NASA Contractor Report 152129

STUDY OF AERODYNAMIC TECHNOLOGY FOR VSTOL FIGHTER/ATTACK AIRCRAFT

PHASE I FINAL REPORT

Walter R. Burhans, Jr.
Vincent J. Crafa, Jr.
Nicholas F. Dannenhoffer
Frank A. Dellamura
Robert E. Krepski

GRUMMAN AEROSPACE CORPORATION
Bethpage, N.Y. 11714

CONTRACT NAS 2-9770
MAY 1978

National Aeronautics and
Space Administration

Ames Research Center
Moffett Field, California 94035

1. Report No.	2. Government Accession No.	3. Recipient's Catalog No.
NASA CR-152129		

4. Title and Subtitle	5. Report Date
Study of Aerodynamic Technology for VSTOL Fighter/Attack Aircraft	May 23, 1978
	6. Performing Organization Code

7. Authors	8. Performing Organization Report No.
W. Burhans, V. Crafa, N. Dannenhoffer, F. Dellamura, R. Krepski	PDR-623-24
	10. Work Unit No.

9. Performing Organization Name and Address	11. Contract or Grant No.
Grumman Aerospace Corporation. Bethpage, New York 11714	NAS2-9770
	13. Type of Report and Period Covered: Contractor Final Report. Nov. 1, 77 – May 23, 78

12. Sponsoring Agency Name and Address	14. Sponsoring Agency Code
NASA, Ames Research Center, Moffett Field, Calif. 94035 David Taylor Naval Ship Research & Development Center Bethesda, Md. 20084	

15. Supplementary Notes

Ames Research Center Technical Monitor-W.P. Nelms (415) 965-5855
NSRDC Point of Contact – R.L. Schaeffer (202) 227-1180

16 Abstract

Studies by the Navy indicate potential for VSTOL Fighter/Attack Aircraft that can be accommodated on ships smaller than present aircraft carriers. In general, concepts displaying VSTOL capability, supersonic dash capability, and transonic agility are of interest. The areas covered in this report are:

- Description of viable V/STOL fighter/attack configuration (a high wing, close-coupled canard, twin-engine, control configured aircraft) which meets or exceeds specified levels of vehicle performance
- Estimates of vehicle aerodynamic characteristics and the methodology utilized to generate them
- Description of propulsion system characteristics and vehicle mass properties
- Identification of areas of aerodynamic uncertainty
- A test program to investigate the areas of aerodynamic uncertainty in the conventional flight mode

17. Key Words (Suggested by Author(s))	18. Distribution Statement
VSTOL Fighter/Attack Aerodynamic Technology	

19. Security Classif. (of this report)	20. Security Classif. (of this page)	21. No. of Pages	22. Price*
Unclassified	Unclassified		

* For sale by the National Technical Information Service, Springfield, Virginia 22161

NASA-Langley, 1978

CONTENTS (Contd)

CONTENTS (Contd)

ILLUSTRATIONS

ILLUSTRATIONS (Cont.)

ILLUSTRATIONS (Cont.)

ILLUSTRATIONS (Cont.)

TABLES

SYMBOLS AND ABBREVIATIONS

a	Acceleration
A/B	Afterburner On
A_c	Air Intake Capture Area, Square Inches (Sq. in.)
A_J	Jet Exit Area, Ft^2 ($Meter^2$)
ADEN	Augmented Deflector Exhaust Nozzles
b_{REF}	Reference Wing Span, Ft. (Meters)
B	Body
B*	Body-Glove-Nacelle
B. L.	Butt Line
BCA	Best Cruise Altitude, Ft. (Meters)
BMN	Best Cruise Mach Number
c	Chord, In. (Meters
$\bar{c}$	Mean Geometric Chord, Inches (Meters)
c_{AVE}	Average Chord, Inches (Meters)
C	Canard
C_D	Drag Coefficient $= \frac{D}{qS_{REF}}$
$C\ell$	Rolling Moment Coefficient $= \frac{l}{q\, S_{REF}\, b_{REF}}$
	2-D Lift Coefficient $= \frac{l}{q\, c}$
C_L	Lift Coefficient $= \frac{L}{q\, S_{REF}}$
C_m	Pitching Moment Coefficient $= \frac{m}{q\, S_{REF}\, \bar{c}}$
C_η	Yawing Moment Coefficient $= \frac{\eta}{q\, S_{REF}\, b_{REF}}$
C_P	Pressure Coefficient $= \frac{\Delta P}{q}$

SYMBOLS AND ABBREVIATIONS (Cont.)

C_Y	Sideforce Coefficient $= \frac{Y}{q S_{REF}}$
CAP	Combat Air Patrol
CG	Center of Gravity
D	Drag, Lbs. (Newtons)
DLI	Deck Launched Intercept
FRL	Fuselage Reference Line
FS	Fuselage Station, In
g	Gravitational Acceleration
GW	Gross Weight, Lbs (Kilograms)
n	Altitude, Feet (Meters)
i	Incidence, Degrees
I_{YY}	Pitch Inertia, Slug-Ft^2 ($Kg-m^2$)
I_{XX}	Roll Inertia, Slug-Ft^2 ($Kg-m^2$)
I_{ZZ}	Yaw Inertia, Slug-Ft^2 ($Kg-m^2$)
l	Rolling Moment, Ft.-Lbs. (Newton-Meters)
l	Two-Dimensional Lift, Lbs. (Newtons)
L	Lift, Lbs. (Newtons)
L/D	Lift to Drag Ratio
LHA	Amphibious Assault Ship
LO	Lift Off
LPH	Amphibious Assault Ship
m	Pitching Moment, Ft.-Lbs. (Newton-Meters)
M	Mach Number
mac	Mean Aerodynamic Chord

SYMBOLS AND ABBREVIATIONS (Cont.)

η	Yawing Moment, Ft.-Lbs. (Newton-Meters)
N	Nacelle
o, OL	Zero Lift
P_S	Specific Excess Power, Feet/Sec. (Meters/Sec.)
q	Free Stream Dynamic Pressure, Lbs./Ft^2 (Newtons/$Meter^2$)
RALS	Remote Augmented Lift System
RCS	Reaction Control System
S_{GR}	Ground Roll Distance, Feet. (Meters)
S_{REF}	Reference Wing Area, $Feet^2$. ($Meters^2$)
SFC	Specific Fuel Consumption, Lbs Fuel/Lbs Thrust/Hr. (Kg Fuel/Newton Thrust/Hr.
SSS	Subsonic Surface Surveillance
STO	Short Take-Off
T	Gross Thrust, Lbs. (Newtons)
t/c	Thickness to Chord Ratio
T/W	Thrust to Weight Ratio (Newtons/Kilogram)
TOGW	Take-Off Gross Weight
TV/SC	Thrust Vectoring/Supercirculation
V	Vertical Tail
V	Velocity, Feet/Sec. (Meters/Sec.)
V_e	Effective Velocity Ratio $= \sqrt{\frac{2 A_J q}{T}}$
VTO	Vertical Take-Off
W	Weight, Lbs (Kilograms)
W	Wing
W.L.	Waterline, In.

SYMBOLS AND ABBREVIATIONS (Cont.)

W/S	Wing Loading, Lb/Ft^2 (Kilogram/Meter)
WOD	Wind Over Deck, Kts (Meters/Sec.)
2-D	Two-Dimensional
3-D	Three-Dimensional
α	Angle of Attack, Degrees
β	Sideslip Angle, Degrees
γ	Flight Path Angle, Degrees
δ_A	Aileron Deflection $\left(=\frac{\delta_{LEFT} - \delta_{RIGHT}}{2},\right)$ Degrees
δ_F	Flap Deflection, Degrees
δ_{LC}	ADEN Nozzle Deflection, Degrees
δ_R	Rudder Deflection, Degrees
δ_{RALS}	RALS Nozzle Deflection, Degrees
δ_{T_2}	Ratio of Total Pressure at Compressor Face to Sea Level Standard Pressure
δ_{W_X}	Variable Camber Element Deflection Angle, Degrees
ΔD	Jet-Induced Interference Drag, Lbs. (Newtons)
ΔE_S	Change in Aircraft Energy, Feet (Meters)
ΔL	Jet-Induced Interference Lift, Lbs. (Newtons)
ΔM	Jet-Induced Interference Pitching Moment, Lbs.-Ft. (Newton-Meters)
θ	Twist Angle, Degrees
θ_{T_2}	Ratio of Total Temperature at Compressor Face to Sea Level Temperature
$\ddot{\theta}$	Pitch Acceleration, Rad/Sec^2
$\ddot{\phi}$	Roll Acceleration, Rad/Sec^2
$\ddot{\psi}$	Yaw Acceleration, Rad/Sec^2

1 - SUMMARY

This report represents the results of Grumman's "Study of Aerodynamic Technology for V/STOL Fighter/Attack Aircraft under contact NAS2-9770. During this effort a configuration was developed to meet NASA-specified guidelines, its aerodynamic characteristics estimated, areas of aerodynamic uncertainty were identified and a wind tunnel program to be conducted at NASA/AMES was developed to investigate as many of the areas of aerodynamic uncertainty as possible.

In 1973, Grumman and General Electric participated in a Navy exhaust nozzle development program. The resulting Grumman Design 623 using the General Electric ADEN nozzle has since been extensively tested in wind tunnels both here and abroad. This testing has ranged from VTOL hot gas tests to transonic and supersonic powered and flow-through model tests. This background data provided a starting point for this study.

Since its initial conception five years ago, advances in the state-of-the-art in propulsion, aerodynamics and materials, as well as a better understanding of the VTOL requirements has allowed Grumman to update Design 623 into a more potent fighter/attack aircraft.

Although this report is primarily directed toward the aerodynamic technology studies, the propulsion and materials are discussed in sufficient detail to show that the overall result is a viable aircraft.

To provide a comparison with previous studies, the baseline sizing mission was selected to be a Deck Launched Intercept (DLI) mission. It is in no way intended that this is the most critical mission for this vehicle but provides for a consistent evolution of the vehicle.

The technique used to develop each design was through the Grumman computer program known as the Computerized Initial Sizing Estimate (CISE). The program serves as an aid in making early decisions about an airplane's optimum size and general characteristics as well as determining sensitivity to major changes such as mission radius or engine type. This report presents these sensitivity results in such a way that the effect of each change is readily apparent.

The final configuration, which is presented in this study as Grumman Design 623-2024, is a high-wing close coupled canard, twin engine, control configured aircraft. Propulsion is provided by two General Electric variable cycle engines with a Remote Augmented

Lift System (RALS) as the forward lift thrusters. The wing employs a mechanical variable camber system consisting of multi-segmented leading and trailing edge devices to vary camber and twist, allowing optimization for cruise and maneuver conditions. Aircraft pitch control is through use of a canard which is augmented at low speeds and high angle of attack by its own leading and trailing edge devices. Roll control during conventional flight is achieved by asymmetric deflection of the wing trailing edge devices. Yaw control is by rudder deflection.

This aircraft makes extensive use of graphite composites, and advanced aluminum and titanium alloys to produce a minimum weight aircraft.

A comparison of this aircraft with the Phase I objective guidelines is as follows:

Phase I Guidelines	Grumman Design 623-2024
• Supersonic dash capability with sustained Mach number capability of at least 1.6	• Supersonic dash capability with sustained Mach number capability of 1.8
• Operational from land and from ships smaller than CV's without catapults and arresting gear (i.e., good STO capability).	• Aircraft sized to fit on smallest CV's. VTO capable for the design mission, STO capable with 400 foot deck run.
• Sustained load factor of 6.2 at Mach 0.6, 10,000 feet altitude at 88-percent VTOL gross weight.	• Sustained load factor of 6.8 at Mach 0.6, 10,000 feet altitude at 88-percent VTOL gross weight.
• Specific excess power (P_S) at 1G of 900 fps at Mach 0.9, 10,000 feet altitude at 88-percent VTOL gross weight.	• Specific excess power (P_S) at 1G of 1130 fps at Mach 0.9, 10,000 feet altitude at 88-percent VTOL gross weight.
• VTOL gross weight = 20,000 to 35,000 pounds.	• VTOL TOGW of 37,726 pounds.
• STO sea-based gross weight - VTOL gross weight plus 10,000 pounds.	• STO sea-based gross weight - VTOL gross weight plus 9574 lb, at 0 WOD, VTOL gross weight plus 13,274 lb, at 20 KTS WOD

Therefore, Design 623-2024 does represent a viable aircraft for the 1990 time frame assuming that the technologies are developed as predicted.

The investigation of aerodynamic uncertainties of such a configuration are the purpose for the Phase II wind tunnel program. In the Design of the 623-2024 configuration, the areas of greatest aerodynamic uncertainty are:

- Buffet onset
- Aerodynamic characteristics of wide-body low aspect ratio wing configurations
- Interference effects of close-coupled Canard/Wing configurations
- Thrust Vectoring/Supercirculation
- High Angle of Attack characteristics.

In addition, uncertainties typical of any VTOL aircraft such as jet-induced effects, reingestion and ground effects at forward speed during short take-off (STO) exist. These are very configuration dependent and require a specialized facilities for experimental evaluation.

Grumman has proposed to modify the existing 1/8 scale Design 623 model which is currently at the NASA/Ames Research Center. A detailed test plan as well as the planned modifications to this model are discussed in section 9.0 of this report. In addition, the model is of sufficient size to permit installation of the XM2R engine simulators at some later date if desired.

2 - INTRODUCTION

Grumman has been involved in VSTOL Fighter/Attack aircraft studies for over seven years and has generated a series of designs based on new concepts and technologies. The design which evolved from this study is an extension of Grumman Design 623, a twin engine fighter/attack aircraft intended for a 1995 IOC.

Application of the advanced propulsion and aerodynamics technology forecasted in our ongoing V/STOL programs and our ATS/AFTI-111 Air Force Study contracts ensure a conceptual design which takes full advantage of the forcasted state-of-the-art to meet this IOC date.

The data presented in this report pertains to the latest conceptual design which meets the projected design requirements, reflects the areas of uncertainty and recommends a wind tunnel program to investigate these uncertainties. In Phase II of this study, Grumman has proposed a modification to the existing NAPTC model which is currently scheduled for testing at NASA, Ames. This modification and test program provides an orderly extension of technology progress on VSTOL aircraft design as well as allowing an early analysis of our prediction methods for future technology.

3 - AIRCRAFT DESCRIPTION

3.1 DESIGN PHILOSOPHY

Grumman Aerospace Corporation has had a commitment to fighter/attack V/STOL aircraft since 1971. During seven years of work, the Design 623 family of aircraft has evolved which has an extensive and sound test program as its basis of design. The starting point for this study, Design 623-2004 represents an aircraft benefitting from all previous test data. However, the performance level is considered low for a projected 1995 IOC aircraft. In addition, it reflects technology levels more consistent with 1982-1987 IOC dates rather than 1995.

With this in mind, work was started by updating the technology levels to those of 1995. Since no mission requirements were specified, Grumman chose to use the standard DLI mission to be consistent with earlier designs, thus removing one variable from the study.

From other ongoing work, the latest technology predictions in the area of materials, structures, propulsion and aerodynamics were introduced into the aircraft design process. In addition the performance requirements from the contract guidelines were introduced.

With these basic changes, the aircraft design process was started which brought Design 623 up to the latest projected technology. The end result was Design 623-2024, shown and described in Section 3.3 and Figure 3.3-1.

3.2 DESIGN GROUND RULES

The basic design ground rules were as follows:

- The use of the DLI (Deck Launched Intercept) mission, not from a point of being the critical mission but to provide consistent evolution of configurations
- All materials and structure should represent 1995 technology levels and each component should be representative of these levels, i.e. (wings, tails, etc.)
- Basic payload should consist of
  - (2) AIM-7 (Sparrow)
  - (2) AIM-9 (Sidewinder)
  - (1) 20 mm Gun and Ammo

SI UNIT CONVERSION		
TO CONVERT FROM	TO	MULTIPLY BY
INCHES	METERS	0.0254
FEET	METERS	0.3048

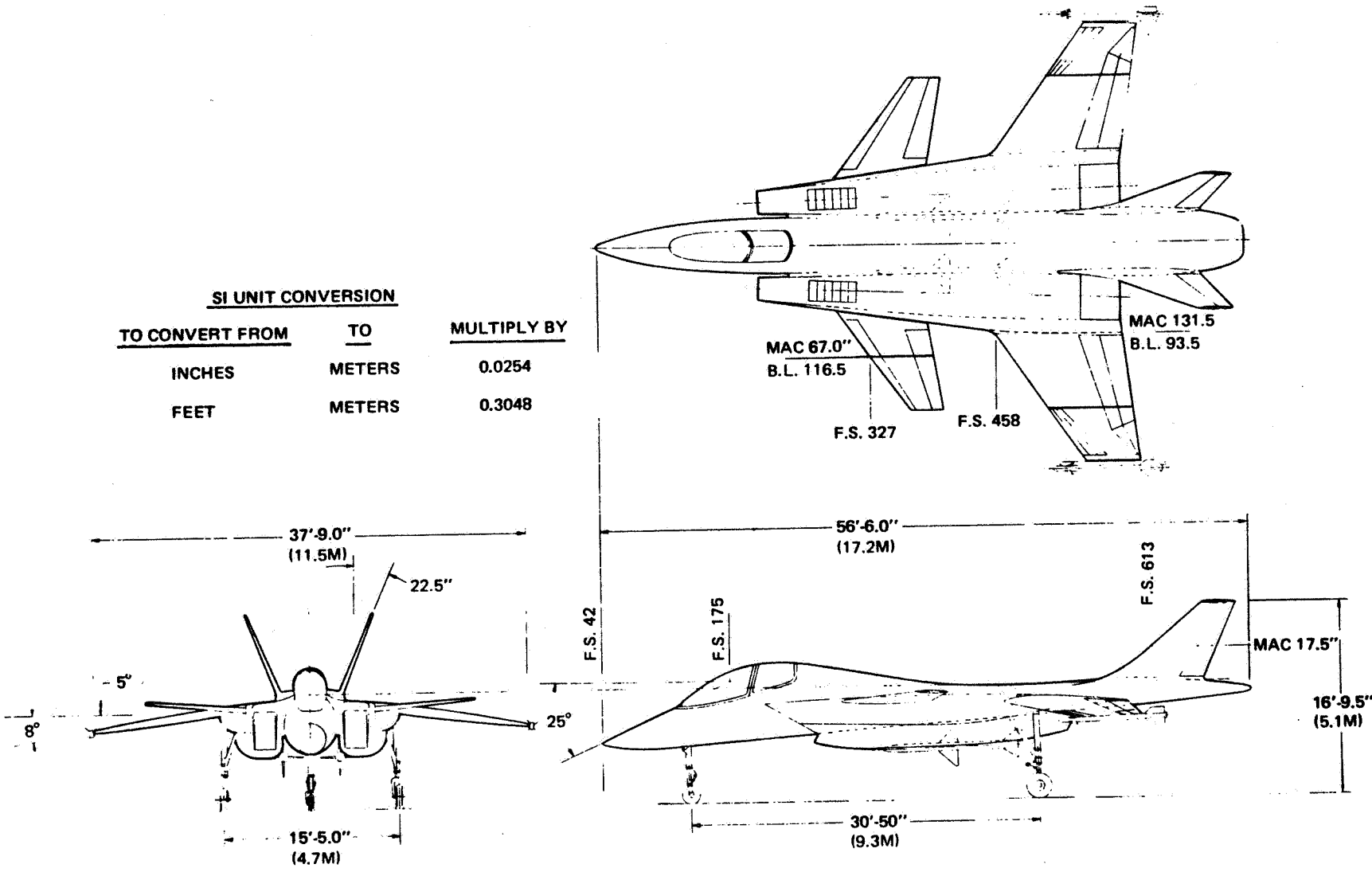

1690-143W

Figure 3.3-1 Design 623 – 2024 General Arrangement

- All fuel for the design mission should be internal with provisions for protected fuel for go-home capability
- Engines shall be of the VCE (Variable cycle engine) type with a RALS (Remote Augmented Lift System) for forward lift
- All other missions which result in higher TOGW's than the design mission shall use STO for takeoff and VTO for landing
- Avionics payload of 1200 lb consistent with today's advanced fighter aircraft. It is assumed that any avionic technology increases will be made in capability or additional features rather than reduced weight.
- The design guidelines would form the minimums for acceptable performance.

3.3 CONFIGURATION DESCRIPTION

In 1973, Grumman and General Electric participated in a Navy sponsored exhaust nozzle development program from which the Design 623 concept evolved. From that effort the ADEN nozzle also evolved and was further developed for our response to the Navy VFAX/VSTOL Presolicitation Notice (PSN) in the summer of 1974. Extensive aerodynamic testing of the basic Design 623 concept has been accomplished in Grumman's 7 x 10 ft low speed tunnel, British Aircraft Corporation's 5.5 M V/STOL tunnel, and the Arnold Engineering Development Center transonic facilities. Hot gas reingestion tests were conducted at VFW/FOKKER hot gas test facility at Bremen, FGR. Configuration modifications necessary to achieve good VTO and STO capabilities were made as a result of conclusions drawn from these tests.

The current Grumman V/STOL Configuration, Design 623-2024, is a high-wing, close-coupled canard, twin-engine, control-configured V/STOL aircraft. The propulsion system employes advanced technology variable cycle engines with two-dimensional Augmented Deflector Exhaust Nozzles (ADEN) to provide both vertical and horizontal thrust. The ADEN nozzle placement in the proximity of the wing trailing edge promotes the formation of beneficial supercirculation effects. A Remote Augmented Lift System (RALS) consisting of twin vectorable nozzles forward of the aircraft center of gravity provides vertical lift augmentation and balance during VTOL AND STOL operation. The general arrangement of the propulsion system provides lateral separation to accommodate the RALS and to ensure fountain formation to offset suckdown effects. Roll control during jet-borne flight is supplied by a wing-tip

Reaction Control System (RCS) jets. RCS flow is supplied by compressor interstage bleed. The RALS nozzles may be deflected laterally to provide yaw control during jet-borne flight modes. Flow shifting between the forward RALS and aft ADEN nozzles provides pitch control during hover and transition.

Advanced aerodynamic technology is employed, consistent with the envisaged IOC date of 1995. A mechanical variable camber system, consisting of multi-segmented leading and trailing edge devices, is employed to vary the wing camber and twist from a cruise configuration to a configuration more suited for maneuver conditions. The aircraft is configured to have negative static longitudinal stability at subsonic and transonic speeds, and thus benefits from minimized trim drag penalties. A canard is employed for pitch control during conventional flight modes, the configuration thus benefiting from positive lift due to trim during maneuver. During operation at high angle of attack and low speeds, control effectiveness of the slab canard surface is augmented by deflection of canard leading and trailing devices. Roll control during conventional flight is supplied by asymmetric deflection of the wing trailing edge devices. Symmetric deflection of these trailing edge devices (other than that used for camber/twist optimization) may be used to augment aerodynamic lift during short takeoff (STO) operation and transition. Yaw control is supplied by rudder deflection

The Design 623-2024 takes full advantage of advanced materials and manufacturing technology. Extensive use of graphite composites, advanced aluminum and titanium alloys are employed to produce a minimum weight aircraft. A summary weight statement is presented in Figure 6.3-1 and 6.3-2.

Primary avionics are carried in three bays: one fore and one aft of the cockpit and one in the aft fuselage. Equipment locations are shown on the inboard profile presented in Fig. 3.5-1. The primary fuel load is totally in the fuselage located in eight main tanks, five bladder tanks between the engines (three forward and two aft of the wing box), plus one integral fuel tank in the center wing box. In addition, two self-sealing fuel tanks are located below the center wing box.

Seven external store stations are provided. Two AIM-7 Sparrow missiles may be mounted tangentially on the inboard nacelle chines. AIM-9 Sidewinder or equivalent advanced missile may be mounted on each wing-tip. Additional stores may be carried on the fuselage centerline and at a single pylon station on each wing panel. In addition, a 20-mm gun is carried internally in the forward fuselage.

3.4 AIRCRAFT CHARACTERISTICS

Dimensional and weight characteristics are shown in the following Table and Figure 3.4-1.

WING				
AREA (REF)	380 FT^2	(35.3 m^2)	AIRFOIL SECTION	
AREA (EXP)	174.5 FT^2	(16.2 m^2)	ROOT – TIP	GRUMMAN K MODIFIED
ASPECT RATIO	3.75		INCIDENCE	
SWEEP L.E.	35°		GLOVE – TIP	0° – 2°
TAPER RATIO	.3		ANHEDRAL	8°
CANARD				
AREA (REF)	85 FT^2	(7.9 m^2)	AIRFOIL SECTION	
AREA (EXP)	85 FT^2	(7.9 m^2)	ROOT – TIP	GRUMMAN K MODIFIED
ASPECT RATIO	1.56/PANEL		INCIDENCE	
SWEEP L.E.	37.5°		GLOVE – TIP	0°
TAPER RATIO	.37		DIHEDRAL	5°
VERTICAL TAIL				
AREA (REF)	84 FT^2	(7.8 m^2)	AIRFOIL SECTION	
AREA (EXP)	84 FT^2	(7.8 m^2)	ROOT – TIP	005 – 64
ASPECT RATIO	1.37/PANEL		CANT	22.5°
SWEEP L.E.	47.5°			
TAPER RATIO	.37			
WEIGHT				
TAKEOFF GROSS WT	37 726 LBS (17 112 Kg)			
FLT DESIGN GROSS WT	33 479 LBS (15 186 Kg)			
LDG DESIGN GROSS WT	27 867 LBS (12 640 Kg)			
EMPTY WT	24 256 LBS (11 002 Kg)			
INTERNAL FUEL	11 618 LBS (5 270 Kg)			
DESIGN LOAD FACTOR	7.0			
WING LOADING	100 LB/FT^2 (488 $Kg/_{m}2$)			
POWERPLANT				
ENGINE TYPE & DESIGNATION – VARIABLE CYCLE TURBOFAN – G.E. SYS – G.E. 16/VVCES STUDY D3				
S.L.S. MAX RATED	27 729 LBS (12 578 Kg)			
INLET CAPTURE AREA	6.4 FT^2 (.6 m^2)			
WETTED AREA				
WING	349 FT^2	(32.4 m^2)	BODY 687 FT^2 (63.8 m^2)	
CANARD	170 FT^2	(15.8 m^2)	GLOVE 167 FT^2 (15.5 m^2)	
VERT. TAIL	175 FT^2	(16.3 m^2)		
NAC	448 FT^2	(41.6 m^2)		
TOTAL = 1996 FT^2 (185.4 m^2)				

1690-140W

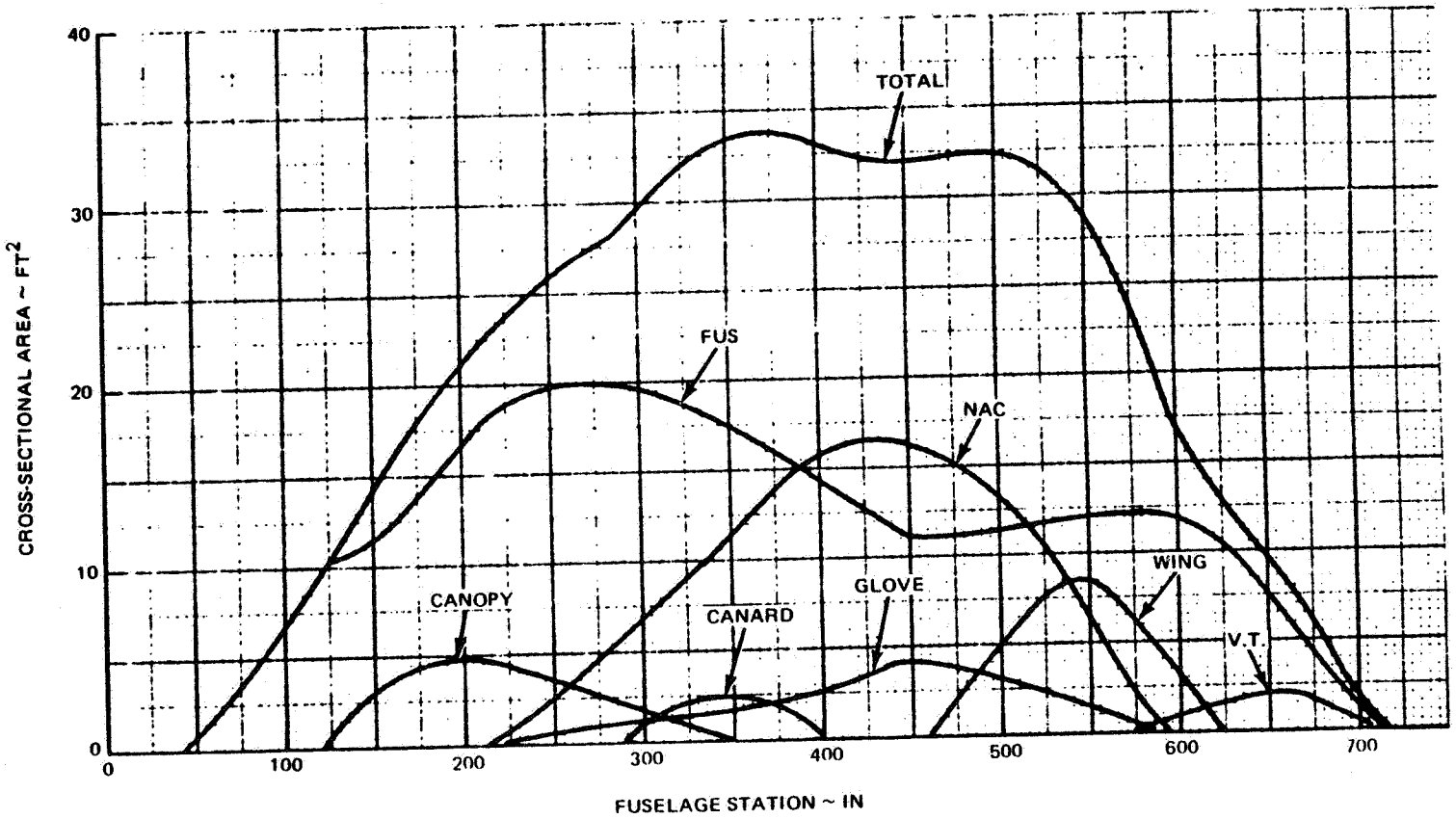

1690-141W

Figure 3.4-1 Design 623 - 2024 Cross-Sectional Area Distribution

3.5 INBOARD PROFILE

Design 623 provides a total internal volume which exceeds the projected volume required for the candidate systems. Figure 3.5-1 shows the arrangement of the subsystems and the location of equipment compartments with major consideration to maintainability, vulnerability, balance and growth potential.

The avionic subsystem such as the multi-function radar and EW/ECM system are located and arranged to maximize performance and minimize installation complexity. The remaining avionic subsystems are arranged to optimize their specific accessibility requirements.

Location of the primary environmental control system (ECS) equipment minimizes the interface requirements to other subsystems while permitting adequate accessibility for routine maintenance and inspection. Forward of the ECS compartment and in close proximity to the cockpit an onboard oxygen generating system (OBOG) is provided.

The arrangement and location of redundant engine/aircraft accessories and hydraulic systems permits periodic maintenance and inspection while providing the necessary vulnerability protection. Internal volume is provided for fuel and armament systems featuring self-sealing feed tanks and a 400 round capacity 20mm ammunition drum.

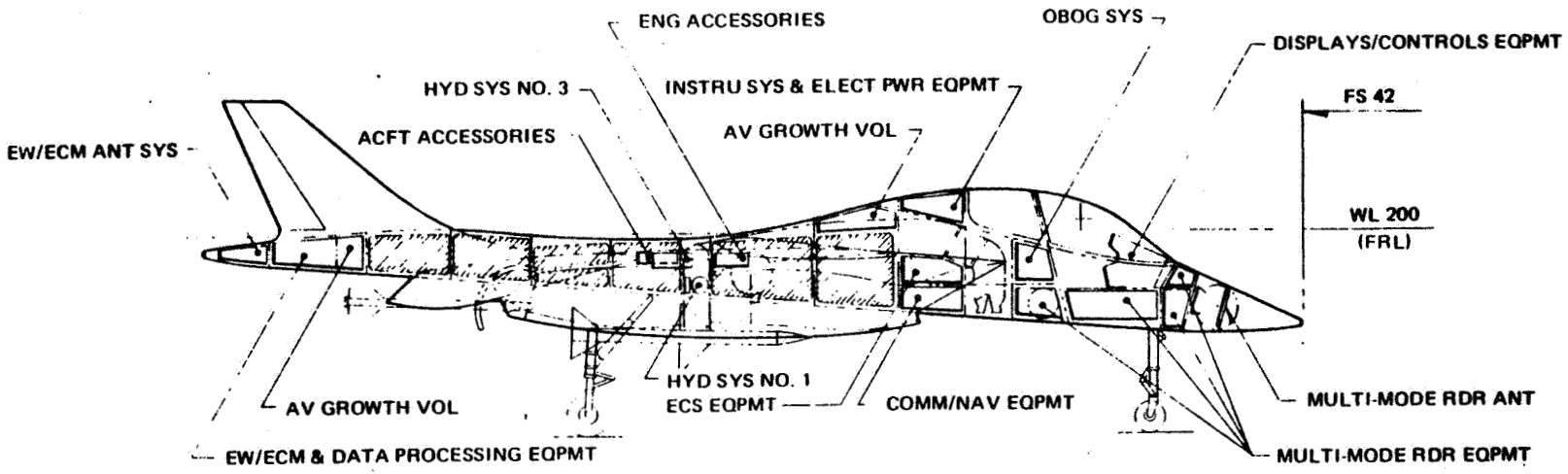

RHS INBD PROFILE

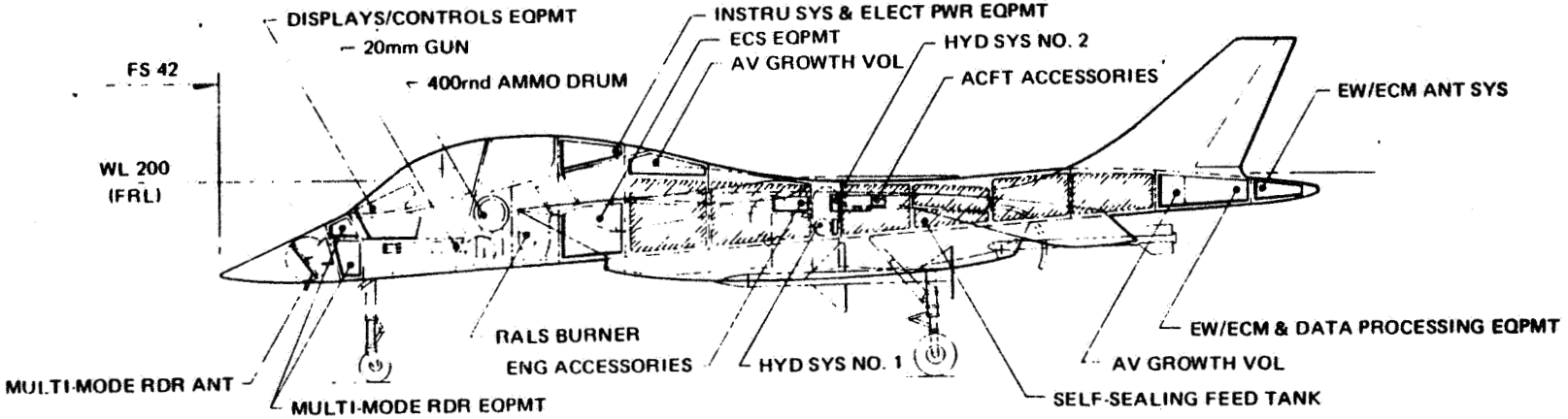

LHS INBD PROFILE

1690 142W

Figure 3.5-1 Design 623 – 2024 Inboard Profile

4 - AERODYNAMIC CHARACTERISTICS

Basic aerodynamic characteristics of the Design 623-2024, as well as the methodology utilized to obtain them are presented in the following sections. This information forms the aerodynamic basis for the performance analyses contained in Section 7.0 as well as the areas of aerodynamic uncertainity discussed in detail in Section 8.

4.1 LONGITUDINAL CHARACTERISTICS

4.1.1 Wing Design

The wing design of Design 623-2024 was based on a number of considerations. Wing planform was chosen on the basis of the results of parametric sizing studies for the baseline DLI mission combined with STO performance considerations as enumerated in Section 7.0. The airfoil design procedure for this chosen planform is discussed below.

Different airfoil geometry is necessary for optimum wing performance when operating at high lift coefficients at a maneuver condition as opposed to the comparatively low lift coefficients encountered during cruise flight (Figure 4.1.1-1). Resolution of these different requirements can be accomplished by employing a variable camber system consisting of multiple element leading and trailing edge devices. For maneuver, the wing employs a highly cambered supercritical airfoil designed to operate in the range of $1.0 < C_{l_{2-D}} < 1.5$, which is decambered to produce an airfoil designed to operate at $.25 < C_{l_{2-D}} < .35$. The appropriate airfoil geometry was determined through use of Grumman's wing design methodology (References 4.1.1-1 thru 4.1.1-3).

The Grumman "K" supercritical airfoil section was selected for the major part of the maneuver wing. This is an aft cambered section having t/c = .065 and trailing edge deflection of approximately -.065c. For the wing spanload distribution at maneuver, the 2-D airfoil section lift coefficients ($C_{l_{2-D}}$) vary from about 1.15 to 1.50, at $M_{2-D} = .554$ (based on $\Lambda_{C/2} = 22.5^{\circ}$). Figure 4.1.1-2 shows a pressure distribution on the "K" maneuver airfoil at $C_{l_{2-D}} = 1.40$, corresponding to $\eta = .75$. It was computed using a program developed at Grumman under NASA sponsorship (Reference 4.1.1-2). This program incorporates a refined treatment of the boundary layer which permits a variation within the boundary layer of the static pressure normal to the airfoil surface, thus improving the solution in the region of the trailing edge, and making the drag and angle of attack values more accurate. The pressure distribution shown is characteristic of the "K" airfoil at maneuver C_l. The upper and

lower surface pressure gradients are small, and no separation is predicted. The airfoil operates shock-free, and flow velocities are subcritical except for a small area near the leading edge. Camber was removed over the rear 35% of this section to produce a cruise airfoil section. This is made possible by use of a variable camber mechanism to adjust the wing shape from cruise to maneuver. Figure 4.1.1-3 presents a pressure distribution on the cruise airfoil section at $M_{2\text{-}D} = .739$, $C1_{2\text{-}D} = .35$, corresponding to $M\infty = .8$ at $C_L = .30$. At this condition the airfoil is entirely subcritical.

Twist distributions were derived using the Grumman 3-D wing/body lifting surface computer program (Reference 4.1.1-3), which is well suited to configurations of this type because it permits multiple (wing and canard) lifting surfaces to be modelled. This capability is important because the canard generates a downwash and a tip vortex ahead of the wing, which affects the desired twist distribution on the wing. The fuselage is represented as a body of revolution having an ogival radius variation near the nose and a constant radius section aft of the canard leading edge. Wing and canard carryover lift on the body is accounted in computed wing spanloads. Since the canard and wing are almost coplanar, the optimum total spanload is designed to be elliptical. The canard spanload is also designed to be elliptical with the total canard lift satisfying the condition of pitching moment equilibrium. The remaining spanload is carried by the wing.

Spanload distributions for cruise and maneuver are presented in Figures 4.1.1-4 and 4.1.1-5 respectively. Both distributions have a spanwise efficiency factor of .91. For cruise, at a design angle of attack of 2°, the moderate canard loading results in a wing twist distribution having 0° root incidence and 2° washout at the tip, as shown in Figure 4.1.1-6. For maneuver, at a design angle of attack of 5°, the canard carries a proportionately larger load, and its induced effects on the wing are larger. The canard downwash requires increased wing incidence in the region of the wing behind the canard, so that the airfoil sections operate at their optimum angle of attack. Outboard of the tip of the canard, the inflow to the wing is more nearly aligned with the free stream, so airfoil sections outboard of the tip of the canard must be twisted leading edge down, relative to the rest of the wing. The maneuver twist distribution is also shown in Figure 4.1.1-6. From the side of the nacelle ($\eta = .366$) to $\eta = .84$, the maneuver twist is the same as the cruise twist distribution, except for a constant 3.5° increase in incidence which is obtained by deflecting the trailing edge segments of the wing variable camber system into the "K" maneuver airfoil section. Outboard of $\eta = .84$, the wing is twisted leading edge down, to an incidence of -4.7° at the tip. This is accomplished by deflecting leading edge devices on the main wing, outboard of the tip of the canard, and progressively removing the trailing edge camber

in the aft region of the wing. At $\eta = .92$, tip airfoil 4 is used, varying to tip airfoil 6 at near the wing tip. Two-dimensional, computed pressure distributions on these sections at maneuver conditions are given in Figures 4.1.1-7 and 4.1.1-8 for completeness.

Coordinates and computer generated plots of the cruise and maneuver airfoil sections are included in the Proprietary Appendix consisting of Section 10 of this report.

4.1.2 Lift and Pitching Moment Characteristics

The vortex-lattice method, as described in Reference 4.1.2-1, was used to determine the longitudinal aerodynamic characteristics of Design 623-2024 at subsonic speeds. This method is an extension of the finite step lifting-line method originally described in Reference 4.1.2-2 and applied in Reference 4.1.2-3. This method assumes steady, irrotational, inviscid, incompressible attached flow. Potential flow theory in the form of the Biot-Savart law is used to represent disturbances created in the flow field by the lift distribution of the planform.

The planform is divided into many elemental panels. Each panel is replaced by a horseshoe vortex. The horseshoe vortex is composed of three vortex lines: a bound vortex which is swept to coincide with the elemental panel quarter chord sweep angle in the plane of the wing and two trailing vortices which extend chordwise parallel to the freestream to infinity behind the wing.

The vortex lattice laid out is used in place of the real planform to generate the same flow field and to determine the forces and moments acting on the real planform. To perform these functions, the flow must be constrained so that it does not pass through the vortex lattice at specified points. This flow constraint is called the "no flow" condition and is equivalent to requiring that the flow be tangent to the real planform mean camber surface. The circulation required to satisfy this tangent flow boundary condition is then determined by solving a matrix equation. Then, the Kutta-Joukowski therorem for list from a vortex filament is used to determine the lift of each elemental panel. These individual lifts are then summed to obtain the lift and pitching moment.

These results were then modified to take into account Grumman experience with fighter/attack configurations incorporating canards, (References 4.1.2-4 and 4.1.2-5) and blended wing/body/nacelle design (Reference 4.1.2-6). This approach has been successful in providing reliable estimates of the variation of longitudinal characteristics with angle of attack in the linear angle of attack range for configurations similar to Design 623-2024 (Reference 4.1.2-7).

Estimates for angle of attack for zero lift (α_{L_0}) and zero lift pitching moment (C_{m_0}) were generated from airfoil characteristics generated during the wing design process (see Section 4.1.1) and from Grumman test experience with similar blended wing-body configurations (Reference 4.1.2-4).

The extension of the estimates through the full range in Mach number was achieved by using the techniques found in Reference 4.1.2-8 modified by Grumman test experience with similar configurations (Reference 4.1.2-4).

A component build-up of the lift and pitching moment data are shown in Figures 4.1.2-1 to 4.1.2-10. The vehicle possesses negative static longitudinal stability at subsonic and low transonic speeds, in keeping with the control configured vehicle concept. Based on our previous experience, these characteristics are expected to be linear for the angle of attack range shown. It should be noted that the characteristics depicted are applicable to the cruise configuration wing.

4.1.3 Longitudinal Control Effectiveness

Canard control effectiveness, presented in Figure 4.1.3-1, was estimated using the techniques of Reference 4.1.2-8 adjusted to reflect Grumman experience with canard configurations. The method of Reference 4.1.2-8 is based on configuration geometry. Carryover effects are included.

The close-coupled canard configuration introduces highly configuration dependent mutual interference between the wing and canard not included in the method of Reference 4.1.2-8. This effect has been established from an earlier Grumman study, Reference 4.1.2-4, of a generically similar configuration and from correlation studies between experimental and predicted results (Reference 4.1.2-5).

4.1.4 Drag Analysis

4.1.4.1 Thrust/Drag Bookkeeping - The separation of drag and thrust effects for the Design 623-2024 aircraft follows a logical and consistent procedure. In keeping with widely accepted practice, those terms affecting thrust minus drag which are functions of power setting are considered thrust effects and therefore included in the installed engine performance (Section 5.0). Those which are not, are included in the aerodynamic drag polar.

The drag data which is contained in the following sections is based on a reference aircraft configuration which does not include any drag forces on the ADEN nozzle. These forces (including skin friction and boattail drag) have been accounted for in the nozzle in-

stallation drag utilized to generate the installed engine performance contained in Section 5.0.

4.1.4.2 Drag At Zero Lift - The drag at zero lift (C_{D_o}) is comprised of the following effects:

- Skin Friction Drag
- Wing Profile Drag
- Wave Drag
- Supercritical Inlet Spillage Drag
- Roughness and Excrescence Drag
- Drag Due to Cooling and Ventilation.

Skin friction drag is determined via a component buildup technique based on methods contained in References 4.1.4-1 and 4.1.4-2. The flat plate skin friction coefficient based on fully turbulent flow is determined for each configuration component and adjusted by a form factor to account for pressure drag. This procedure is applied at various combinations of Mach number and altitude which are part of the aircraft flight envelope. A representative skin friction drag buildup employing this procedure is presented in Figure 4.1.4-1.

The additional pressure (profile) drag due to airfoil shape not included in the above analysis was obtained from the results of the wing/airfoil design effort elaborated on in Section 4.1.1. The value of this term is $\Delta C_D = .00020$ subsonically.

An additional correction was made for the presence of the canopy in the subsonic and transonic speed regimes (supersonically, the effect of this component is included in the analysis of wave drag). A subsonic incremental drag coefficient of .00132 was used for this effect, based on information contained in Reference 4.1.4-1.

Wave drag at supersonic speeds is based on a far field linearized approach in which an aircraft configuration is described by a series of planar surfaces (wing, canard, tail) and bodies of revolution (fuselage and nacelle). At each Mach number, a family of equivalent bodies of revolution is determined by passing several series of parallel cutting planes (inclined at the specific Mach angle) through the configuration. These cutting planes are oriented at various angles with respect to the aircraft axis. The area of the equivalent body of revolution at each station may be defined as the projection on to a plane normal to the aircraft axis of the area intercepted by the cutting plane. The wave drag of each equivalent body is determined by the von Karman slender body equation, which relates the drag to free stream conditions and the equivalent body area distribution. The wave drag of the aircraft

at a given Mach number is the integrated average of the equivalent body wave drags. This method is developed and verified in References 4.1.4-3, 4.1.4-4 and 4.1.4-5.

The computer code utilized to obtain the wave drag of the design 623-2024 (Reference 4.1.4-6) has been shown to give excellent correlation with experimental data (Reference 4.1.4-7).

The variation in drag between the subsonic and supersonic speed regimes is based on a conservative estimate of the drag divergence characteristics of the cruise airfoil section modified to 3-D conditions.

A number of miscellaneous drag terms must be added to the values of aerodynamic drag to obtain a realistic assessment of the total C_{D_o} of the aircraft. Supercritical inlet spillage drag is depicted in Figure 4.1.4-2 and comprises inlet cowl drag, drag due to upper inlet door bypass bleed air and the additive drag due to inlet stream tube contraction. Drag of other miscellaneous effects is shown in Figure 4.1.4-3. Statistically derived values of drag due to roughness for supersonic fighter/attack type aircraft were used to account for this effect. Allowance for drag due to excrescences was obtained from a detailed estimate for a comparable aircraft. Cooling and ventilation drag representative of this class aircraft were utilized to account for these effects in the Design 623-2024 drag at zero lift.

The total zero lift drag coefficient as a function of Mach number is shown in Figure 4.1.4-4 for an altitude of 36,089 ft. The variation of C_{D_o} with altitude is depicted in Figure 4.1.4-5. A comparison of the subsonic minimum drag with those of contemporary supersonic aircraft illustrates the credibility of the methodology employed (Figure 4.1.4-6.)

4.1.4.3 Drag-Due-To-Lift - The subsonic drag-due-to-lift was based on the results of the wing design effort, Section 4.1.1. For the actual near-optimum chordwise and spanwise total load distributions (canard plus wing), a spanwise efficiency factor was determined along with profile and wave drag-due-to-lift. The total induced drag is then the sum of the above components. This procedure was followed at a number of values of lift coefficient to take into account the variable camber aspect of the Design 623-2024 wing.

The transonic/supersonice induced drag is based on a combination of theoretical and empirical methods that reflect the improved performance achievable with advanced (supercritical, variable camber) technologies. The methodology is based on developing aircraft Oswald factor, e, as a function of flight conditions (Mach number, lift coefficient) and configuration geometry (aspect ratio, wing leading edge sweep, wing thickness, taper ratio). This methodology is based on Grumman's experience in advanced variable camber wing design.

At low to moderately high lift coefficients a relatively high Oswald factor is achieved through appropriate wing design. Above this break lift coefficient, progressive separation or shock wave formation ultimately degrades the lifting efficiency to the same low level obtained with a simple sharp edged planar wing (no leading edge suction).

The above methodology has been computerized and is documented in Reference 4.1.4-8.

The results of the analysis are presented in Figure 4.1.4-7.

4.1.4.4 Untrimmed Drag Polar - The results of the analyses described in the two previous sections have been combined to generate the total untrimmed drag polar for the Design 623-2024 aircraft depicted in Figure 4.1.4-8 for the reference altitude of 36,089 ft. (11,000 m). Corresponding drag levels for other altitudes may be obtained by applying the data contained in Figure 4.1.4-5. Variations of the lift-to-drag ratio (L/D) with lift coefficient for a number of difference Mach numbers is presented in Figure 4.1.4-9.

4.1.4.5 Trim Drag - Relaxed levels of static longitudinal stability inherent to the control configured design philosophy utilized in the evolution of the configuration ensures minimal trim drag penalties. Values of canard deflection required for trim during the DLI mission using the estimated stability, control and center of gravity information presented elsewhere in this report do confirm that this is true. Hence, the drag polar presented in Figure 4.1.4-8 is used to represent the Design 623-2024 trimmed drag polar.

4.1.4.6 Installed Drag of External Stores - Incremental drag due to external stores for the baseline DLI and alternate Combat Air Patrol (CAP) mission loading of two nacelle mounted AIM-7 Sparrow and two wing tip mounted AIM-9 Sidewinder missiles is depicted in Figure 4.1.4-10. Installed Sparrow drag was obtained from data contained in Reference 4.1.4-9, while drag due the addition of the two AIM-9 Sidewinders was generated from information contained in References 4.1.2-4 and 4.1.4-10.

Incremental external store drag information for the alternate Subsonic Surface Surveillance (SSS) mission is presented in Figure 4.1.4-11. Incremental drag of the two pylon mounted AGM-84A Harpoon missiles was generated from unpublished free-flight data adjusted by installation factors presented in Reference 4.1.4-11. Incremental drag for the centerline mounted 300 gallon drop tank and both wing and centerline pylons was established utilizing data contained in References 4.1.4-10 and 4.1.4-11.

4.1.5 High Lift Characteristics

The subsonic level of maximum lift coefficient for the Design 623-2024 configuration was established from an unpublished Grumman-developed empirical procedure which relates the total lifting ability of a configuration to the ratio of total planform area to reference wing area. This method has been shown to give good, if conservative, estimates of maximum lift coefficient for configurations possessing moderately low aspect ratio wings and relatively wide bodies. Trending with Mach number was determined by extracting the trends exhibited by similar high technology fighter configurations from flight test results contained in Reference 4.1.5-1. Levels of maximum usable lift coefficient in the supersonic speed regime were ascertained from control limit considerations and trends exhibited by generically similar configurations. The resultant variation of maximum usable lift coefficient for the Design 623-2024 configuration is presented in Figure 4.1.5-1.

Conventional procedures for predicting buffet onset (such as Reference 4.1.5-2) are not applicable to configurations such as Design 623-2024 which possess blended wing-bodies and incorporate variable camber/supercritical wing technology. Due to the aft shock location characteristic of supercritical airfoils, the area influenced by shock induced separation is substantially less than that of a corresponding wing employing conventional airfoil sections. The lack of available pertinent data on low aspect ratio blended wing-body configurations causes the assessment of the buffet onset characteristics of the Design 623-2024 to be an area of aerodynamic uncertainty.

4.1.6 Supercirculation Effects

Although it has been experimentally verified that beneficial supercirculation effects are present for the Design 623 cruise nozzle/airframe configuration (Reference 4.1.6-1), the impact of such effects on the size/performance of the design has not been accounted for. This conservative approach has been followed for a number of reasons:

- The sparcity of supercirculation data pertinent to the configuration precludes reliably accounting for the impact of this phenomenon in all applicable regions of the flight envelope.
- Supercirculation effects are configuration dependent. To date, experimental data for configurations combining advanced supercritical/variable camber wing design with potential for supercirculation is lacking and there exists some uncertainty as to the additive quality of these effects.

- Studies conducted at Grumman utilizing the applicable experimental data available indicate that the impact of supercirculation on vehicle size/performance is extremely configuration dependent. The DLI mission utilized to size the Design 623-2024 aircraft results in a comparatively small impact of supercirculation on vehicle size. (Less than 10% of total fuel is used furing transonic cruise)

It should be noted (as shown in Section 7.1) that, without taking any benefit for supercirculation, the performance of Design 623-2024 far exceeds the performance requirements enumerated in the Statement of Work.

Configuration dependency, as well as the lack of an applicable experimental data base, makes this phenomenon an area of aerodynamic uncertainty and a candidate for further experimental investigation.

4.2 LATERAL/DIRECTIONAL CHARACTERISTICS

4.2.1 Lateral/Directional Stability Characteristics

Estimated lateral/directional derivatives for the Design 623-2024 are obtained by correlating established empirical techniques with prior wind tunnel test results for generically similar aircraft. The empirical techniques used were obtained from References 4.1.2-8 and 4.2.2-1 combined with data correlation from Reference 4.1.2-4 and Reference 4.1.2-6. Where no technique was available, the trends with Mach number were established from test data on similar configurations.

The sideforce derivative (C_{Y_β}) were calculated for the wing-body, nacelle, canard and vertical tail components of the total configuration. The subsonic derivative was calculated as described in Reference 4.1.2-8. The wing-body, wing-nacelle and canard-body increments were treated as invariant with Mach number. The vertical tail increment at subsonic and supersonic Mach numbers was obtained from the methods of Reference 4.1.2-8. Trending in the transonic speed regime is based on data contained in Reference 4.1.2-4. The variations in sideforce with Mach number for each component and the total configuration are presented in Figures 4.2.1-1 to 4.2.1-4. Based on previous Grumman experience, C_{Y_β} should be relatively invariant with angle of attack for the range under consideration.

The directional stability derivative (Cn_β) was calculated for the vertical tail and wing body components as described in Reference 4.2.1-1. The nacelle and canard were found to have no effect on the directional stability level, based on correlation studies performed utilizing the data contained in References 4.1.2-6 and 4.1.2-4, respectively. The

wing-body component was estimated to be invariant with Mach number. The vertical tail component was computed from the incremental side force data described previously. A component buildup of C_n vs. β is shown for several Mach numbers in Figures 4.2.1-5 to 4.2.1-8. Again, based on previous experience, these levels are expected to remain relatively invariant for moderate ranges of angle of attack (i.e., less than 15 degrees).

The lateral stability derivative (C_{ℓ_β}) was calculated as a function of Mach number and angle of attack by the method shown in Reference 4.1.2-8. The correlation procedure revealed that close agreement is achieved with wide body-nacelle configurations like Design 623-2024 when the exposed wing aspect ratio is used rather than the geometric aspect ratio. The body and nacelle were treated as a single body for this calculation. The vertical tail component was also calculated using Reference 4.1.2-8, and the data of Reference 4.1.2-6 which is a similar configuration. The canard component was calculated as if it were a wing, using only the exposed geometry. The resulting component was then scaled to the full scale wing reference area and span. The component buildup and total level is shown as it varies with Mach number and angle of attack in Figures 4.2.1-9 to 4.2.1-12.

4.2.2 Lateral-Directional Control Effectiveness

Roll control in conventional flight is provided by asymmetric deflection of the wing trailing edge devices; the effectiveness of which was estimated by utilization of the methods contained in Reference 4.1.2-8. Variations of $C_{\ell_{\delta_a}}$ and $C_{n_{\delta_a}}$ with Mach number ($C_{Y_{\delta_a}}$ being insignificant) are displayed in Figure 4.2.2-1. These values are applicable for the cruise wing in the linear angle of attack range. Satisfactory levels of rolling performance based on MIL-F-8785B (ASG) are attained utilizing the levels shown.

Rudder effectiveness was determined by treating the vertical panel as a wing with a plain flap. The method presented in Reference 4.2.2.1 was used to determine the side force generated per degree of rudder deflection ($C_{Y_{\delta_R}}$). Rudder yaw effectiveness ($C_{n_{\delta_R}}$) and roll effectiveness ($C_{\ell_{\delta_R}}$) were determined by multiplying $C_{Y_{\delta_R}}$ by the proper moment arm from the panel center of pressure to the aircraft center of gravity. The variation of rudder effectiveness with Mach number was accounted for by using the variation of the vertical tail ΔC_{Y_β} with Mach number. All three effectiveness parameters are shown in Figure 4.2.2-2 as a function of Mach number.

4.3 PROPULSION-INDUCED EFFECTS

4.3.1 Hover Flight Mode

The level of jet-induced interference lift (commonly referred to as suckdown) utilized to establish T/W required for VTO operation was generated from parametric experimental data published in Reference 4.3-1. These data, obtained from model tests of a generically similar configuration, are presented in Figure 4.3.1-1 as jet-induced interference lift (non-dimensionalized by gross thrust) as a function of height (non-dimensionalized by equivalent nozzle diameter) for various lateral spacings of the ADEN lift/cruise nozzles. The test article from which the data were obtained possessed the same forward/aft nozzle spacing as the Design 623-2024 aircraft and was tested at the same fore/aft thrust split as the current configuration. Although the test article possessed a single forward nozzle, the data obtained should be applicable, as the spacing of the twin RALS nozzles of the current configuration is small enough to insure that the two emanating flows will coalesce and act as a single jet. Based on these data, a value of $\Delta L/T$ of -0.077 at static gear height was employed in the propulsion system sizing procedure. It should be noted that the experimental data contained in Reference 4.3.1-2 indicate that this level should be relatively invariant with nozzle deflection for $80° \leq \delta_{L/C} \leq 100°$, (90°, being the nominal deflection for hover) thus facilitating the use of nozzle deflection angle to minimize reingestion thrust losses in the hover flight mode.

4.3.2 Transition

During the transition from fully jet-borne to fully wing-borne flight (and vice-versa) the deflection of the forward RALS and aft ADEN nozzles are geared together to maintain moment balance of direct thrust effects. Due to structural/geometric considerations, there is a limitation on aft deflection of the twin RALS nozzles. When this aft deflection point is reached (say in a transition from hover to fully wing-borne flight), the power setting of the RALS is reduced to retain the moment balance. This gearing scheme is depicted in Figure 4.3.2-1.

Levels of jet-induced interference lift, pitching moment and drag (non-dimensionalized by gross thrust and wing reference chord in the case of pitching moment) are presented in Figures 4.3.2-2 through 4.3.2-6 as a function of effective velocity ratio (V_e). Variations are depicted for several deflections of the lift/cruise (ADEN) nozzle (0^o deflection corresponding to conventional flight). The RALS deflection angles corresponding to these ADEN nozzle deflections are the same as those presented in Figure 4.3.2-1. These data

are based on the test results reported on in Reference 4.3-1 and were utilized in the transition analysis presented in section 7.5.

4.3.3 STO

As in the transition flight mode, deflection of the ADEN and RALS nozzles follows the gearing relationship presented in Figure 4.3.2-1. Jet-induced interference lift and drag are presented in Figures 4.3.3-1 and 4.3.3-2 in an identical format to those of the preceding section and are based on data contained in the same reference. Interference pitching moment effects are not presented as the STO performance of the vehicle was analyzed utilizing a two degree-of-freedom approach which did not include pitching moment effects (see section 7.6).

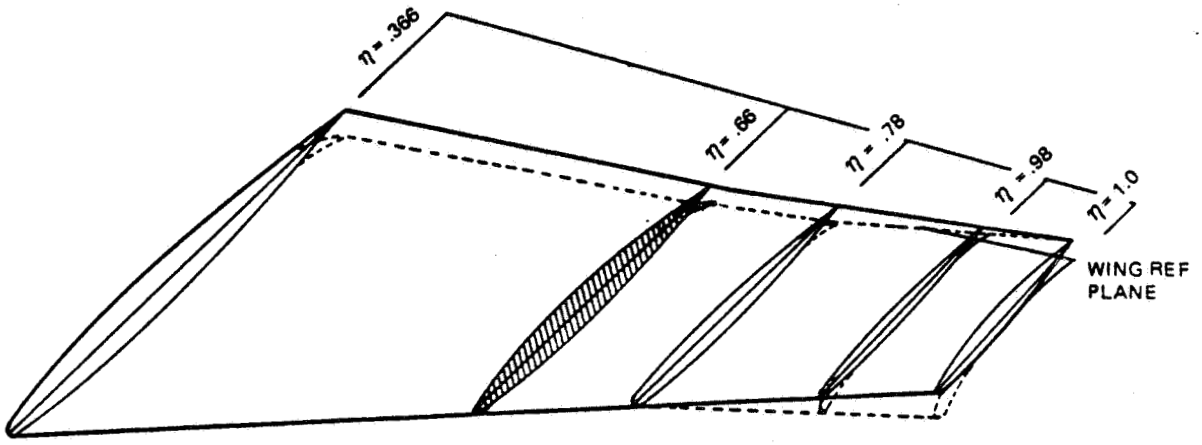

1690-092

Figure 4.1.1-1 Wing/Airfoil Geometry Required For Cruise and Maneuver Flight

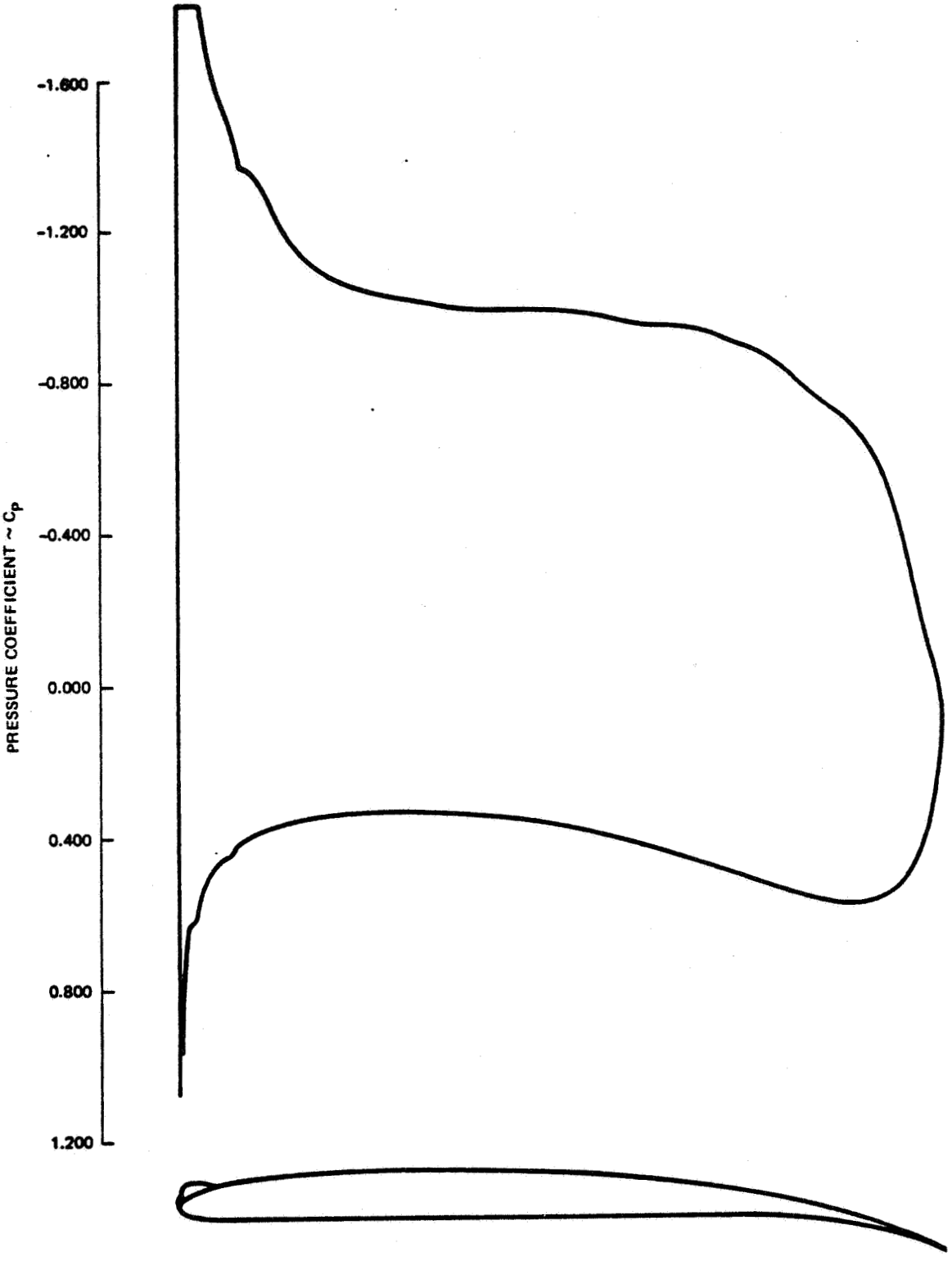

1690-093

Figure 4.1.1-2 "K" Maneuver Airfoil Pressure Distribution $C_{\ell_{2\text{-}D}} = 1.40$ $M_N = 0.554$

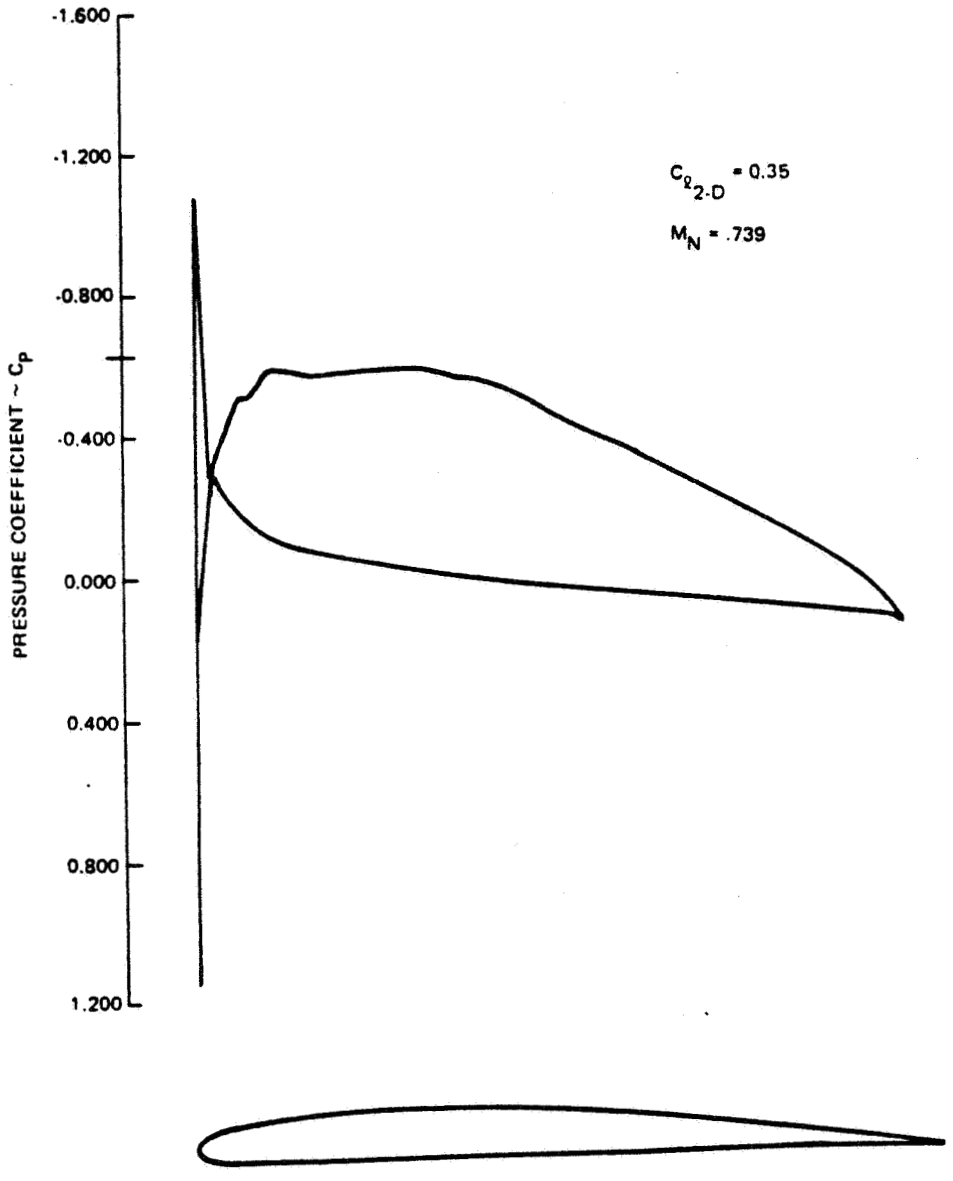

1690-094

Figure 4.1.1-3 Cruise Airfoil Pressure Distribution $C_{\ell_{2\text{-}D}}$ = 0.35 M_N = 0.739

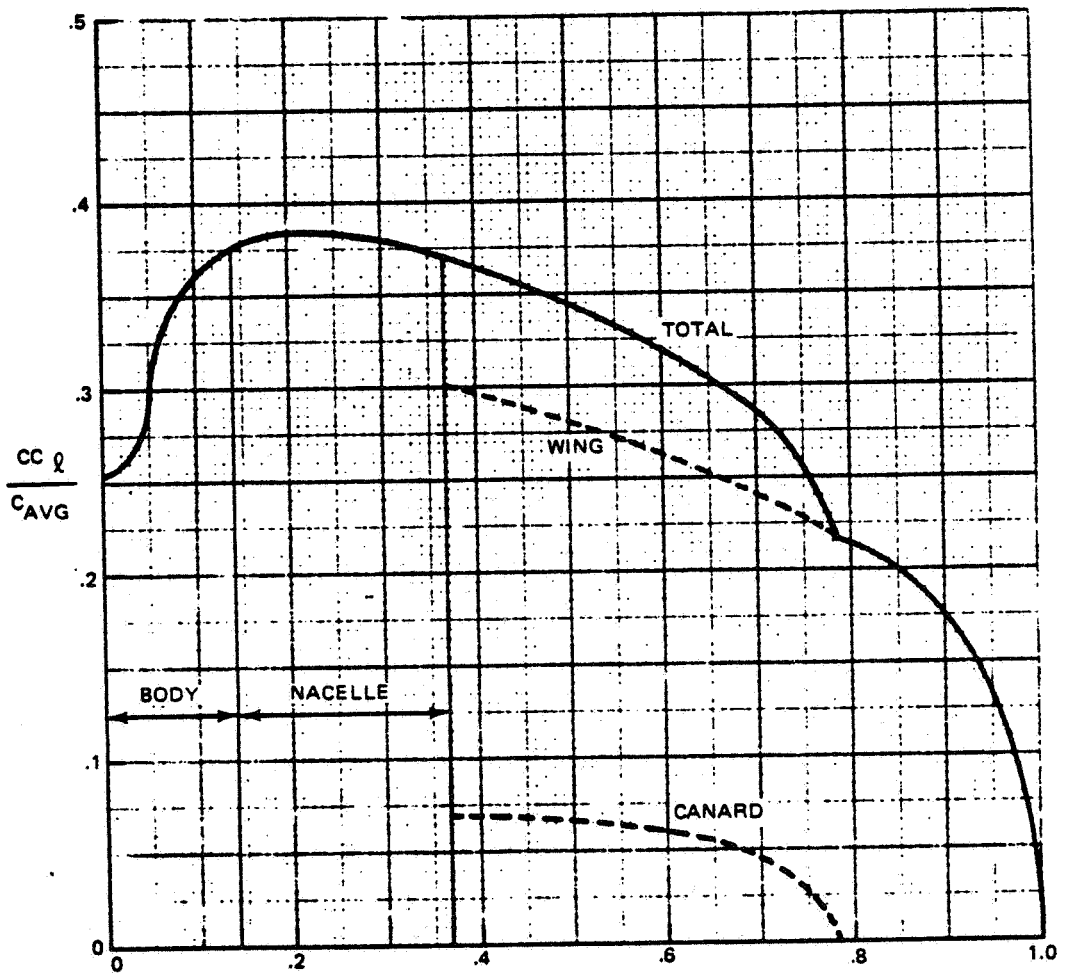

1690-095

Figure 4.1.1-4 Cruise Spanload Distribution
C_L = .3

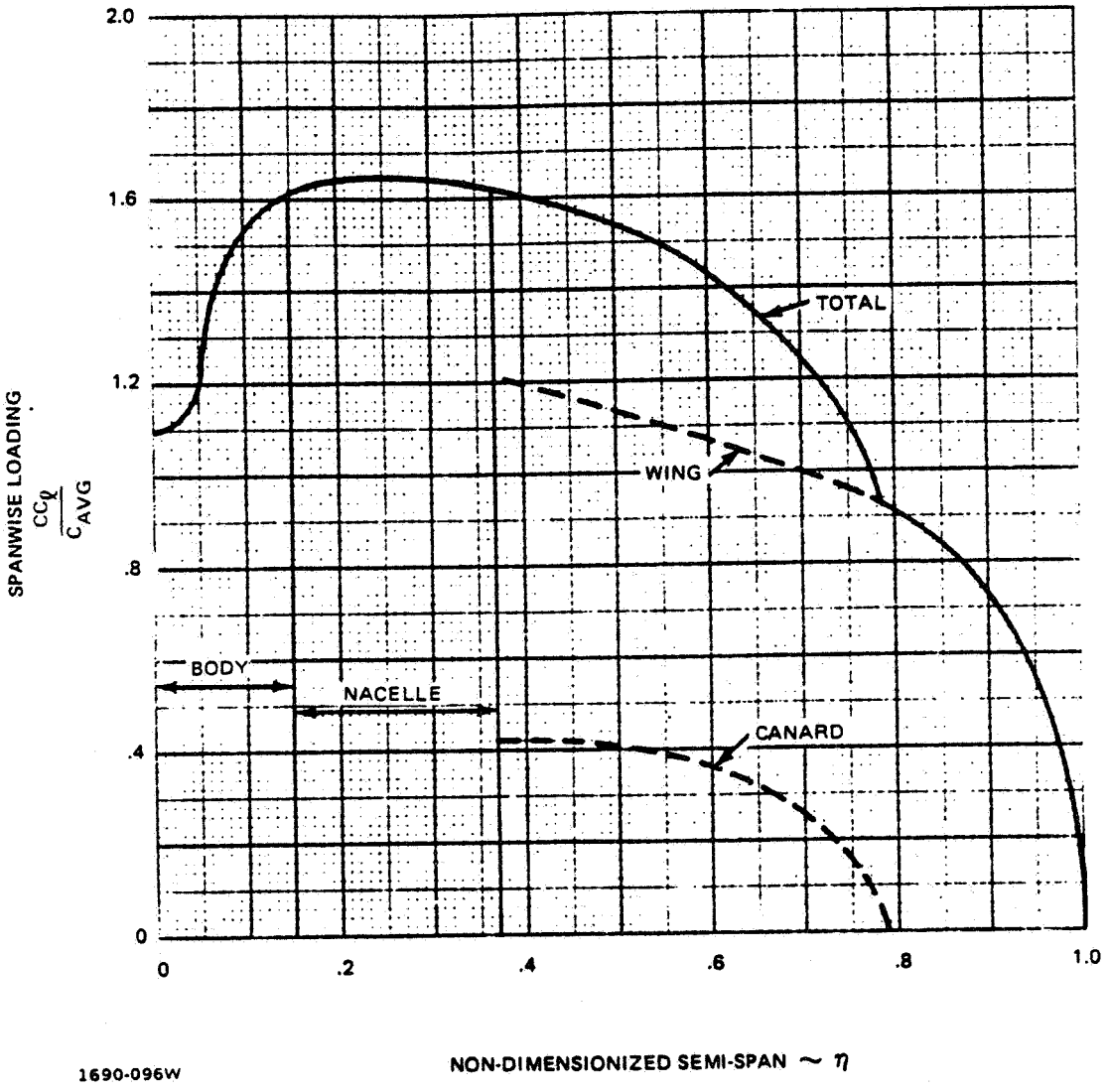

Figure 4.1.1-5 Maneuver Spanload Distribution C_L = 1.3

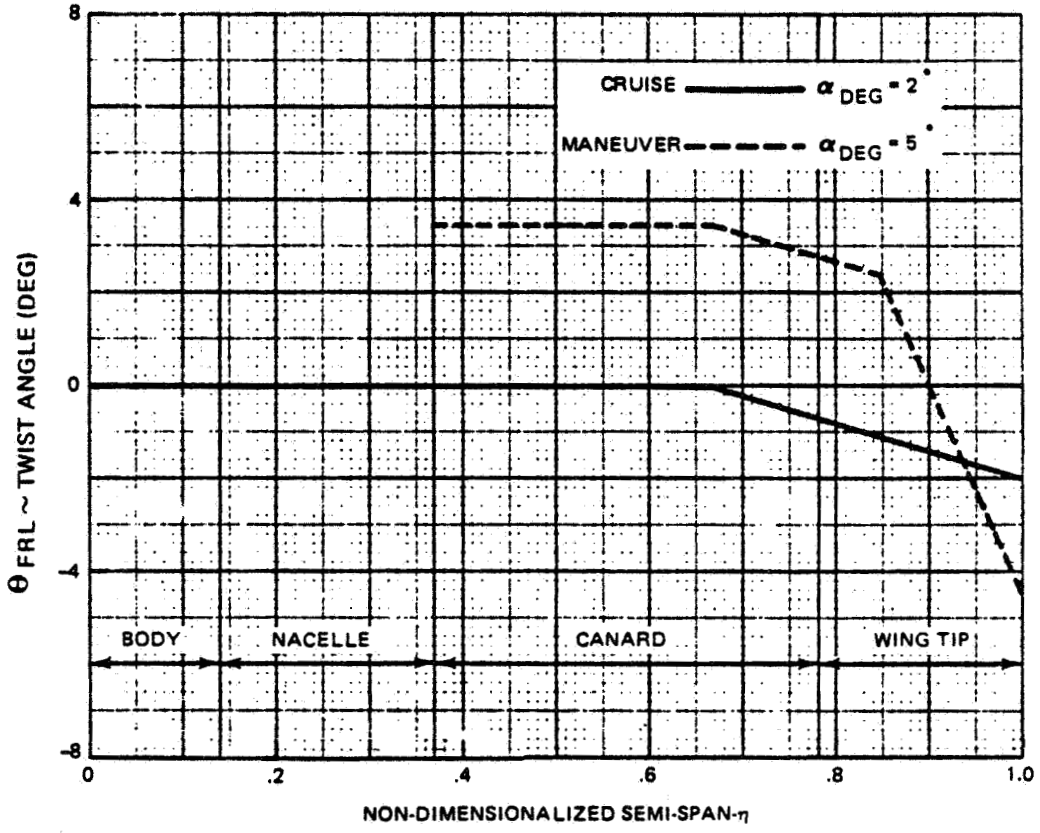

1690-097

Figure 4.1.1-6 Wing Twist Distribution

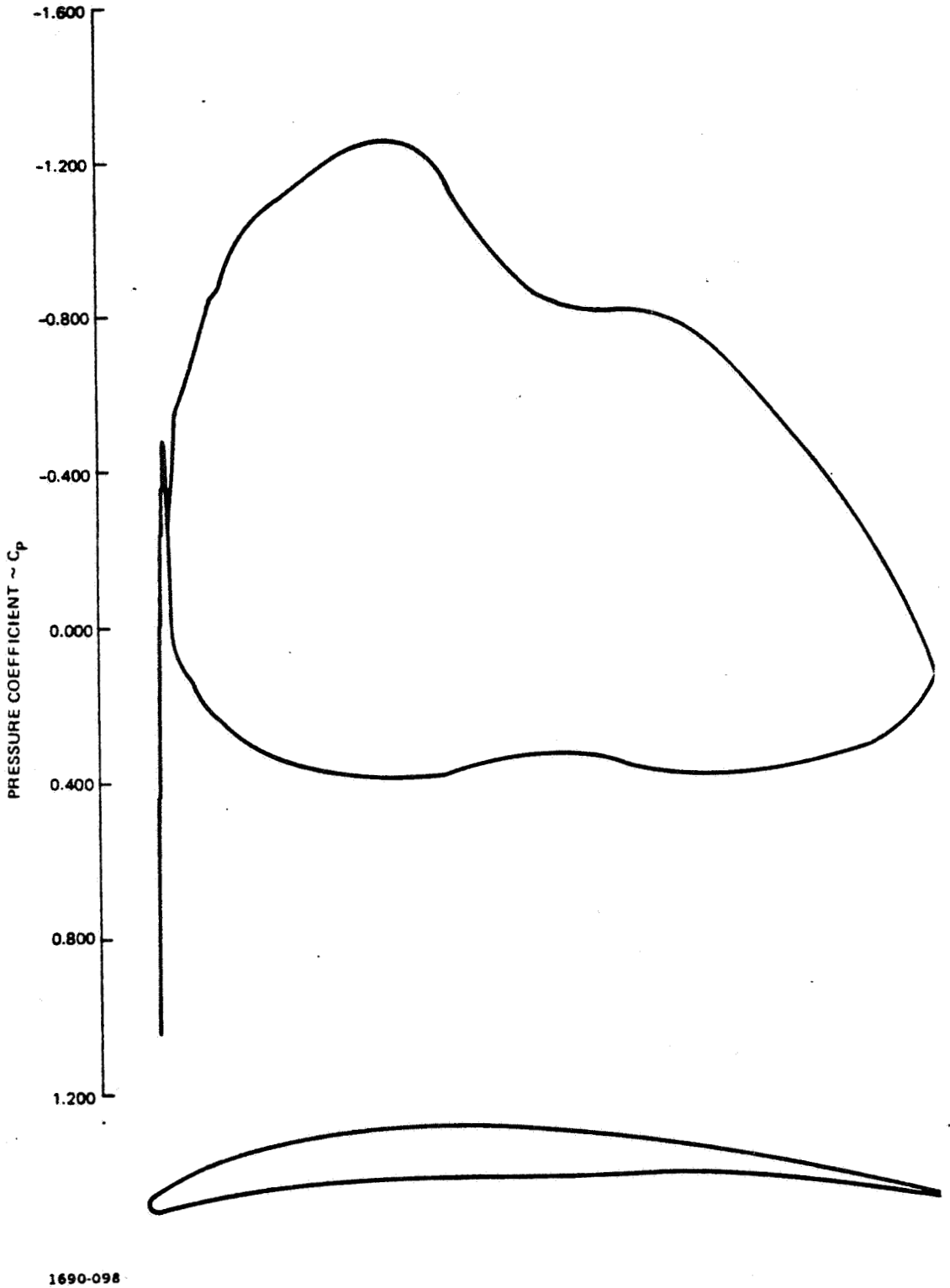

Figure 4.1.1-7 Pressure Distribution Airfoil 4 $\eta = 0.92$ $M_N = 0.554$

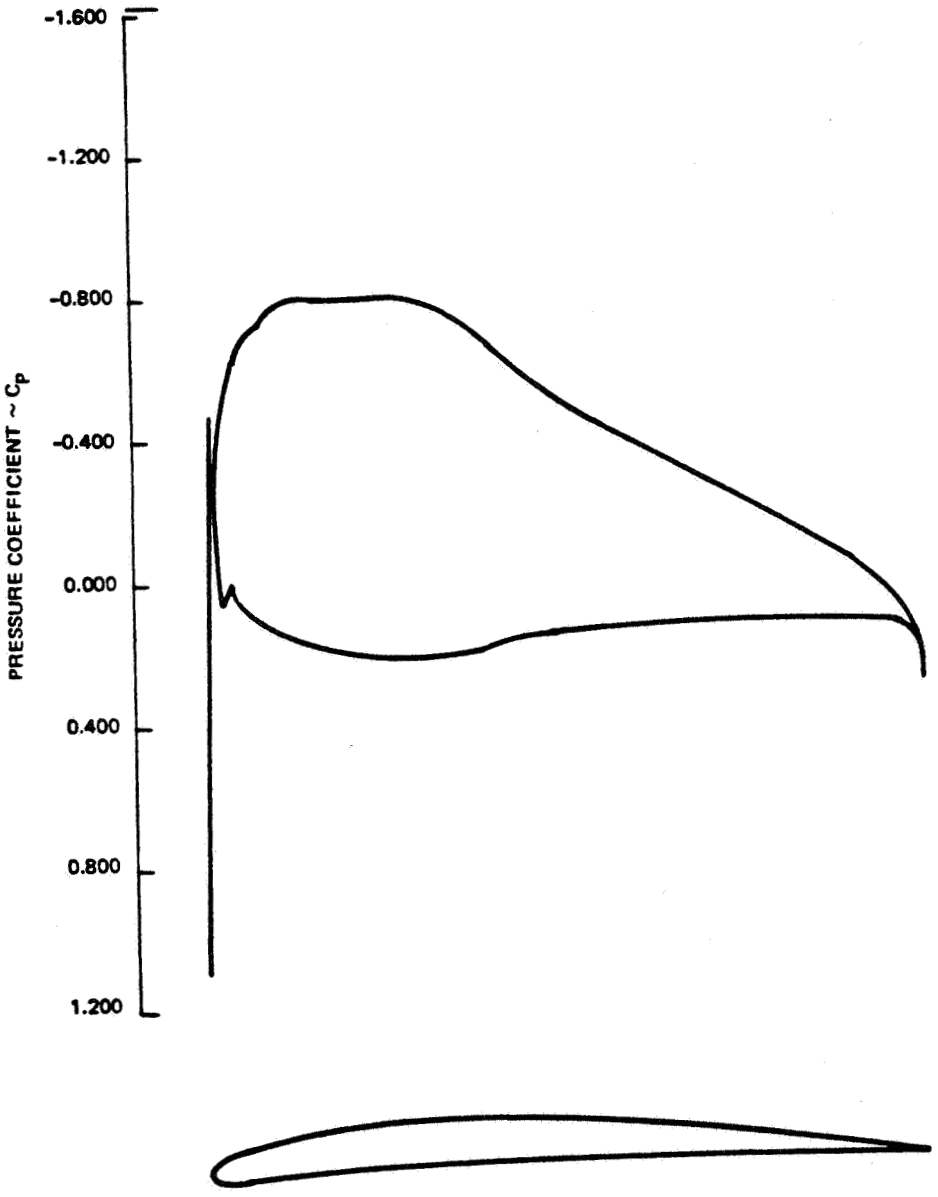

Figure 4.1.1-8 Pressure Distribution Airfoil 6 η = 1.00 M_N = 0.554

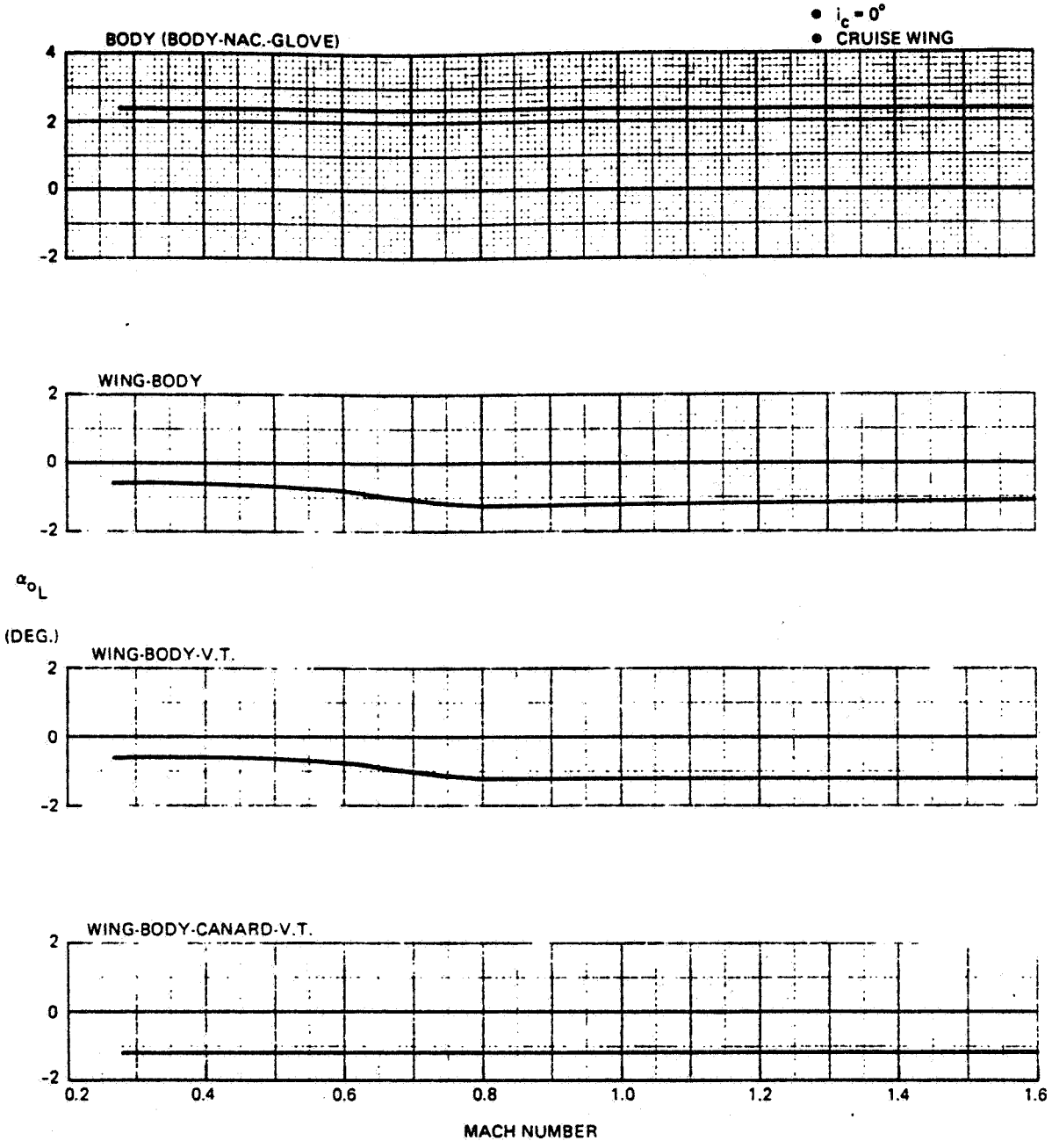

Figure 4.1.2-1 Design 623 – 2024 Zero Lift Angle of Attack

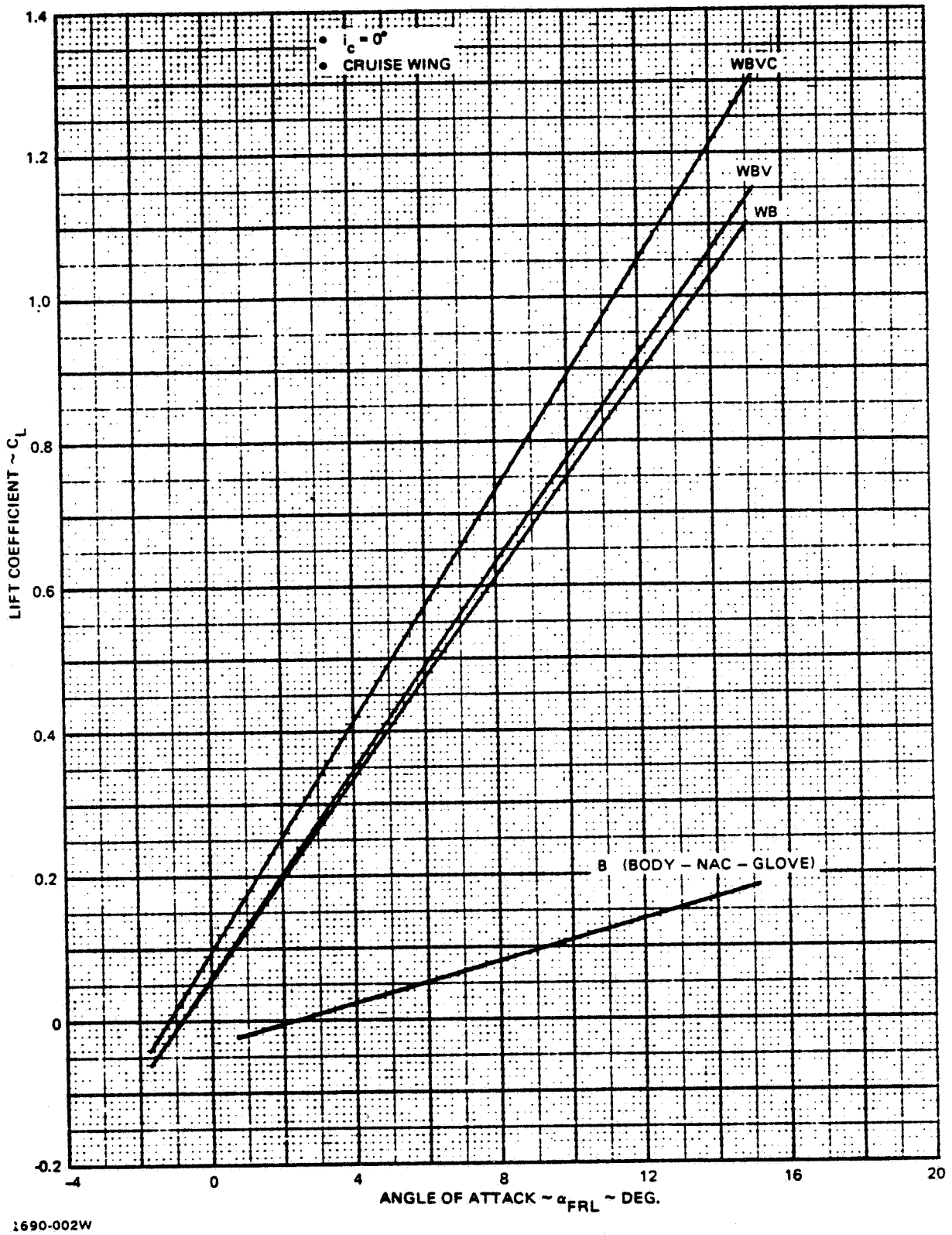

1690-002W

Figure 4.1.2-2 Design 623 – 2024 Lift Coefficient vs Angle of Attack M = 0.60

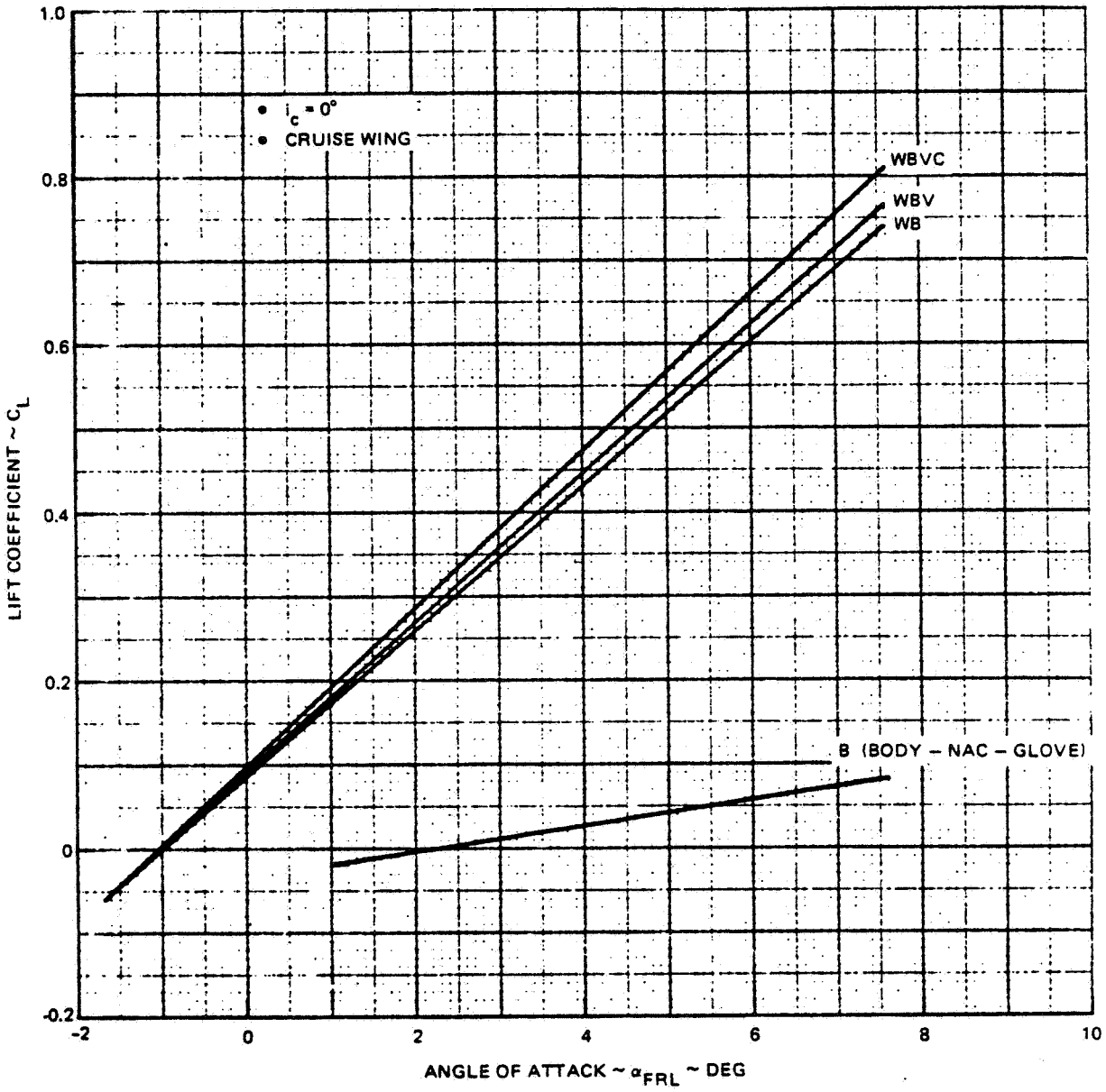

1690-003W

Figure 4.1.2-3 Design 623 – 2024 Lift Coefficient vs Angle of Attack M = 0.90

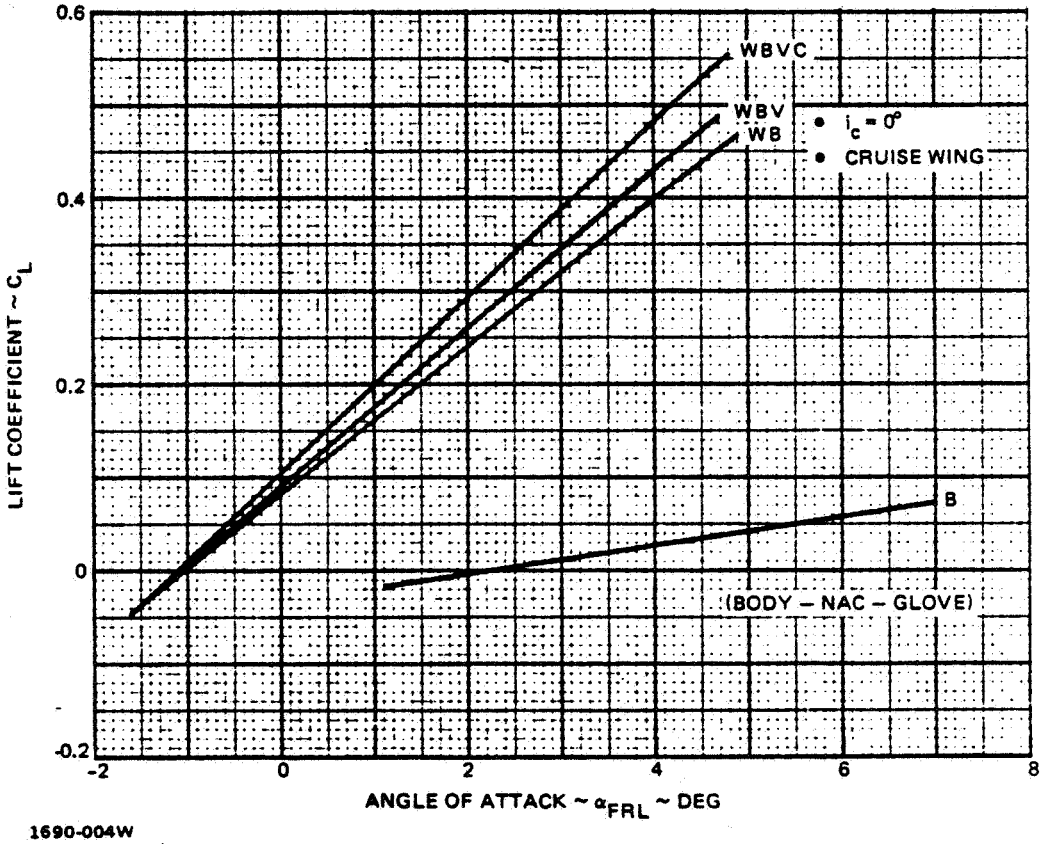

Figure 4.1.2-4 Design 623 – 2024 Lift Coefficient vs Angle of Attack M = 1.2

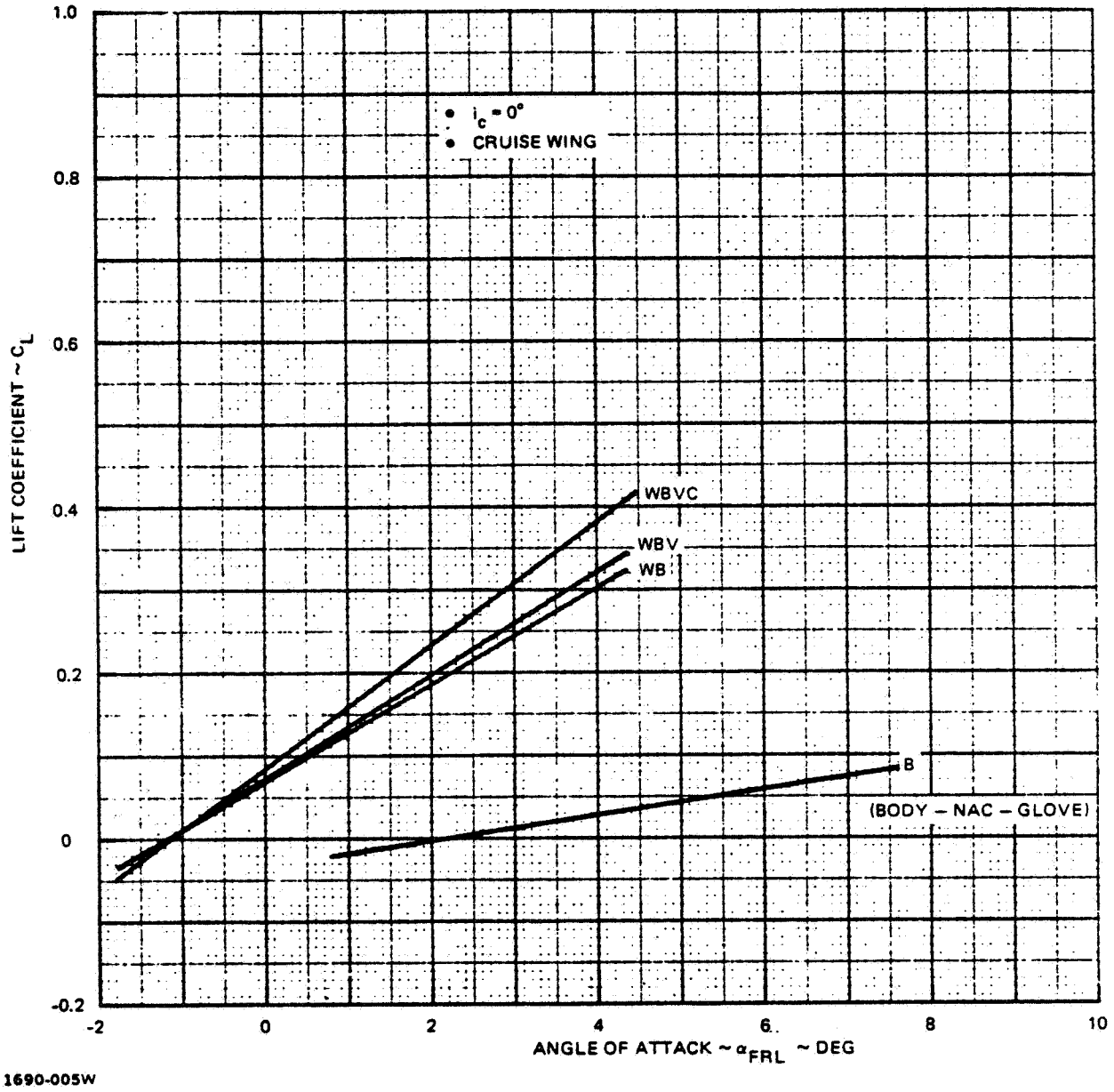

Figure 4.1.2-5 Design 623 – 2024 Lift Coefficient vs Angle of Attack M = 1.6

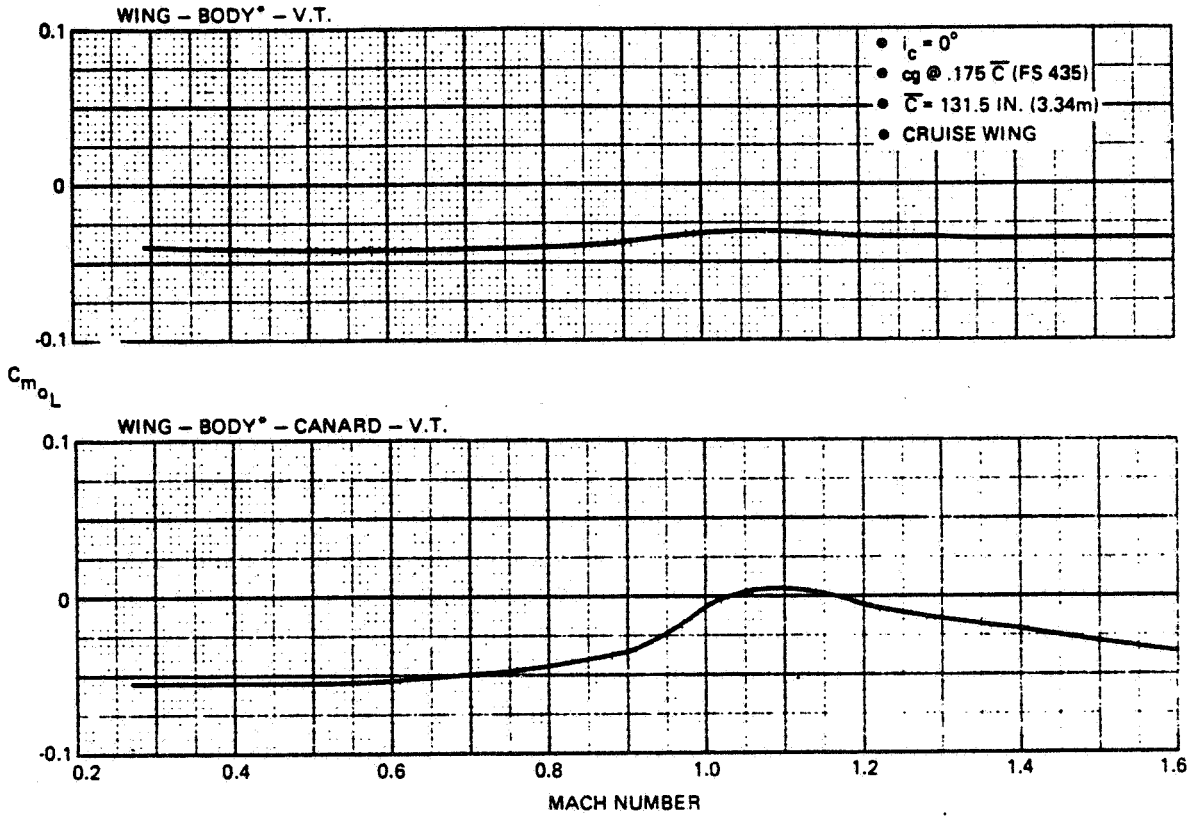

*BODY: BODY – NAC. – GLOVE

1690-006W

Figure 4.1.2-6 Design 623 – 2024 Zero Lift Pitching Moment

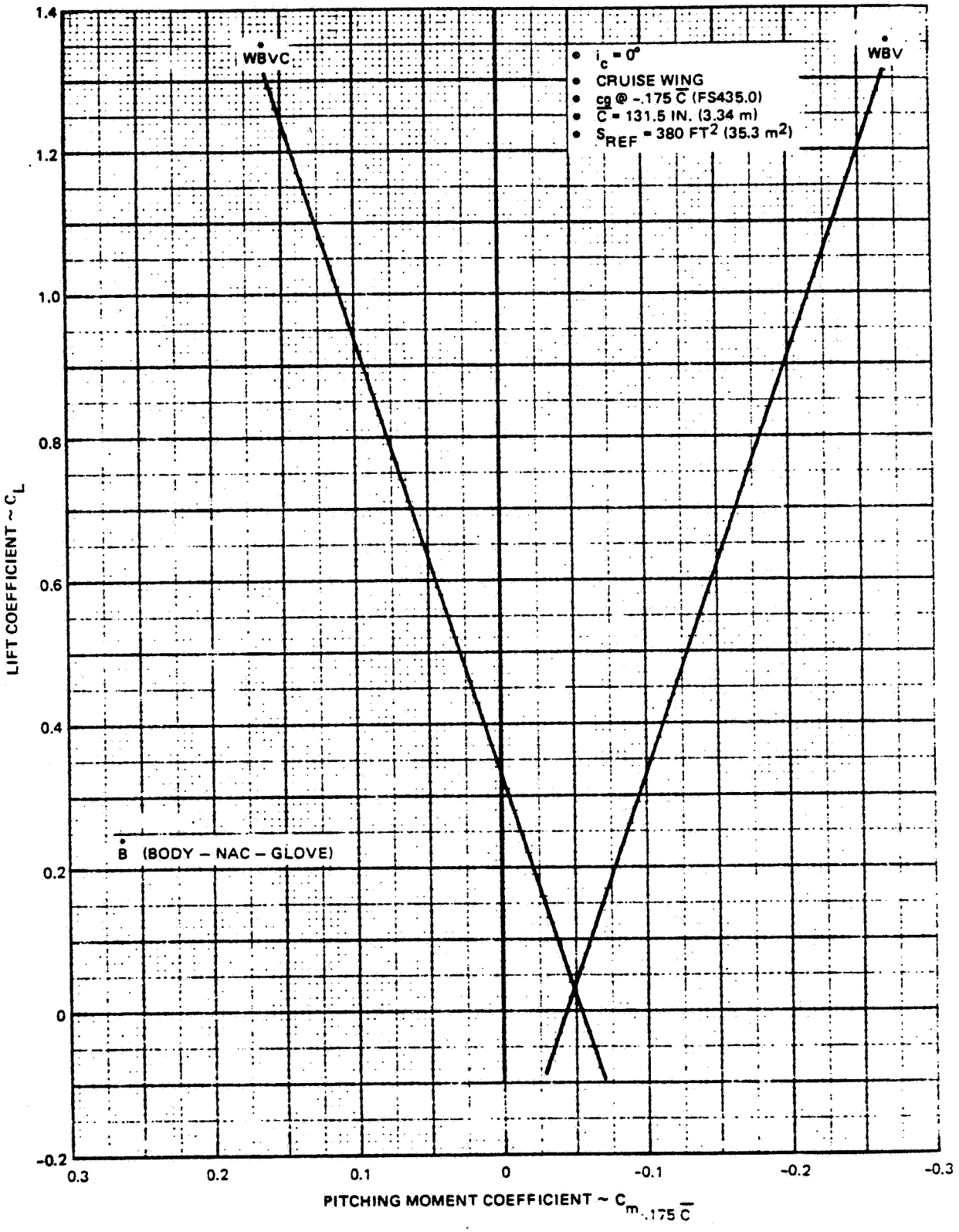

1690-007W

Figure 4.1.2-7 Design 623 – 2024 Longitudinal Stability M = 0.60

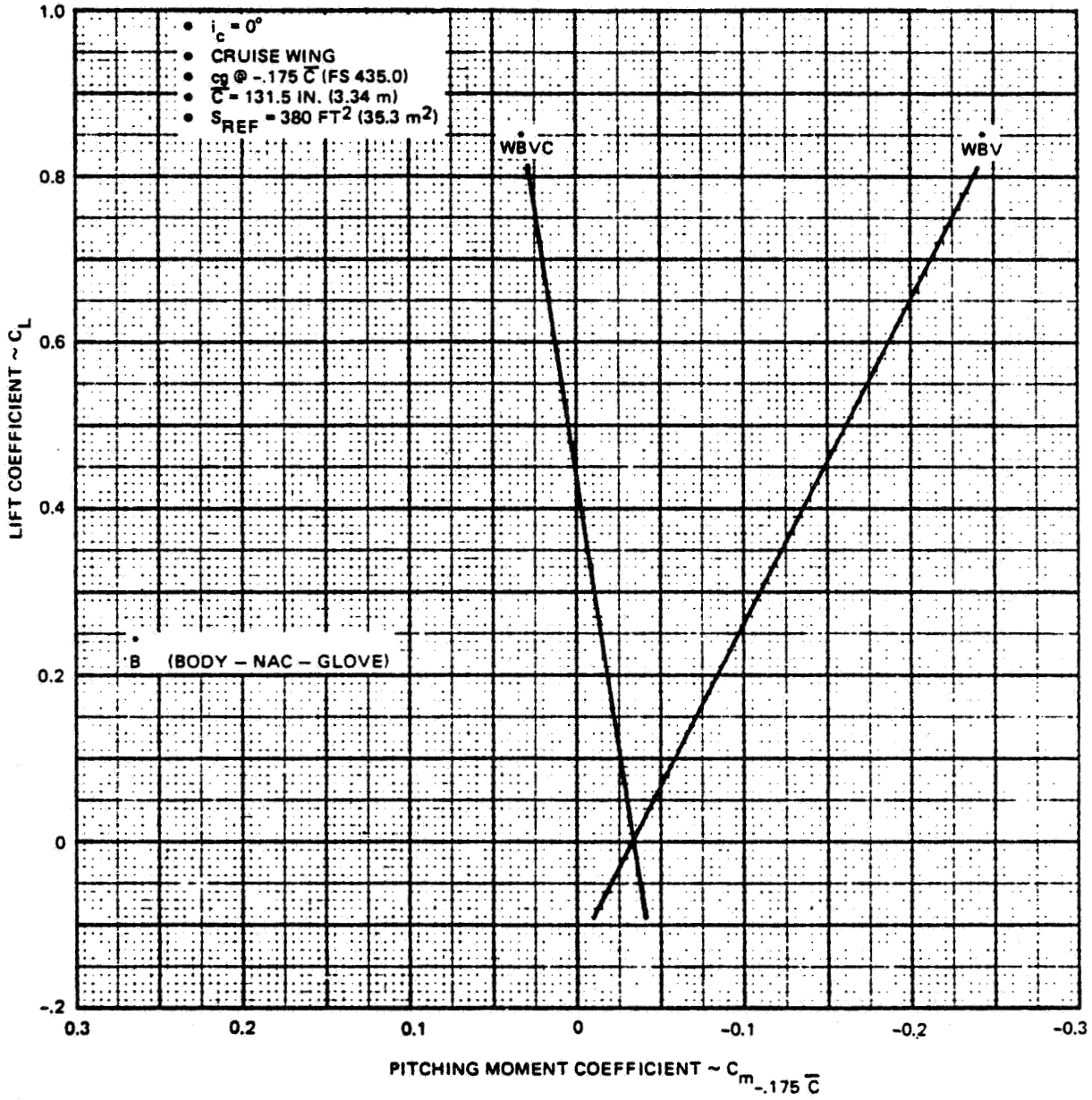

1690-008W

Figure 4.1.2-8 Design 623 – 2024 Longitudinal Stability M = 0.90

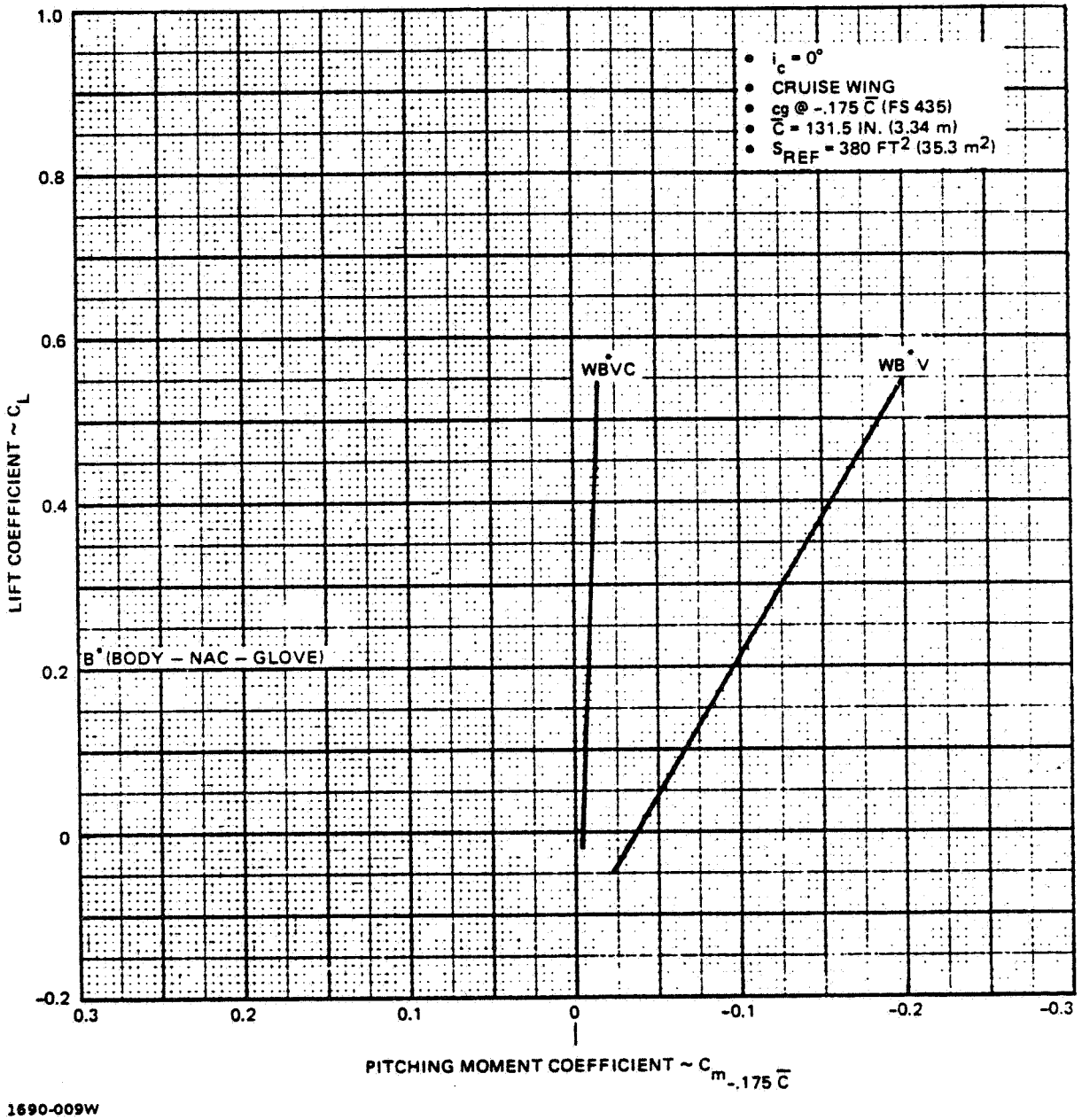

1690-009W

Figure 4.1.2-9 Design 623 – 2024 Longitudinal Stability M = 1.2

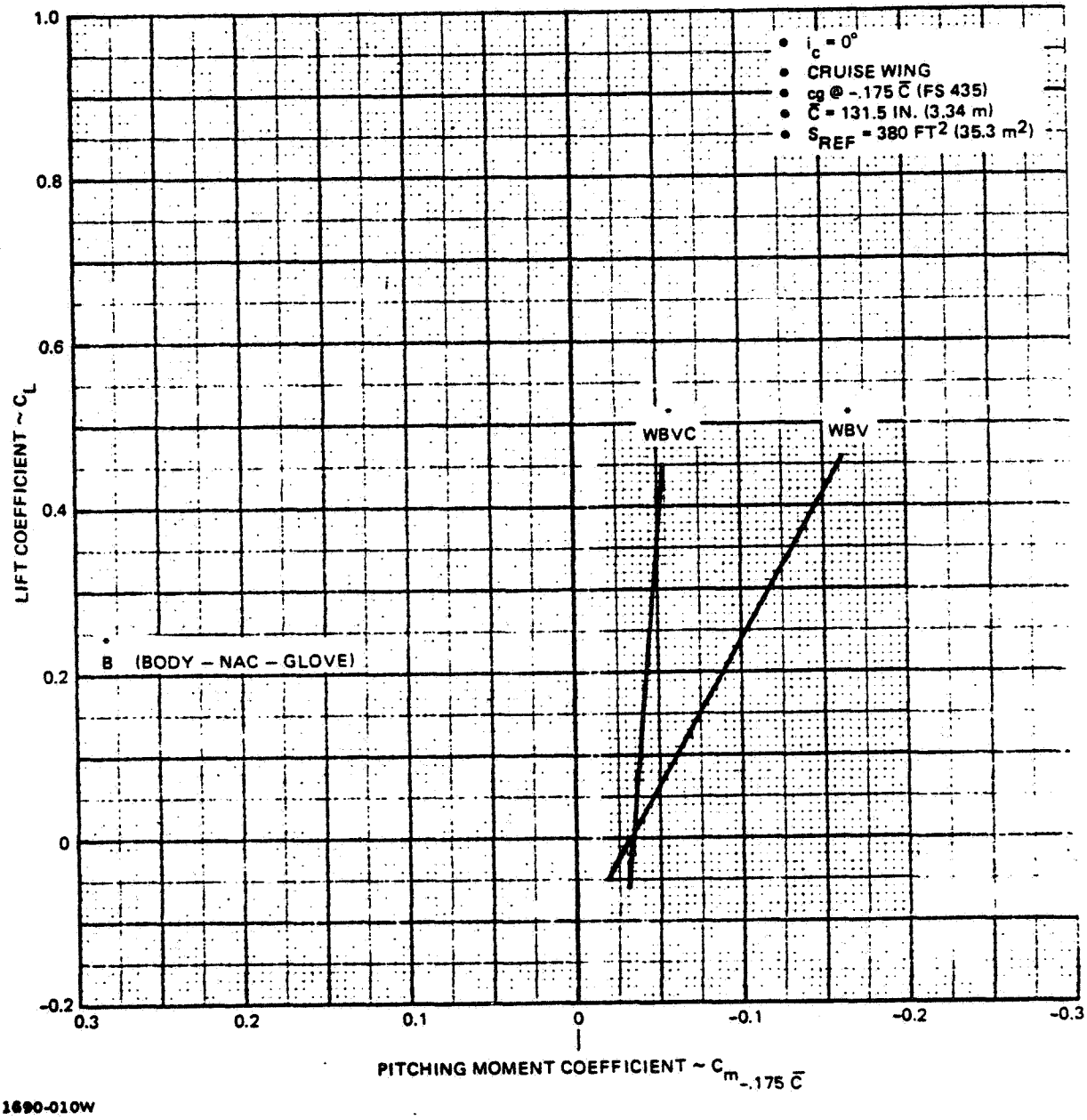

1690-010W

Figure 4.1.2-10 Design 623 – 2024 Longitudinal Stability M = 1.6

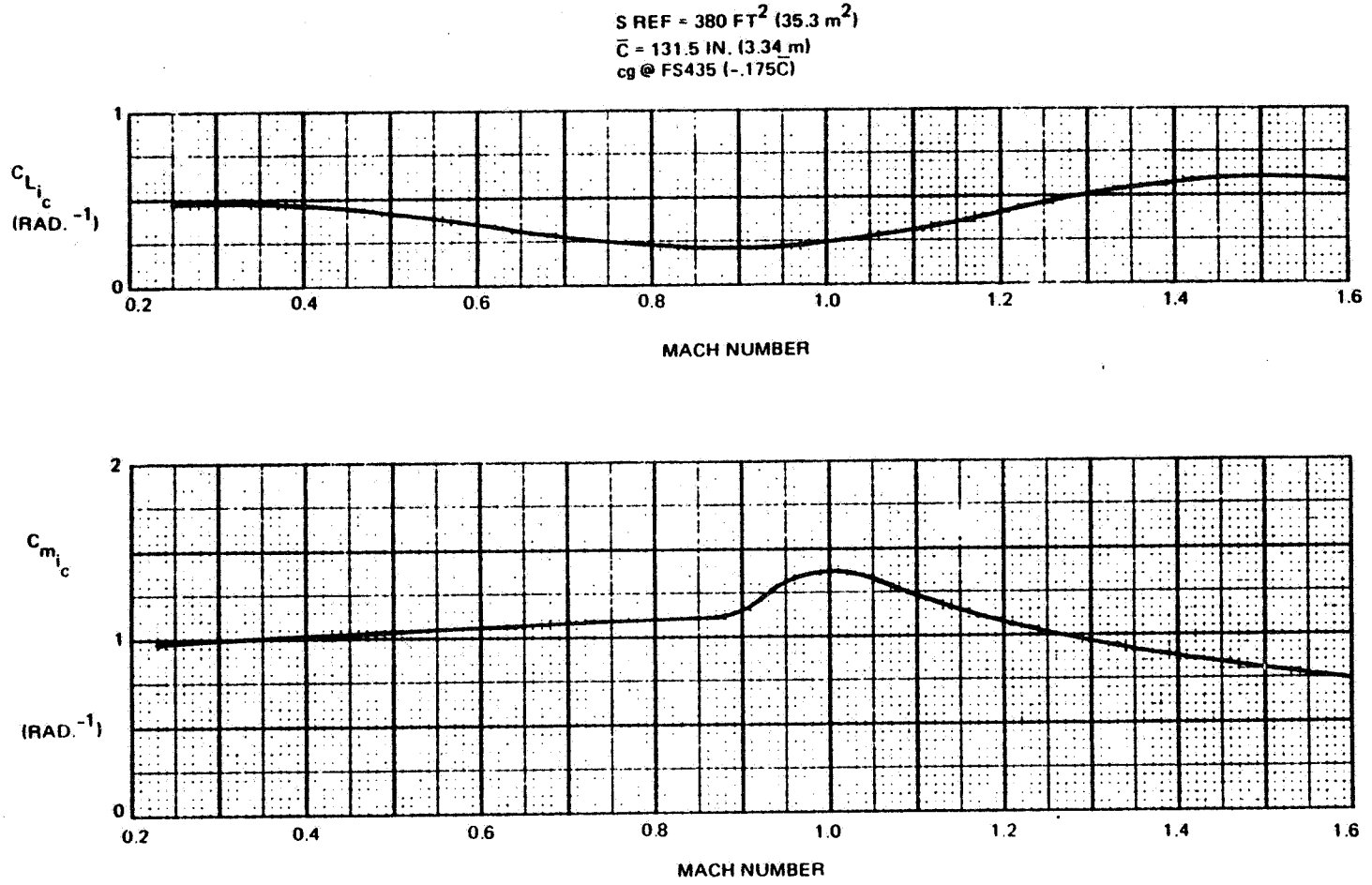

1690 011W

Figure 4.1.3-1 Design 623 – 2024 Canard Longitudinal Control Effectiveness

COMPONENT	WETTED AREA S_{WET}	CHARACTERISTIC LENGTH	REYNOLDS NUMBER	FORM FACTOR	FULLY TURBULENT FLAT PLATE DRAG COEFFICIENT ~ C_f	$C_D S_{WET}$
WING	349 FT^2	8.17 FT	1.32×10^7	1.0995	.00276	1.059 FT^2
CANARD	170	5.58	9.02×10^6	1.0903	.00294	.545
VERTICAL TAIL	175	5.96	9.64×10^6	1.0903	.00291	.561
NACELLES	448	31.50	5.09×10^7	1.0852	.00223	1.084
FUSELAGE	687	56.33	9.11×10^7	1.0476	.00205	1.475
GLOVE	167	17.33	2.80×10^8	1.0407	.00245	.426

$S_{WET_{TOTAL}} = 1996\ FT^2\ (185.4\ m^2)$

$C_D S_{WET_{TOTAL}} = 5.15\ FT^2$

$C_{f_e} = .00258$

1690-012W

Figure 4.1.4-1 Design 623 – 2024 Skin Friction Drag Buildup h = 36 089 Ft (11 000 m) M = 0.70

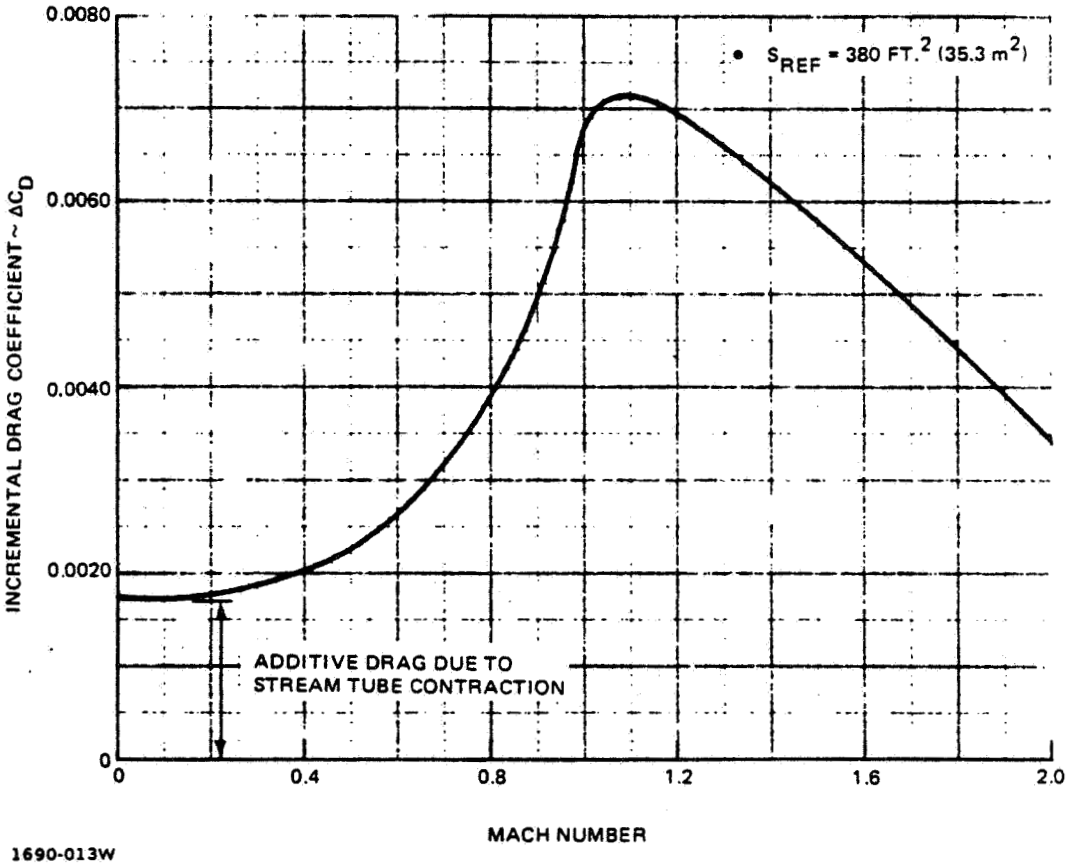

1690-013W

Figure 4.1.4-2 Design 623 – 2024 Supercritical Inlet Spillage Drag

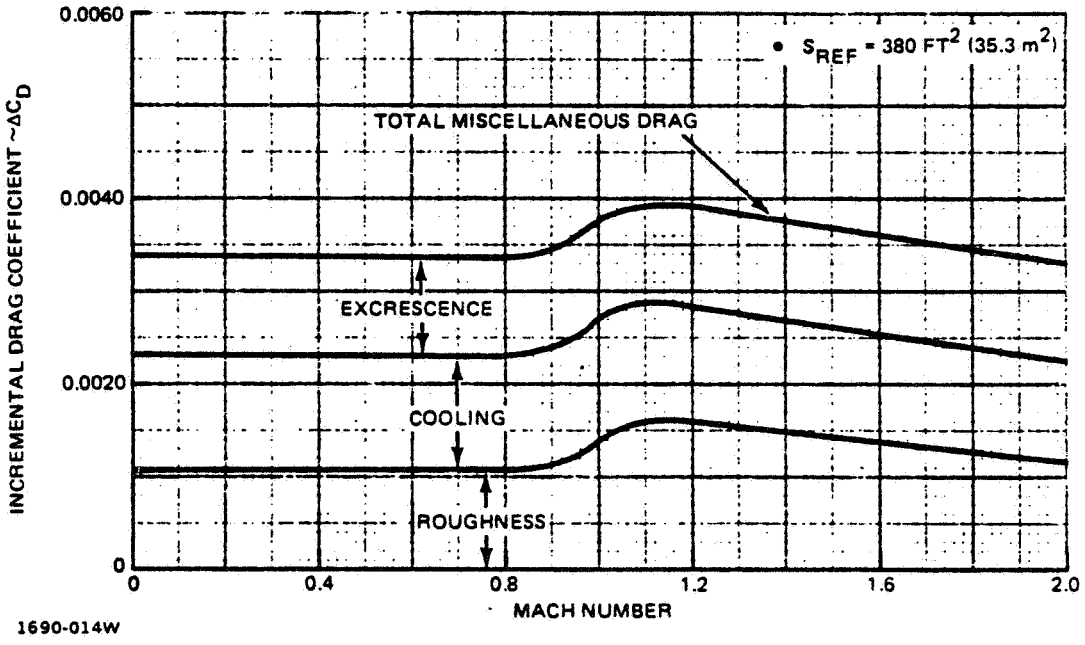

Figure 4.1.4-3 Design 623–2024 Drag Due to Miscellaneous Items

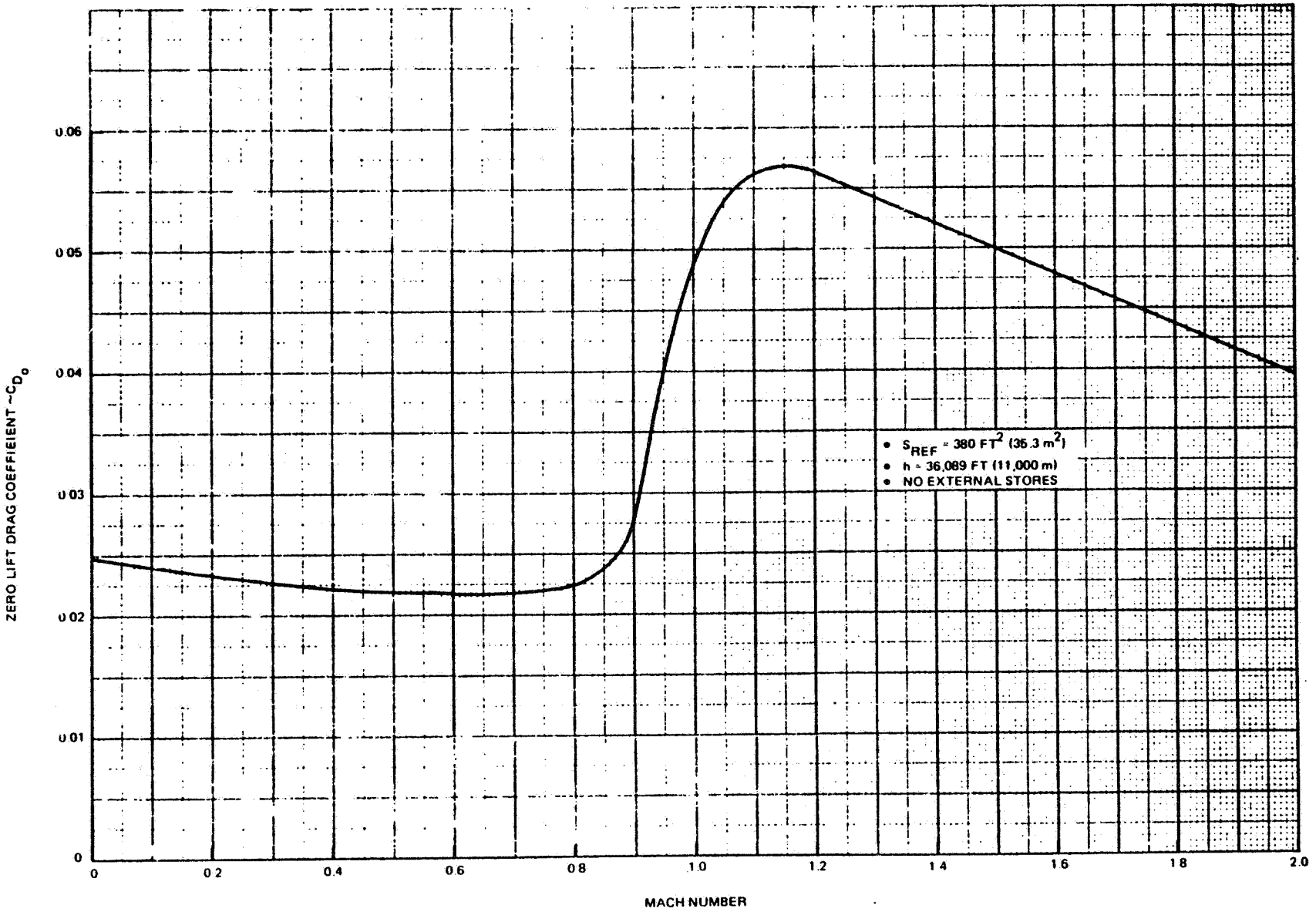

1690 015W

Figure 4.1.4-4 Design 623 – 2024 C_{D_o} vs Mach Number

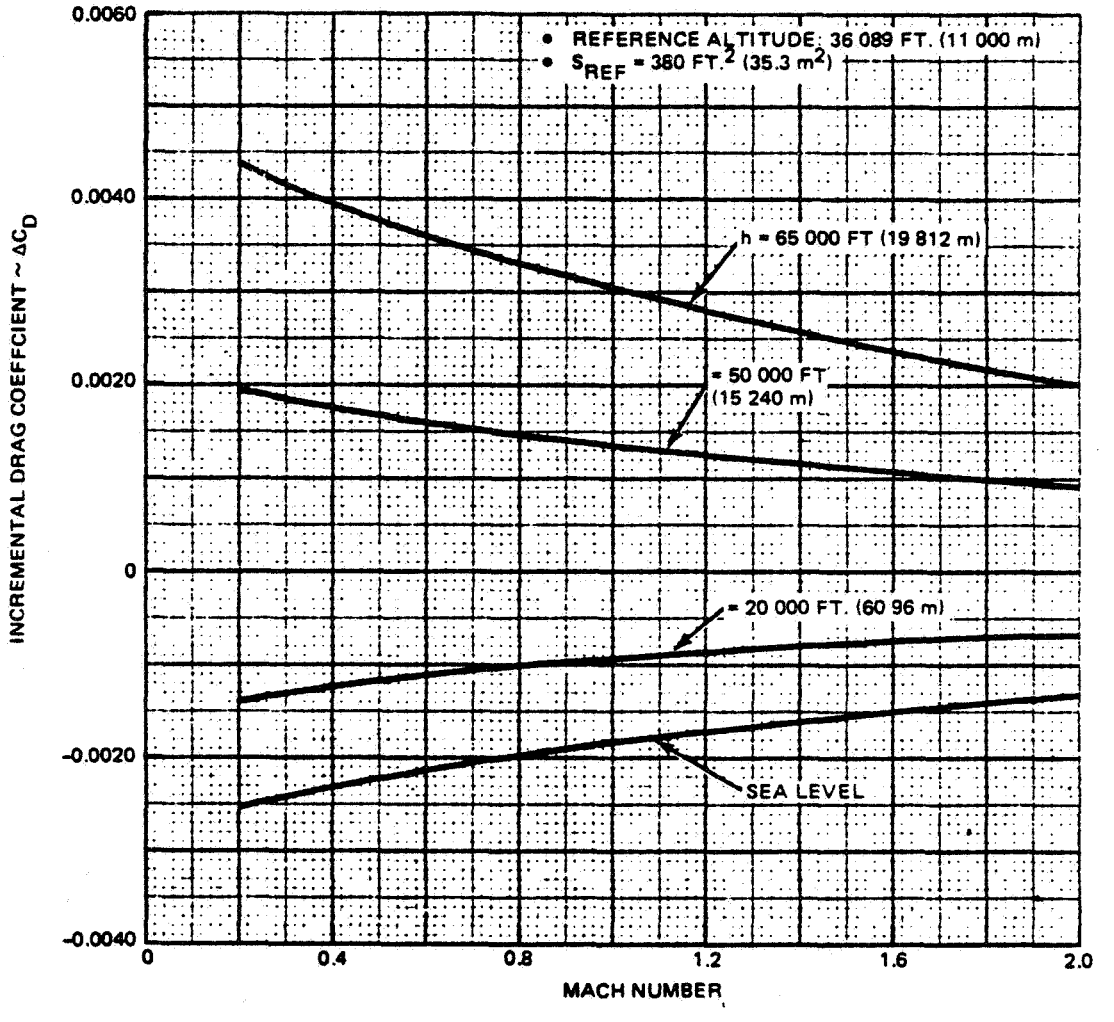

1690-016W

Figure 4.1.4-5 Design 623 – 2024 Effect of Altitude on Drag Level

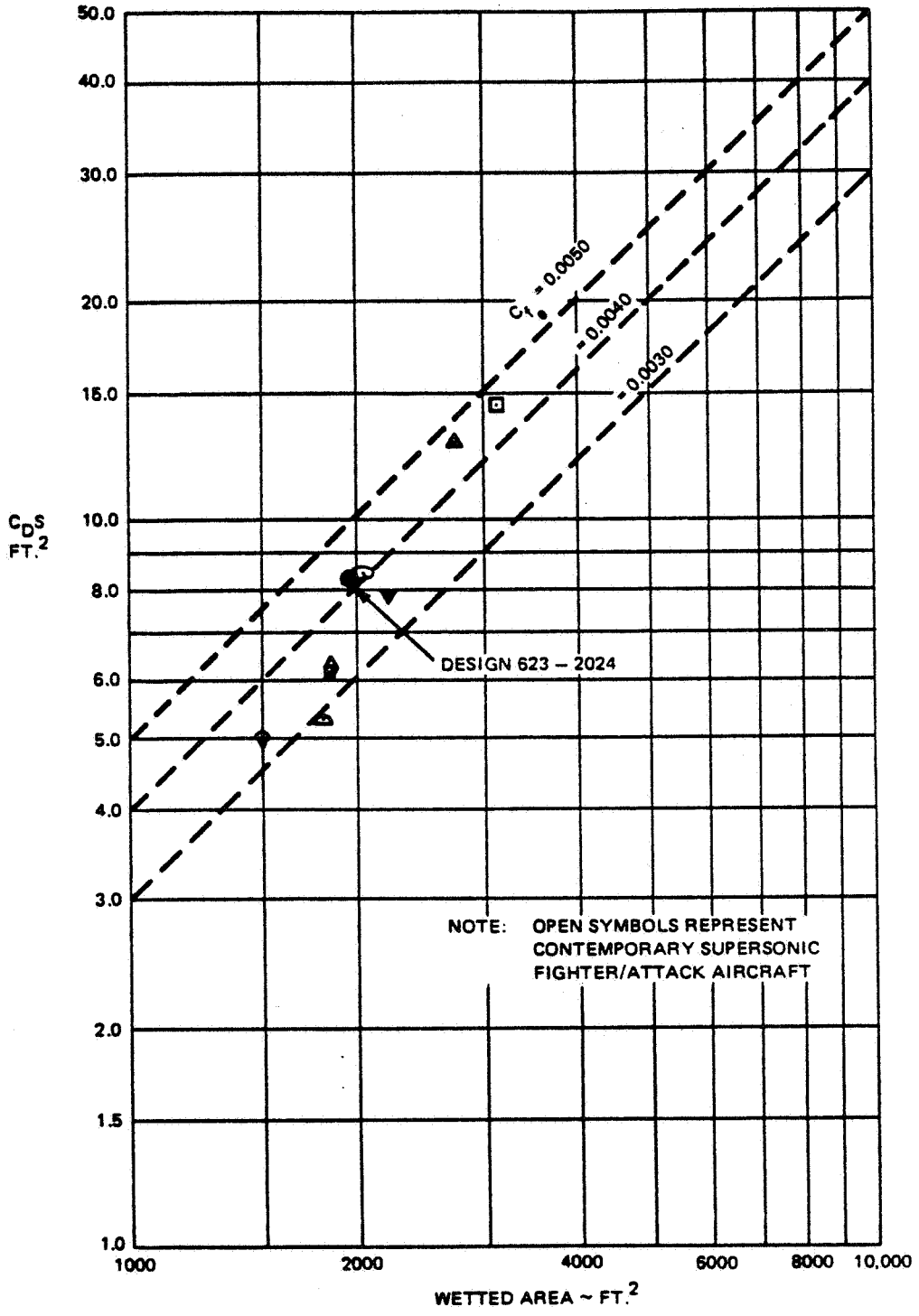

1690-017W

Figure 4.1.4-6 Design 623 – 2024 Minimum Drag Comparison

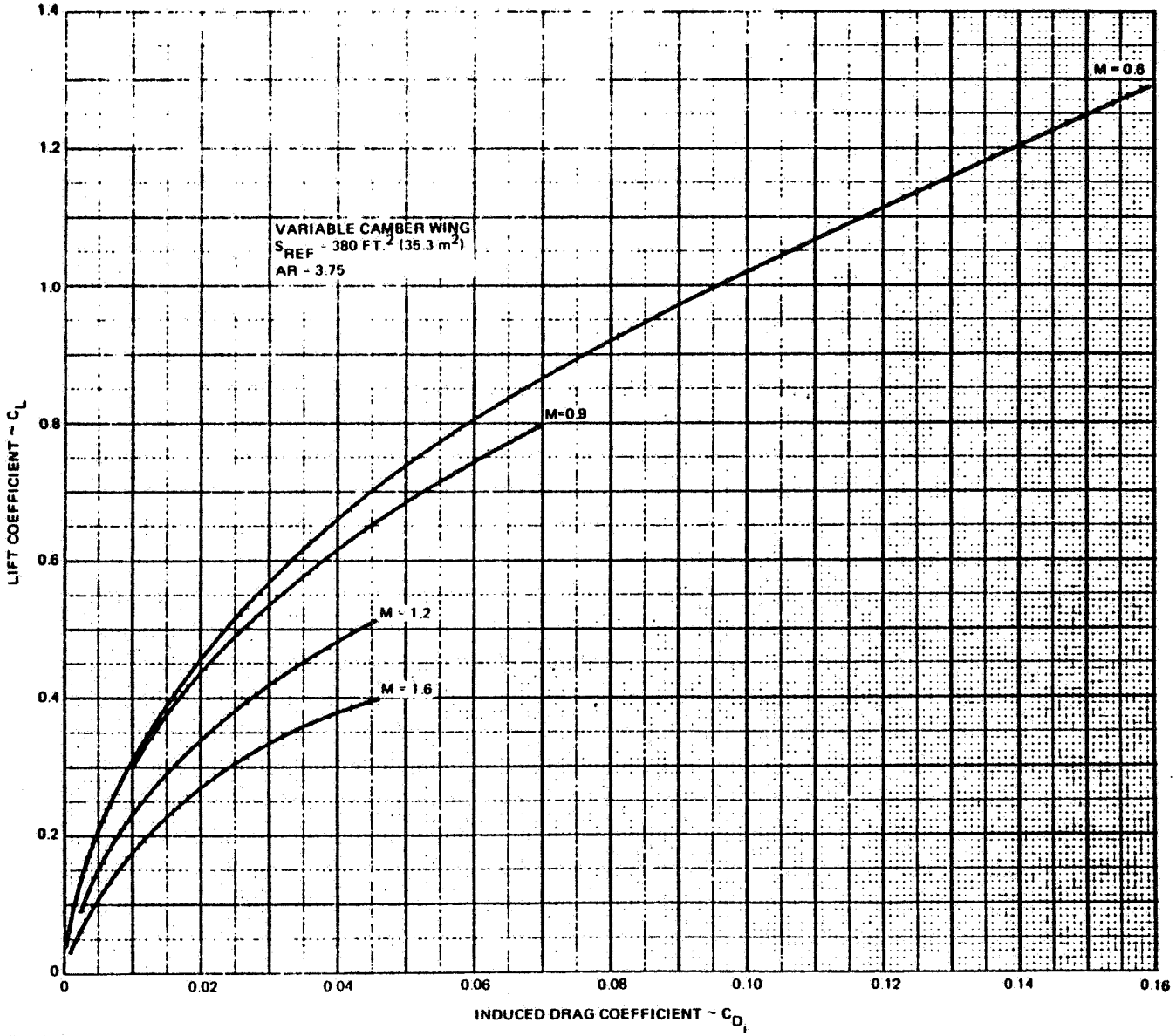

Figure 4.1.4-7 Design 623 – 2024 Drag Due to Lift

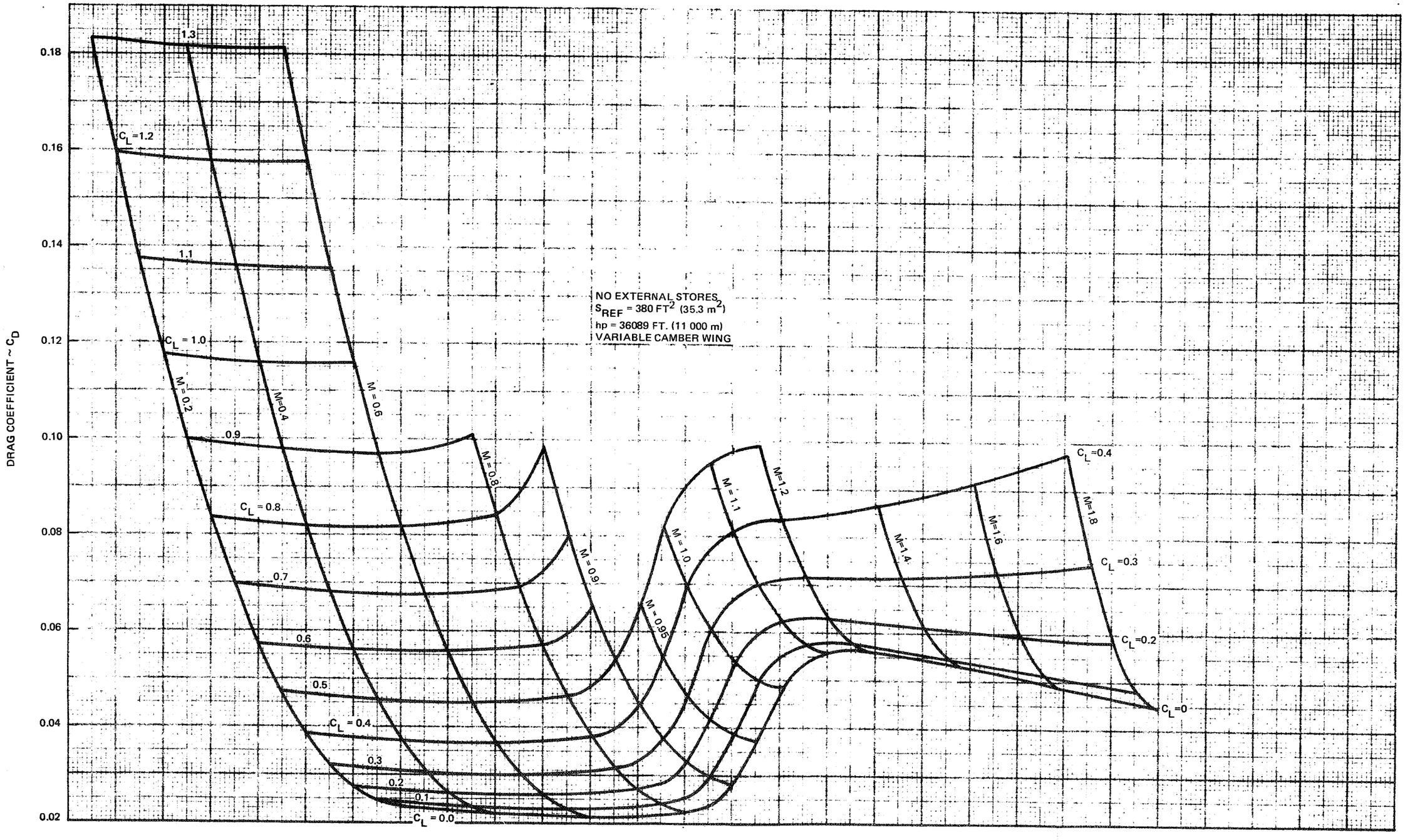

1690-019W

Figure 4.1.4-8 Design 623 – 2024 Untrimmed Drag Polar

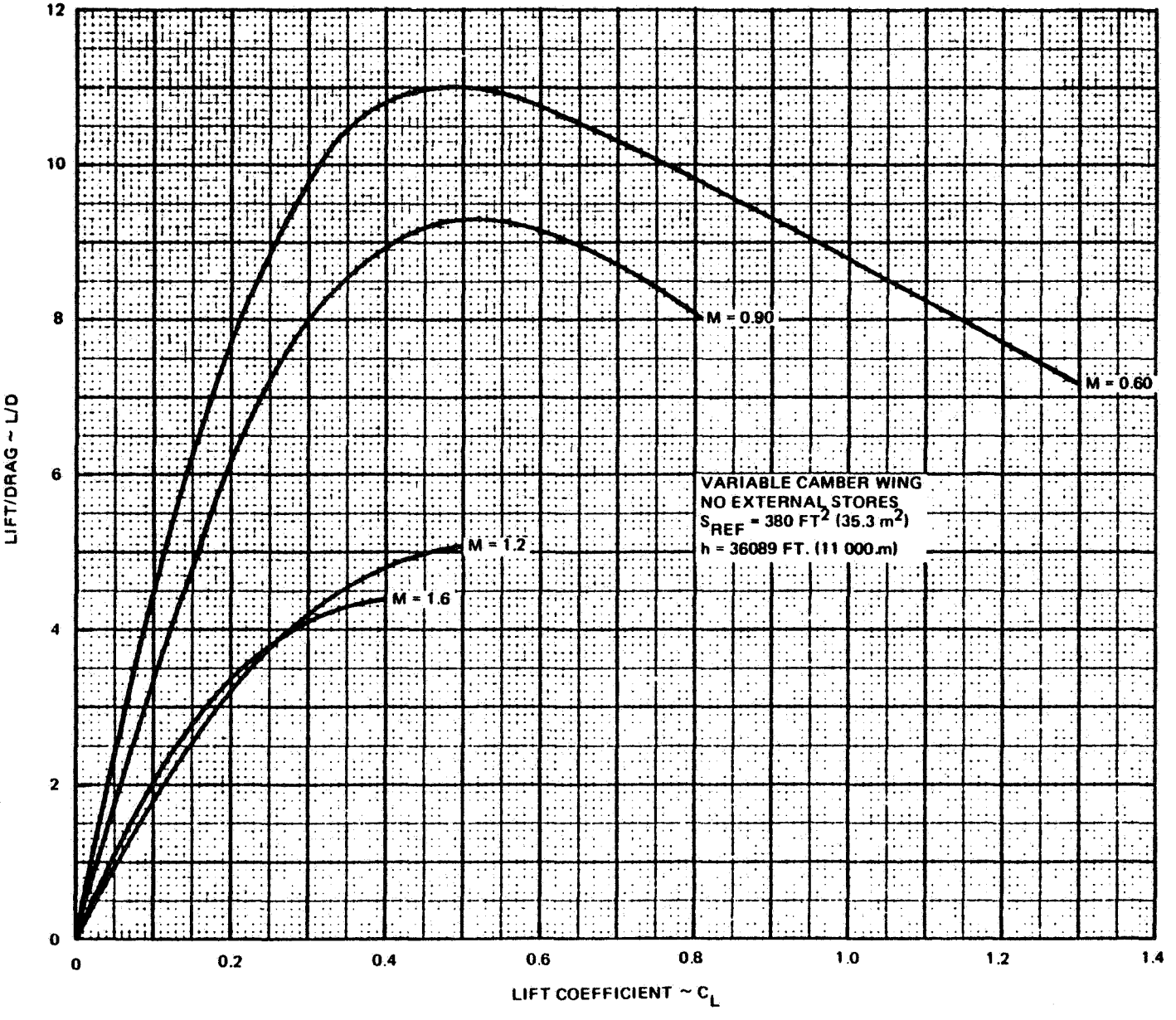

1690-020W

Figure 4.1.4-9 Design 623 – 2024 Lift-to-Drag Ratio

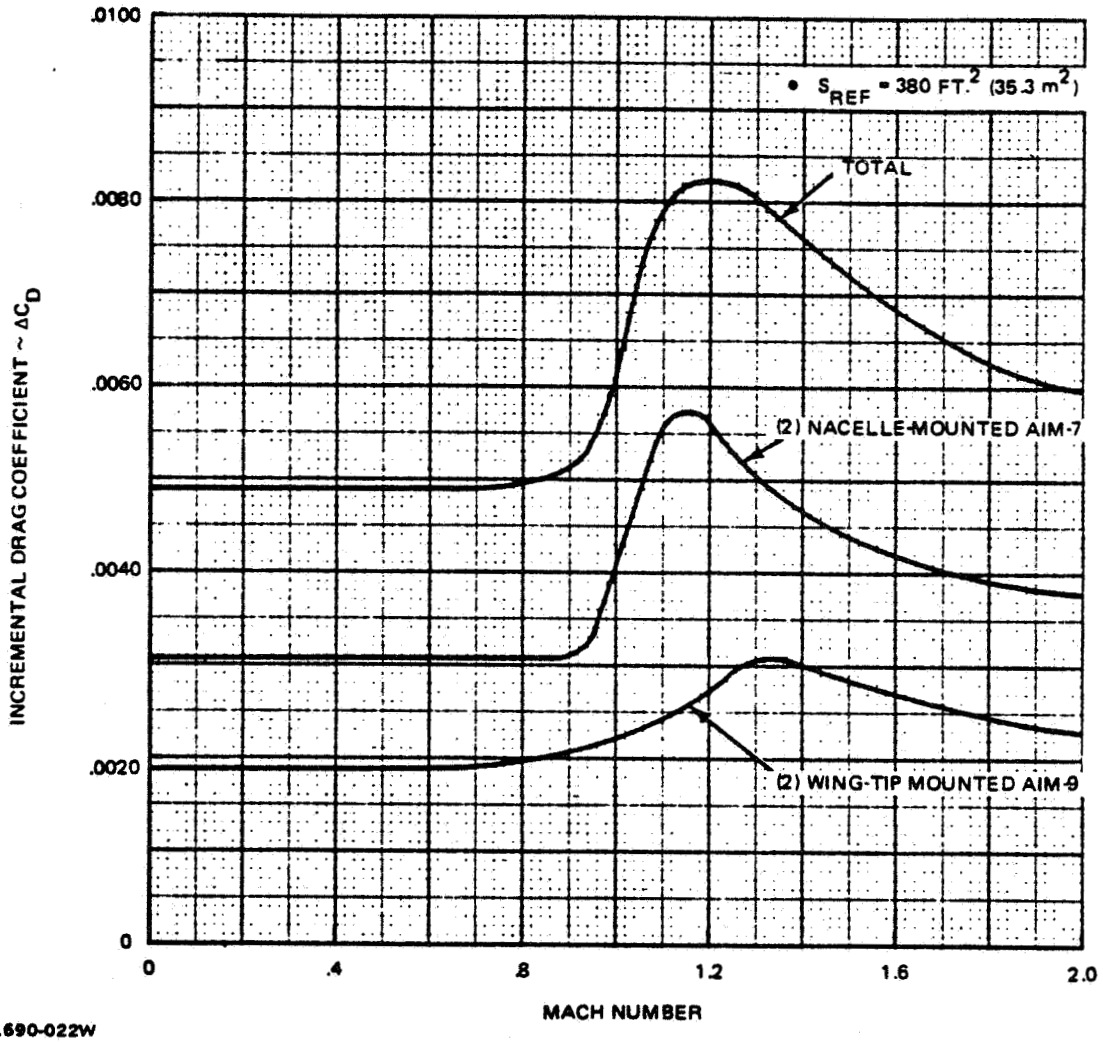

1690-022W

Figure 4.1.4-10 Design 623–2024 Installed Drag of External Stores; DLI and CAP Missions

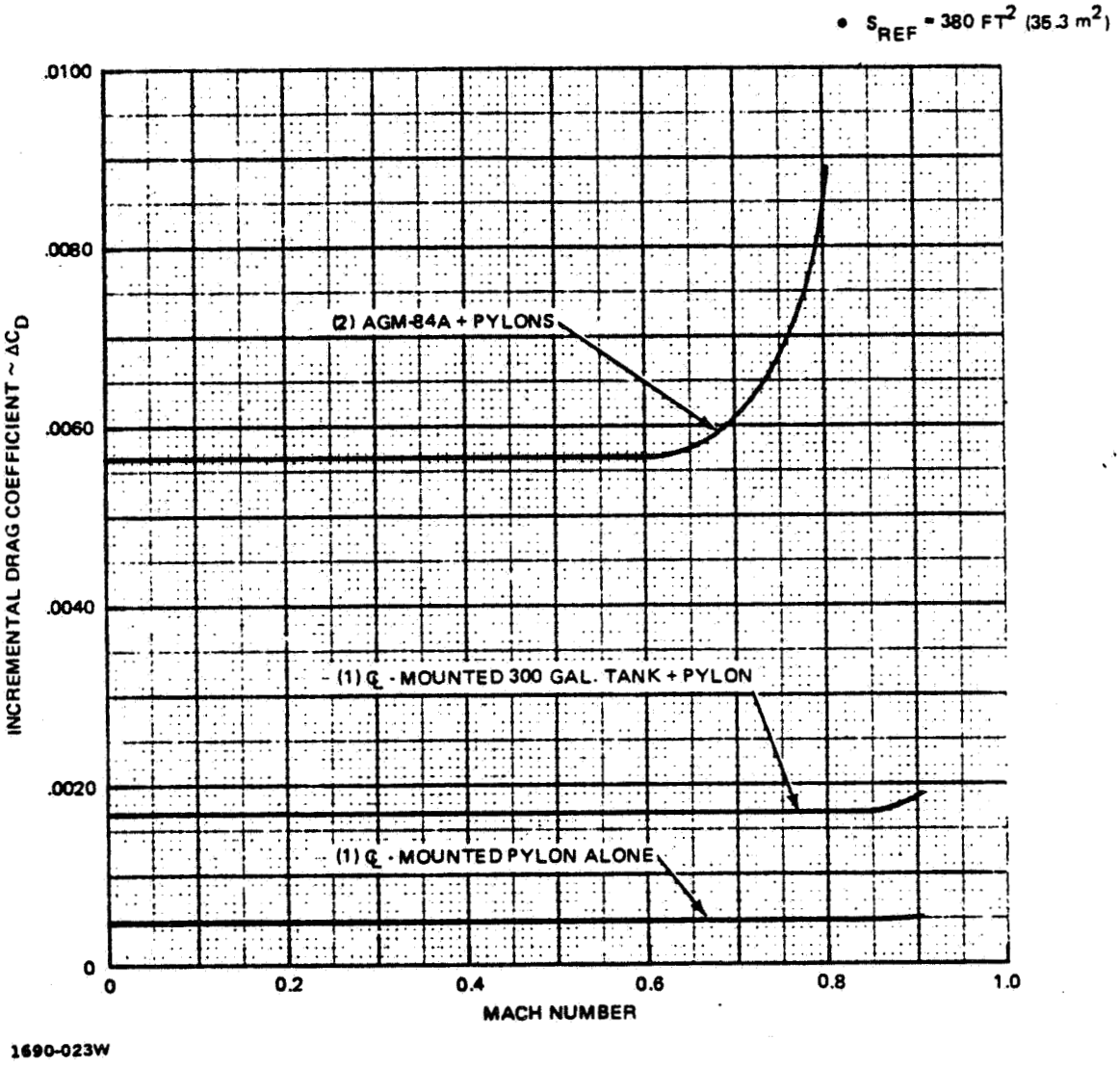

Figure 4.1.4-11 Design 623 – 2024 Installed Drag of External Stores SSS Mission

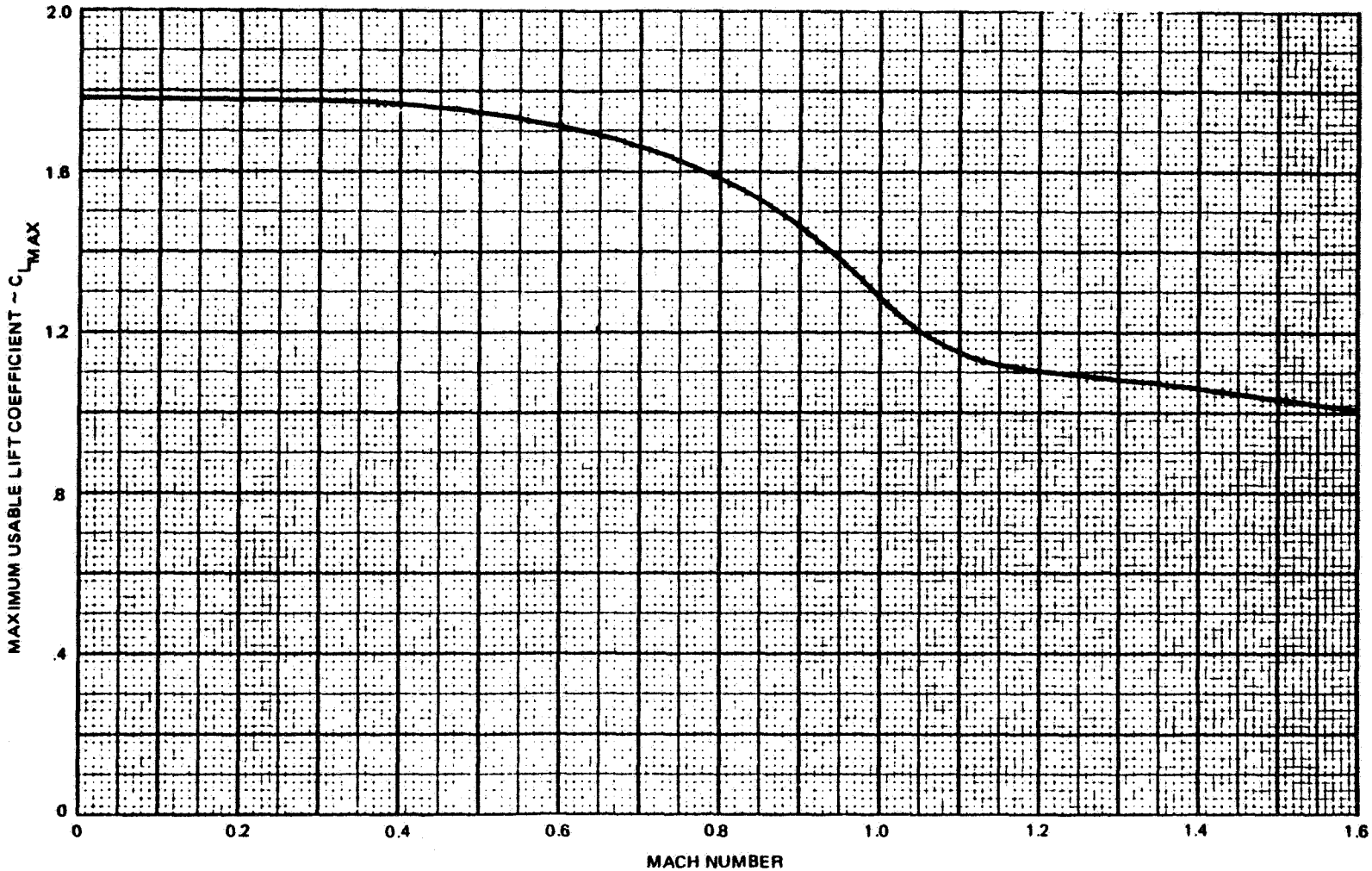

1690-024W

Figure 4.1.5-1 Design 623-2024 Maximum Usable Lift Coefficient

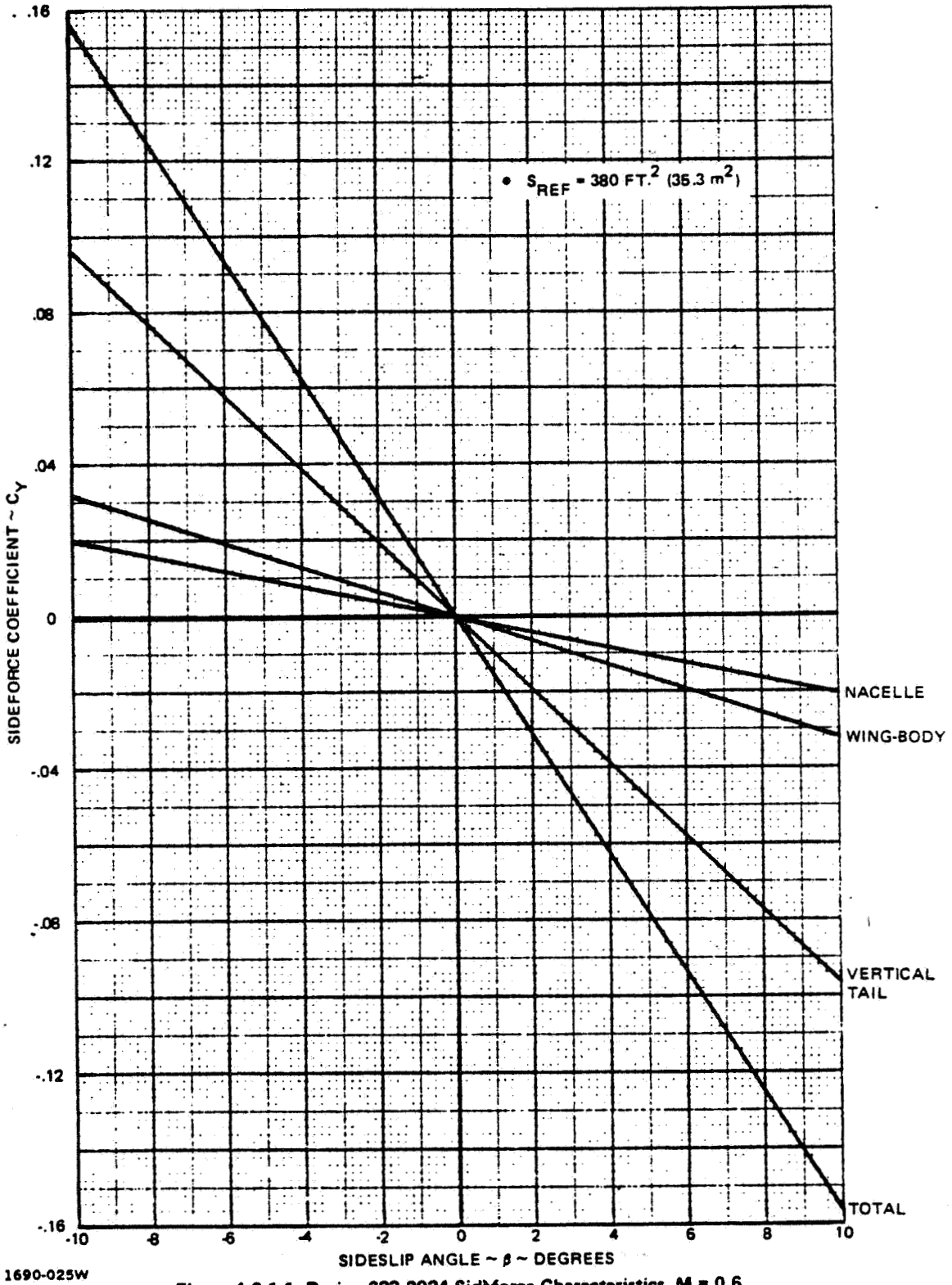

Figure 4.2.1-1 Design 623-2024 Sideforce Characteristics, M = 0.6

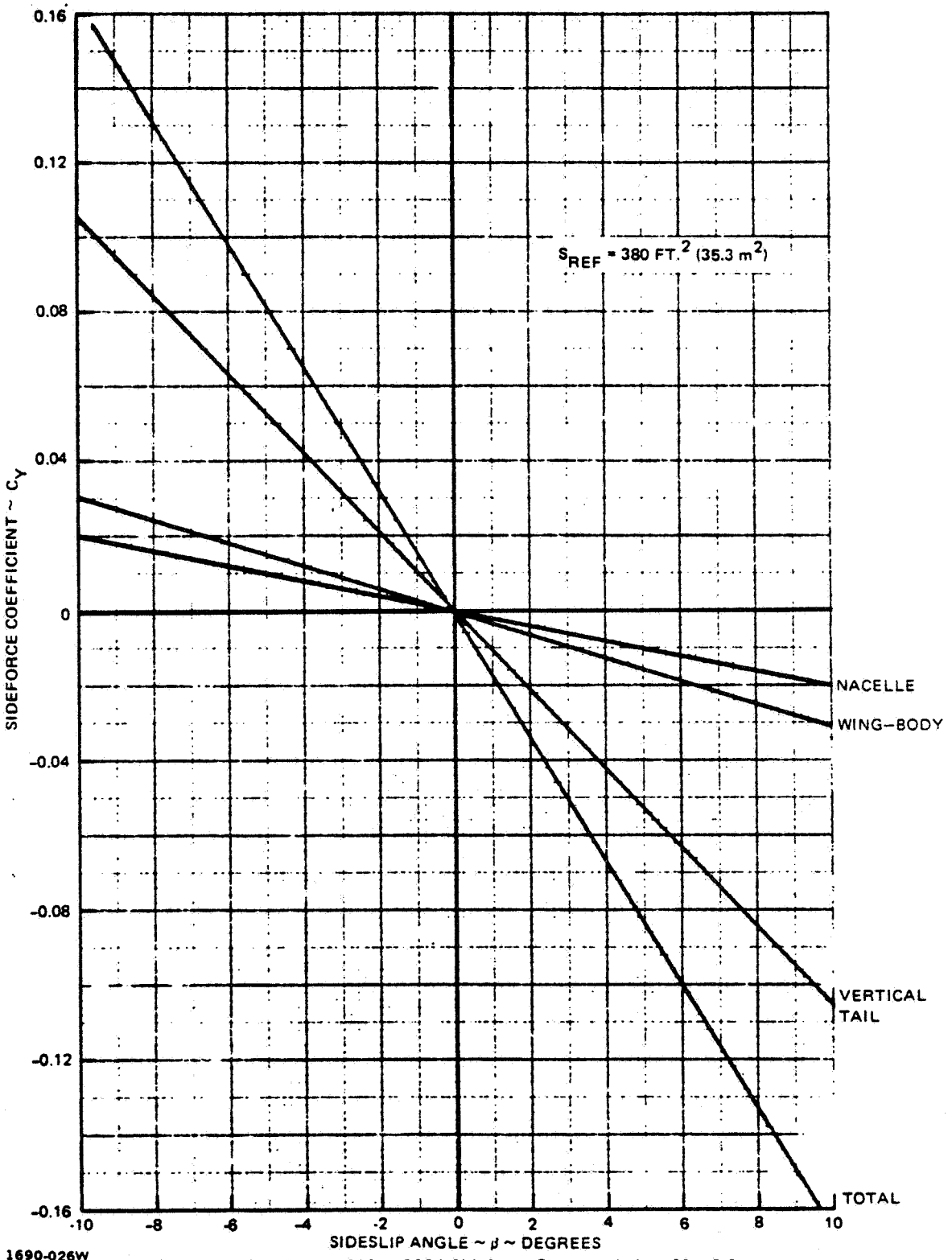

Figure 4.2.1-2 Design 623 – 2024 Sideforce Characteristics M = 0.9

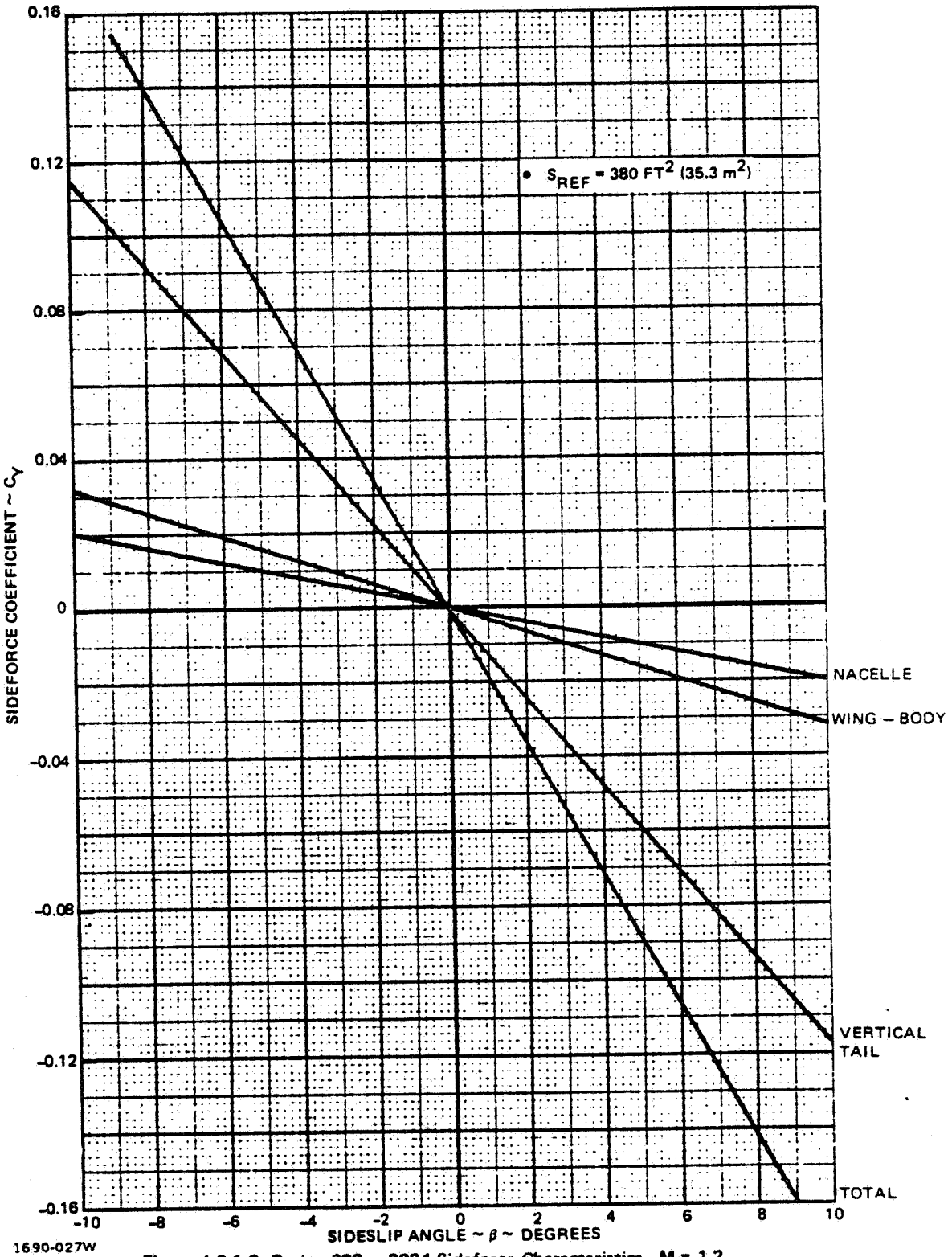

Figure 4.2.1-3 Design 623 – 2024 Sideforce Characteristics M = 1.2

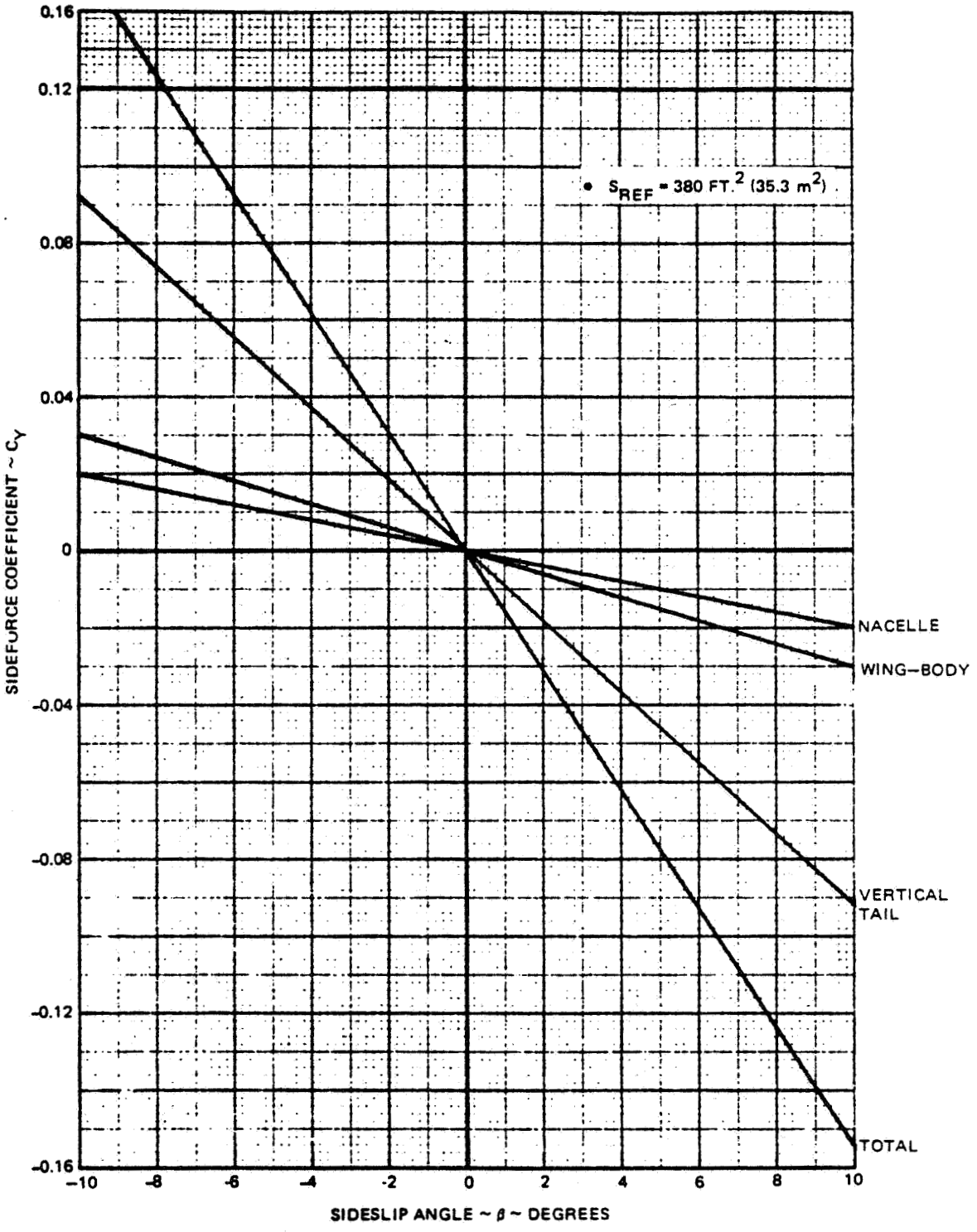

1690-028W

Figure 4.2.1-4 Design 623 – 2024 Sideforce Characteristics M = 1.6

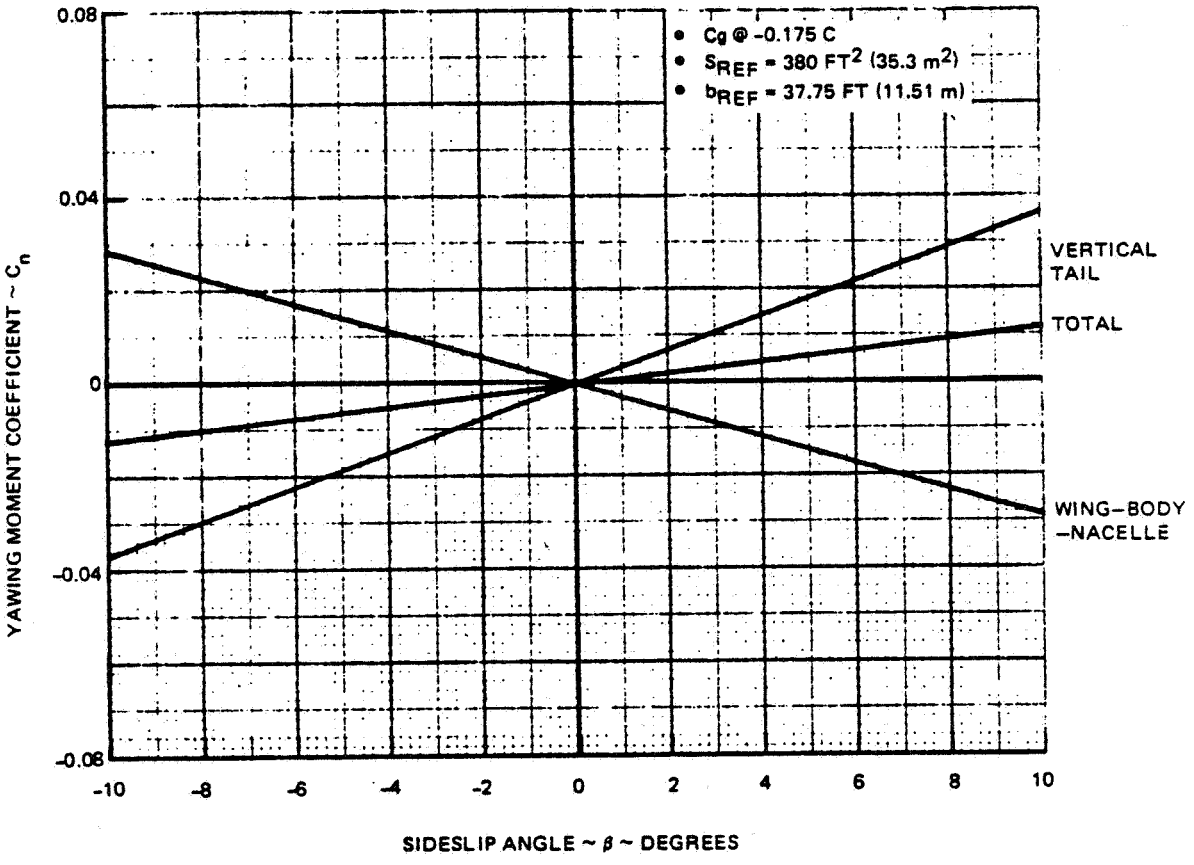

1690-029W

Figure 4.2.1-5 Design 623 – 2024 Directional Stability M = 0.6

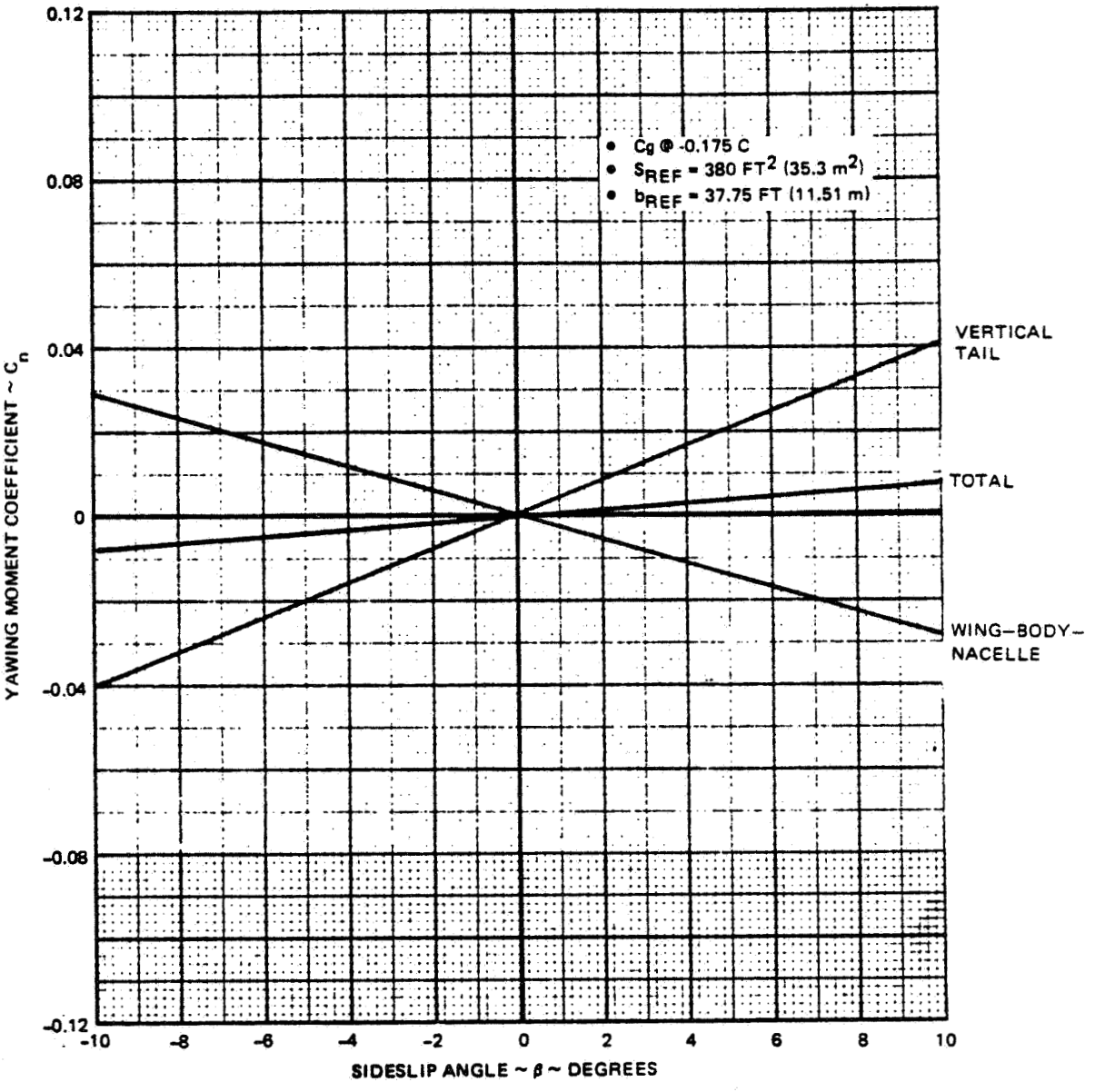

1690-030W

Figure 4.2.1-6 Design 623 – 2024 Directional Stability M = 0.9

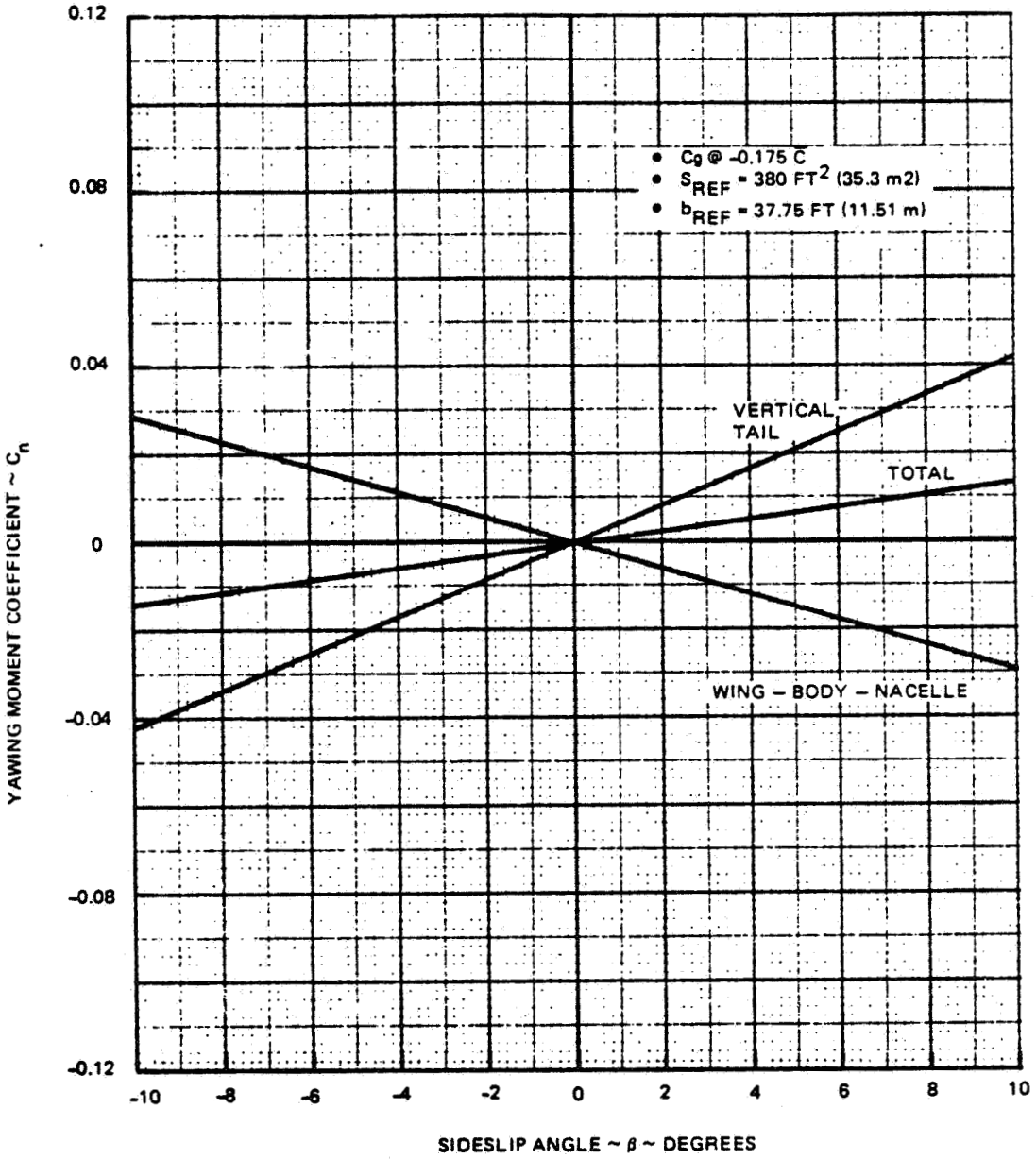

1690-031W

Figure 4.2.1-7 Design 623 – 2024 Directional Stability M = 1.2

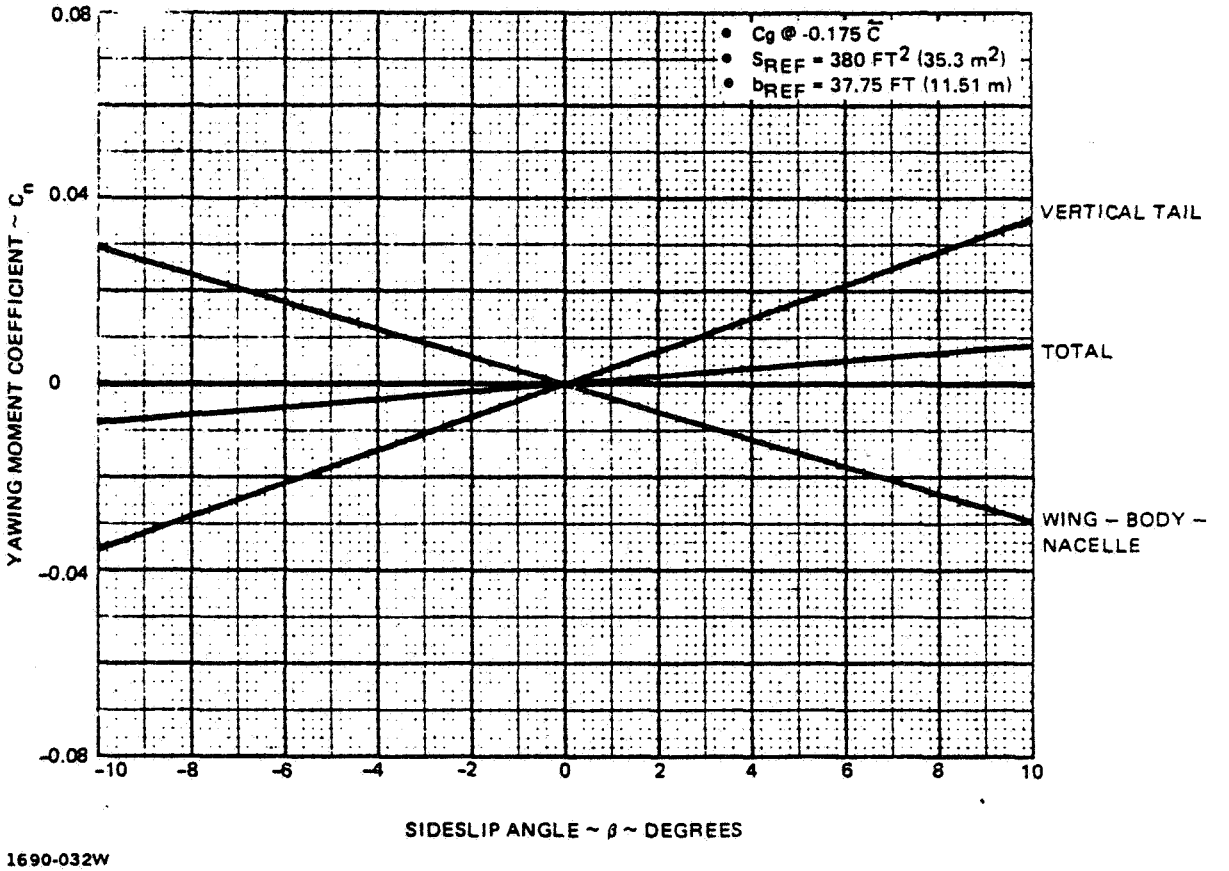

1690-032W

Figure 4.2.1-8 Design 623 - 2024 Directional Stability M = 1.6

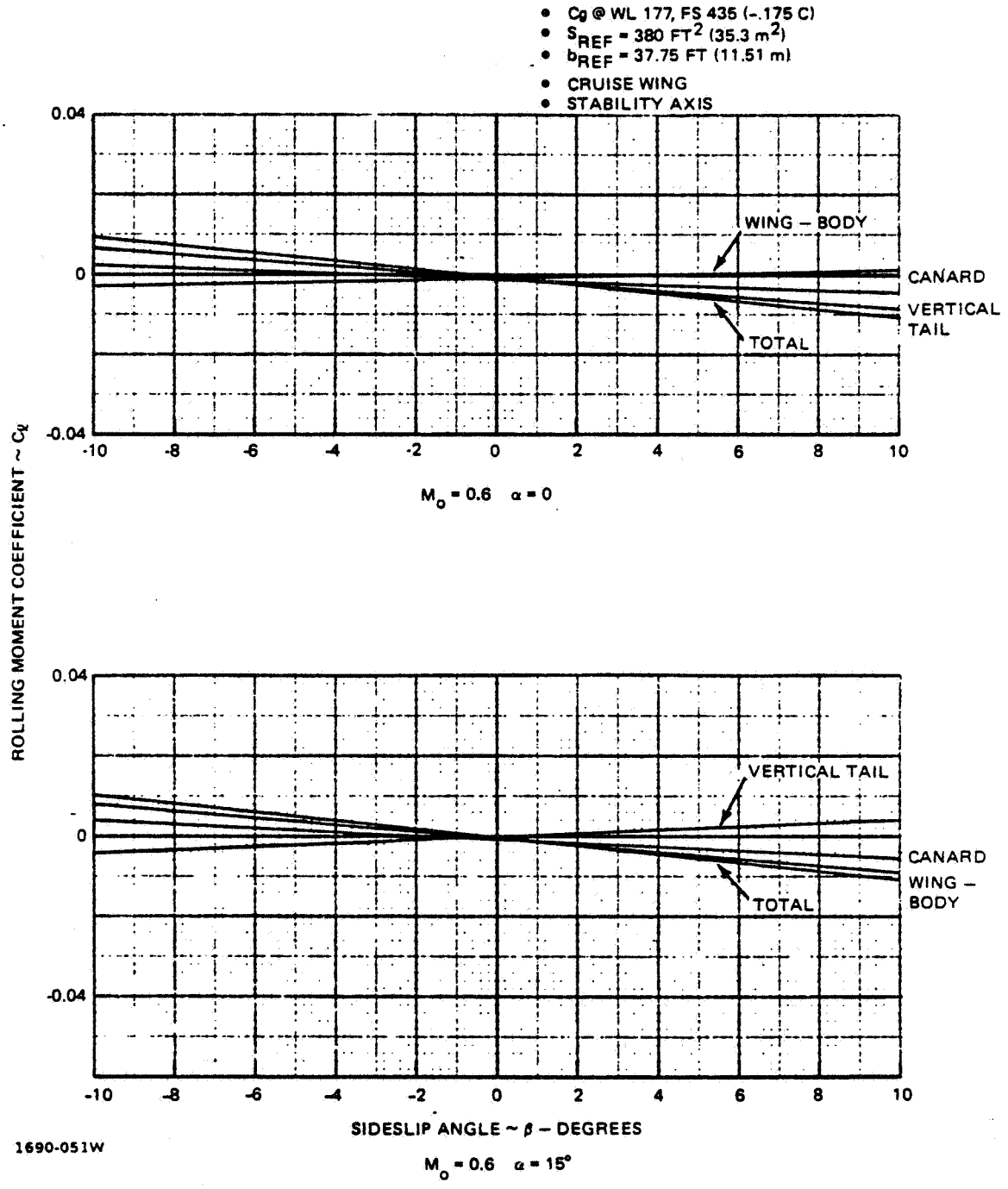

Figure 4.2.1-9 Design 623 – 2024 Lateral Stability

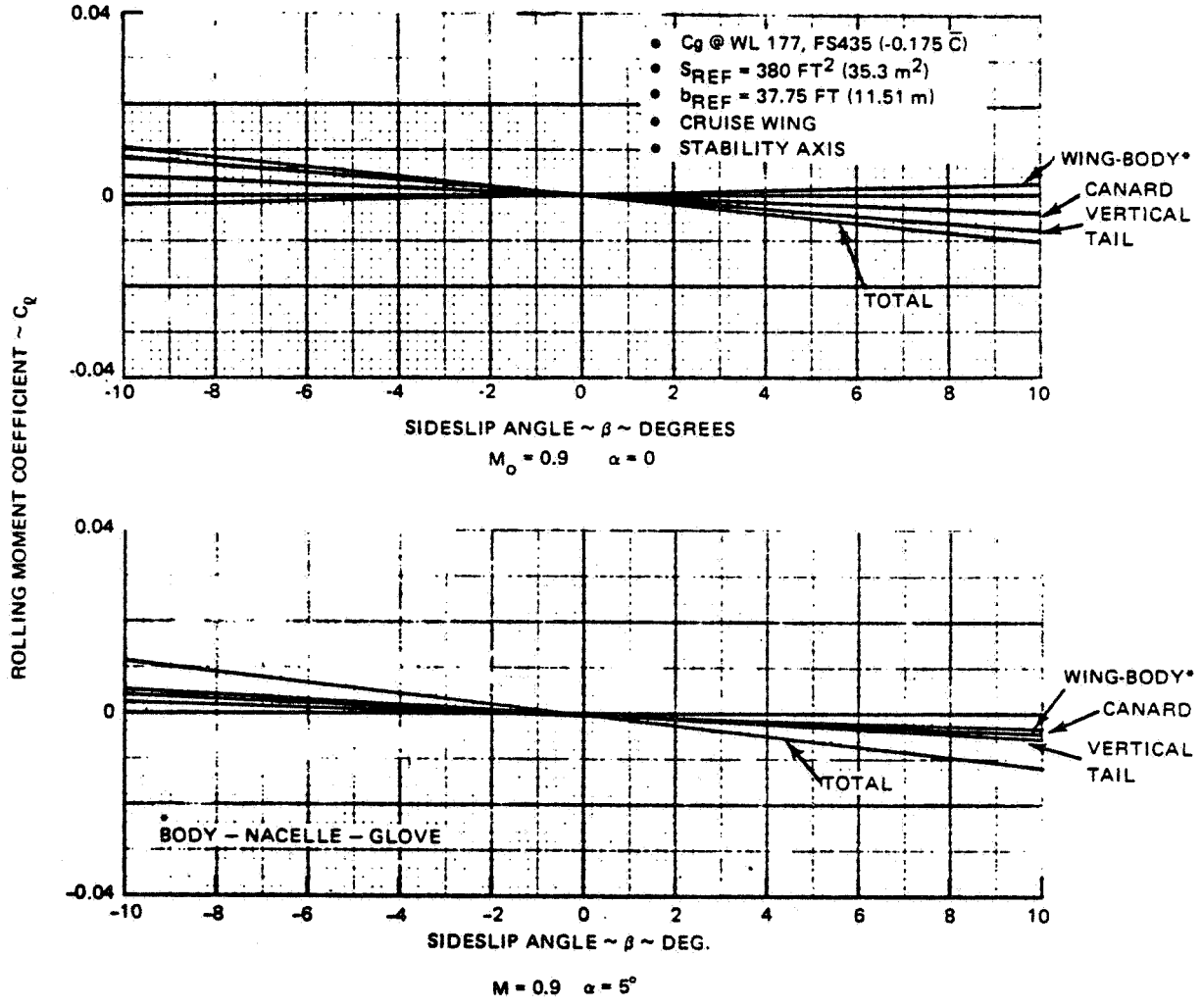

1690-052W

Figure 4.2.1-10 Design 623 – 2024 Lateral Stability

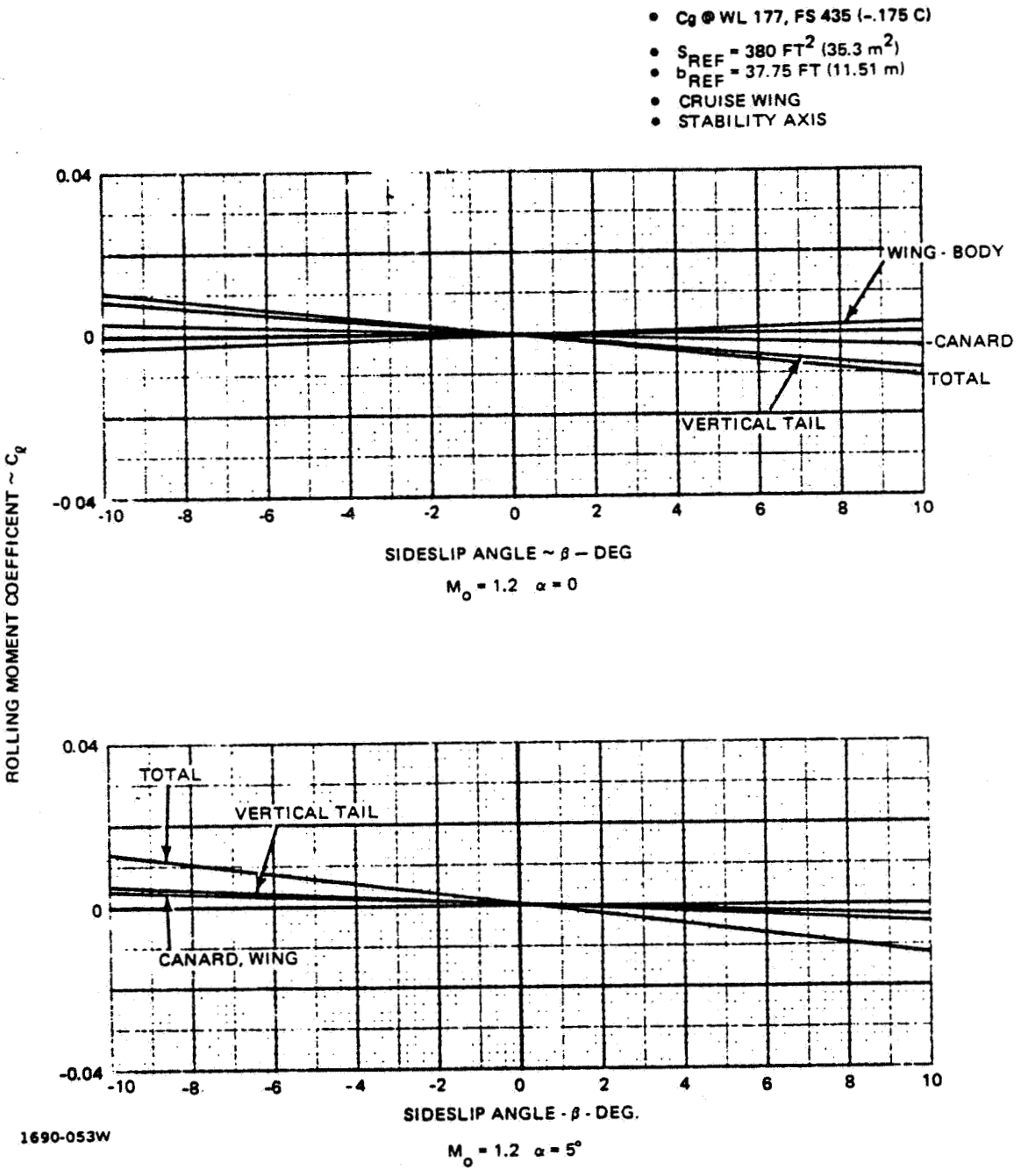

Figure 4.2.1-11 Design 623 — 2024 Lateral Stability

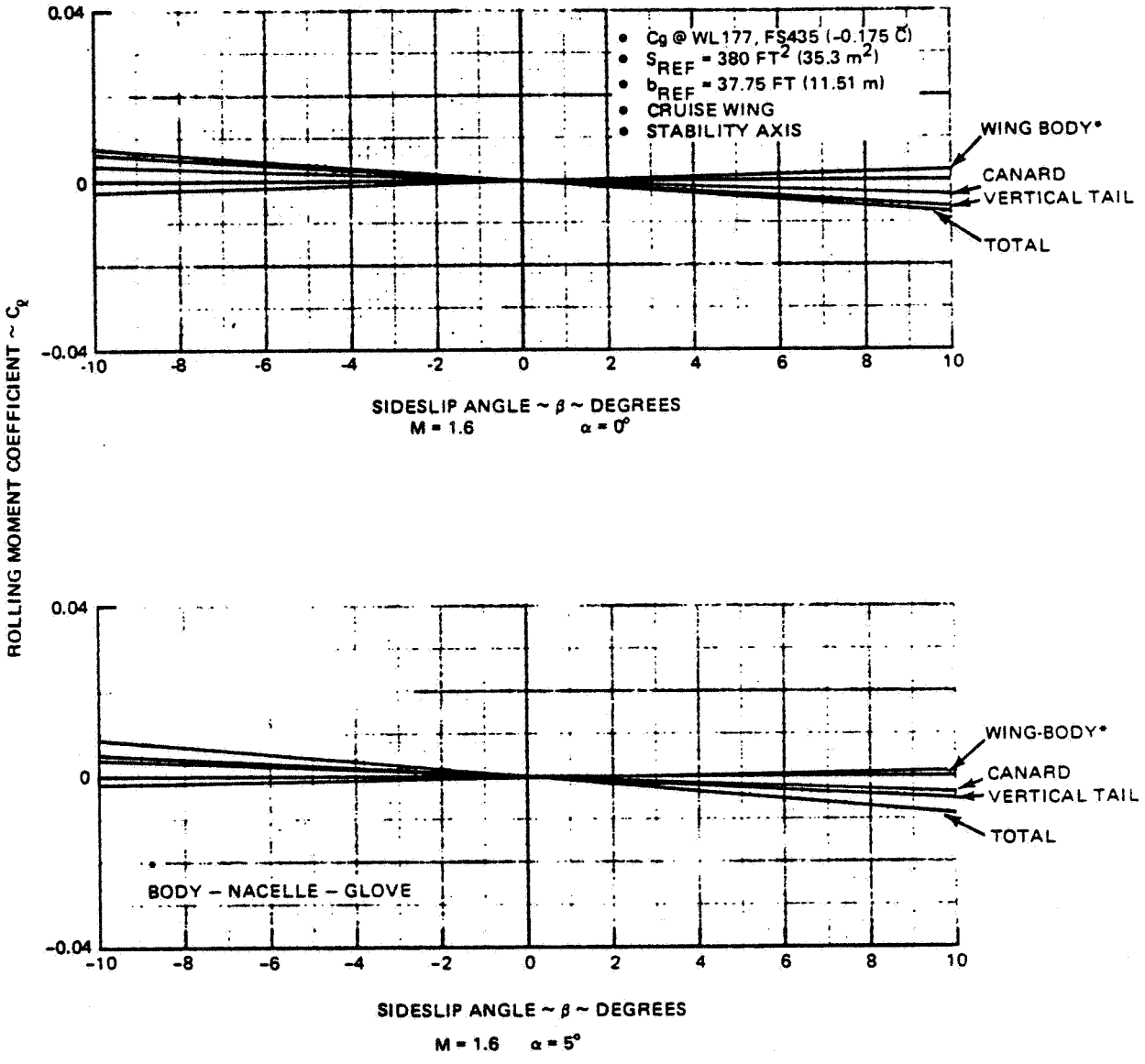

Figure 4.2.1-12 Lateral Stability

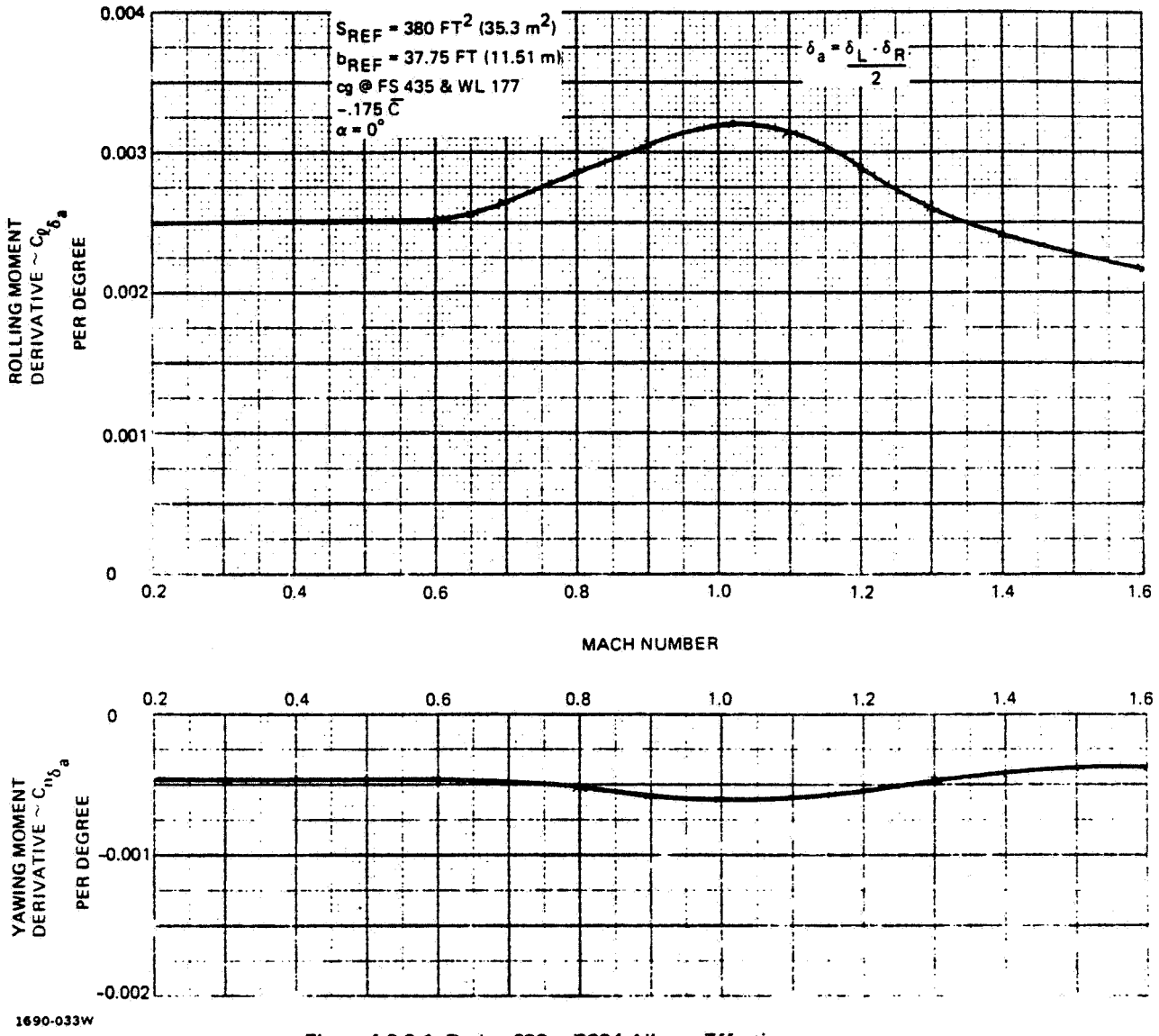

Figure 4.2.2-1 Design 623 – 2024 Aileron Effectiveness

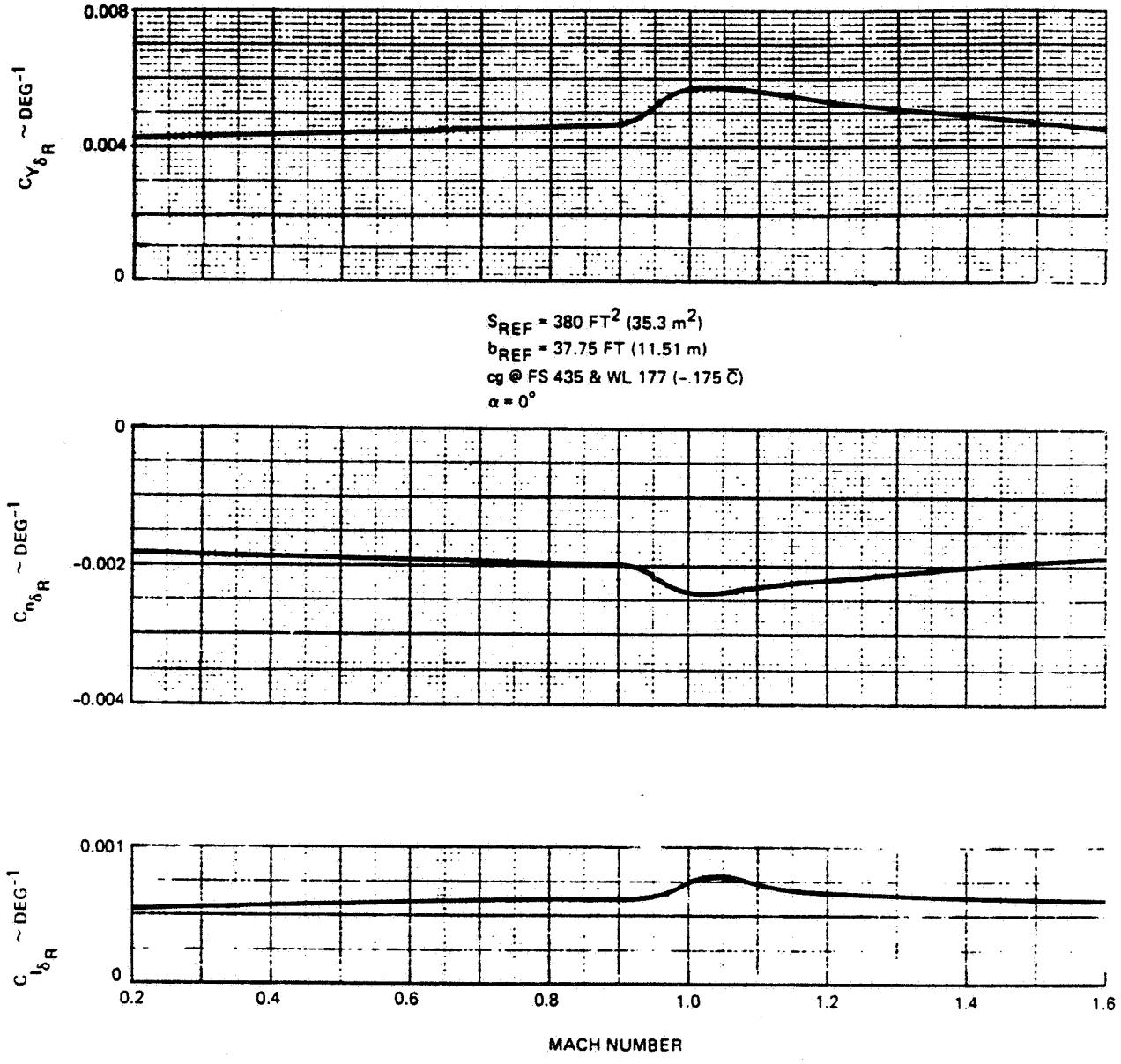

1690-034W

Figure 4.2.2-2 Design 623 - 2024 Rudder Effectiveness

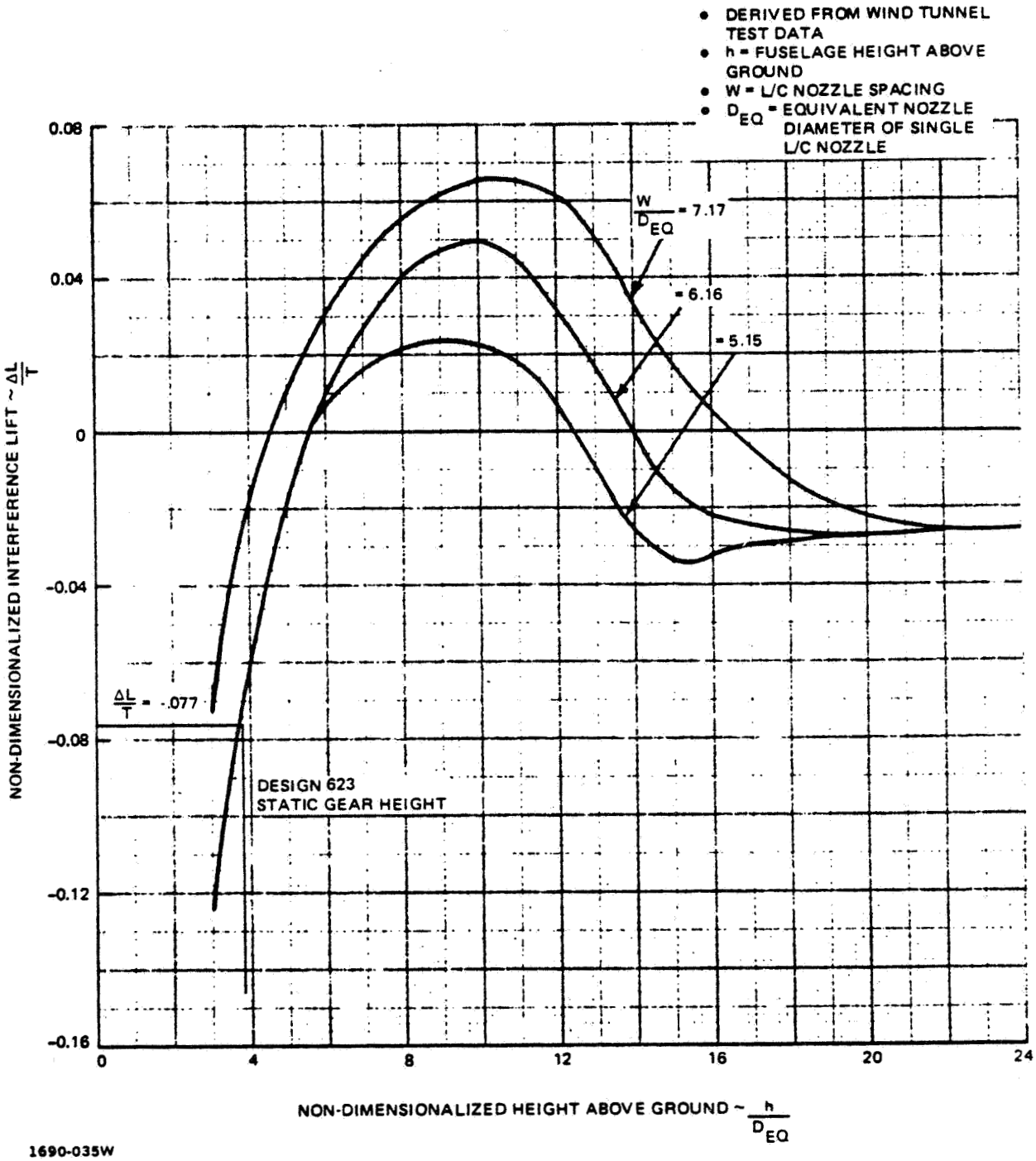

Figure 4.3.1-1 Determination of ΔL/T Used To Define T/W Required For VTO

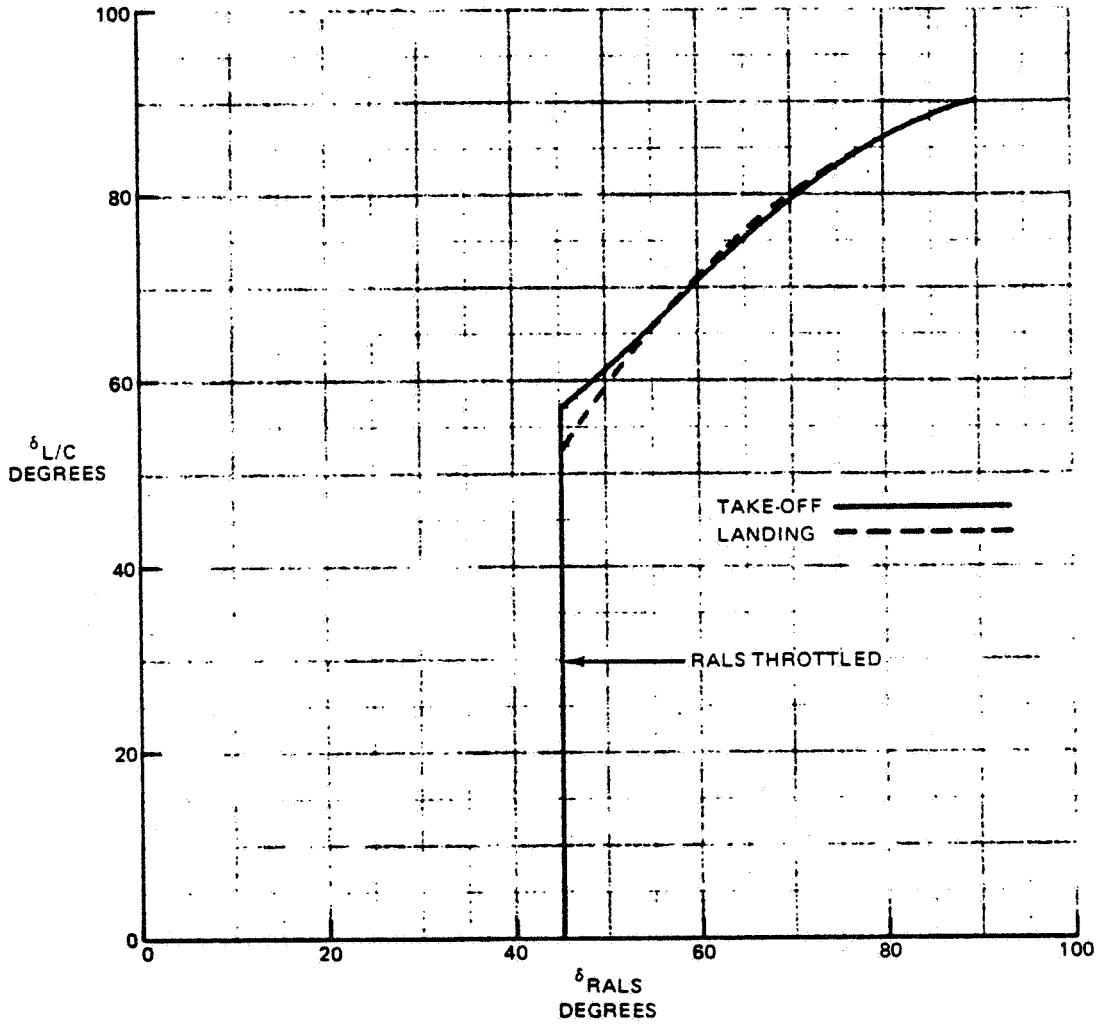

1690-036W

Figure 4.3.2-1 Design 623-2024 Nozzle Gearing for Static Thrust Moment Balance

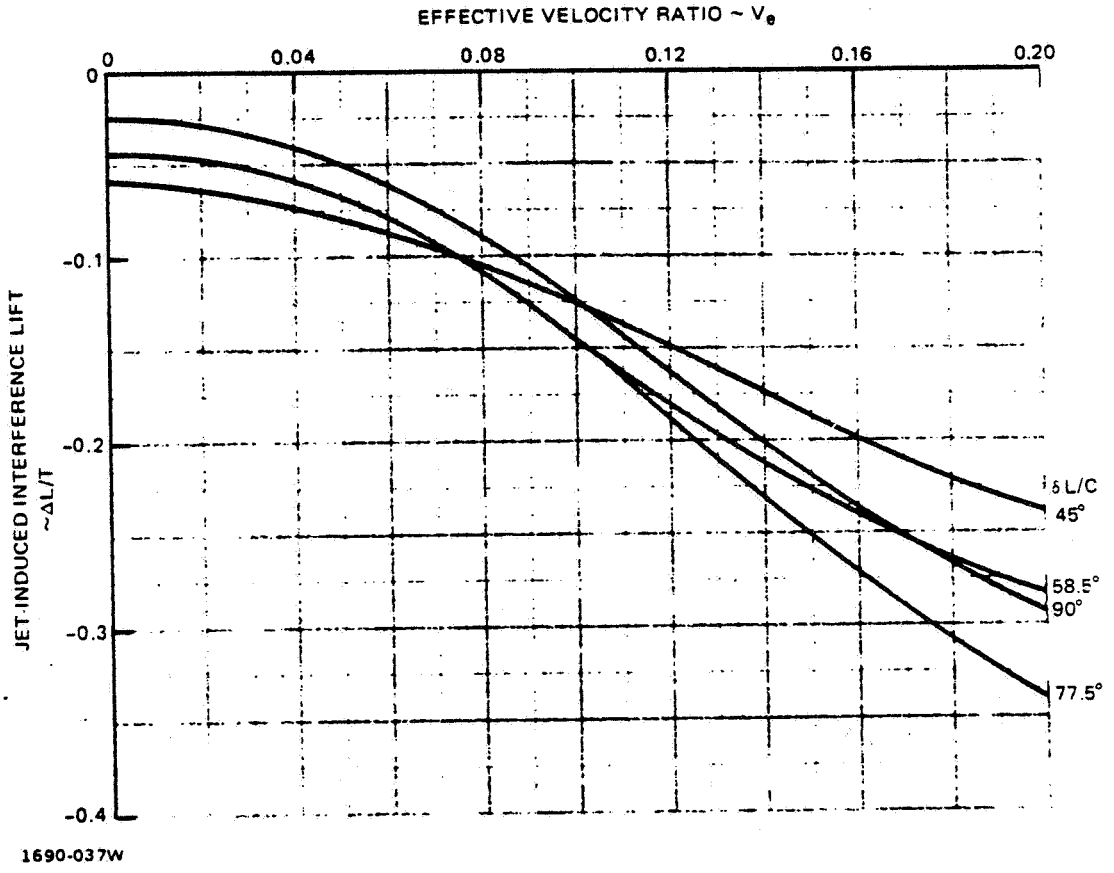

Figure 4.3.2-2 Design 623-2024 Estimated Jet-Induced Interference Effects Out of Ground Effect $\alpha = 0^\circ$

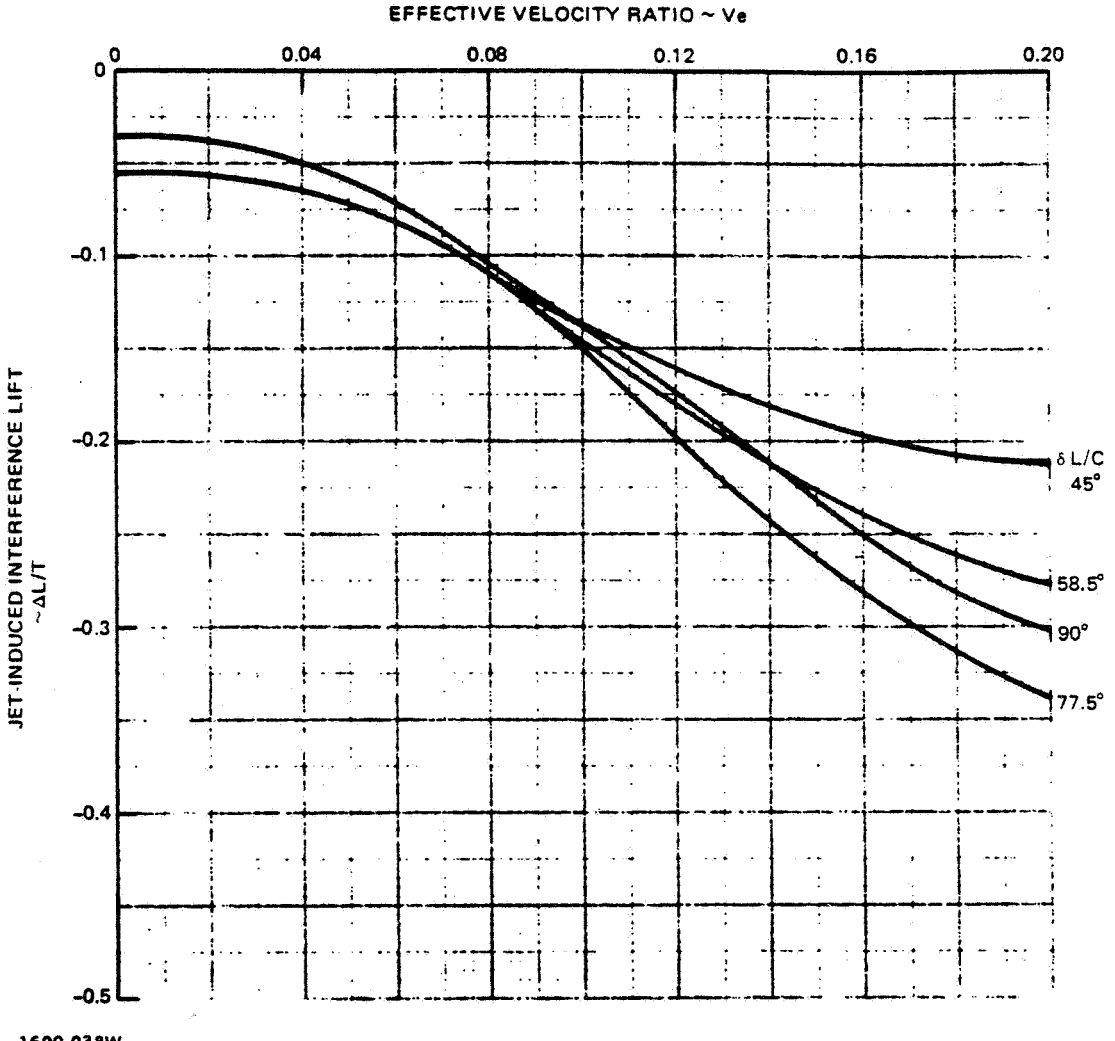

1690-038W

Figure 4.3.2-3 Design 623-2024 Estimated Jet-Induced Interference Effects Out of Ground Effect $\alpha = 11^\circ$

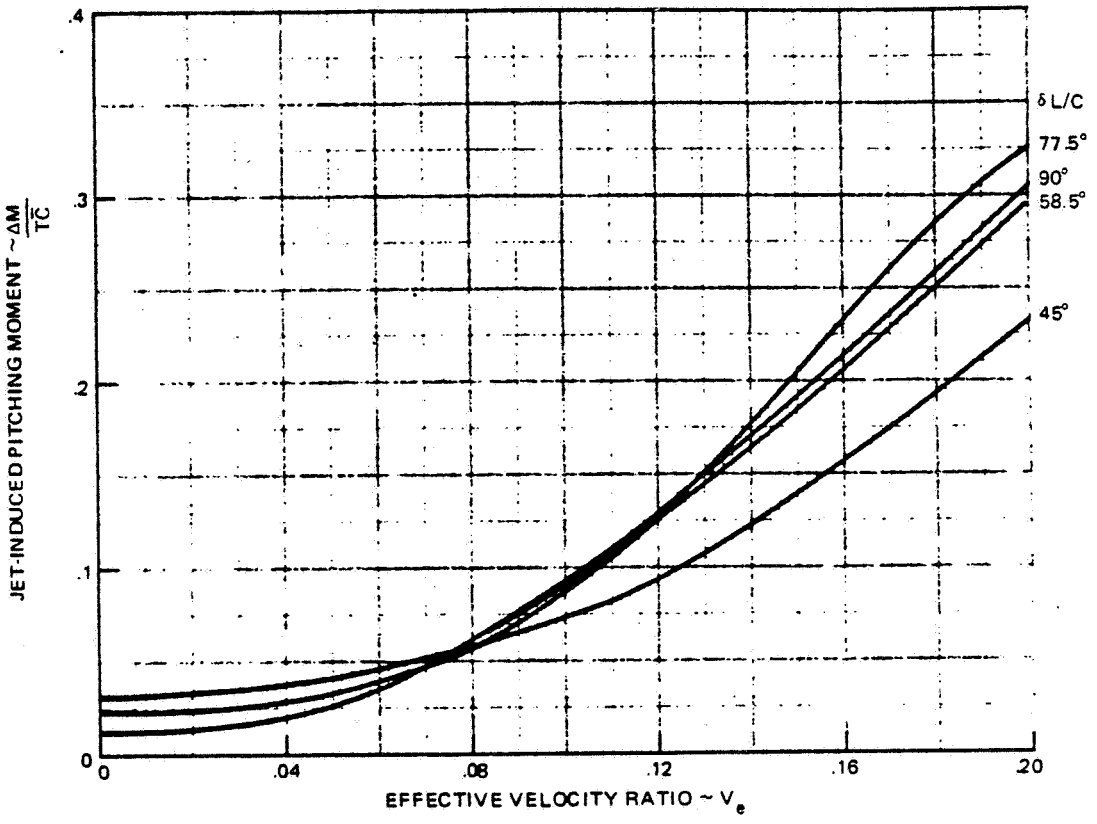

1690-039W

Figure 4.3.2-4 Design 623-2024 Estimated Jet-Induced Interference Effects Out of Ground Effect $\alpha = 0°$

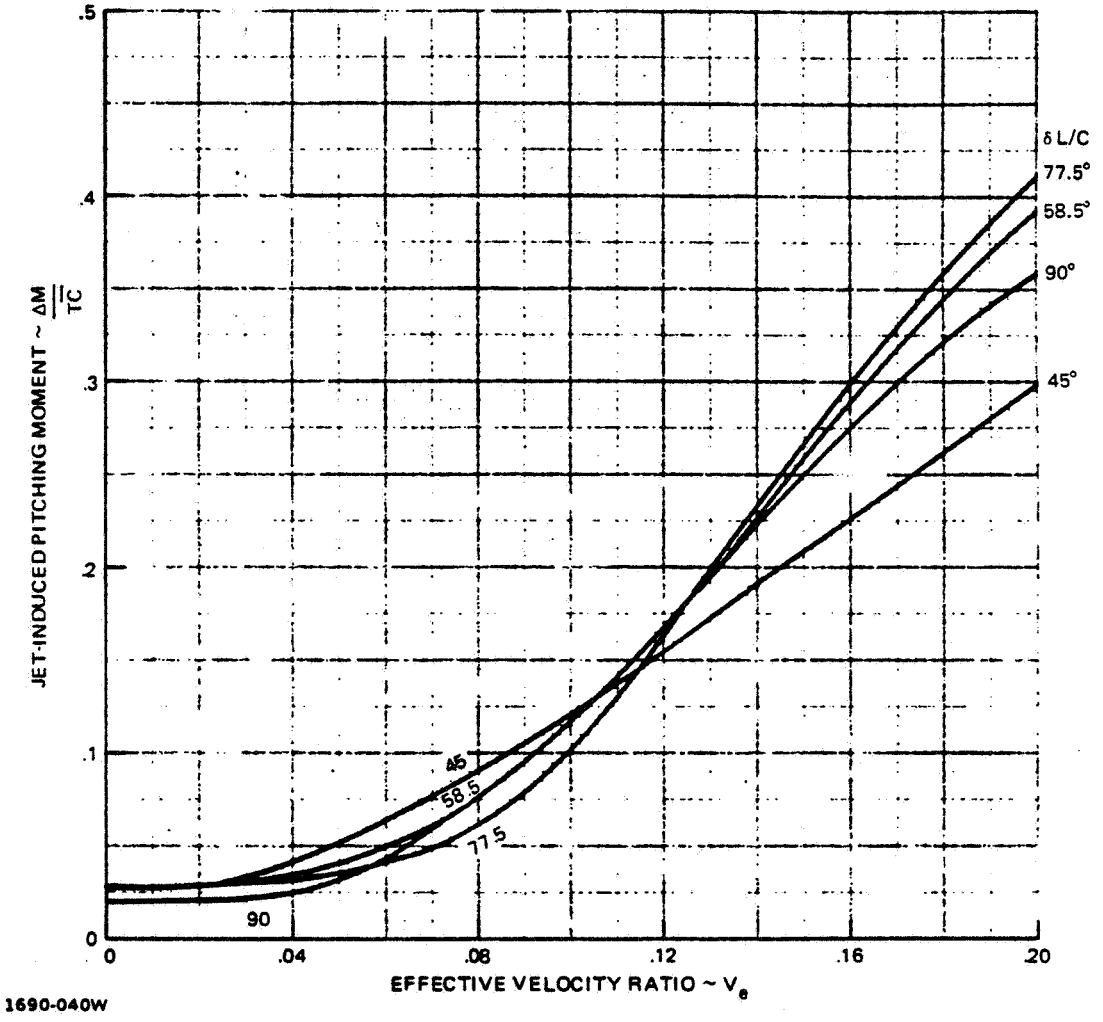

Figure 4.3.2-5 Design 623-2024 Estimated Jet Induced Interference Effects Out of Ground Effect α = 11°

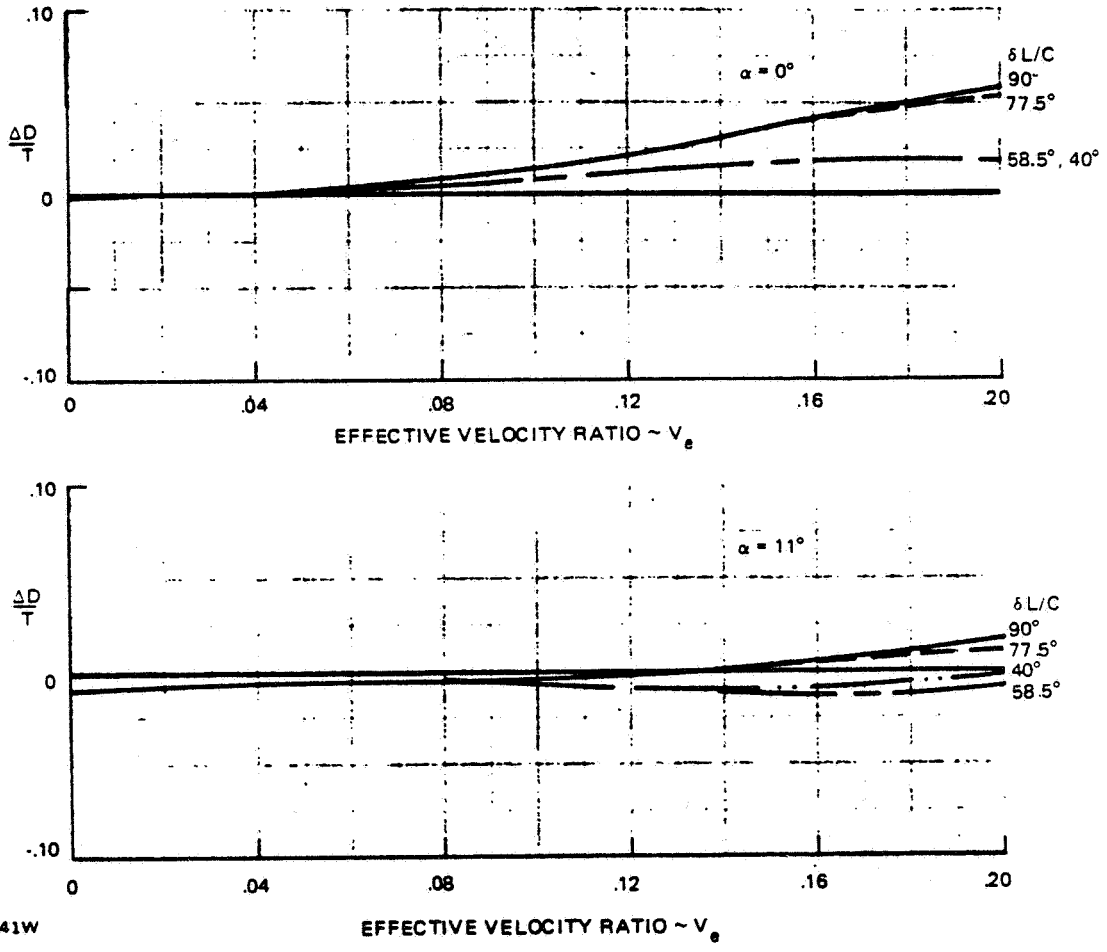

Figure 4.3.2-6 Design 623-2024 Estimated Jet-Induced Interference Effects Out of Ground Effect

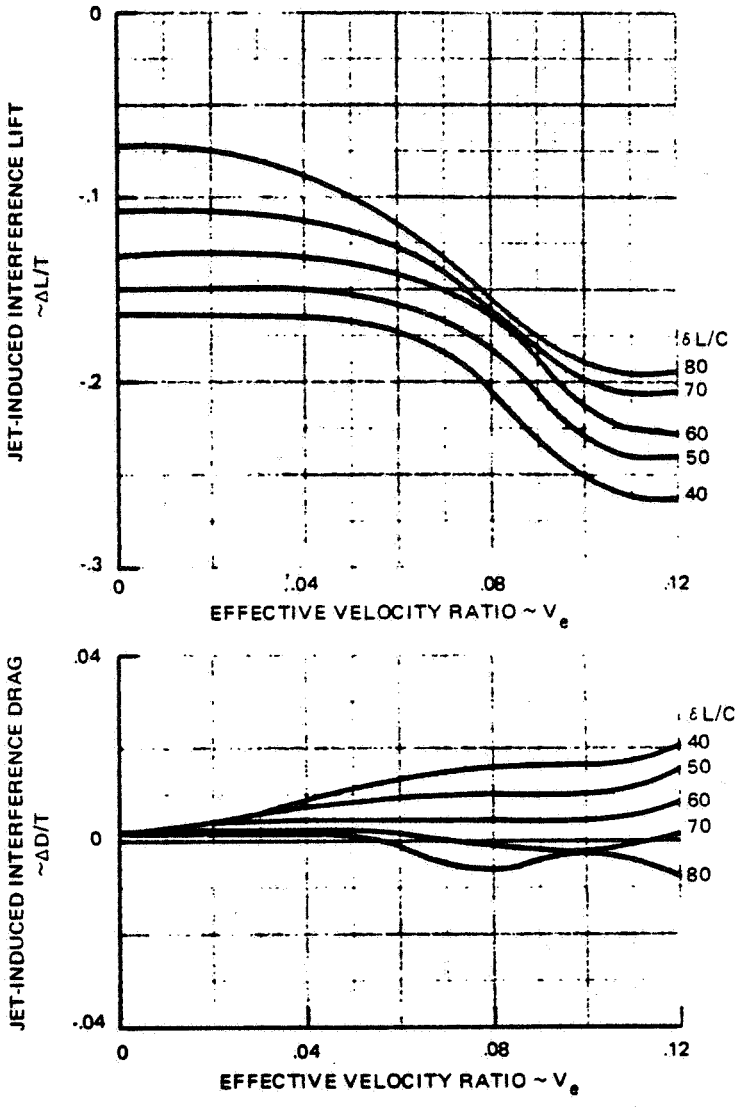

1690-042W

Figure 4.3.3-1 Design 623-2024 Estimated Jet-Induced Interference Effects In Ground Effect $\alpha = 0°$

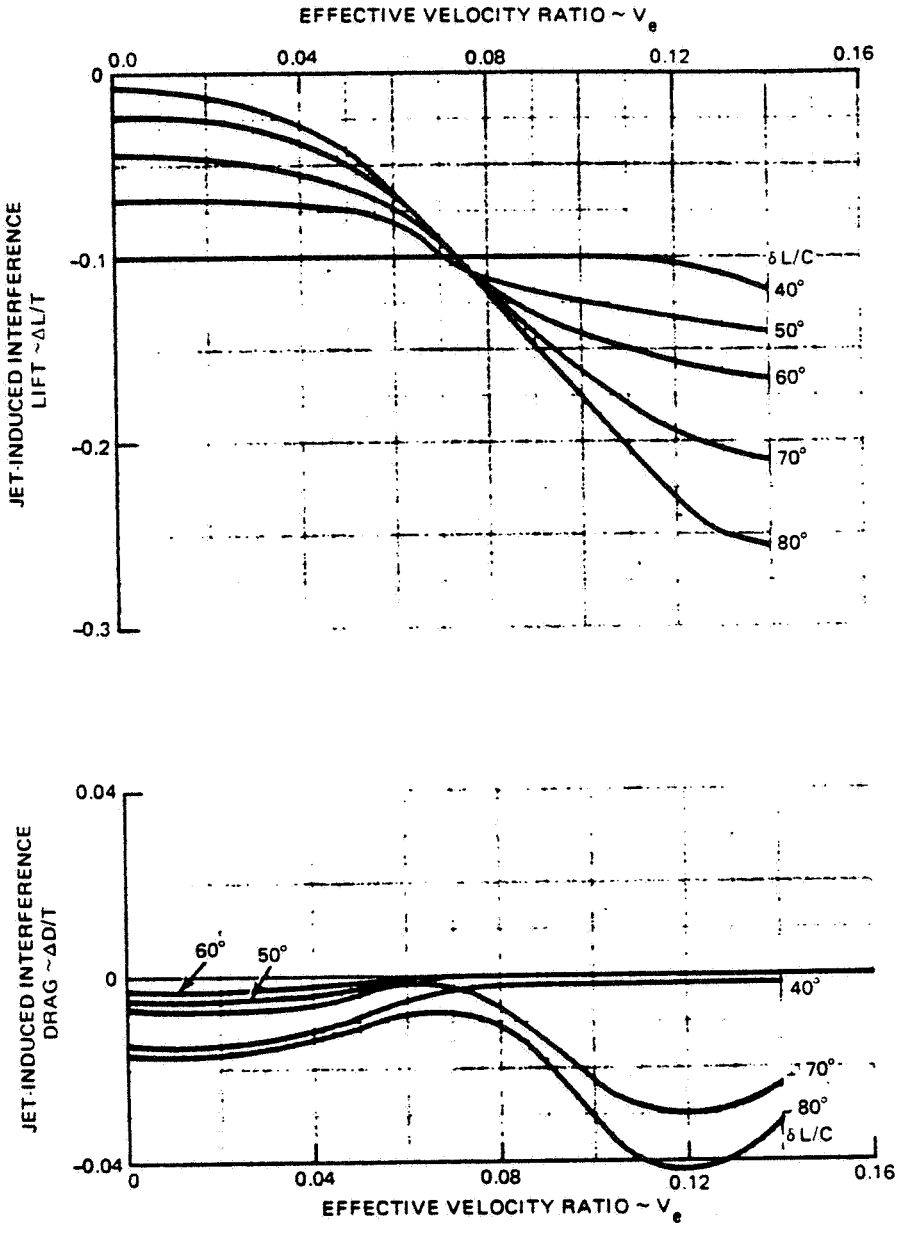

1690-043W

Figure 4.3.3-2 Design 623 – 2024 Estimated Jet-Induced Interference Effects In Ground Effect $\alpha = 11^\circ$

5 - PROPULSION CHARACTERISTICS

The Design 623-2024 propulsion system consists of two advanced technology variable cycle turbofans; high performance inlets, and a vectorable two-dimensional exhaust nozzle for each engine. In addition, remote augmentors, using fan discharge air, provide lift forward of the aircraft center of gravity. Aircraft pitch and yaw control is achieved in hover and transition by thrust modulation of the remote augmentors and the exhaust nozzles - both vector controlled. Compressor discharge bleed is used to power roll control nozzles located at each wing tip.

5.1 ENGINE DESCRIPTION

Power for Design 623-2024 is provided by the General Electric SYS-GE16/VVCE5 Study D3 Remote Augmented Lift System (RALS) (Reference 5.1-1). This system, shown schematically in Figure 10.2-1 (Proprietary Section), incorporates a variable cycle turbofan with the following features:

- Bypass ratio of 0.95
- Split, oversized fan to provide additional flow for VTOL and transonic acceleration
- Variable geometry in the fan and core stators
- Forward and aft Variable Area Bypass Injectors (VABI) in the fan stream.

The engine operates as a conventional mixed-flow turbofan at high power to maximize specific thrust. At the reduced power settings required for loiter and subsonic cruise, the engine variable geometry features reduce fuel consumption by increasing the bypass ratio. Additional performance improvements derived from the engine cycle variability are:

- Airflow is scheduled to obtain better inlet matching in the Mach number range of 0.8 to 2.0.
- Inlet spillage drag is reduced subsonically by maintaining airflow at its maximum as engine power is reduced to approximately 50% thrust. This has the added benefit of using larger nozzle jet areas (relative to a conventional engine), and thereby reducing the nozzle boattail drag.

Air bleed from the fan is reheated in a remote augmentor to provide lift forward of the aircraft center of gravity during VTOL operation. The D3 engine is capable of supplying up to 43% of the inlet flow to the remote augmentor during this mode of operation.

5.1.1 Engine Selection

The RALS D3 engine used in this configuration was selected from six candidates offered by the General Electric Company. Only RALS engines were considered for this study because they provide:

- High thrust to weight
- Flight performance exceeding that of current operational engines
- VTOL capability without the use of a lift engine

Additionally, the aerodynamic configuration developed for this mission is adaptable to a lift plus lift/cruse system without major redesign.

Engine cycle studies designated A1, C1, D1 and D3 were used for initial configuration studies as shown in Figure 10.2-2. The A1 and C1 cycles were not considered for the configuration because VTO balance could not be achieved with the design thrust splits. All four initial candidates were used for preliminary aircraft sizing studies to determine sensitivities to the differences in engine cycle parameters. The results of these studies showed that the smallest airplane would be configured with an A1 engine. Two configurations met the hover/thrust balance requirements, the A3 and the D1, the D1 resulting in the lightest airplane. Additional configuration studies with this engine revealed that there was inadequate RCS thrust available for aircraft control during hover.

Based on the results of these studies, two additional candidates, designated VVCE6 Study H1 and VVCE5 Study D3 were evaluated. Both engines have the ability to vary VTO thrust split in the ranges shown with only an insignificant change in total thrust. This feature can be utilized to provide for aircraft pitch control during hover. Studies with these two candidates showed the H1 engine would give the smallest airplane, but aircraft thrust balance and hover RCS requirements could not be attained within the H1 thrust split range. The aircraft was therefore configured with VVCE5 Study D3 engine, which is the optimum of the six candidates studied.

5.2 INLET DESCRIPTION

The inlet selected for this configuration is the Grumman A-88V high flow design, which is well suited to the trasonic high-flow capabilities of the Study D3 engine. The inlet is a fixed geometry, external compression design, with an auxiliary door located on the lower nacelle surface for operation at high mass flow ratios. Louvers are provided on the upper cowl surface for efficient hover and low speed performance, and to discharge bleed/bypass air at higher speeds. Data from Reference 5.2-1 and later sizing studies with the G. E.

D3 engine, indicated that a 5% aircraft weight reduction can be achieved with a high flow inlet relative to a conventional fixed design. Operation of the inlet during three significant flight modes is shown in Figure 5.2-1.

The inlet is sized for the supersonic cruise Mach number of 1.6, with an acceleration capability up to Mach 2.0. Because of the increased levels of distortion and turbulence encountered at higher Mach numbers, the airplane was limited to Mach 1.8 for this study. Further definition of the inlet performance at higher Mach numbers is required to accurately set the high speed limit.

A seven square inch model of the inlet design has been tested in the Grumman high speed wind tunnel over a Mach number range of 0.8 to 1.2. Results of this test and other analytical studies, (References 5.2-1 and -2), were used to size the study configuration.

Figure 5.2-2 is an illustration of the matching of the high flow inlet and to the requirements of the D3 engine. The effect of the lower auxiliary door opening is reflected in the increased inlet flow capability below Mach 1.4. In the Mach range from 0.9 to 1.4, the auxiliary inlet area schedule is somewhat oversized for the requirements of the D3 engine, because the area was sized (15% of capture area) for a engine using high flow only at selected flight conditions. The D3 engine is capable of high flow operation at all Mach numbers. As additional engine cycle studies are conducted, further tailoring of the inlet/engine flow schedules will result in more optimum matching.

In the range of M_o = 1.4, the auxiliary inlet is almost completely closed. Operation of the inlet in this region is near critical, and should be addressed as further studies of this design are undertaken.

5.3 NOZZLE DESCRIPTION

The RALS engine uses an Augmented Deflector Exhaust Nozzle (ADEN). The ADEN is a fully vectorable, two-dimensional nozzle that provides thrust vectoring from 0 to 110 degrees. The nozzle was designed and developed by General Electric under contract to the Naval Air Propulsion Test Center. It was evaluated along with several other candidates by Grumman under contract to General Electric in both single and twin engine supersonic airplanes (Reference 5.3-1). This study and later hardware testing by General Electric demonstrated the superiority of this installation in this airplane class. The ADEN has demonstrated high thrust vectoring performance, and excellent forward mode performance over a wide range of throat areas and nozzle pressure ratios.

Other desirable characteristics are:

- Low nozzle boattail drag
- Vectoring capability in afterburning
- In-flight thrust vectoring
- Reduced IR signatures in several viewing angles

5.4 INSTALLATION FACTORS

Performance data supplied by General Electric in Reference 5.1-1 were corrected to reflect installation in Design 623-2024. Installed engine performance accounts for inlet/engine matching, aircraft bleed and power extraction, nozzle interference drag and ambient temperature variations. The following sections describe the levels of corrections used for this study.

5.4.1 Inlet Performance

Total pressure recovery for the high-flow inlet is shown in Figure 5.4.1-1 for all flight modes. These data were derived from the analytical studies and model tests described in References 5.2-1 and -2. The recovery data in Figure 5.4.1-1 reflects operation of the auxiliary inlets during hover, transition and transonic flight.

Also shown are the inlet spillage drag characteristics which include additive drag, lip suction and bleed/bypass drag. These values are included in the thrust data since they vary with engine power setting. Supercritical spillage drag, shown in Figure 4.1.4-2, is independent of engine power setting and is included in the aircraft drag polar.

5.4.2 Nozzle Performance

Performance data for the Study D3 engine include internal performance of the ADEN nozzle for all modes of operation.

Installed propulsion data are corrected for nozzle interference drag using data measured on a 1/8 scale model at the Arnold Engineering Development Center. These programs, sponsored by the Air Force Flight Dynamics Laboratory, provide the basis for realistic estimates of installed nozzle interference drag for this design. Test data developed from these tests show nozzle interference drag as a function of nozzle pressure ratio, flight Mach number, airplane angle of attack, and nozzle flap deflection angle. The data shown in Figures 5.4.2-1 through -6 were derived from these test data (Reference 5.4-1), and correct for the drag difference between the reference nozzle configuration in the aerodynamic polar and the actual nozzle installation. The drag polar developed for Design 623-2024 (see

Section 4.1.4) references a free-flowing nozzle operating at flow-through pressure ratios. The nozzle interference drag data shown also are corrected for Design 623-2024 angle of attack at each altitude and flight Mach number, and are for the nozzle external flap set at 0^{o}.

5.4.3 Bleed Horsepower Extraction

Performance data supplied by General Electric (Reference 5.1-1) includes 0.35 lbs/sec and 60 horsepower extraction per engine for aircraft use.

Past design experience with this type of aircraft indicate that these levels are adequate for the aircraft subsystems.

5.4.4 Exhaust Gas Reingestion

Performance data calculated in ground effect includes allowance for reingestion of engine exhaust gases. Grumman has run extensive hot gas model test programs jointly with the VFW-Fokker of Bremen, FGR, on a 1/12 scale model of Grumman Design 623-2024. Results of these tests (Reference 5.4.4-1) show that the mean inlet temperature rise is strongly dependent on nozzle deflection. Acceptable levels of mean inlet temperature rise of 10^{o}F were obtained with lift and lift/cruise nozzle deflections of 10^{o} aft. VTO performance in ground effect accounts for the loss in thrust for an inlet rise of 10^{o}F and a 10^{o} aft tilt of the thrust vector.

5.5 ENGINE PERFORMANCE

Installed performance data for a scaled General Electric SYS-GE16/VVCE5 Study D3 engine are contained in Section 10.2 (Proprietary).

5.5.1 Conventional Flight Performance

Installed in-flight engine performance for the General Electric SYS-GE16/VVCE5 Study D3 engine are shown in Figures 10.2-3 through 10.2-27 (Proprietary Section). The following notes apply to these data:

- Standard Day
- All data per engine
- Horsepower extraction and engine bleed included as described in Paragraph 5.4.2.
- Nozzle drag included per Figures 5.4.2-1 through -6
- Inlet performance of Figure 5.4.1-1

- Engine data scaled to a Sea Level Static thrust of 27729 lbs using the scaling laws of Reference 5.1-1
- Fuel flows are increased 5%.

5.5.2 VTO Performance

The installed thrust calculation for vertical takeoff condition is shown in Figure 10.2-28. Engine thrust is sized to account for:

- Thrust loss due to reingestion of engine exhaust gases
- Change in aircraft lift due to jet induced interference (discussed in Section 4.3.1)
- Rearward tilt of the ADEN and RALS nozzles of 10^{o} to minimize reingestion losses
- Recovery of Reaction Control System thrust
- Tropical day temperature.

Vertical takeoff on a tropical day is the sizing point for the RALS D3 engine.

5.5.3 Transition Performance

The transition from hover to fully wing-borne flight is achieved by rotating the ADEN and RALS nozzles aft from the vertical according to the schedule shown in Fig. 4.3.2-1, and utilizing thrust modulation for pitch control.

Installed thrust used for the aircraft transition analysis of Section 7.5 are presented in Figures 10.2-29 through 10.2-32. The total gross thrust plot in Figure 10.2-29 represents RALS burner plus ADEN thrust, from Intermediate to Maximum Power. At Intermediate Power both the RALS burner and the ADEN afterburner are not operating and the thrust is therefore developed without reheat. Figure 10.2-31 shows the variation of the thrust split in this range of power settings, which is within flow shifting capability of the engine. Further reductions in power setting below Intermediate are scheduled to stay within the limits shown for 60% maximum A/B power in Figure 10.2-31.

The nozzle velocity ratios in Figure 10.2-32 were computed for the total gross thrust (ADEN & RALS burner) allowing for full expansion to ambient pressure.

5.6 REACTION CONTROLS

Aircraft control during the hover and transition mode of operation is provided by engine thrust control and core bleed air.

Pitch control is achieved by modulating the thrust split within the design capability of the engine. Nominal aircraft thrust balance is achieved with the ADEN developing 65% of the thrust split and the RALS burner providing the remaining 35%. The Study D3 engine has the capability to vary this split almost instantaneously to an upper limit of 46% for the RALS (ADEN thrust of 54%) and to a lower limit of 25% RALS thrust (ADEN at 75%). This variation in thrust split is provided by adjusting the fan airflow distribution using the internal bypass injectors, and adjusting the RALS and ADEN nozzle areas accordingly. Exhaust gas temperature is maintained throughout the flow transfer operation.

Yaw control is achieved by deflecting the RALS nozzle to the side. A total of ± 15 degrees yaw vectoring capability is available in the current design.

Roll control is provided by ducting core bleed air to roll control nozzles located in the wing tips of the aircraft. Hover engine performance includes an engine thrust penalty for this bleed flow, which is 10.6 lbs/sec/engine. To provide for maximum thrust recovery, roll control thrust vectors are directed down on both wing-tips. Roll is achieved by shifting bleed flow to the appropriate side by changing the corresponding nozzle areas.

Thrusts available for aircraft reaction control are shown in Figure 10.2-33.

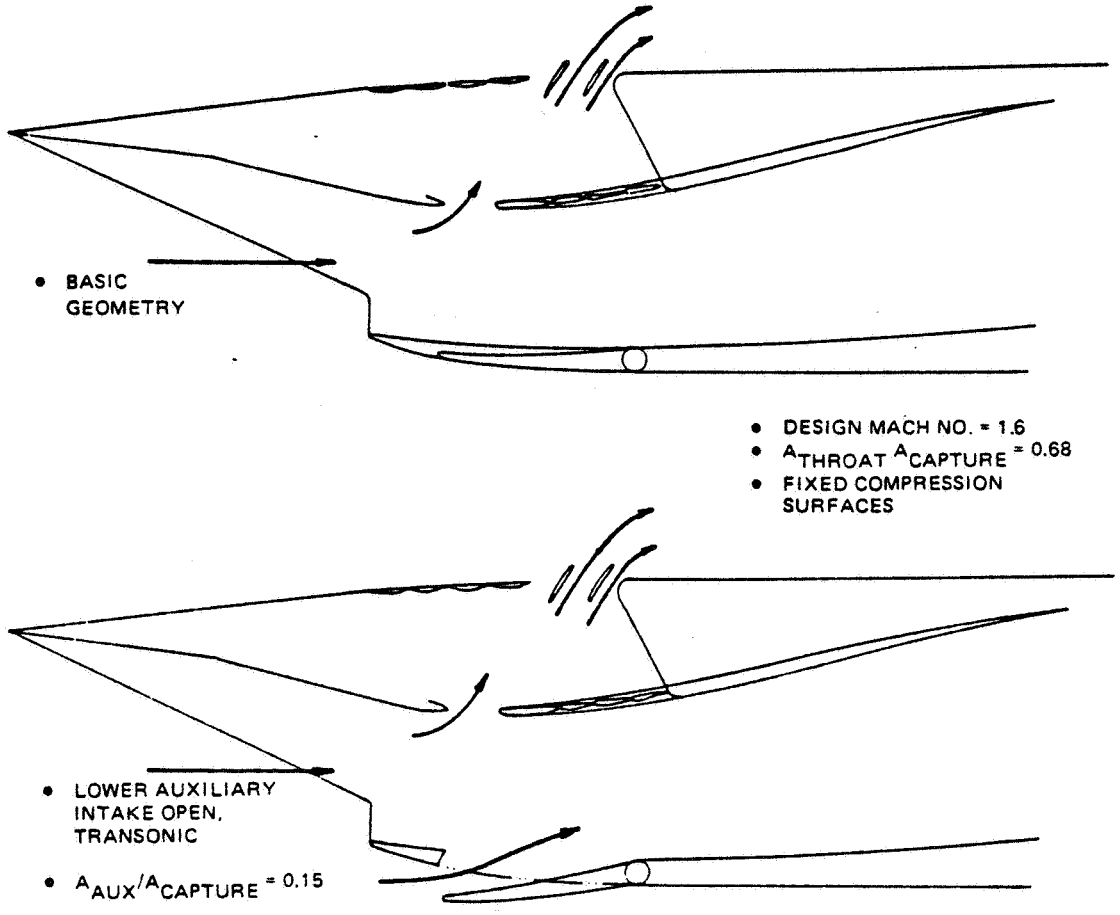

1690-165W

Figure 5.2-1 High Flow Inlet Design

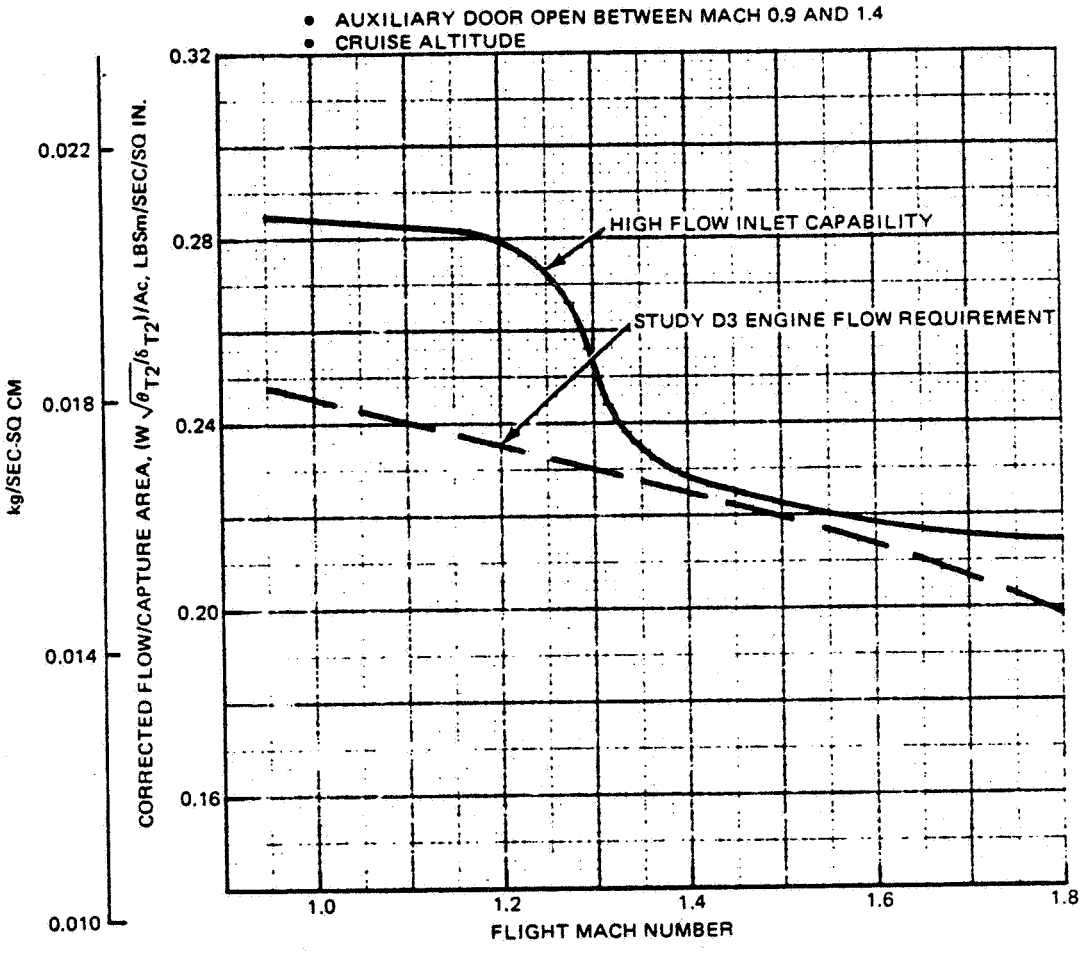

1690-127W

Figure 5.2-2 Inlet/Engine Matching for High-Flow System

- FIXED COMPRESSION SURFACES
- $M_{O_{DES}} = 1.6$
- $A_{THROAT}/A_{CAPTURE} = 0.68$
- AUXILIARY INLET OPEN AT MACH 0.9 & 1.2

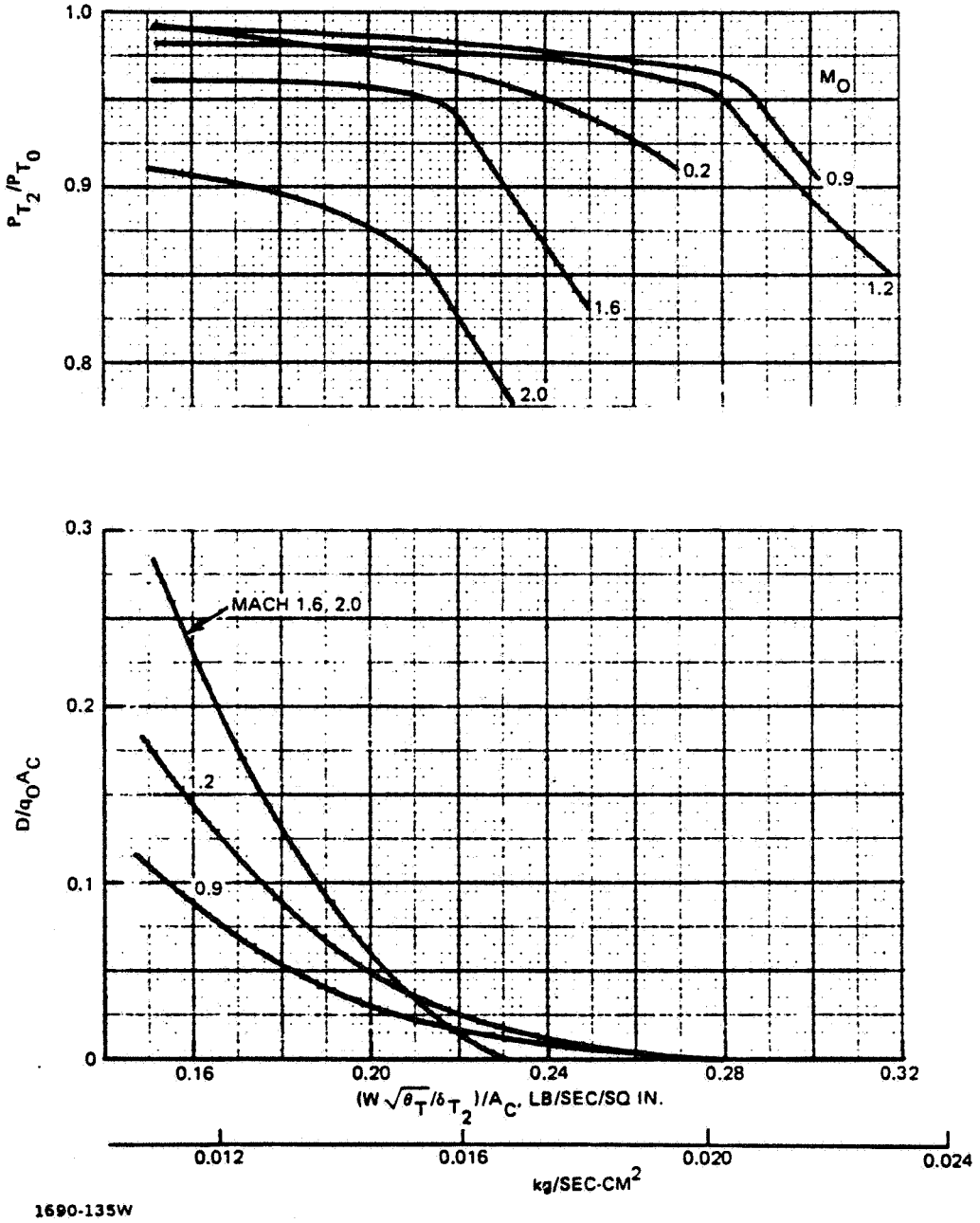

Figure 5.4.1-1 High-Flow Inlet Performance Characteristics

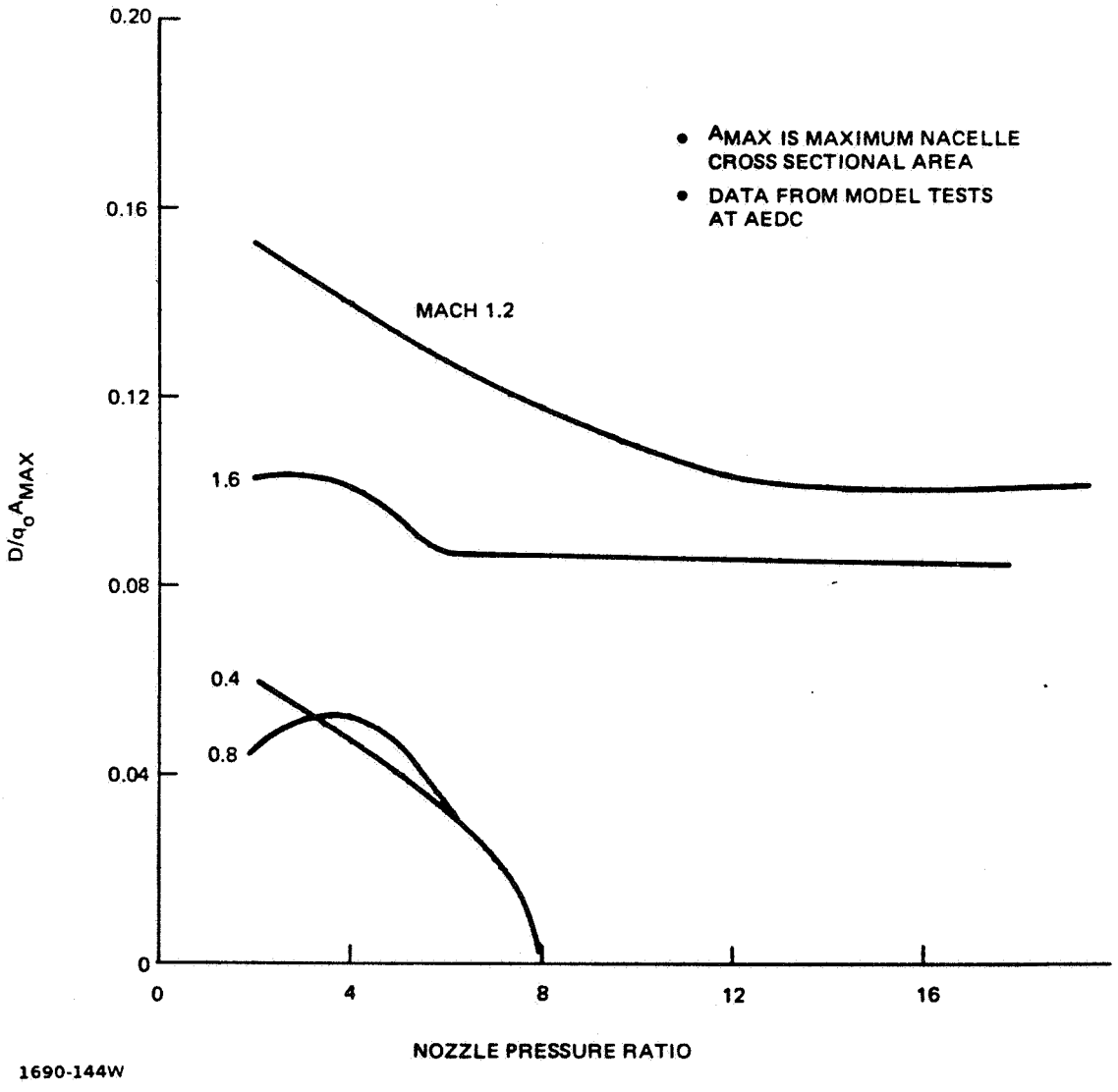

Figure 5.4.2-1 ADEN Nozzle Interference Drag Coefficient, Non-Afterburning, Sea Level

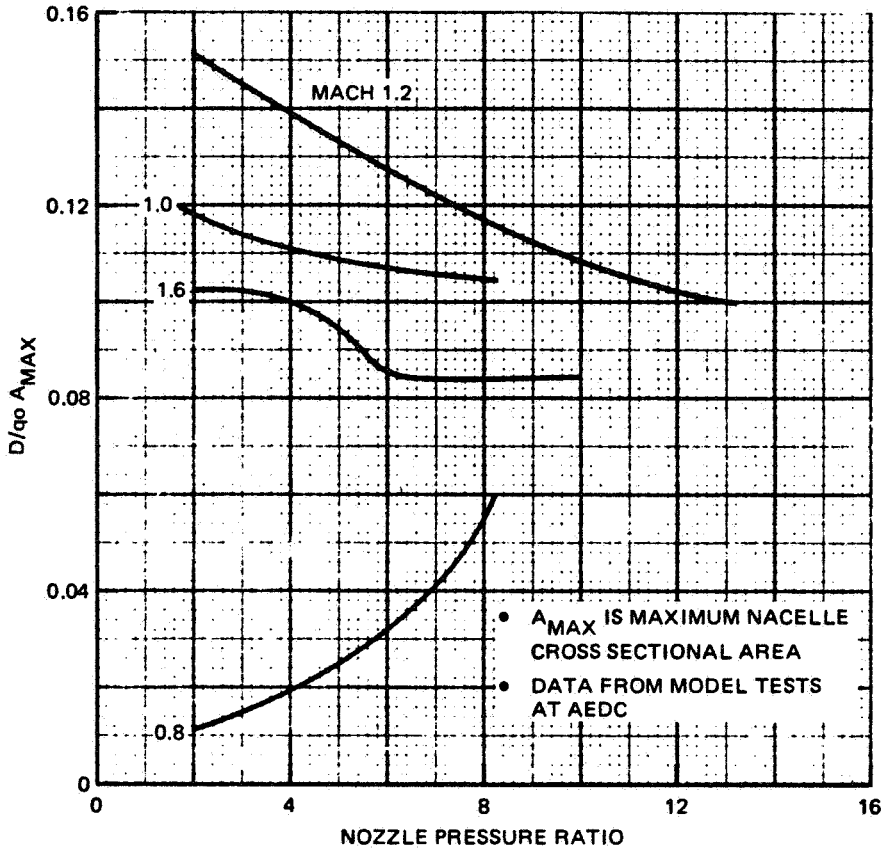

Figure 5.4.2-2 ADEN Nozzle Interference Drag Coefficient, Non-Afterburning, 40 000 Ft (12 192 m)

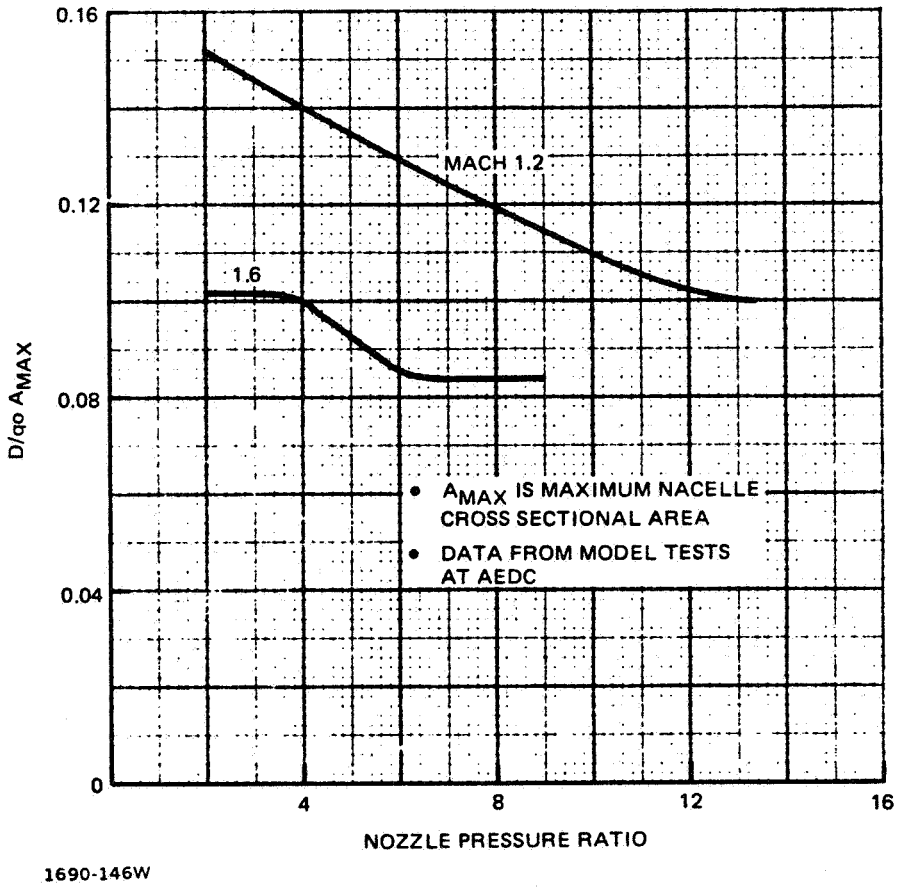

Figure 5.4.2-3 ADEN Nozzle Interference Drag Coefficient, Non-Afterburning, 70 000 Ft (21 336 m)

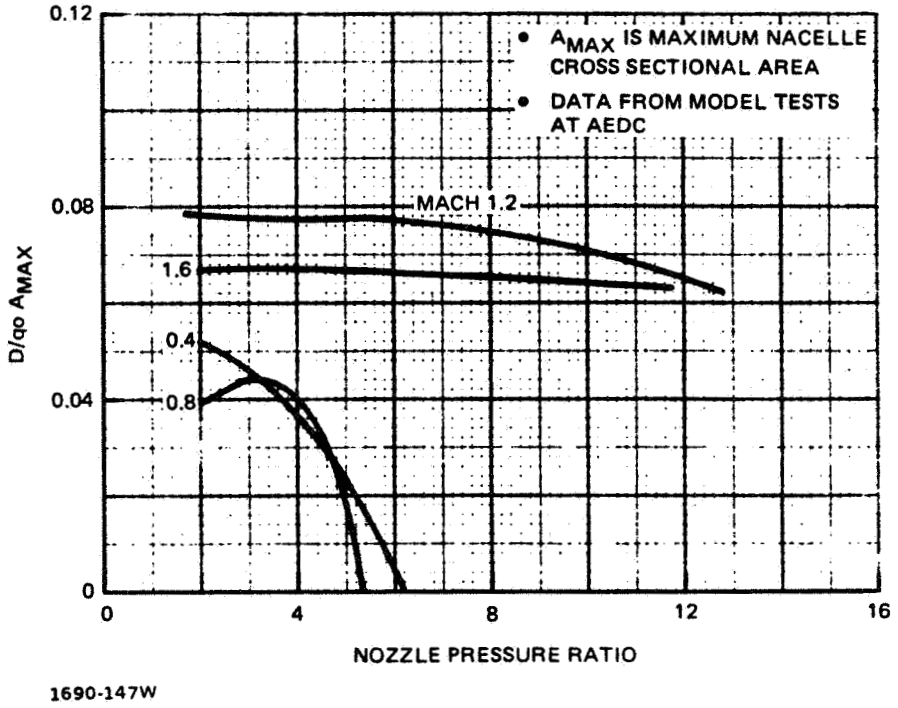

Figure 5.4.2-4 ADEN Nozzle Interference Drag Coefficient, Afterburning, Sea Level

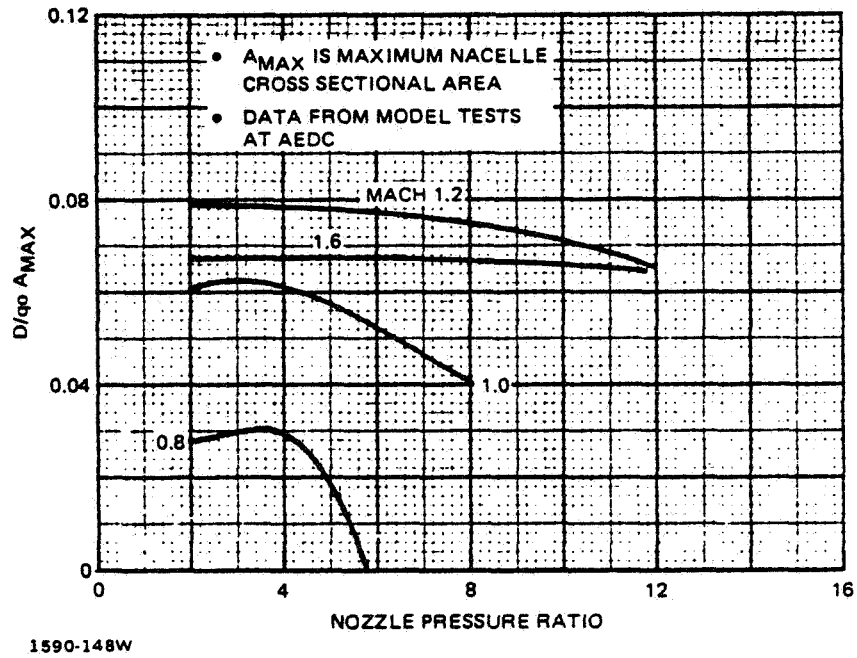

Figure 5.4.2-5 ADEN Nozzle Drag Coefficient, Afterburning, 40 000 Ft (12 192 m)

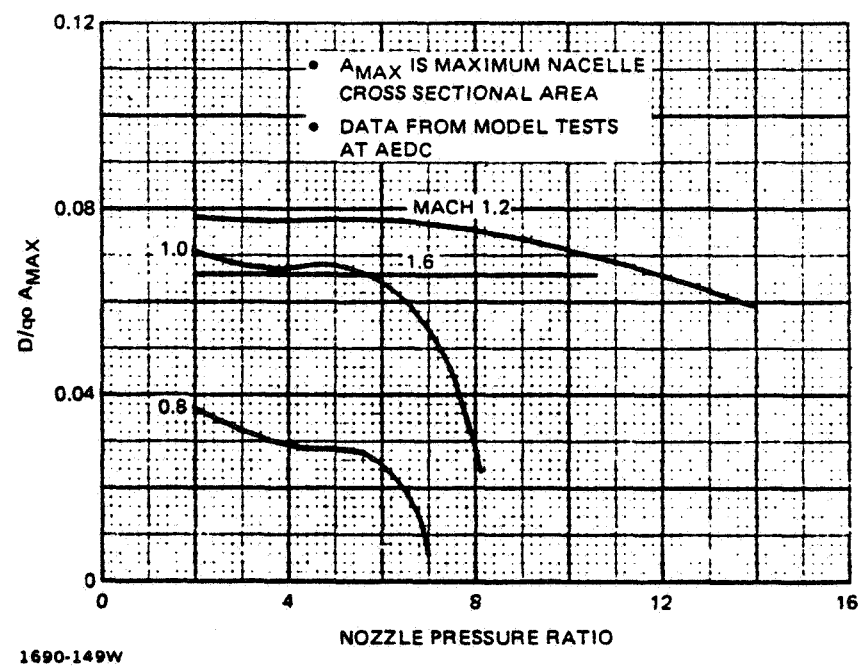

Figure 5.4.2-6 ADEN Nozzle Drag Coefficient, Afterburning, 70 000 Ft (21 336 m)

6 - AIRCRAFT DESIGN

6.1 FLIGHT CONTROLS

Control is provided by a triple digital channel fly-by-wire (FBW) flight control system. Pilot input to the flight computers is accomplished by triplex transducing signals. Rate and acceleration inputs are provided by cone-configured, skewed axis gyro and accelerometer packages. The flight control system handles all aspects of aerodynamic flight as well as control in the hover and transition flight modes. Table 6.1-1 shows the primary control modes and control functions.

6.2 STRUCTURAL DESIGN DESCRIPTION

Design 623-2024 structural components are a blend of advanced composites and metallic materials applying advanced manufacturing technology appropriate to a 1995 IOC airframe.

The primary structural materials are:

(A) Non-metallic

- Graphite, Boron, Kevlar/Epoxy
- Graphite/Polyimide

(B) Metallic

- Advanced Aluminum alloys
- Aluminum powder and wrought alloys
- Advanced Titanium alloys
- Advanced Titanium powder alloys.

Manufacturing technology includes automated tape layup and co-curing, for the composites/epoxy matrix materials, and extensive use of powder-metallurgy, super-plastic forming (SPF), weld, adhesive and diffusion bonding (DB) for the advanced metallic structure.

The projected weight savings, discussed in section 7.3.1, are a result of in-house studies that applied the advanced materials and manufacturing technologies to conceptual airframes (Reference 6-1).

6.2.1 Wing Structure

The wing consists of a thru-box with continuous covers extending from wing fold joint to wing fold joint. Multi-spar semi-sine wave beam construction is used to obtain maximum

Table 6.1-1 Flight Control Mode and Function Summary

MODE	CONTROL FUNCTION				WING LOAD OPTIMIZATION
	ROLL	PITCH	YAW	THRUST	
VTOL/HOVER	• RCS	• MODULATED ADEN & RALS THRUST	• LATERAL RALS	• ADEN+RALS+RCS	–
STOL/TRANSITION	• RCS • DIFFERENTIAL FLAPS	• MODULATED ADEN & RALS THRUST • CANARD • CANARD LE/TE DEVICES	• LATERAL RALS • RUDDERS	• ADEN+RALS+RCS	–
WING-BORNE	• DIFFERENTIAL FLAPS	• CANARD • CANARD LE/TE DEVICES	• RUDDERS	• ADEN	• WING LE/TE DEVICES • LE DEVICE

1690-136W

structural efficiency for the desired low thickness ratio wing section. The wing is predominantly graphite/epoxy (covers and spars) with boron/epoxy reenforcement in the highly loaded areas. The rear beam is titanium as are the major rib fittings, fuselage attachment and wing store support ribs. Leading and trailing edge variable camber surfaces use aluminum skins supported and actuated by high strength steel elements.

6.2.2 Fuselage Structure

The fuselage structure uses a combination of advanced composite and metallic construction. Extensive use is made of large skin/stiffener/frame sub-assemblies fabricated from co-cured graphite/epoxy and SPF/DB titanium. The major load-carrying bulkheads and frames are predominantly titanium. Hot areas are fabricated from titanium, graphite/polyimide and, in selected areas, high strength steel.

Graphite-epoxy shear panels are assumed designed for buckling at ultimate load to gain the weight advantage of post-buckled graphite/epoxy shear panel strength. Composite skin and shear panels use integral and co-cured stiffeners selectively strengthened with boron/epoxy where load intensity is high. Titanium skins are beaded or corrugation-stiffened using the SPF/DB technique. Aluminum skins employ weld or adhesive bonded stiffeners and beads.

6.2.3 Canard and Vertical Tail

The canard and vertical tail covers are pre-cured graphite/epoxy covers bonded to reinforced plastic (HRP) core substructure. The canard flap leading and trailing edge devices and rudders are similarly constructed. The canard pivot fitting is titanium as are the fore and aft canard spars which must distribute the canard flap loads.

6.2.4 Alighting Gear

The main landing gear materials are projected as high strength steel and titanium. Advanced graphite/epoxy is projected for the drag braces. Brake assemblies are carbon composition.

6.2.5 1995 IOC Material Usage

The projected material usage for the 1995 IOC airframe assumed in this study is shown in Figure 6.2-1. The material mix forms the basis for the anticipated structural weight savings discussed in section 7.3.1.

MATERIAL	% USAGE
GRAPHITE	41.1
GLASS	4.3
TITANIUM	26.7
ALUMINUM	14.6
STEEL	8.4
MISCELLANEOUS MTLS	4.9

1690-100W

Figure 6.2-1 Design 623 – 2024 1995 IOC Material Mix

6.3 MASS PROPERTIES

Design 623-2024 Design Take-Off Gross Weight (TOGW) was derived by the use of the Computerized Initial Sizing Estimate (CISE) program. CISE employs a level I and II series of weight prediction equations developed for fighter/attack aircraft. Modifications were made to account Design 623-2024's unique features. A more detailed description of CISE follows in section 7.2.

Figures 6.3-1 and 6.3-2 present the group weight-empty statement and mission loading. The mission loading tables show loadings for the Deck Launched Intercept (DLI) mission as well as the alternate Combat Air Patrol (CAP) and Subsonic Surface Surveillance (SSS) alternate STOVL missions.

The mission loadings show a maximum internal fuel load of 11618 lb (5270 kg) (refer to STOVL/CAP mission, Fig. 6.3-2) and a VTO internal fuel load of 10618 lb (4816 kg) in VTO. The additional fuel, above VTO fuel required, resulted from additional internal volume generated during the final configuration development. The additional volume is allotted to fuel for STOVL missions.

Figure 6.3-3 shows the center of gravity (CG) location and inertias for take-off-gross weight and landing weight in tabular form. Figure 6.3-4 shows the CG travel graphically.

6.4 CREW STATION

Design 623 as depicted in Figure 3.5-2 (general arrangement drawing) provides a single seat crew station capable of accepting future cockpit displays and controls. The canopy/nose design permits desired external visibility and meets the VTOL over the nose vision requirement of 25 degrees (Ref. MIL-STD-850B). The one piece canopy/windshield design eliminates conventional windshield bow obstruction of the external visibility envelope.

GROUP	WEIGHT, LB (kg)	
WING	3 109	(1 410)
CANARD	460	(209)
VERTICAL TAIL	354	(161)
BODY	4 652	(2 110)
ALIGHTING GEAR	1 798	(816)
ARRESTING GEAR	—	—
ENGINE SECTION	173	(78)
AIR INDUCTION	580	(263)
STRUCTURE WEIGHT (SUB TOTAL)	11 126	(5 047)
PROPULSION	7 018	(3 184)
FUEL SYSTEM	956	(434)
FLIGHT CONTROLS	1 113	(505)
AUXILIARY POWER PLANT	—	—
INSTRUMENTS	180	(82)
HYDRAULICS AND PNEUMATICS	543	(246)
ELECTRICAL SYSTEM	465	(211)
AVIONICS (INST. FACTOR 1.25)	1 500	(680)
ARMAMENT	191	(87)
FURNISHINGS AND EQUIPMENT	205	(93)
AIR CONDITIONING & ANTI ICING	452	(205)
LOAD AND HANDLING	9	(4)
CONTINGENCY	498	(226)
WEIGHT EMPTY	24 256	(11 003)

1690-077W

Figure 6-3.1 Design 623 – 2024 Group Weight Statement

	VTO/DLI MISSION		STOVL/CAP MISSION		STOVL/SS MISSION		STOVL/SSS MISSION EXTENDED	
CREW	180	(82)	180	(82)	180	(82)	180	(82)
FUEL-UNUSABLE	49	(22)	49	(22)	49	(22)	49	(22)
-USABLE	10 618	(4 816)	11 618	(5 270)	11 618	(5 270)	13 568	(6,154)
OIL	149	(68)	149	(68)	149	(68)	149	(68)
EQUIPMENT	60	(27)	60	(27)	60	(27)	60	(27)
(2) AIM-7 SPARROW	1 000	(454)	1 000	(454)	–	–	–	–
(2) AIM-9 SIDEWINDER	390	(177)	390	(177)	390	(177)	390	(177)
(2) AGM-84 HARPOON	–	–	–	–	2 300	(1 043)	2 300	(1 043)
(1) GUN/AMMO	674	(306)	674	(306)	674	(306)	674	(306)
PYLONS & RACKS	350	(159)	350	(159)	372	(169)	492	(223)
300 GALLON (1136 ℓ) TANK	–	–	–	–	–	–	198	(90)
TOTAL USEFUL LOAD	13 470	(6 110)	14 470	(6 563)	15 792	(7 163)	18 060	(8 192)
WEIGHT EMPTY	24 256	(11 003)	24 256	(11 003)	24 256	(11 003)	24 256	(11 003)
TAKE-OFF GROSS WT.	37 726	(17 113)	38 726	(17 566)	40 048	(18 166)	42 315	(19 196)

1690-078W

Figure 6-3.2 Design 623-2024 Mission Load and Take-Off Gross Weight, lb (kg)

CONDITION	WEIGHT LB (kg)	CG % MAC	Ixx SLUG-FT^2 (kg-m^2)	Iyy SLUG-FT^2 (kg-m^2)	Izz SLUG-FT^2 (kg-m^2)
TAKE-OFF VTO	37726 (17113)	-17.2	31754 (23441)	123412 (91103)	149940 (110686)
LANDING WEIGHT	27867 (12640)	-23.0	30974 (22865)	103794 (76621)	130048 (96001)

1690-102W

Figure 6.3-3 Design 623 – 2024 CG and Inertia DLI - Mission Loading

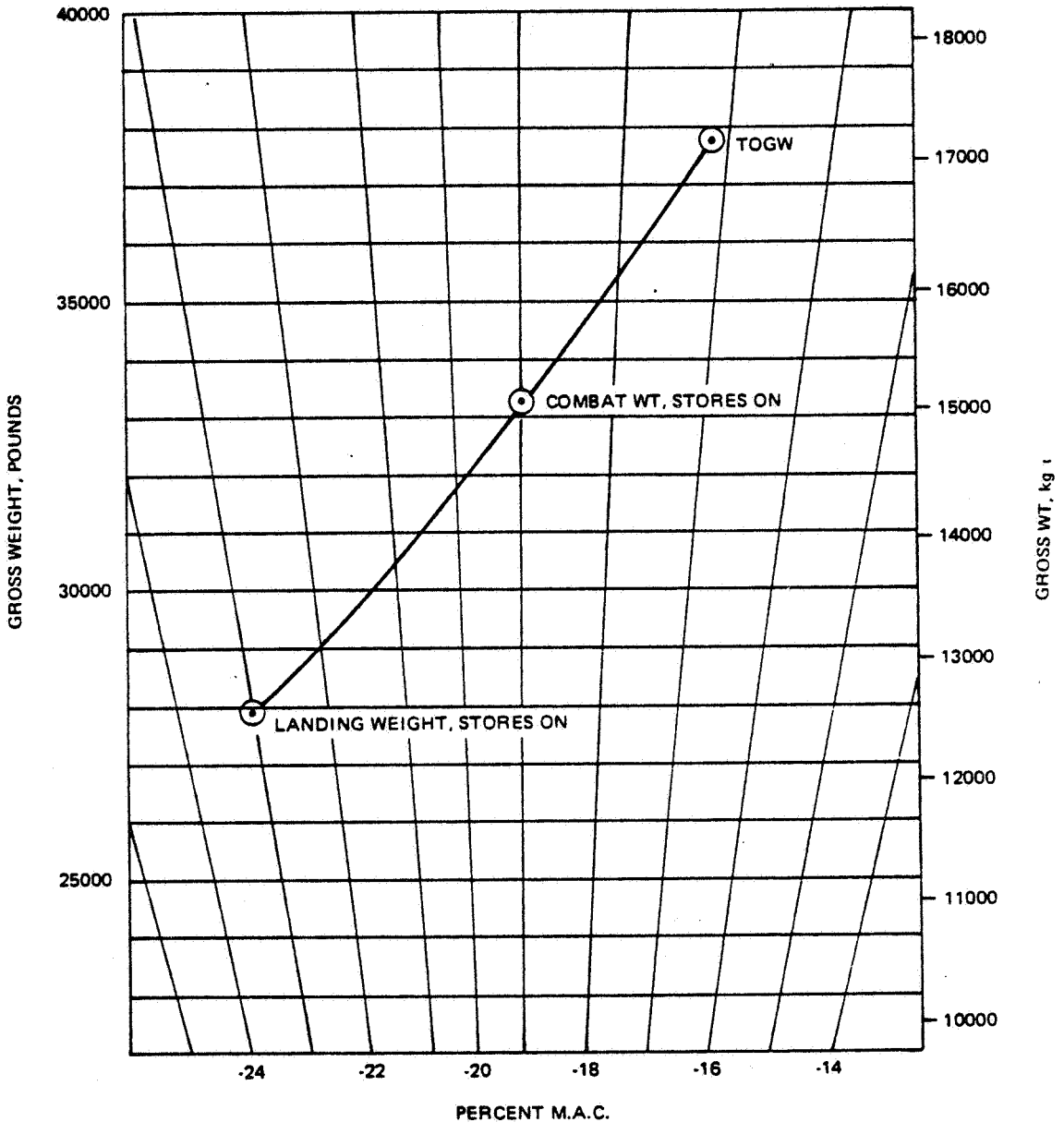

Figure 6-3.4 Design 623 – 2024, Center of Gravity Travel DLI Mission Load

6.5 SUB SYSTEMS

6.5.1 Pilot Station

The primary controls, for conventional flight and VTOL/Hover, are as follows:

- Two-Axis DHC (Displacement Hand Controller), Central Location
- Rudder Pedals
- Thrust Control Quadrant

The DHC controls roll and pitch via transducer inputs to the FBW flight control system. Yaw is facilitated by rudder pedals. Translation, forward, aft and laterally, is accomplished by the combined use of the thrust vector control quadrant and the DHC.

Primary flight information is handled by a head-up-display (HUD) system. Alternate display and information is provided by command/voice warning.

6.5.2 Flight & Hover Controls

Control of aero surfaces and VTOL dedicated equipment (nozzle vectoring and modulation) will be by servo-feed-back actuation commanded by the digital FBW system using the pilot and/or flight control and navigation computer systems. The FBW flight control is configured as a fail-operational - operational (fail-op^2) digital system consistent with the control configured levels of instability in Design 623. The power for actuators are provided by three independent hydraulic systems consistent with the state of the art for the 1990 time period.

6.5.3 Electrical Power Systems

There are two potential systems which are applicable for Design 623: The Variable Speed Constant Frequency (VSCF) generating system and the High Voltage DC (HVDC) generating system. Final recommendations regarding electrical system type will result from continuing and future studies.

6.5.4 Environmental Control System (ECS)

The conceptual ECS for Design 623 is derived from a basic bootstrap air cycle machine using ram air as the heat sink.

The ECS provides cockpit cooling or heating and thermal control of avionics and weapons. It will also provide cockpit pressurization, wind screen anti-icing, rain removal and canopy defogging.

6.5.5 Avionics

A baseline functional avionics system concept has been generated to support V/STOL vehicle sizing studies. The V/STOL baseline avionics concept includes a multi-mode, (air-to-air and air-to-surface) search/track fire control radar system. Air-to-air combat avionics capability is configured for multiweapon/multi-target attack with advanced air-to-air missiles and/or gun. The radar features a noncooperative target recognition capability, allowing beyond visual range weapon launch. An antiship standoff weapon delivery attack function using a Synthetic Aperture Radar (SAR) mode is included to enhance the V/STOL role in sea control. Accurate conventional or guided weapon delivery against land targets under all-weather conditions is an additional feature.

6.5.6 Armament

Weapons configuration for the basic DLI mission consists of:

- (2) AIM-7 Sparrow - Externally mounted
- (2) AIM-9 Sidewinder - Externally mounted
- (1) 20 mm gun and ammunition - internally mounted

Additional external store provisions are provided on the aircraft fuselage centerline and under-wing locations. External store stations are supplied with electrical, ECS and fluid couplings to enable the carriage of a wide variety of stores.

6.5.7 Fuel System

A single point pressure fueling station is provided. The primary fuel load is located in eight main tanks, five bladder tanks between the engines (three forward and two aft of the wing box), plus one integral fuel tank in the center wing box, with two self-sealing fuel tanks just below.

7 - AIRCRAFT PERFORMANCE

7.1 COMBAT PERFORMANCE

The maneuverability of the Design 623-2024 aircraft is indicated by the variations of specific excess power (P_s) with normal load factor depicted in Figures 7.1-1 thru 7.1-5 for various altitudes at the Mach numbers specified in the Statement of Work. These data are applicable to the configuration with the DLI mission external store loading of two AIM-7 and two AIM-9 missiles at a combat weight which equals 88 percent of VTO weight. Due to the combination of high T/W required for VTO operation and advanced technology in aerodynamics, propulsion and materials, the performance requirement of the Statement of Work are far exceeded. From Figure 7.1-2, it may be seen that the sustained normal load factor at M=0.60 and an altitude of 10,000 feet (3048m) is 6.8 (vs a requirement of 6.2), nearly equal the 7.0g structural limit of the aircraft. The specific excess power (P_s) available during level flight at a Mach number of 0.90, 10,000 feet (3048m) altitude is 1130 fps (344 m/s) as shown in Figure 7.2-3, far exceeding the required value of 900 fps (274 m/s). It should be noted that this outstanding maneuver capability has been obtained by conservatively not taking any benefit for supercirculation effects.

The acceleration and maximum Mach number capability of the design are depicted in Figures 7.1-6 and 7.1-7, respectively. Due to the high T/W of the propulsion system, excellent acceleration times are achieved. Maximum Mach number capability of the aircraft emanates from inlet and structural design considerations.

7.2 CONFIGURATION SELECTION

The technique used to develop Design 623-2024 is based on a Grumman developed computer program known as the Computerized Initial Sizing Estimate (CISE). CISE enables the initial sizing of airplanes in the "zero" level of design (i.e. before a layout is made). The program serves as an aid in making early decisions about an airplane's optimum size and general characteristics (e.g. engine size, wing area, aspect ratio). CISE provides a rapid and efficient method of determining aircraft sensitivity to major changes such as mission-radius or engine type.

Figure 7.2-1 is an abbreviated flow chart of the program. The initial assumption of TOGW is generated by an equation that accounts for mission load and radius. The value of the initial assumption, however, does not affect the final answer because the program is

designed to iterate on TOGW until it converges to an acceptable solution. Assuming there is no previous geometric data on an airplane that would fulfill a given set of mission requirements and that no bias pre-exists (e.g. "let us use a canard design"), CISE will initially create a geometry based on "historical" trends.

After an initial solution is reached a map of principle parameters (e.g. aspect ratio, wing loading, sweep, thrust-to-weight) is generated in order to determine an optimum configuration. The required fuel (for a given TOGW and geometry) is determined by using tabular engine data and a combination of analytical and empirical aerodynamics methods.

7.2.1 Optimum Configuration Selection

As an aid to the selection of an optimum configuration a series of carpet plots of thrust-to-weight t/w and wing load w/s was generated using CISE. To further assist the configuration selection, carpet plots of specific excess power (P_S), acceleration time and sustained g's were generated relative to t/w and w/s over a range of aspect ratios, and wing sweep values. The parametric ranges are:

- Aspect ratio: 3.0 to 4.5
- Wing sweep: 30, 35, 40 degrees
- Wing loading: 90 to 110 lb/ft^2 (439-537 kg/m^2)
- Thrust-to-Weight: 1.3 to 1.5

Figure 7.2-2 presents a typical carpet plot, for an aspect ratio of 3.75, leading edge sweep of 35 degrees, showing the effects on TOGW of the geometry and performance parametrics discussed. Superimposed on the carpet is the thrust to weight constraint for VTO.

An evaluation of the carpet plot series, along with other pertinent considerations (e.g. STOL performance, aerodynamics) enabled the final Design 623 configuration to be established.

7.2.2 Design Mission Definition

In order to establish Design 623-2024 a design mission must be inputted into CISE. The selected design mission is the VTO Deck Launched Intercept (DLI) profile. Airplane and mission loading is:

- 1200 lb (544 kg) Avionics (uninstalled weight)
- (2) AIM-7 Sparrows (external)
- (2) AIM-9 Sidewinder (external)
- Gun/Ammunition carried internally.

The inputted mission profile is described in Figure 7.2-3 and is inputted into CISE along with airplane aerodynamic performance characteristics, as described in Section 4.1, Figures 4.1.4-5 thru 8, and engine performance data for the SYS-GE16-VVCES Study D-3 RALS engine. 1995 IOC materials and manufacturing technology are inputted to generate the proper levels of structural weight. Figure 7.2-4 presents the DLI mission fuel, Mach number, distance and altitude summary for a radius of 150 nm (278 km).

7.3 DESIGN MISSION SENSITIVITIES

In order to establish a reasonable configuration (e.g. weight, fuel load, dimensions) an understanding of the vehicle "drivers" is required. The approach used was to vary the airplane's significant parameters, in the CISE program, within the DLI mission requirements.

7.3.1 Materials and Manufacturing Technology

Since the airplane is to be designed for an Advanced IOC, the applicable material technology must be inputted into CISE. The input format is in the form of projected structural weight savings percentage broken down by groups as follows:

- Wing
- Vertical Tail
- Horizontal Tail (Canard)
- Body
- Alighting Gear
- Air Induction

The percent savings have been developed from a continuing in-house effort, by the Advanced Composites Group and Materials - Process Engineering, and represents the current projected structural savings over a current state-of-the-art "conventional" aluminum aircraft circa 1970. The savings presented assumes the use of non-metallic composites material and manufacturing technology as well as advanced metallic material technology and manufacturing such as aluminum-lithium alloys, diffusion bonded/super-plastic formed titanium alloys.

Figure 7.3-1 presents the inputted structural weight savings for three IOC dates. The selected materials technology for Design 623-2024 is 1995 IOC. Figure 7.3-2 shows the effect on TOGW for the three material technology dates examined.

7.3.2 Combat Allowance Sensitivity

Combat fuel allowance is a strong driver in the DLI mission. As a result the combat allowance was examined in from several points of view.

Figure 7.3-3 and 7-3.4 show the sensitivity of combat allowance to take-off gross weight. It is evident that the combat turn is a larger driver of TOGW than change in total Energy (ΔE_s). Obviously some of the turn capability can be traded off for additional ΔE_s or the ΔE_s fuel can go to increasing the turn. Since the combat allowance was generated by a 1/2-turn plus 41000 ft (12498 m), a look at the fuel breakdown, for combat, would be more informative.

Figures 7.3-5 and 7.3-6 show the fuel required for turns and ΔE_s. The term, ΔE_s, represents the total energy change available to the aircraft. To execute a half turn, at Mach 1.6 and 40000 ft (12192 m) requires 735 lb (333 kg) of fuel while the required ΔE_s value demands 1157 lb (529 kg). The total of 1892 lb (858 kg) of fuel can be apportioned as defined in the DLI mission or can be used to execute additional turn, or generate a higher level of ΔE_s but not simultaneously. The total combat fuel allowance, and its sensitivity on TOGW, is shown in Figure 7.3-7. The implication, in the data presented, is that the DLI mission specifies adequate combat capability, at a radius of 150 nm (278 km). As Figure 7.3-7 indicates an increase in combat fuel (i.e. capability) can be achieved but only at a considerable cost in increased TOGW.

7.3.3 Parametric Sensitivities

Other parametric variations were examined for their effect on TOGW. The parameters examined are:

- Change in Engine t/w (uninstalled)
- Change in Engine SFC
- Uninstalled Avionics Weight

Changes in Engine SFC and t/w appear to be the second biggest drivers to TOGW. A change in ten percent in thrust-to-weight produces a take-off gross weight change of 2175 lb (987 kg). A similar (10%) change in SFC yields a 3375 lb (1531 kg) change in TOGW. While uninstalled avionics drives volume and supporting system weight its sensitivity is not as severe as engine t/w or SFC. For example, a 10% change in avionics weight will yield an 1175 lb (533 kg) change in TOGW. Since the avionics system is potentially the most variable of the weight items it was selected to show vehicle TOGW sensitivity. Figures 7.3-8 and

7.3-9 shows the TOGW sensitivities of engine t/w and SFC. Figure 7.3-10 presents the sensitivity of TOGW to avionics weight.

7.3.4 Mission Sensitivities, DLI Mission

The first parametric investigation performed was the TOGW sensitivity to mission radius in the DLI mission. Figure 7.3-11 indicates a high sensitivity of TOGW to dash-out radius at Mach 1.6, 40000 ft (12192 m). The approximate change rate of TOGW (growth factor) is 80 lb/n.mi (50.4 kg/km).

Figure 7.3-12 shows the effect of dash speed on DLI mission radius. It is interesting to note that for radii of less than 100 nm (185 km) the maximum allowable dash speed permitted is the same as the maximum capable dash speed of the airplane at 40000 ft (12192 m). As the radius increases, beyond 100 nm (185 km), the allowable dash speed must be rapidly reduced. At a radius of 175 nm (324 km) dash speed is low enough so that the airplane can continue without afterburner. Beyond a radius of 275 n. mi (509 km) the dash speed must be subsonic. In other words, for a fixed amount of fuel, the maximum allowable dash Mach number is a function of radius. For a short radius, a higher thrust, and consequently higher SFC is allowed to maximize dash Mach number. For an increasingly longer radius, engine thrust (i.e. lower SFC) must be reduced to achieve the radius and still have fuel for combat and return to base station.

Figure 7.3-13 shows the effect of changing engine SFC on the DLI mission radius. Small changes in predicted engine SFC can produce significant changes in DLI mission radius for a constant gross weight aircraft. The change is more pronounced when SFC is improved (negative change) since an increasingly lower percentage of the total fuel is used for the initial climb and acceleration to dash Mach number.

7.4 ALTERNATE MISSIONS

Two alternate missions have been evaluated for the STO mode of operation. Additionally, ferry range has been estimated for VTO and STO. The alternate missions were evaluated by inputting Design 623-2024 geometry, weights and drag characteristics into CISE as a "frozen" airplane and exercising the mission solution capability of the program.

7.4.1 STOVL Combat Air Patrol (CAP) Mission

The STOVL/CAP mission requires the aircraft to loiter at some radius from its launch point, then be directed to an air target. The mission is subsonic with the exception of the combat leg. Dash to target and combat is conducted supersonically.

The mission loading is:

- (2) AIM-7 Sparrow
- (2) AIM-9 Sidewinder
- (1) Gun/Ammunition

Stores are assumed to be retained throughout the mission. STO weight, for the CAP mission, is 38726 lb (17566 kg) with 11618 lb (5270 kg) of fuel carried internally. The STOVL/CAP mission profile is described in Figure 7.4-1.

7.4.2 STOVL Subsonic Surface Surveillance (SSS) Mission

The STOVL/SSS is an air-to-surface anti-shipping mission that requires the aircraft to loiter at a radius from launch point, then execute a surveillance and/or attack of a surface target. The mission is examined with and without external fuel.

The mission load is:

- (2) AGM-84 Harpoon
- (2) AIM-9 Sidewinder
- (1) Gun/Ammunition
- (1) 300 gallon (1136 l) fuel tank (optional)

STO weight for the SSS mission is 40048 lb (18165 kg) with 11618 lb (5270 kg) of fuel carried internally and, alternately, 42316 lb (19194 kg) when a 300 gallon (1136 l) center line fuel tank is carried. The STOVL/SSS mission profile is described in Figure 7.4-2.

7.4.3 Ferry Range

Ferry ranges are estimated for a clean aircraft (no stores, no ammunition) with 11618 lb (5270 kg) of fuel carried internally. VTO and STO take off weight is 36866 lb (16722 kg).

- VTO ferry range with 11618 lb fuel (5270 kg) 1110 n. mi (2056 km)
- STO ferry range with 11618 lb fuel (5270 kg) 1260 n. mi (2334 km)

The ferry ranges shown are for cruise at Mach 0.8, 48000 feet (14630 m) with 10 minutes loiter capability at sea level plus 5% reserve. Ferry range can be considerably increased if external fuel is carried.

7.4.4 CAP and SSS Mission Performance Summary

Loiter time vs radius for the CAP and SSS STOVL missions are presented in Figures 7.4-3 and 7.4-4. A mission fuel breakdown for the STOVL/CAP and STOVL/SSS missions are presented in Figure 7.4-5 and 7.4-6.

7.5 VTOL ANALYSIS

7.5.1 Hover Control Power

The propulsion system of Design 623-2024 has been sized to provide adequate control power when operating in jet-borne flight. Roll control is provided by wing tip mounted Reaction Control System (RCS) jets. During normal operation, these jets operate in a continuous symmetric (i.e. "down-down") manner. To impart a rolling motion to the aircraft, one RCS nozzle is shut and total RCS flow is exhausted through the remaining open nozzle at the opposite wing tip. Pitch control is attained by changing the thrust split (i.e. flow shifting) between the RALS and ADEN nozzles. Yawing motion is generated by sideward deflection of the RALS nozzle (up to a maximum of 15 degrees).

The maximum control power available about each axis is shown below compared with the minimum levels of reference 7.5-1. These data were generated at the DLI mission VTO weight utilizing the inertia and propulsion information presented in sections 6.3 and 5.5, respectively.

	Design 623-2024	Agard 577 Minimum Value
Roll $\ddot{\phi}$ (rad/sec^2)	0.80	0.80
Pitch $\ddot{\theta}$ (rad/sec^2) nose up	0.99	0.40
nose down	0.95	0.40
Yaw $\ddot{\psi}$ (rad/sec^2)	0.59	0.35

7.5.2 Transition Analysis

Transition trajectories for the Design 623-2024 have been generated for both take-off and landing phases of the VTOL DLI mission. A steady-state method of computerized analysis is employed which determines the static trim characteristics during transition at discrete values of airspeed for fixed values of angle of attack, flight path angle, acceleration and aircraft configuration. The scheme employed to trim the aircraft is contingent on the flight mode. In hover, pitch attitude and thrust of the fore and aft nozzles are used. In transition, the aircraft is trimmed by nozzle deflection angle and thrust. When the ADEN nozzle is at 0° deflection, the vehicle is fully wing-borne and is trimmed by variation of angle of attack, canard deflection, and power setting. At each static trim condition, the computer program also has the capability of determining the maximum instantaneous pitch control power available from both flow shifting between fore and aft nozzles and from deflection of the canard.

Basic aerodynamic data employed in the analysis is contained in Figures 7.5-1 through 7.5-3. These data have been obtained by modifying the basic aerodynamic data of Section 4.1 to account (from information contained in References 4.1.2-6 and 4.3.3-1) for deflection of the wing trailing edge devices which are used to increase aerodynamic lift during transition. Canard control effectiveness used is the same as that contained in Section 4.1.3, while incremental drag due to canard deflection was obtained from Reference 4.1.2-4. The installed engine performance which was used is presented in Section 5.0, the applicable jet-induced interference effects in Section 4.3, and weight, center of gravity and inertia data in Section 6.3.

Transition trajectories are presented in the format of lift/cruise (ADEN) deflection angle necessary for vehicle static trim as a function of airspeed for transitions at fixed combinations of flight path angle and angle of attack. The corresponding deflection angle of the forward RALS nozzle is uniquely defined by the nozzle gearing ratio (Figure 4.3.2-1 is reproduced as Figure 7.5-4 for the reader's convenience). Typical transition trajectories are presented in Figures 7.5-5 and 7.5-6 for the DLI mission takeoff and landing phases, respectively. Approximate conversion speed for both take-off and landing is 200 knots (103 m/s). Flight path angle during the transition has only a moderate effect as shown in Figures 7.5-7 and 7.5-8.

Excellent pitch control is available throughout transition. Figure 7.5-9 depicts the available control power due to both propulsion and aerodynamic control devices during a take-off transition at an angle of attack of 4 degrees. The guideline levels of pitch control power of Reference 7.5-1 are exceeded throughout the transition velocity range.

7.6 STO PERFORMANCE

The STO take-off procedure envisaged for the Design 623-2024 aircraft is a straightforward one designed to minimize pilot workload and vehicle complexity. The deflections of both the RALS and ADEN nozzles are preset to a specified value, which corresponds to the same gearing relationship utilized in transition (see Figure 4.3.2-1). This eliminates pitching moments due to direct thrust effects. Wing trailing edge devices are deflected and the canard is preset to a positive incidence to maximize aerodynamic lift at the end of the ground roll. The throttle is advanced to a power setting equivalent to that used in VTO, which allows sufficient thrust modulation capability to reside in the propulsion system for aircraft rotation once lift-off speed is attained and for pitch control in the transition flight phase. The brakes are released and the ground roll is commenced. Once lift-off speed is attained, the aircraft is rotated to a predetermined angle of attack. The aircraft lifts off and transition to fully wing-borne flight is initiated.

A two-degree-of-freedom method of analysis was employed to evaluate STO performance capability. Pitching moment effects were not considered due to their minimal impact (excellent pitch control power is available through flow shifting between the RALS and ADEN nozzles, direct thrust moments are trimmed out due the nozzle gearing ratio, and generally the effect of jet-induced interference pitching moments is negligible). Lift and drag characteristics employed in the analysis are depicted in Figures 7.6-1 and 7.6-2, respectively. The lift and drag characteristics shown have been generated by modifying the information contained in Sections 4.1.2 and 4.1.3 to take the following effects into account:

- Ground Effects - Obtained from information contained in References 4.3.1-2, 7.6-1 and 7.6-2.
- Deflection of Wing Trailing Edge Devices - Multiple segments are deflected to act as a plain flap. Incremental lift at low angles of attack conservatively estimated by the methods contained in Reference 4.2.2-1. The variations of incremental lift with angle and incremental drag are based on data contained in Reference 4.1.2-6.
- Landing Gear - incremental effects are based on statistical data.

Jet-induced interference effects utilized in the analysis are contained in Section 4.3.3. The appropriate thrust data is contained in Section 5.0.

STO performance capability is presented in Figures 7.6-3 thru 7.6-5 for various values of wind over deck (WOD), for a deck run of 400 ft (122m), which corresponds to operation from ships of the LHA and LPH category, overload capabilities of 9574 lbs (4343 kg), 11,274 lbs (544 kg), and 13,274 lbs (6020 kg), may be obtained at values of WOD of 0, 10 (5.1) and 20 (10.3) knots (m/s), respectively. It should be noted that as the nozzles are rotated from the horizontal (0^{o}) to the vertical (90^{o}), there is a trade-off between horizontal acceleration and direct powered lift. Eventually, the point of minimum acceptable horizontal acceleration (0.065g) is reached and further increases in the powered lift capability become unusable.

7.7 ENGINE-OUT CONSIDERATIONS

Loss of one engine during hover and transition flight will necessitate initiation of procedures to stabilize the aircraft to allow sufficient time for safe pilot egress. At higher speeds/altitudes, the possibility exists for saving both the pilot and aircraft by trading-off altitude for the additional speed necessary to obtain fully wing-borne flight. These aspects of engine-out operation and the ramifications of engine-out during STO operation should be investigated as high speed V/STOL continues to evolve.

In the conventional flight mode, the rudder surfaces have been sized for preliminary design purposes to provide sufficient control to trim out moments due to asymmetric thrust forces from all speeds from conversion to V_{max}. Design 623-2024 will be reconfigured with all-moving slab vertical tail surfaces, should one-engine operation during conventional take-off and landing dictate control requirements.

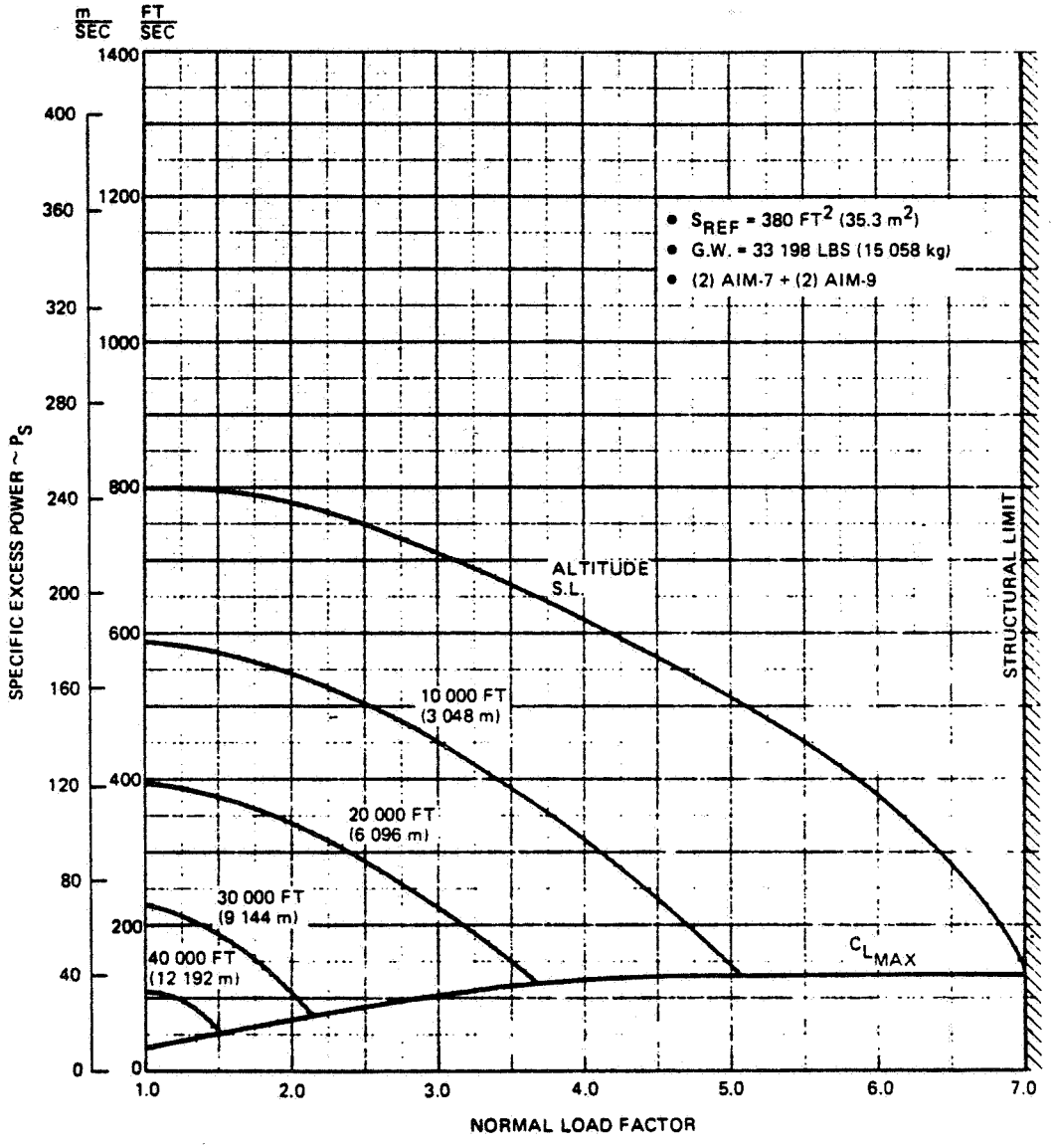

Figure 7.1-1 Design 623 – 2024 Maneuverability M = 0.50

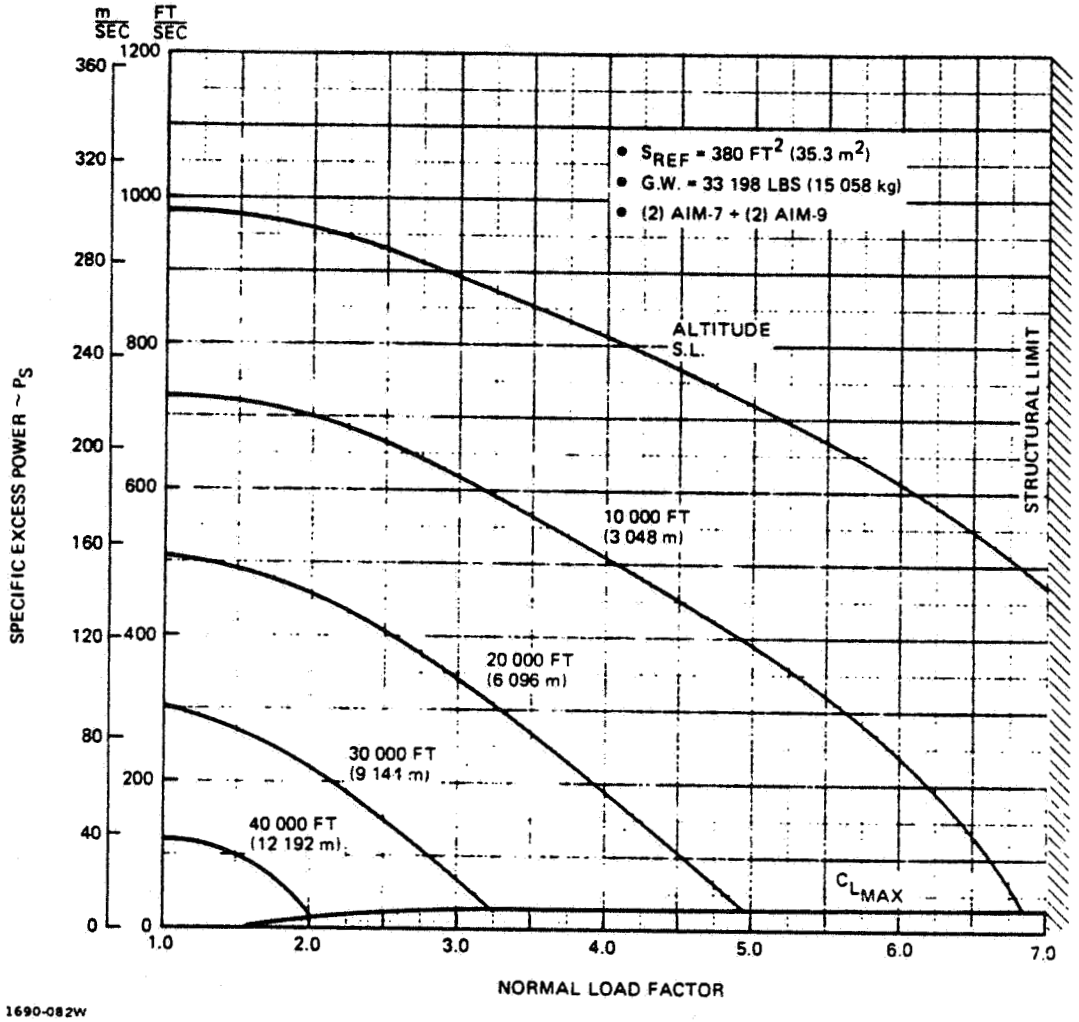

Figure 7.1-2 Design 623-2024 Maneuverability M = 0.60

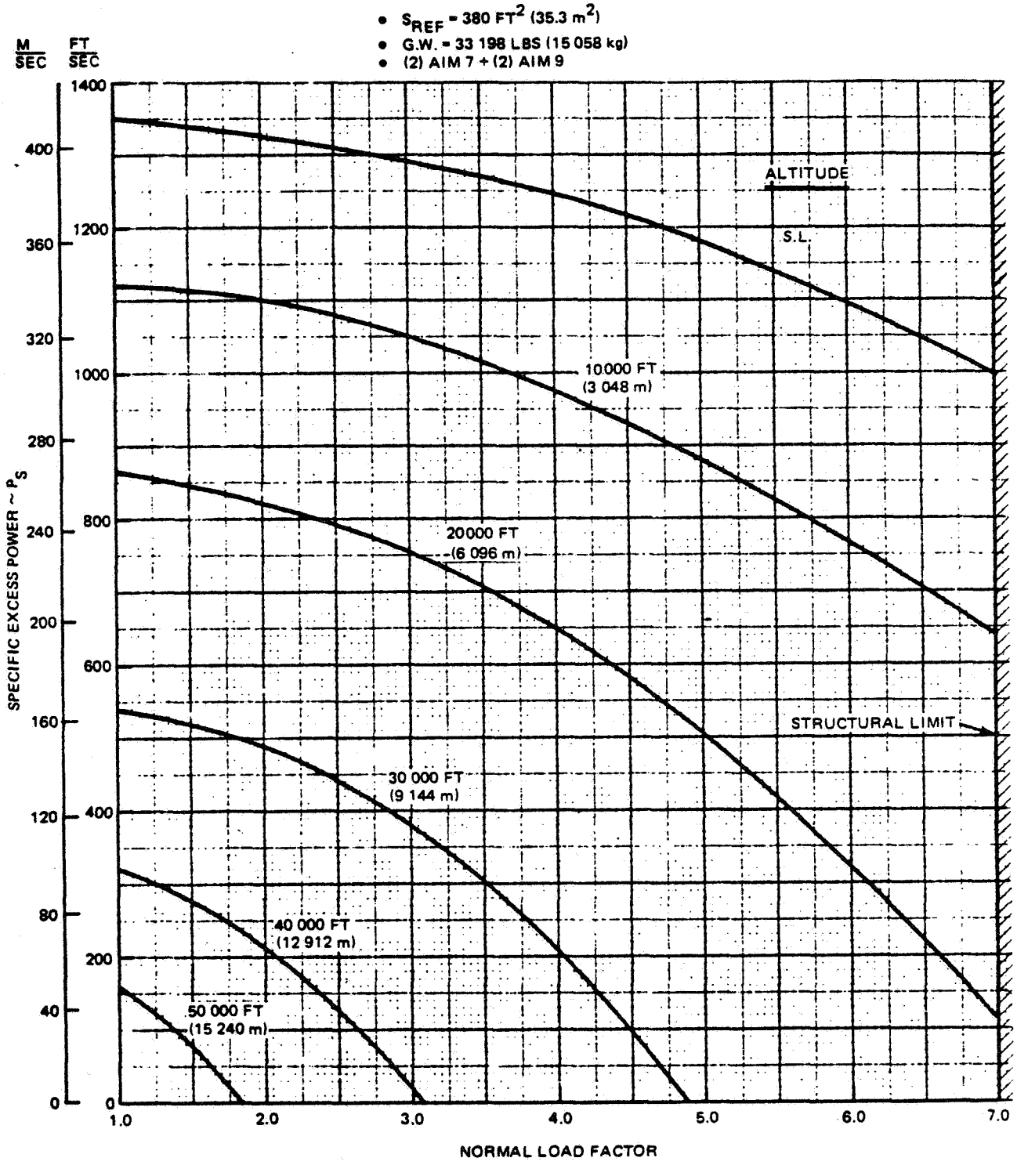

1690-083W

Figure 7.1-3 Design 623 – 2024 Maneuverability M = 0.90

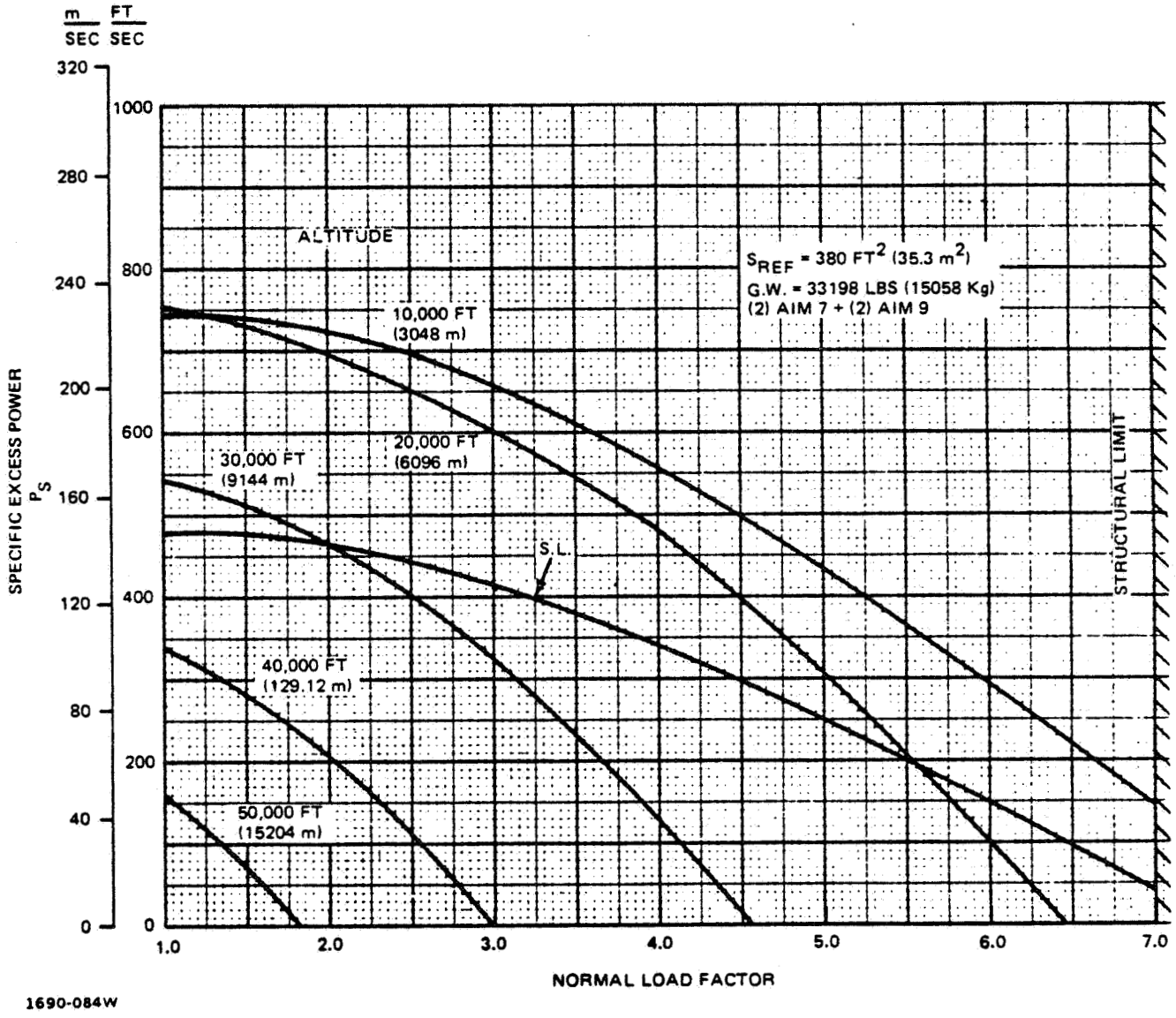

Figure 7.1-4 Design 623-2024 Maneuverability M = 1.2

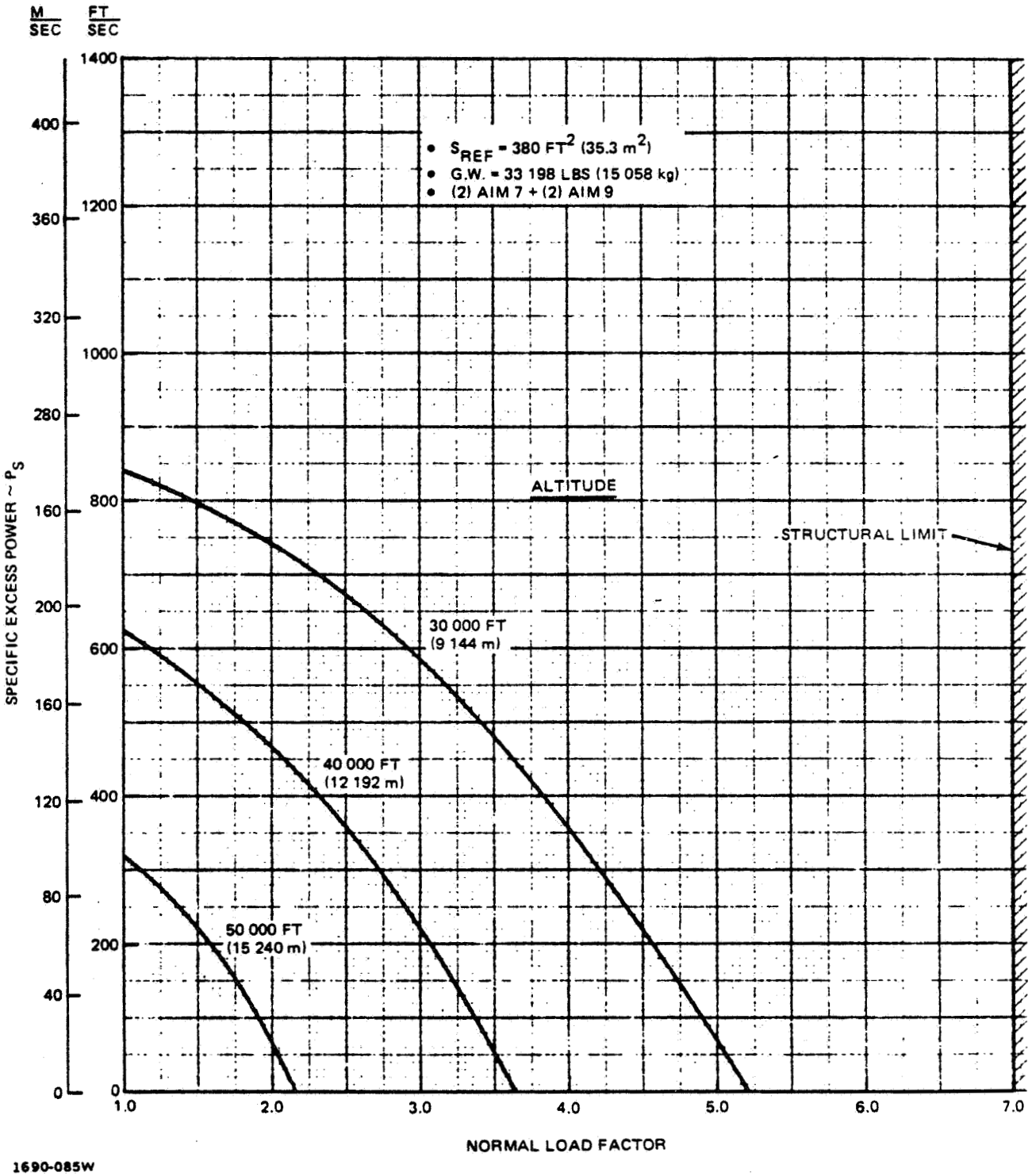

Figure 7.1-5 Design 623 – 2024 Maneuverability M = 1.60

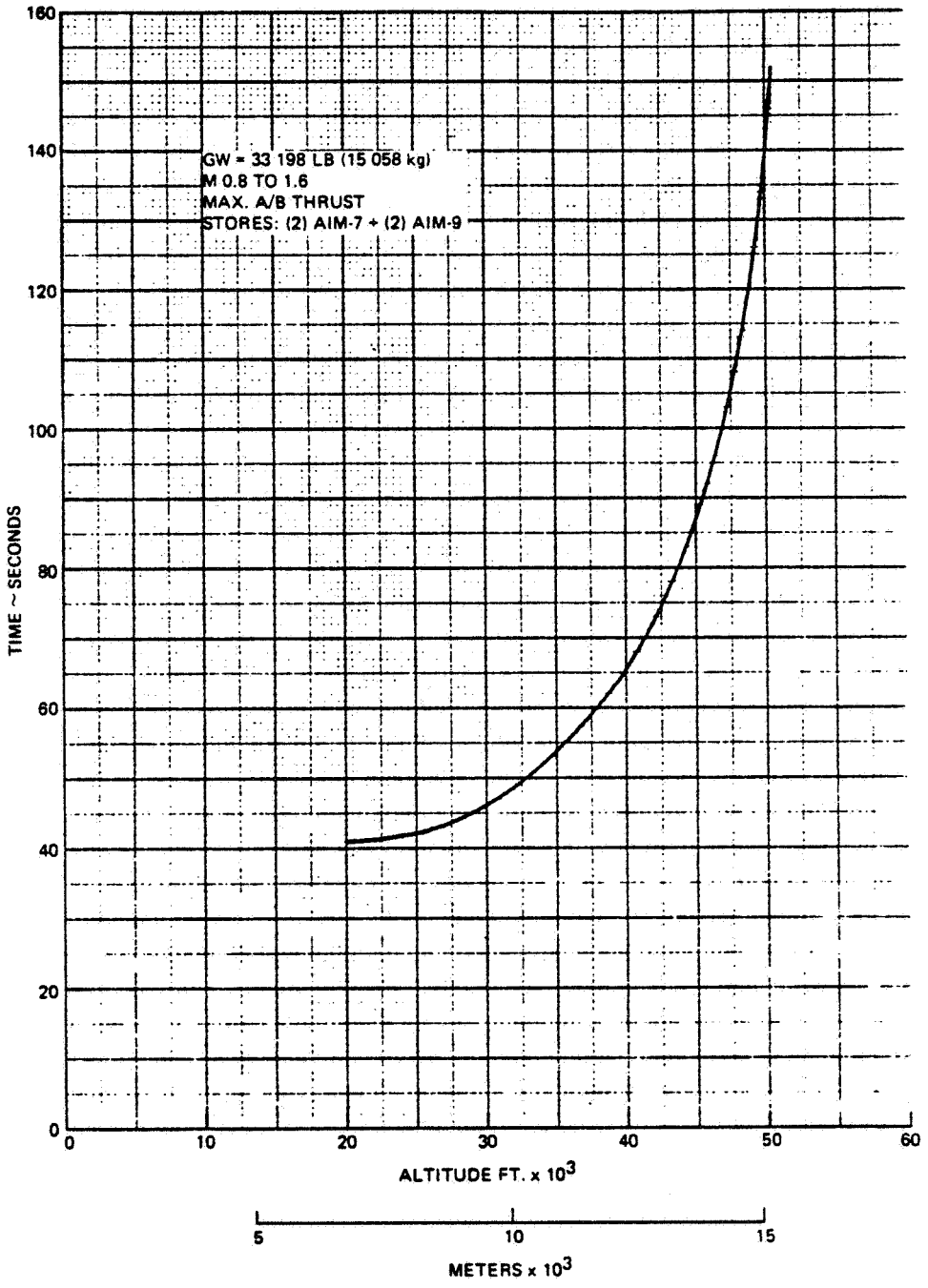

Figure 7.1-6 Design 623 – 2024 Level Flight Acceleration

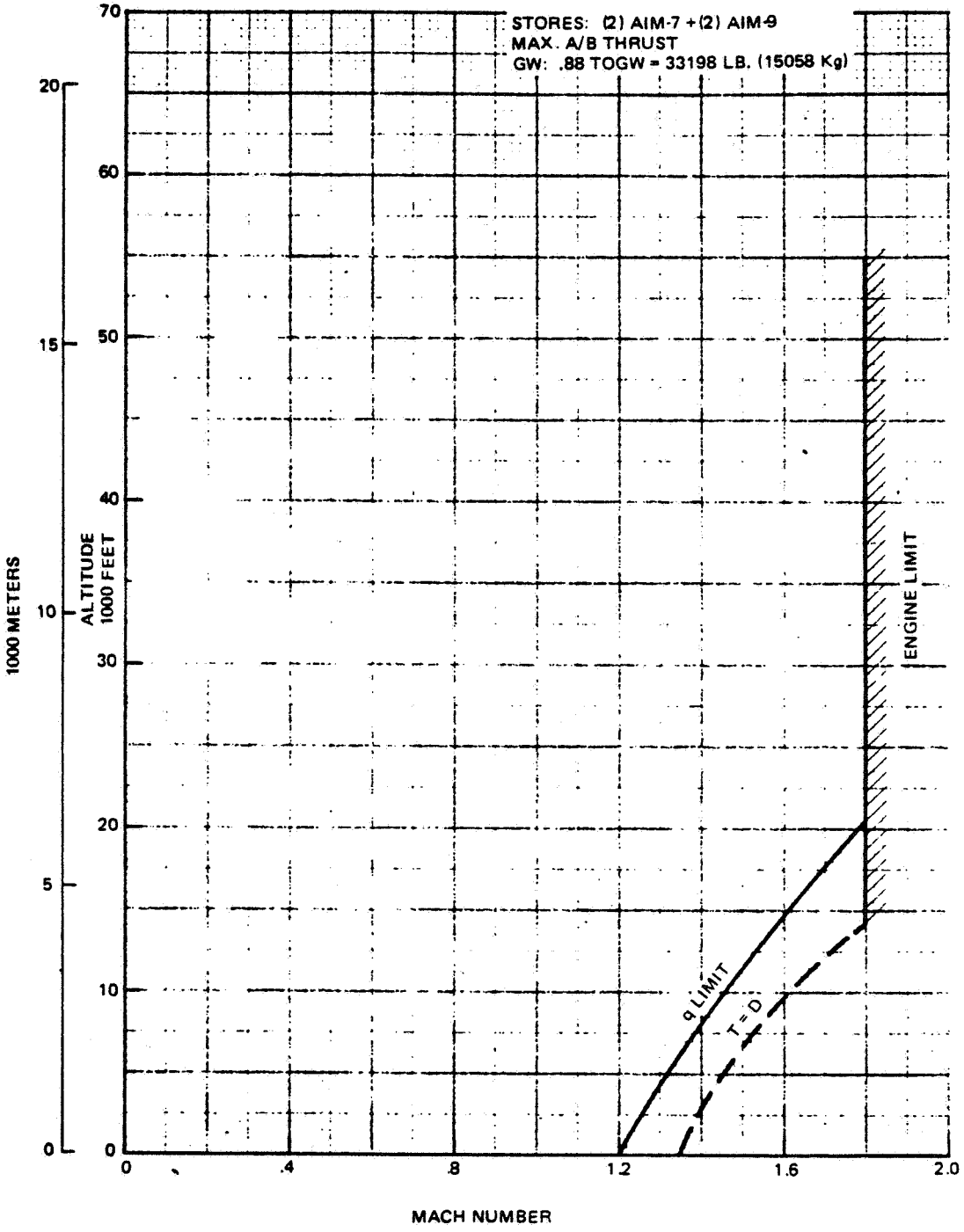

1690-045W

Figure 7.1-7 Design 623-2024 Maximum Mach Number

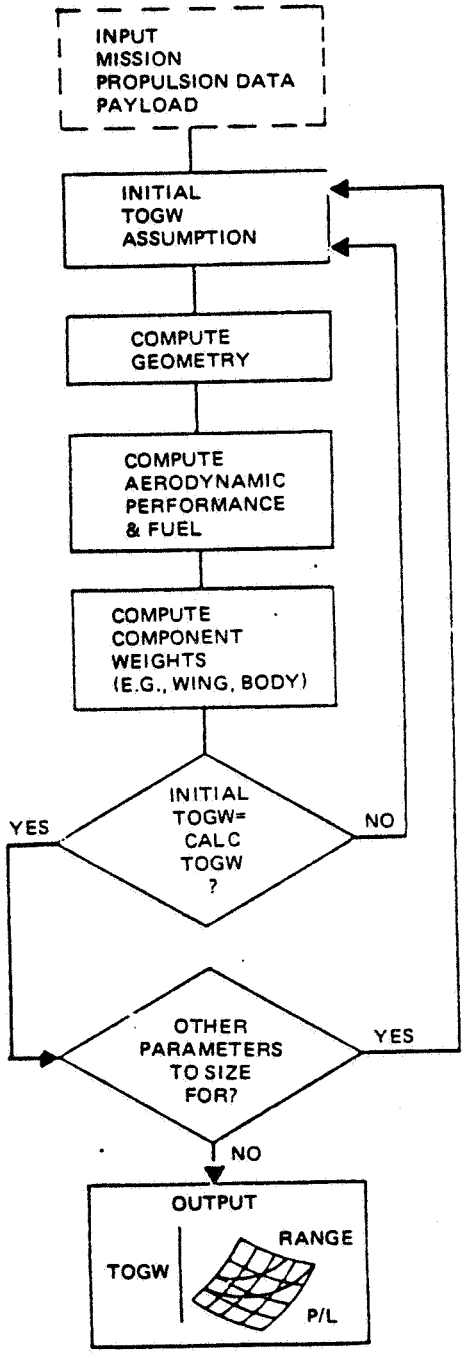

1690-073W

Figure 7.2-1 CISE Flow Chart

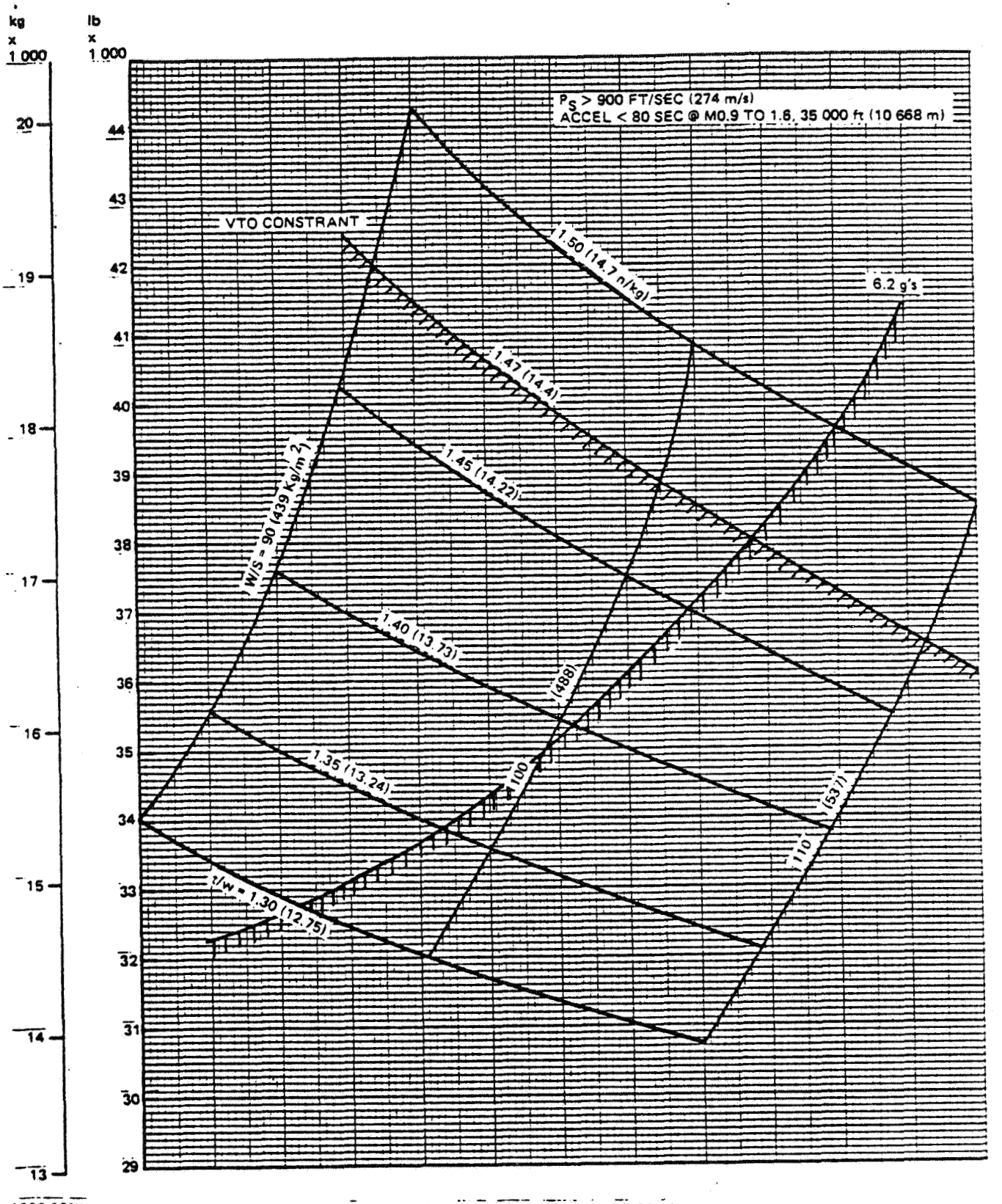

Figure 7.2-2 Des 623 (T/W), (W/S) vs TOGW
AR = 3.75 Λ_{LE} = 35°

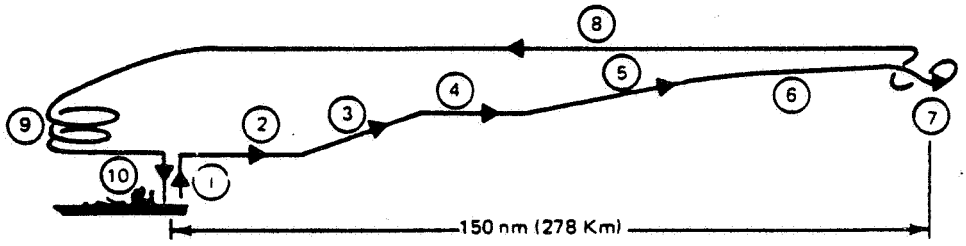

1 VTO FROM SURFACE SHIP

2 ACCELERATE TO MACH 0.9 ATSEA LEVEL

3 CONSTANT MACH NUMBER CLIMB TO 35 000 FT (10668 m)

4 ACCELERATE TO MACH 1.6, 35 000 FT (10668 m)

5 DASH-CLIMB TO BEST CRUISE ALTITUDE (BCA), MACH 1.6

6 DASH-CRUISE AT MACH 1.6, BCA

7 COMBAT ALLOWANCE
- HALF TURN AT MACH 1.6 MAX SUSTAINED G'S
- P_S = 41 000 FT (12 497 m)

8 CRUISE BACK AT BEST MACH NUMBER (BMN) AND BCA

9 LOISTER 10 MINUTES AT SEA LEVEL, BMN

10 VERTICAL LANDING ALLOWANCE WITH 5% RESERVE FUEL

1690-075W

Figure 7.2-3 Design 623 – 2024 VTOL Deck Launched Intercept (DLI) Mission (Stores Retained)

MISSION DESCRIPTION	MACH NO.	ALTITUDE ft (m)	TIME min.	DISTANCE nm (km)	FUEL, lb (kg)
1 VERTICAL TAKE-OFF ALLOWANCE	0	0	3.0	0	2 011 (912)
2 ACCELERATE TO MACH 0.9, SEA LEVEL	0.9	0	0.5	3.6 (7)	254 (115)
3 CONSTANT MACH CLIMB TO 35 000 FT (10 668 m)	0.9	35 000 (10 668)	1.4	11.5 (21)	812 (368)
4 ACCELERATE TO MACH 1.6	1.6	35 000 (10 668)	1.4	16.9 (31)	909 (412)
5 CLIMB TO BEST CRUISE ALT. MACH 1.6	1.6	55 000 (16 764)	0.8	12.3 (23)	648 (294)
6 DASH TO RADIUS, MACH 1.6	1.6	56 000 (17 069)	6.9	105.7 (197.6)	1890 (857)
7 COMBAT ALLOWANCE	1.6	40 000 (12 192)	1.8	—	1892 (858)
8 CRUISE BACK AT BCA/BMN	0.80	45 000 (13 716)	19.6	150 (278)	898 (407)
9 LOITER 10 MINUTES AT SEA LEVEL, BMN	0.27	0	10.0	—	544 (244)
10 LANDING ALLOWANCE PLUS 5% RESERVE	—	—	—	—	760 (345)

1690-076W

Figure 7.2-4 Design 623-2024 VTOL Deck Launched Intercept (DLI) Mission, Radius 180 NM (333 km) VTO TOGW = 37 726 lb (17 113 Kg)

COMPONENT	1987 IOC PCT SAVINGS	1991 IOC PCT SAVINGS	1995 IOC PCT SAVINGS
WING	21	24	28
VERTICAL TAIL	27	30	30
CANARD	18	23	24
BODY	8	15	25
ALIGHTING GEAR	10	11	14
AIR INDUCTION	13	21	26

1690-056W

Figure 7.3-1 CISE Input, Component Weight Savings

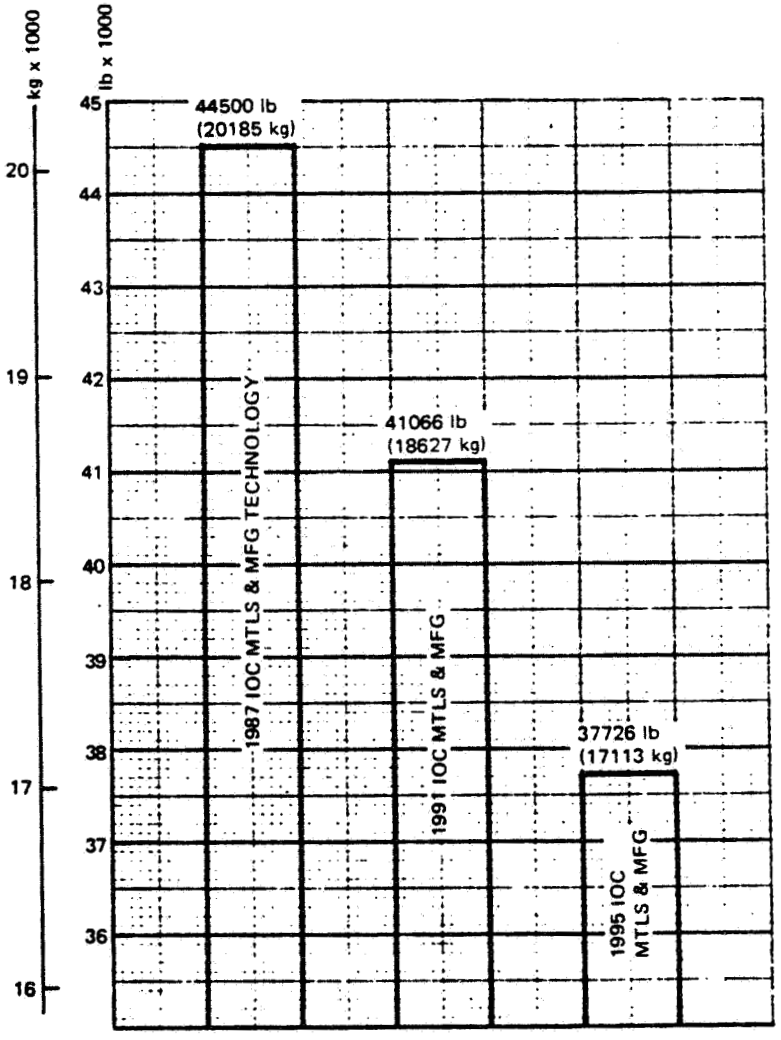

1690-057W

Figure 7.3-2 Design 623–2024 TOGW Sensitivity to Materials & MFG IOC Date, DLI Mission

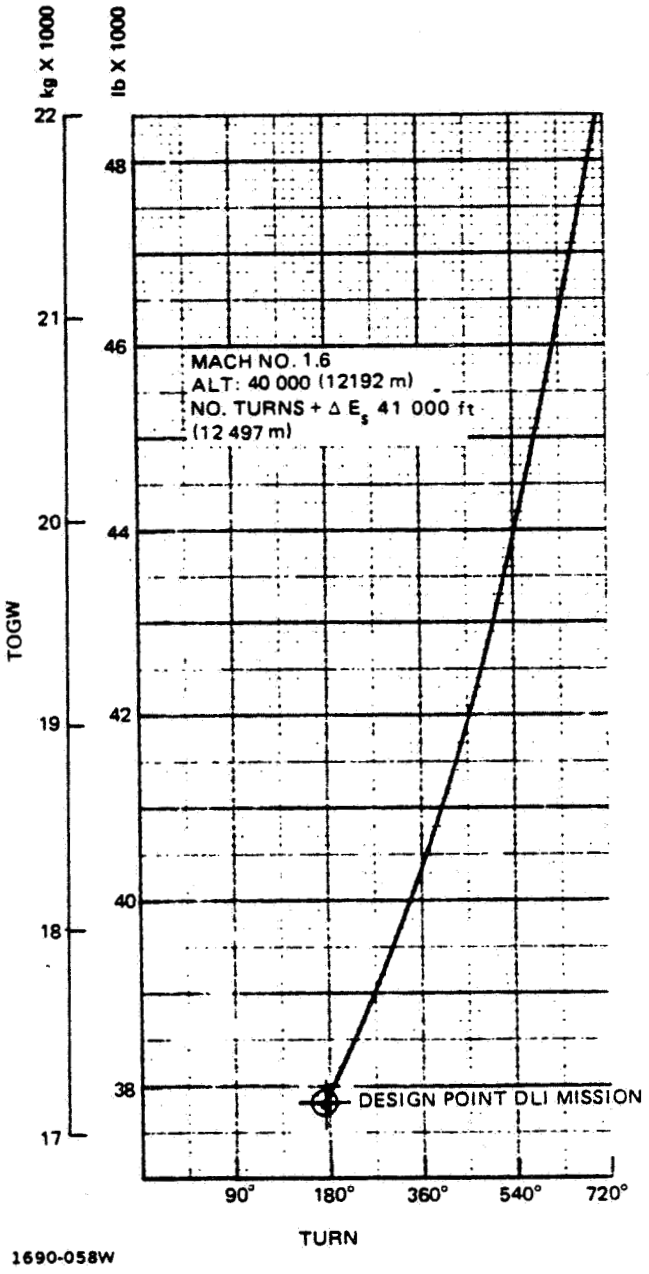

Figure 7.3-3 Design 623–2024 TOGW Sensitivity to No. Turns in Combat

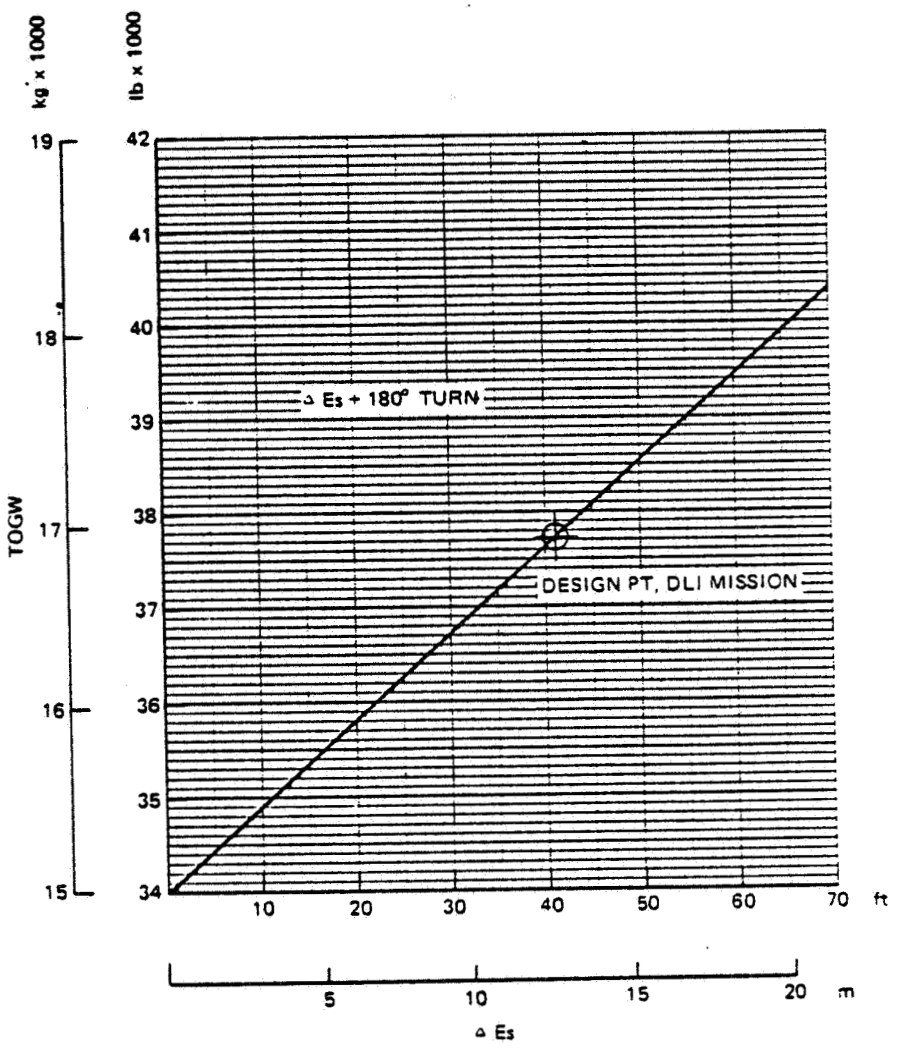

Figure 7.3-4 Design 623–2024 TOGW Sensitivity to Combat – Es @ Macn 1.6, 40 000 FT (12192 m)

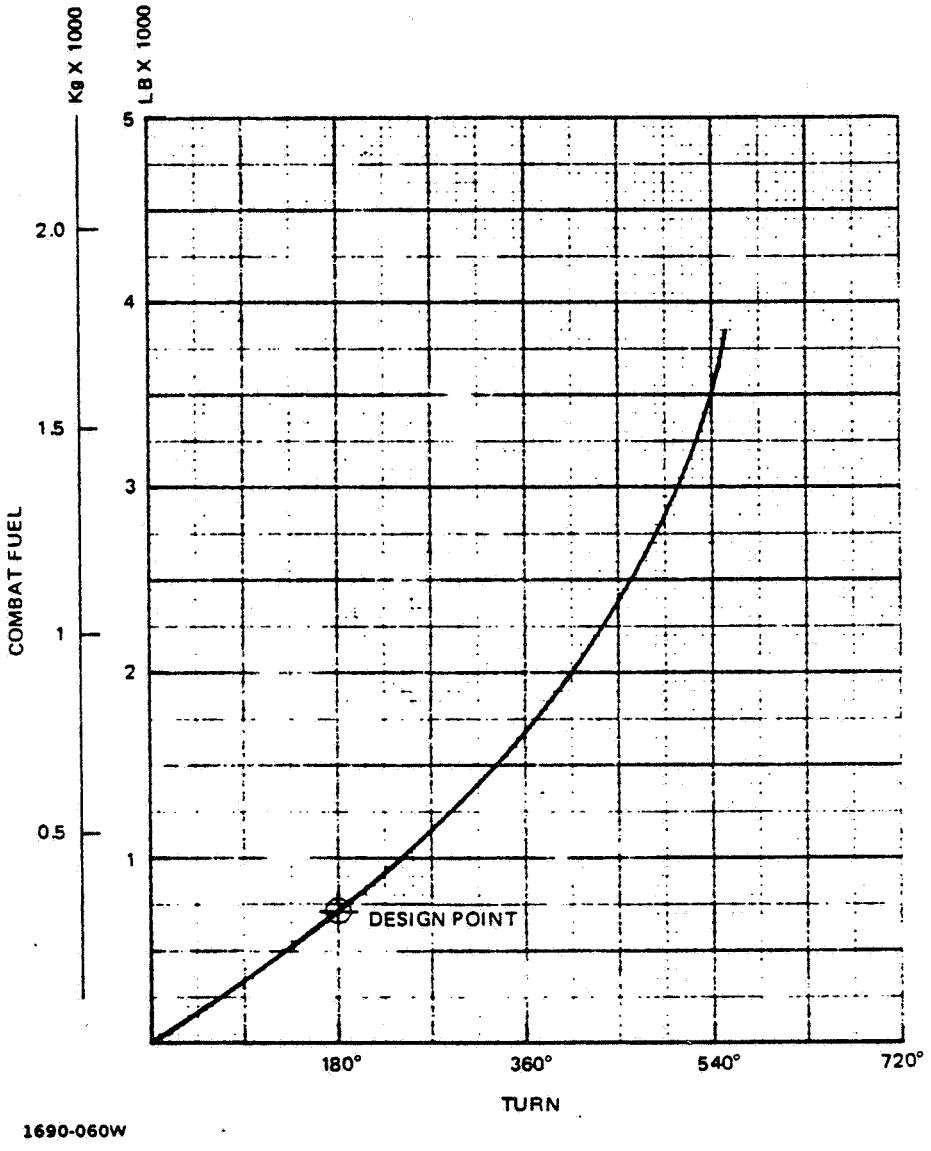

Figure 7.3-5 Design 623-2024 Combat Fuel Req'd vs Turn Mach 1.6, 40000' (12 192 m), DLI Mission

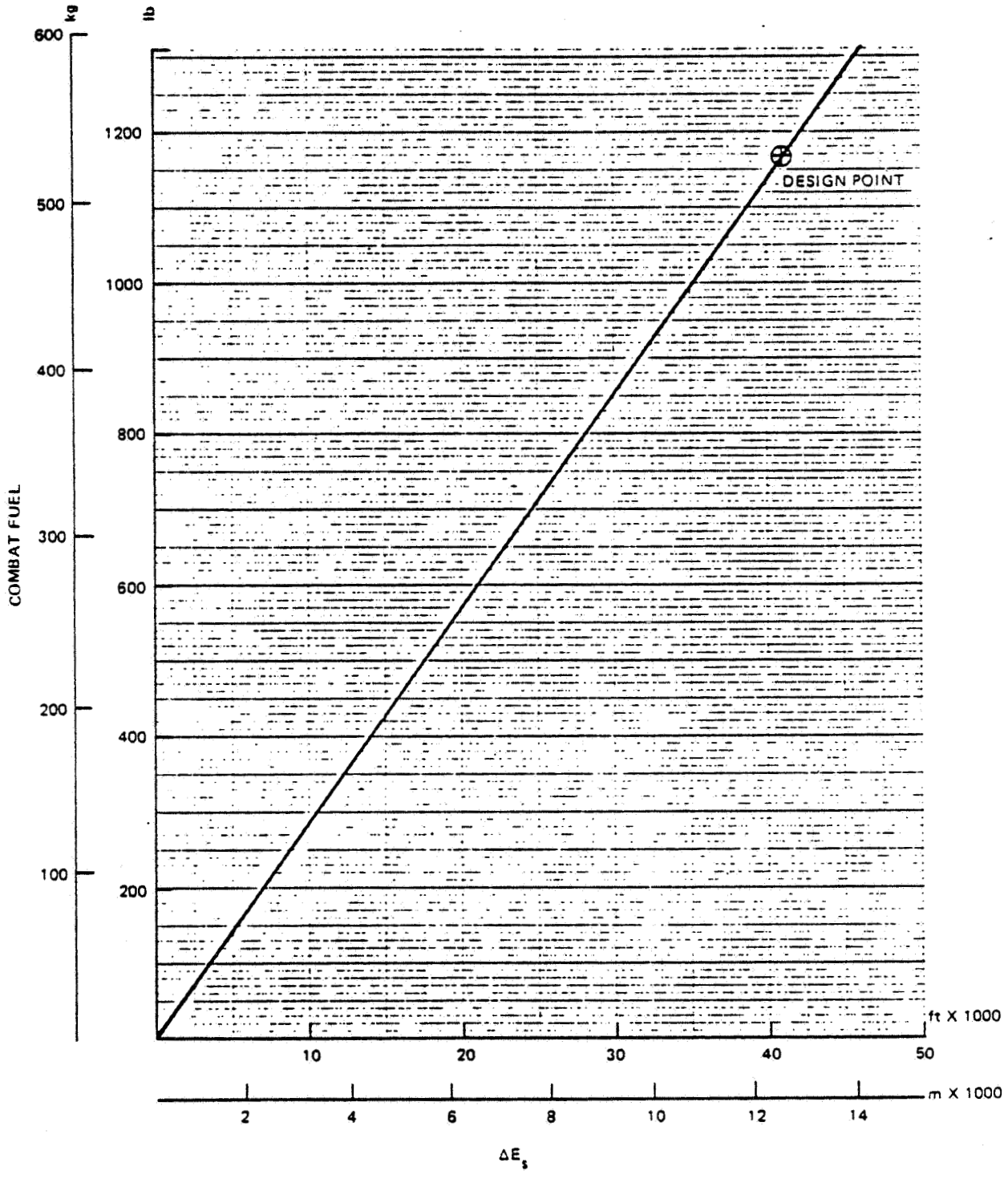

4782-061W

Figure 7.3-6 Design 623-2024 Combat Fuel Req'd vs ΔE_s Mach 1.6, 40000' (12192m), DLI Mission

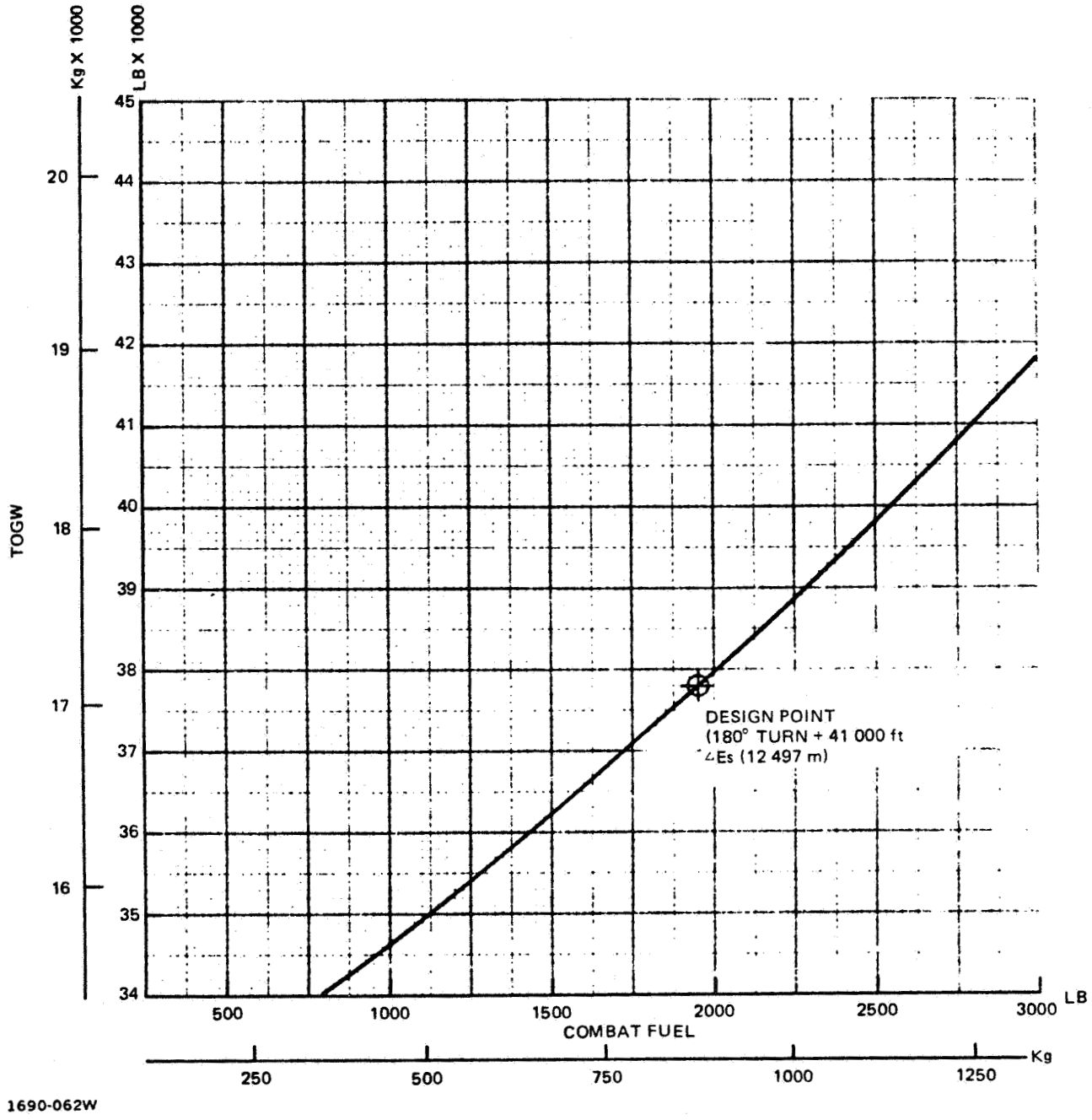

Figure 7.3-7 Design 623-2024 Combat Fuel Allowance vs TOGW Combat Fuel at Mach 1.6, 40000' (12 192 m), DLI Mission

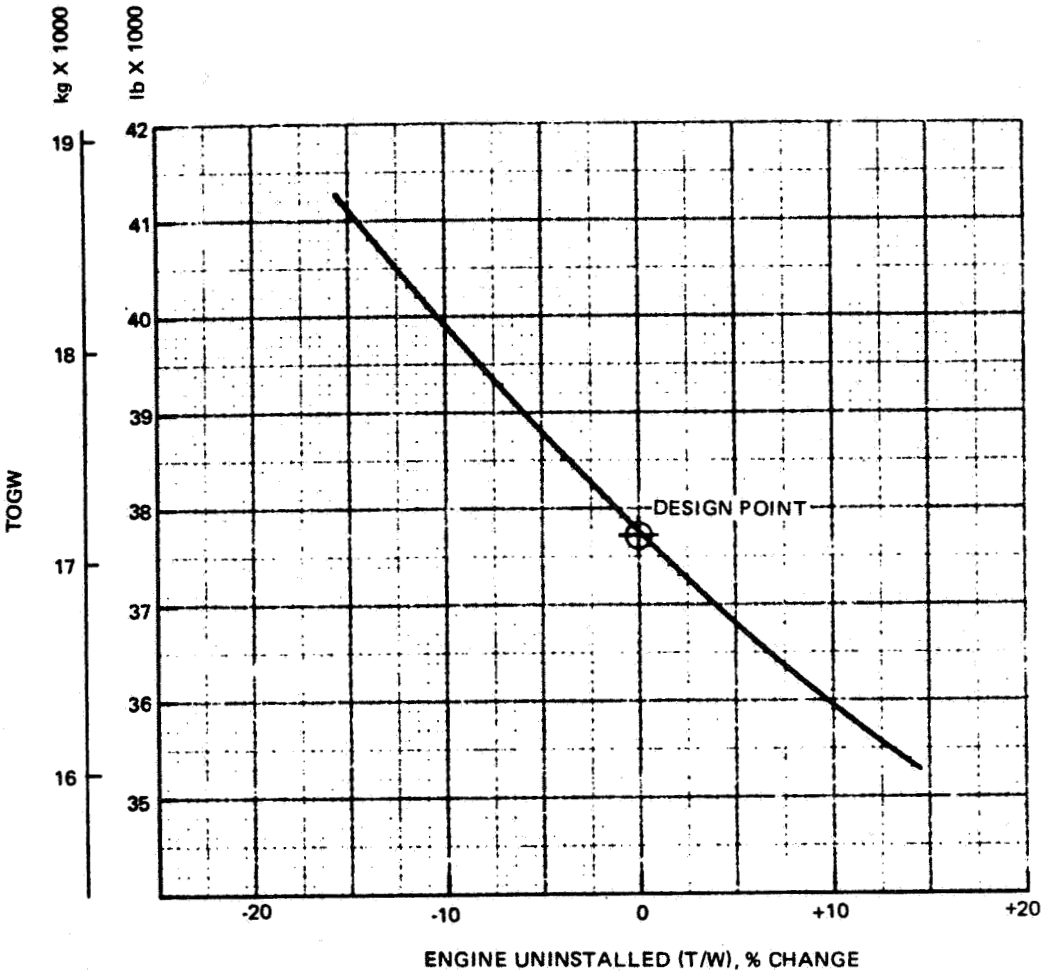

1690-063W

Figure 7.3-8 Design 623-2024 TOGW Sensitivity to Uninstalled Engine (T/W)

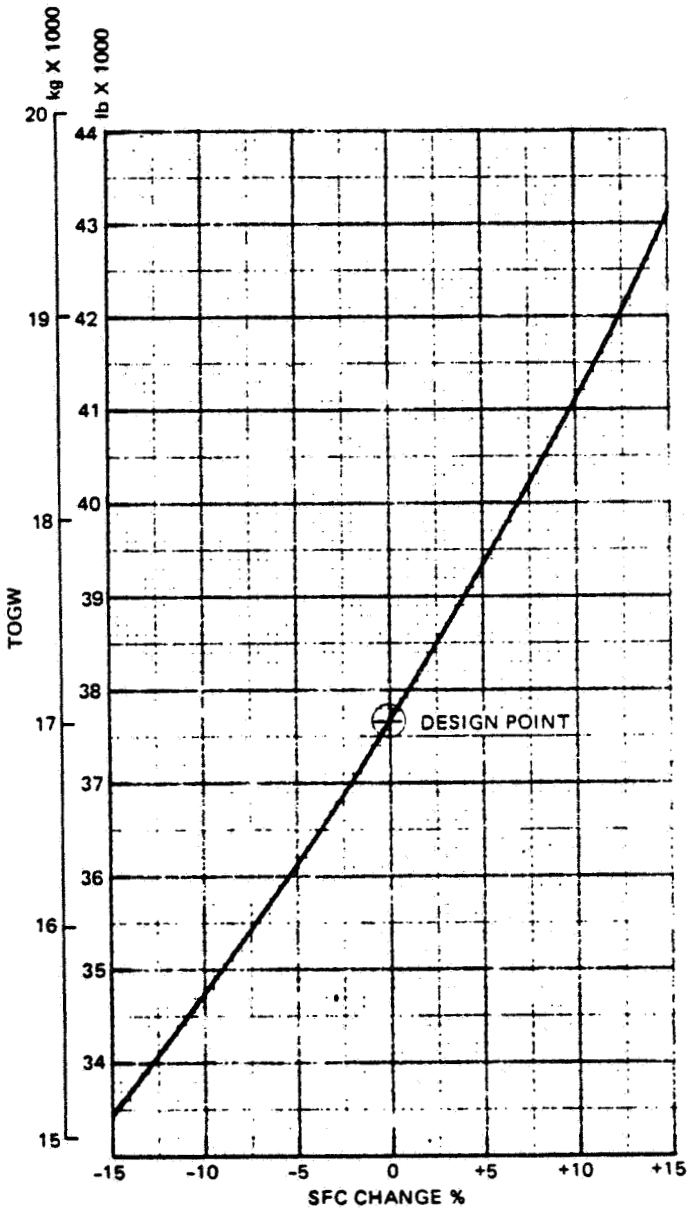

1690-064W

Figure 7.3-9 Design 623–2024 TOGW Sensitivity to Engine SFC Change

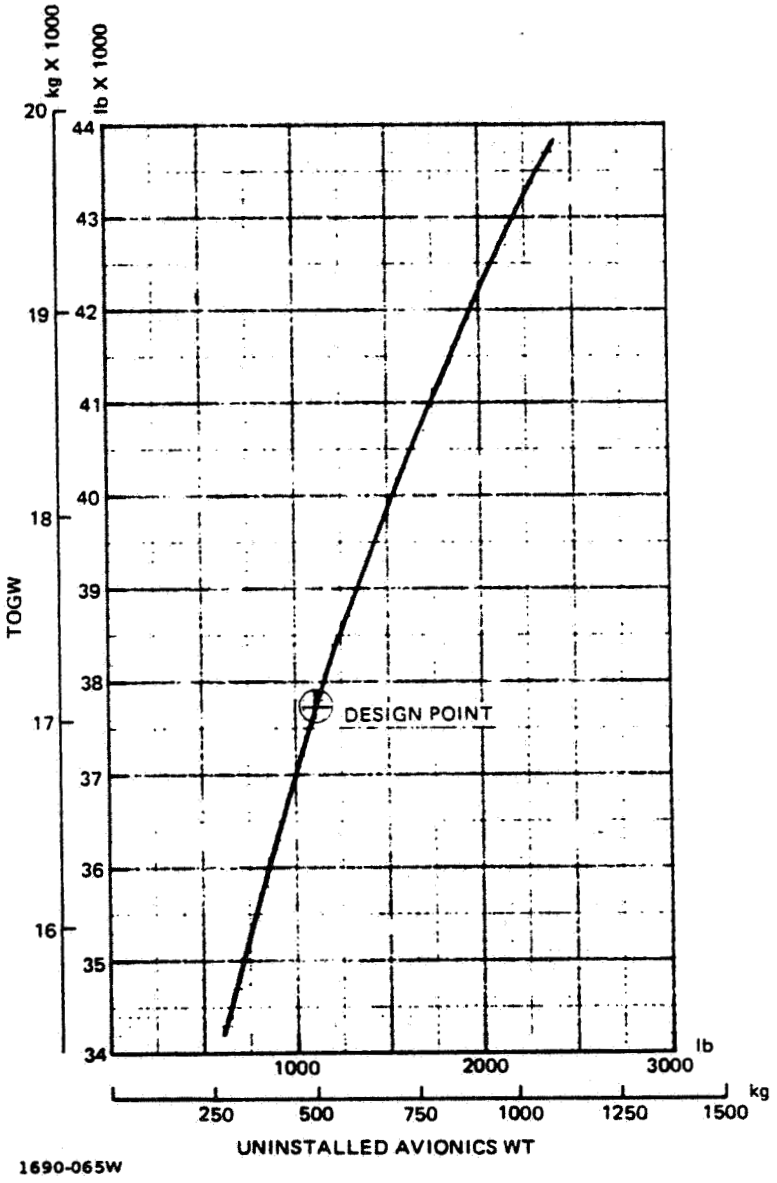

Figure 7.3-10 Design 623-2024 TOGW Sensitivity to Uninstalled Avionics Weight

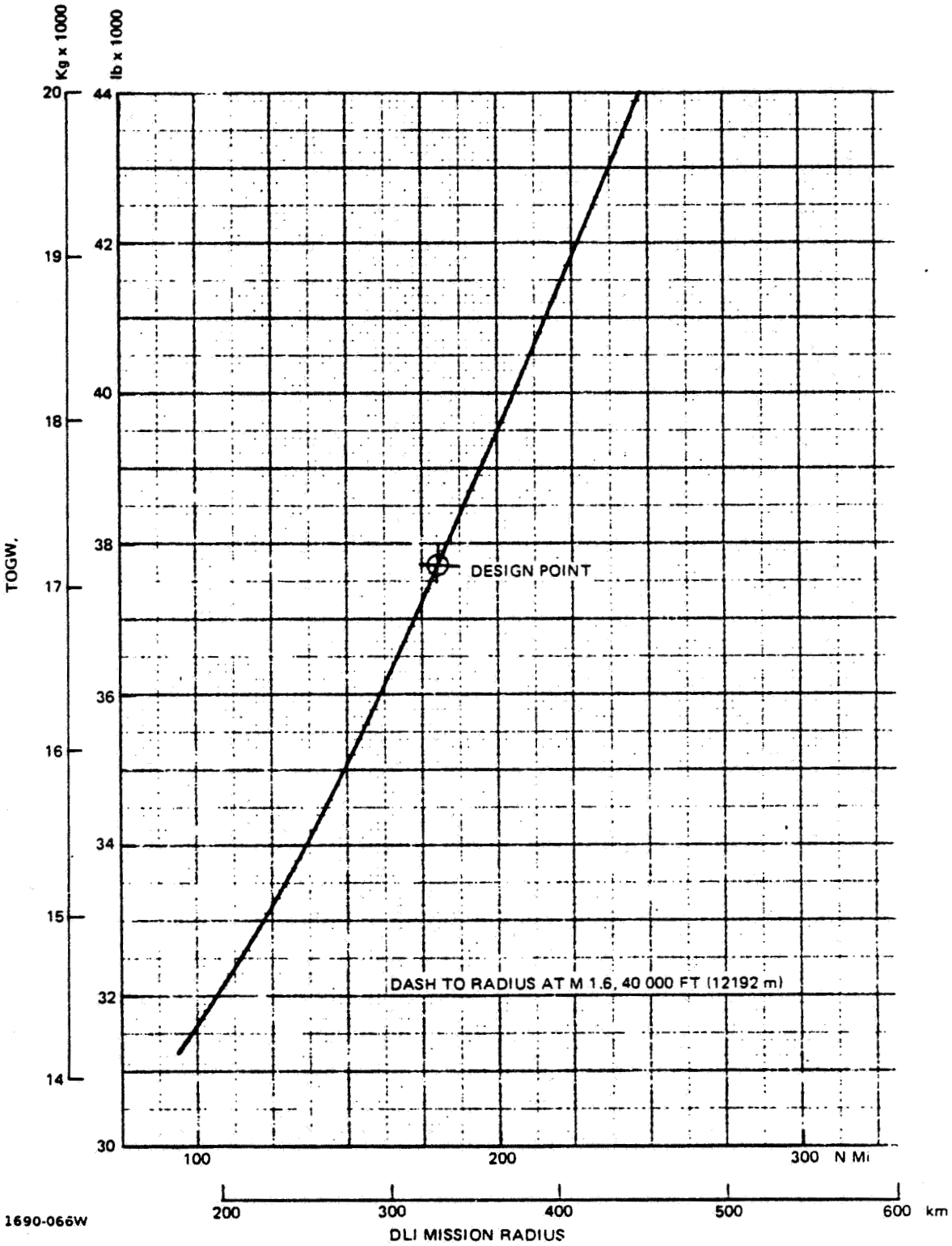

Figure 7.3-11 Design 623–2024 TOGW Sensitivity to DLI Mission Radius

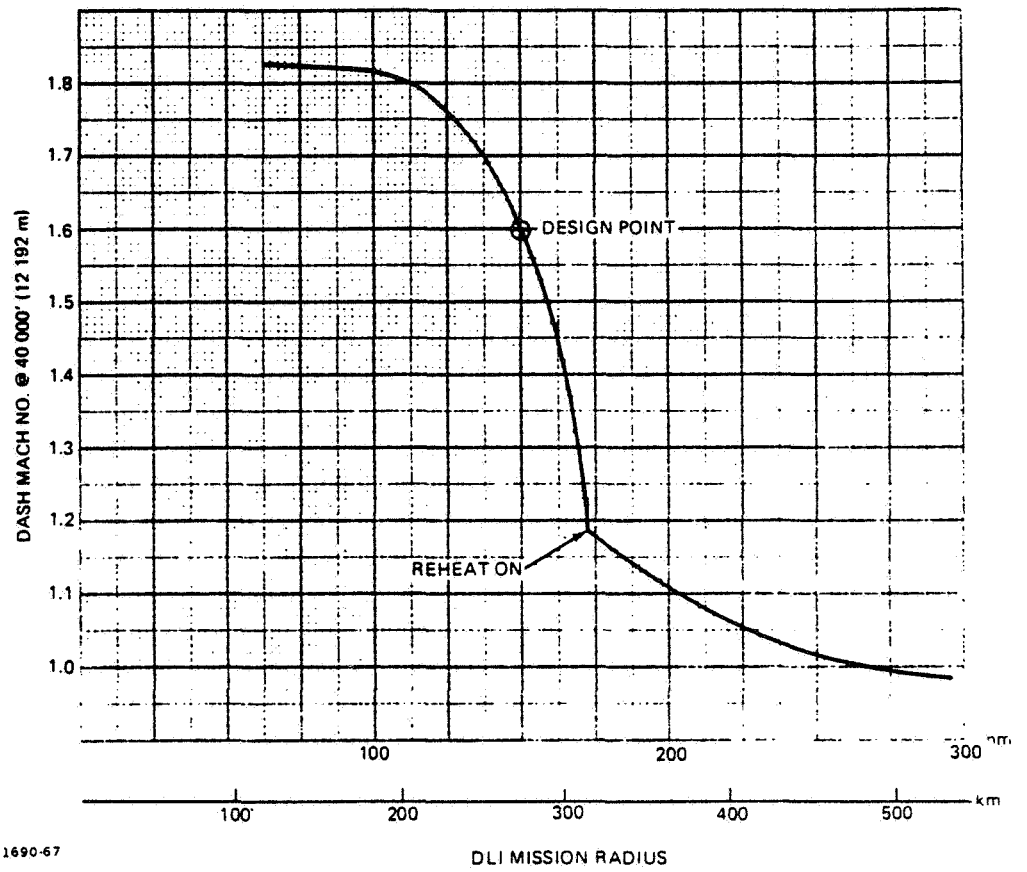

Figure 7.3-12 Design 623 Dash Speed, @ 40 000' (12 192 m), vs Mission Radius, nm, DLI Mission

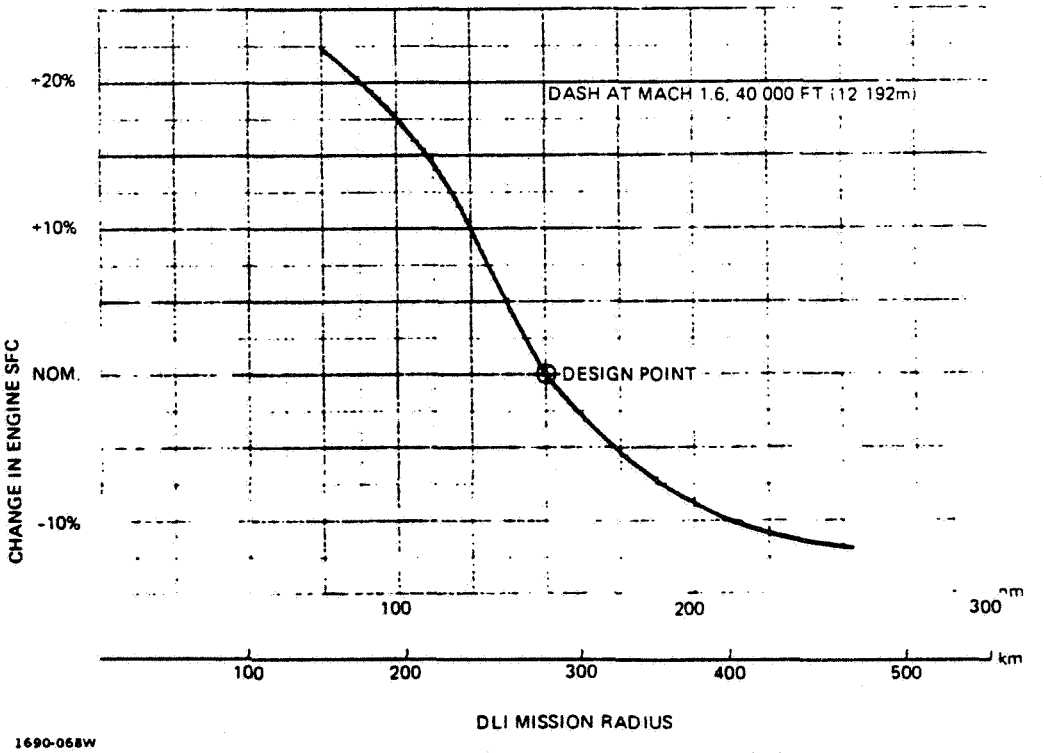

Figure 7.3-13 Design 623-2024 DLI Mission Radius vs. SFC Change

LOADING (2) AIM-7 SPARROW (2) AIM-9 SIDEWINDER, GUN/AMMO (ALL RETAINED)

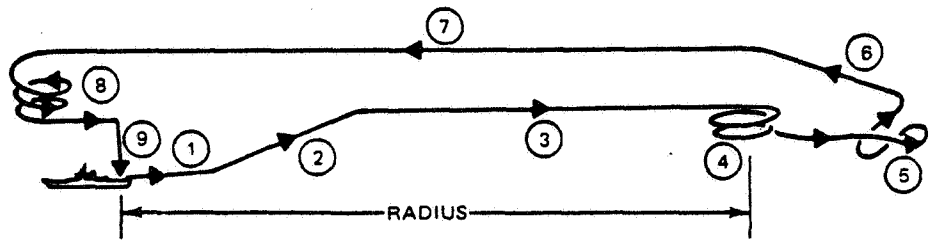

1 SHORT TAKE-OFF

2 MINIMUM FUEL CLIMB TO BEST CRUISE ALTITUDE AND MACH NUMBER (BCA/BMN)

3 CRUISE AT BCA/BMN TO RADIUS

4 LOITER AT RADIUS

5 COMBAT ALLOWANCE
- ACCELERATE TO MACH 1.4
- EXECUTE 180° TURN
- EXPEND ΔE_S = 41 000 ft (12 497 m)

6 MINIMUM FUEL CLIMB TO BCA/BMN

7 CRUISE BACK AT BCA/BMN

8 LOITER 10 MINUTES AT BMN, SEA-LEVEL

9 VERTICAL LANDING WITH 5% FUEL REMAINING

1690-087W

Figure 7.4-1 Design 623–2024 STOVL Combat Air Patrol (CAP) Mission

LOADING: (2) AGM-84 HARPOON, (2) AIM-9 SIDEWINDER, GUN/AMMO (ALL RETAINED)

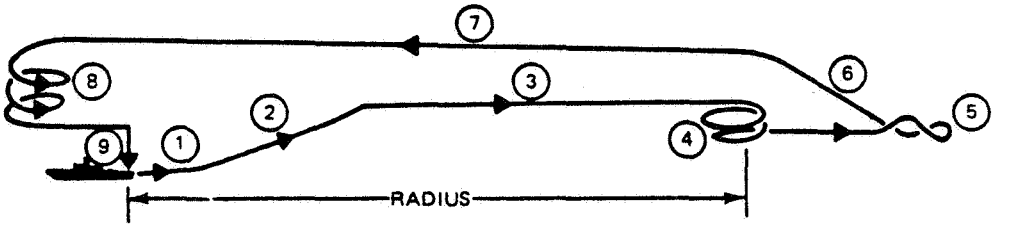

1 SHORT TAKE-OFF

2 MINIMUM FUEL CLIMB TO BEST CRUISE ALTITUDE AND MACH NUMBER (BCA/BMN)

3 CRUISE AT BCA/BMN TO RADIUS

4 LOITER AT BCA/BMN

5 COMBAT ALLOWANCE, 5 MINUTES AT MACH 0.8, 20 000 FT. (6 096 m)

6 MINIMUM FUEL CLIMB TO BCA/BMN

7 CRUISE BACK AT BCA/BMN

8 LOITER 10 MINUTES AT BMN, SEA LEVEL

9 VERTICAL LANDING WITH 5% FUEL REMAINING

1690-086W

Figure 7.4-2 Design 623–2024 STOVL Subsonic Surface Surveillance (SSS) Mission

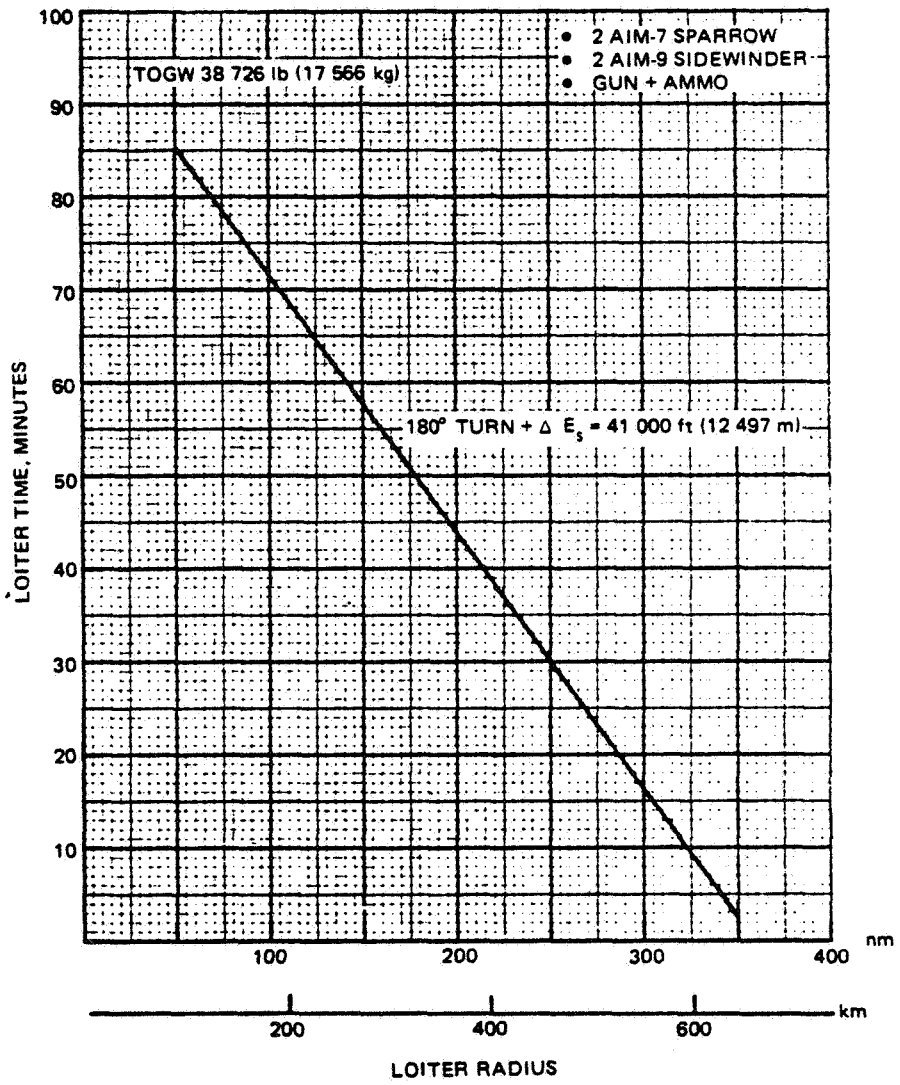

1690-088W

Figure 7.4-3 Design 623-2024 STOVL Combat Air Patrol Mission

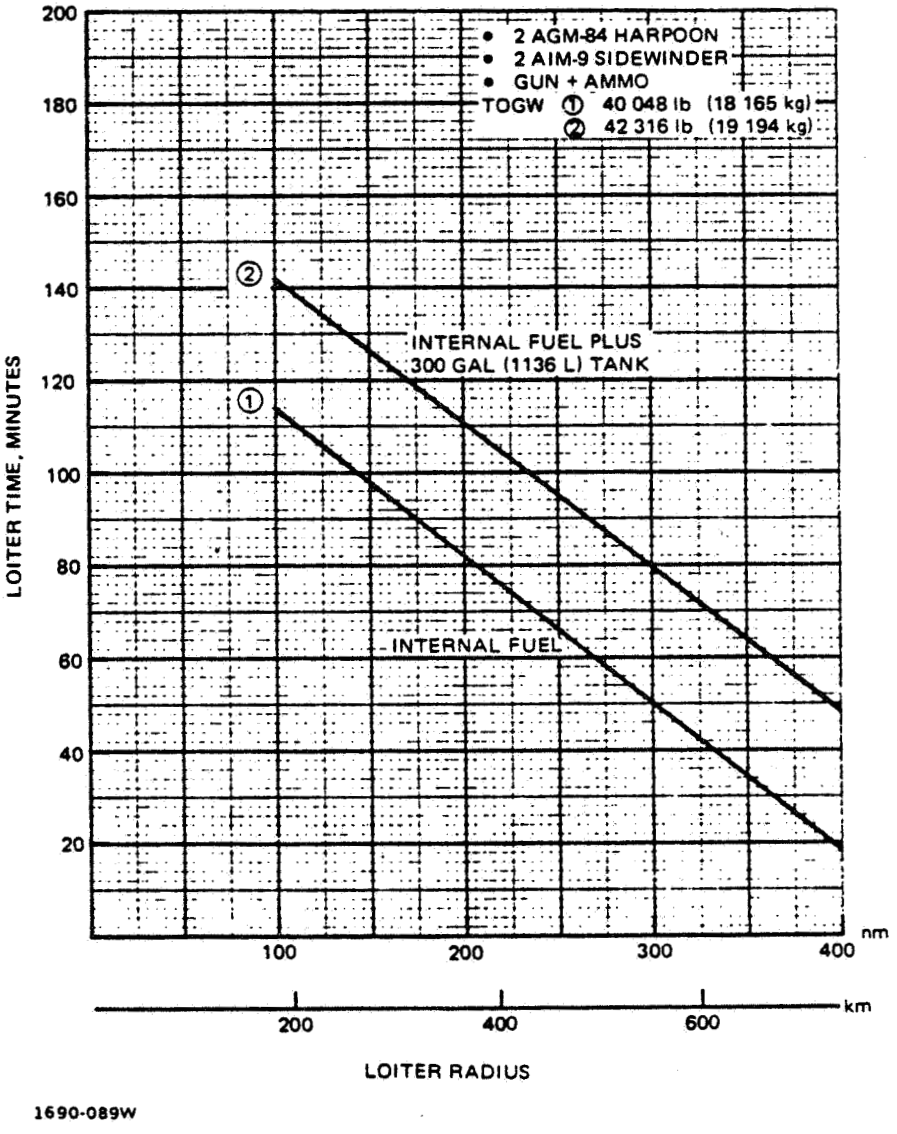

Figure 7.4-4 Design 623-2024 STOVL Subsonic Surface Surveillance

MISSION DESCRIPTION	MACH NO.	ALTITUDE ft (m)	TIME min.	DISTANCE nm (km)	FUEL, lb (kg)
1 SHORT TAKE-OFF	–	0	2.0	0	915 (415)
2 MIN. FUEL CLIMB TO BCA/BMN	0.83	36 000 (10 972)	2.4	18.1 (34)	706 (320)
3 CRUISE TO RADIUS BCA/BMN	0.80	37 000 (11 278)	17.6	131.9 (244)	1055 (479)
4 LOITER AT RADIUS	0.70	38 000 (11 583)	59.6	–	3213 (1457)
5 COMBAT ALLOWANCE					
• ACCELERATE TO MACH 1.4	1.40	20 000 (6 096)	0.6	–	483 (219)
• EXECUTE 180° TURN (6.05g)	1.40	20 000 (6 096)	0.4	–	766 (347)
• EXPEND ΔE_s = 41,000 ft	1.40	20 000 (6 096)	0.19	–	1815 (823)
6 CLIMB TO BCA/BMN	0.87	37 000 (11 278)	1.9	8.2 (15)	234 (106)
7 CRUISE BACK AT BCA/BMN	0.78	40 000 (12 192)	18.6	141.8 (263)	944 (428)
8 LOITER 10 MINUTES AT BMN, SEA LEVEL	0.27	0	10.0	–	547 (248)
9 VERTICAL LANDING	0	0	0.8	–	366 (166)
10 5% FUEL RESERVE	–	–	–	–	581 (264)

1690-090W

Figure 7.4-5 Design 623-2024 STOVL CAP Mission Breakdown 150 nm (278 km) Radius 11618 Lb (5270 kg) Internal Fuel

	MISSION DESCRIPTION	MACH NO.	ALTITUDE ft (m)	TIME min.	DISTANCE nm (km)	FUEL, lb (kg)
1	SHORT TAKE-OFF	0	0	2.0	–	915 (415)
2	MINIMUM FUEL CLIMB TO BCA	0.82	37 000 (11 278)	2.7	21.1 (39)	798 (362)
3	CRUISE AT BCA/BMN TO RADIUS	0.80	40 000 (12 192)	36.3	278.9 (517)	2 332 (1 058)
4	LOITER AT BCA/BMN	0.69	39 000 (11 887)	54.2	–	3 052 (1 384)
5	COMBAT ALLOWANCE	0.80	20 000 (6 096)	5.0	–	582 (264)
6	MINIMUM FUEL CLIMB TO BCA	0.83	41 000 (12 497)	2.0	15.4 (29)	369 (167)
7	CRUISE BACK AT BCA/BMN	0.80	44 000 (13 411)	37.1	284.6 (527)	2 005 (909)
8	LOITER 10 MINUTES AT BMN, SEA LEVEL	0.27	0	10.0	–	584 (265)
9	VERTICAL LANDING	0	0	0.8	–	366 (166)
10	5% RESERVE FUEL	–	–	–	–	579 (263)

1690-091W

Figure 7.4-6 Design 623-2024 STOVL SSS Mission Breakdown 300 nm (556 km) Radius 11618 Lb (5270 kg) Internal Fuel

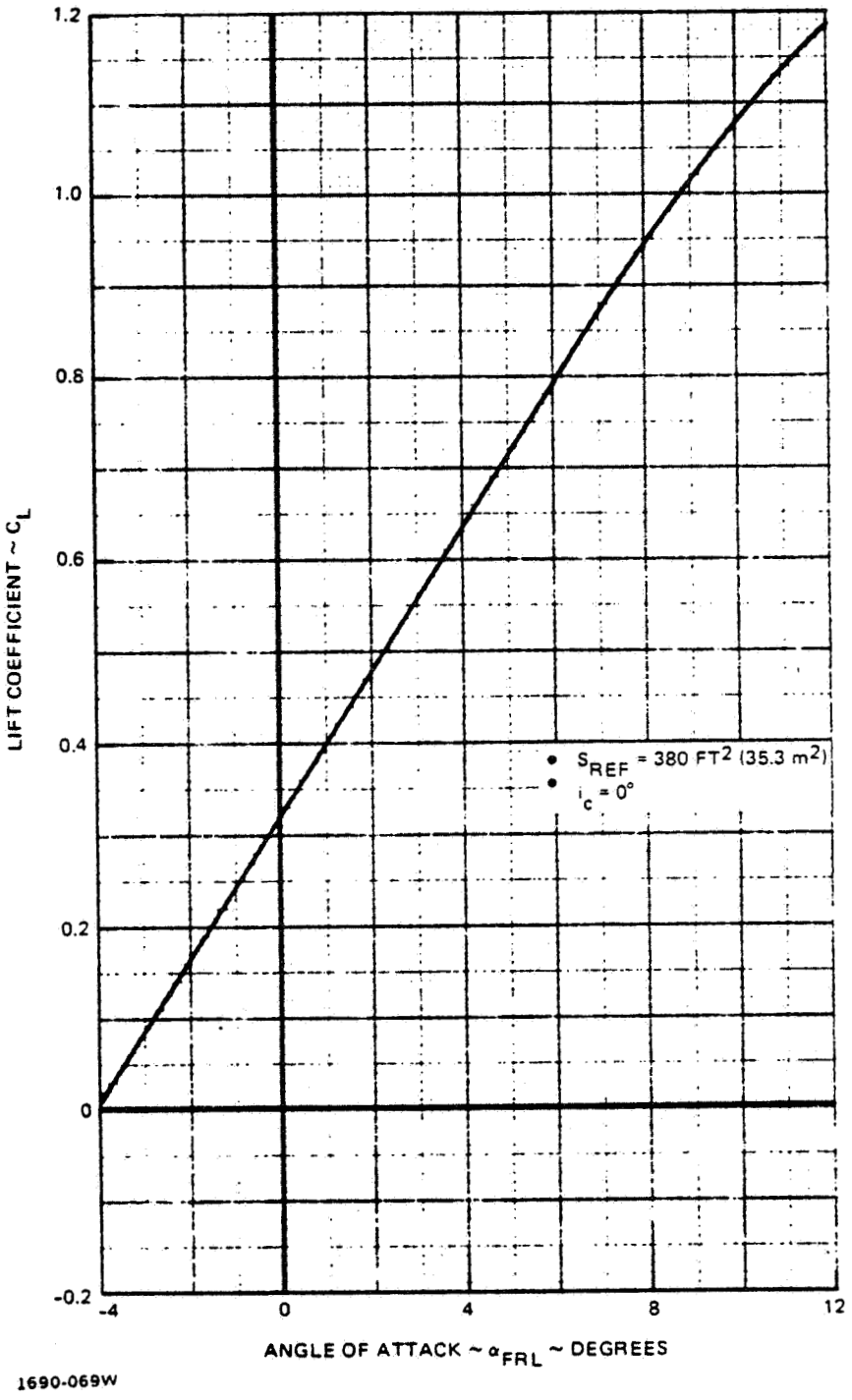

Figure 7.5-1 Design 623 – 2024 Lift Characteristics – Trailing Edge Devices Deflected

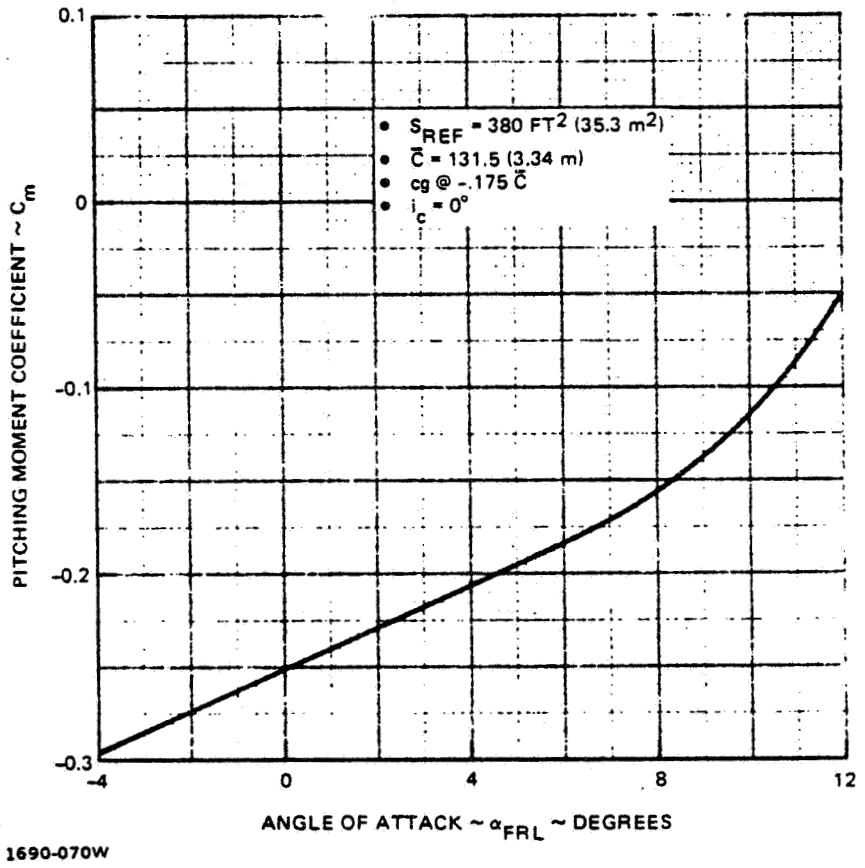

Figure 7.5-2 Design 623 - 2024 Pitching Moment Characteristics – Trailing Edge Devices Deflected

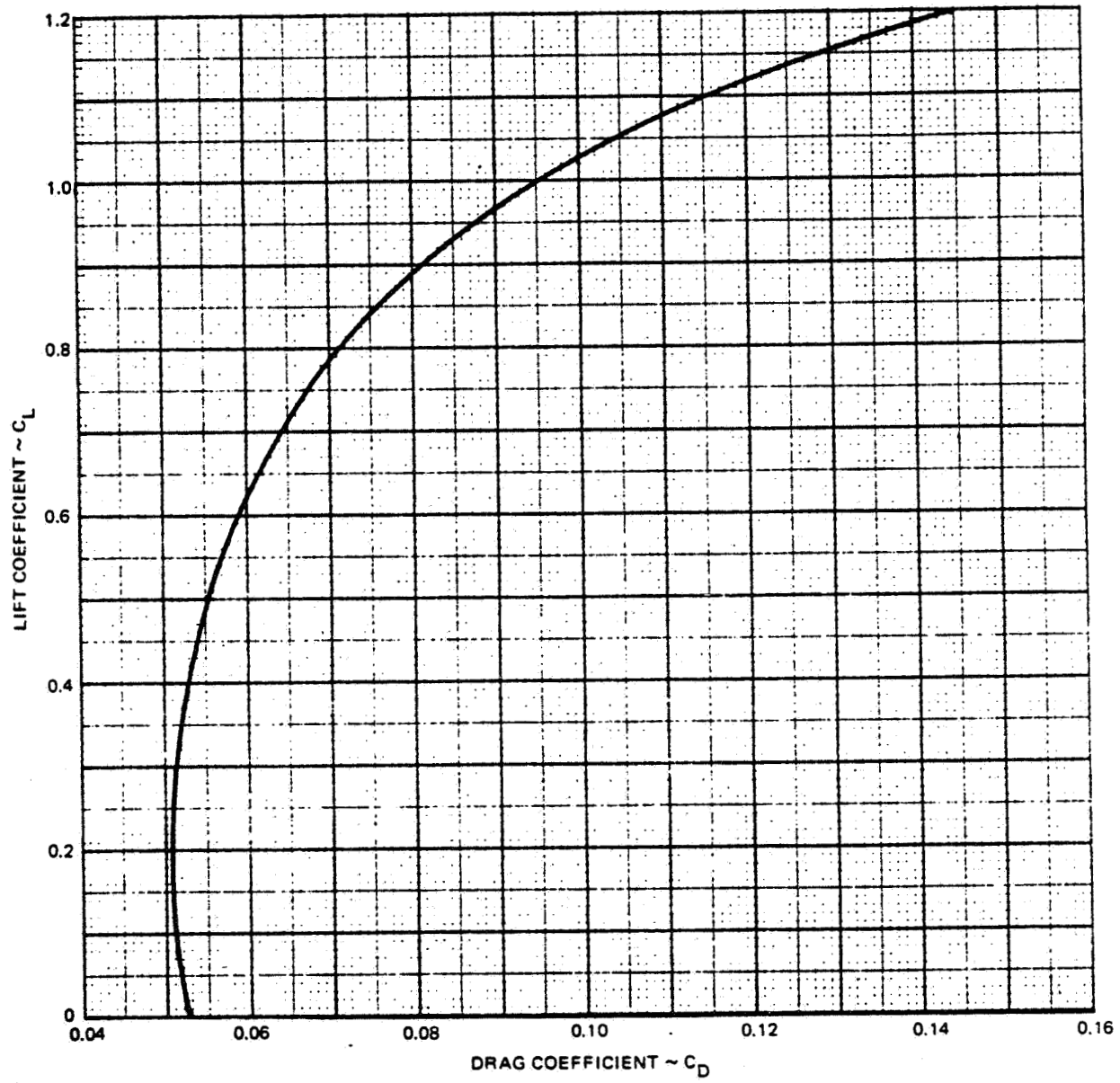

Figure 7.5-3 Design 623 – 2024 Drag Characteristics – Trailing Edge Devices Deflected

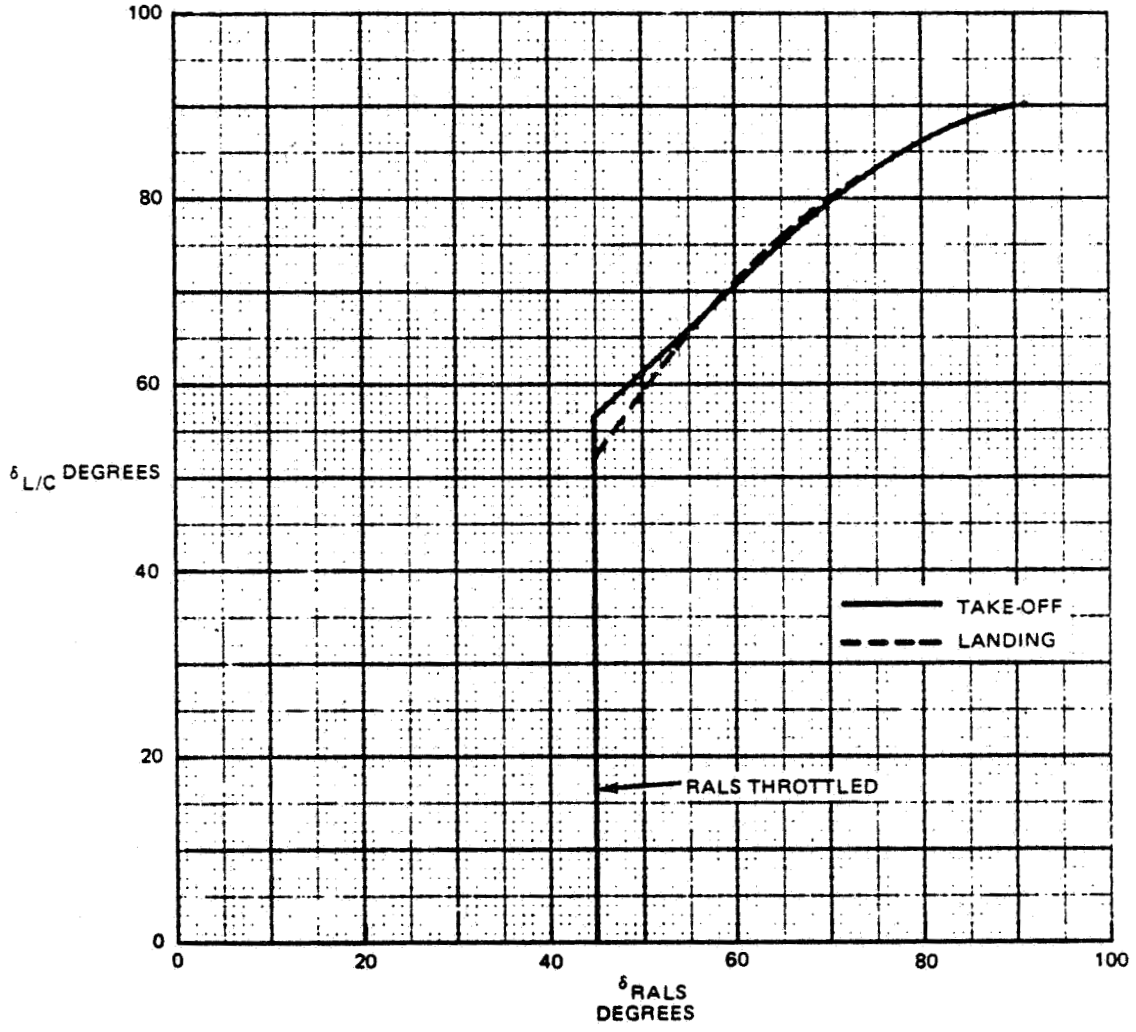

Figure 7.5-4 Design 623 – 2024 Nozzle Gearing for Static Thrust Moment Balance

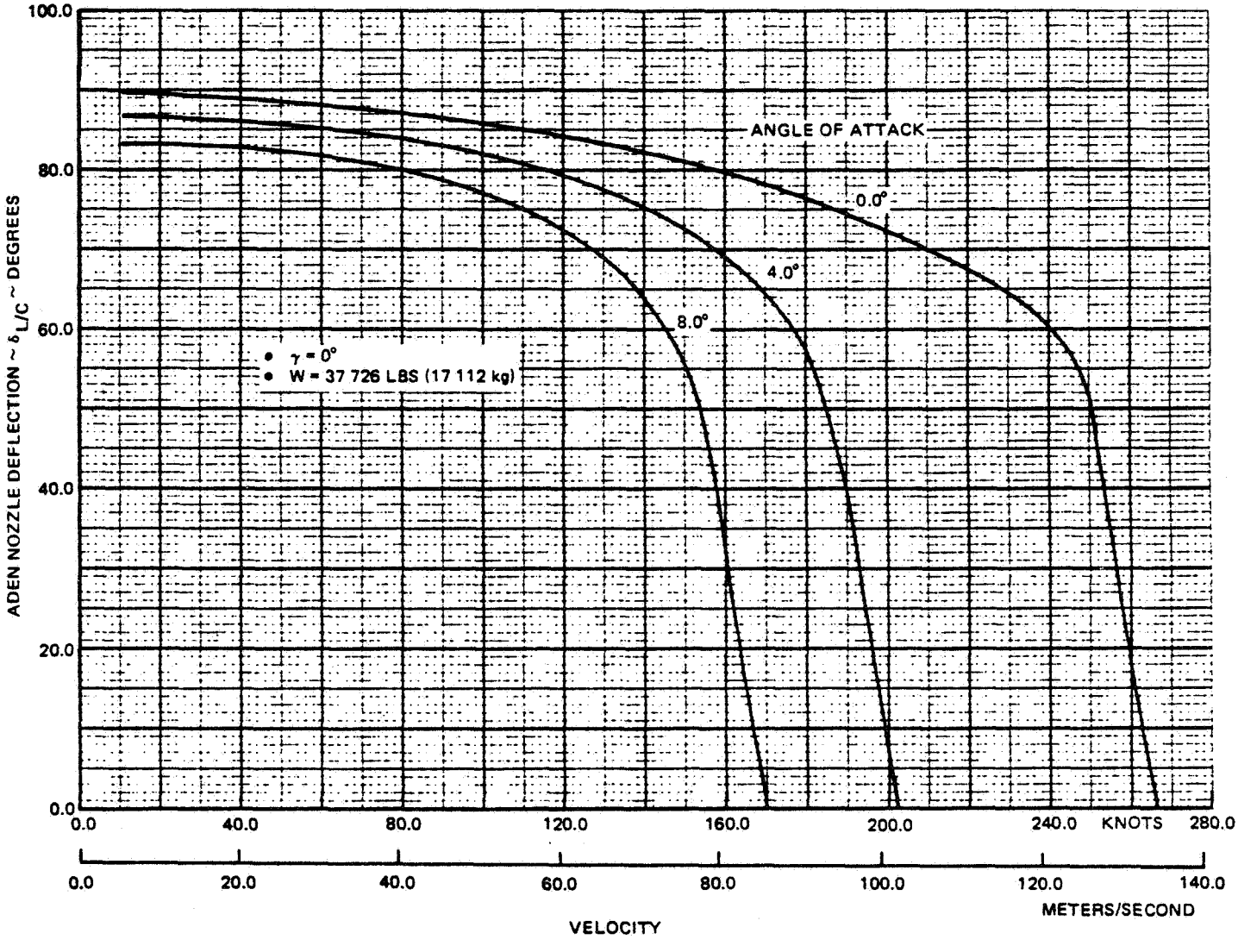

Figure 7.5-5 Design 623 - 2024 Takeoff Transition, Effect of Angle of Attack

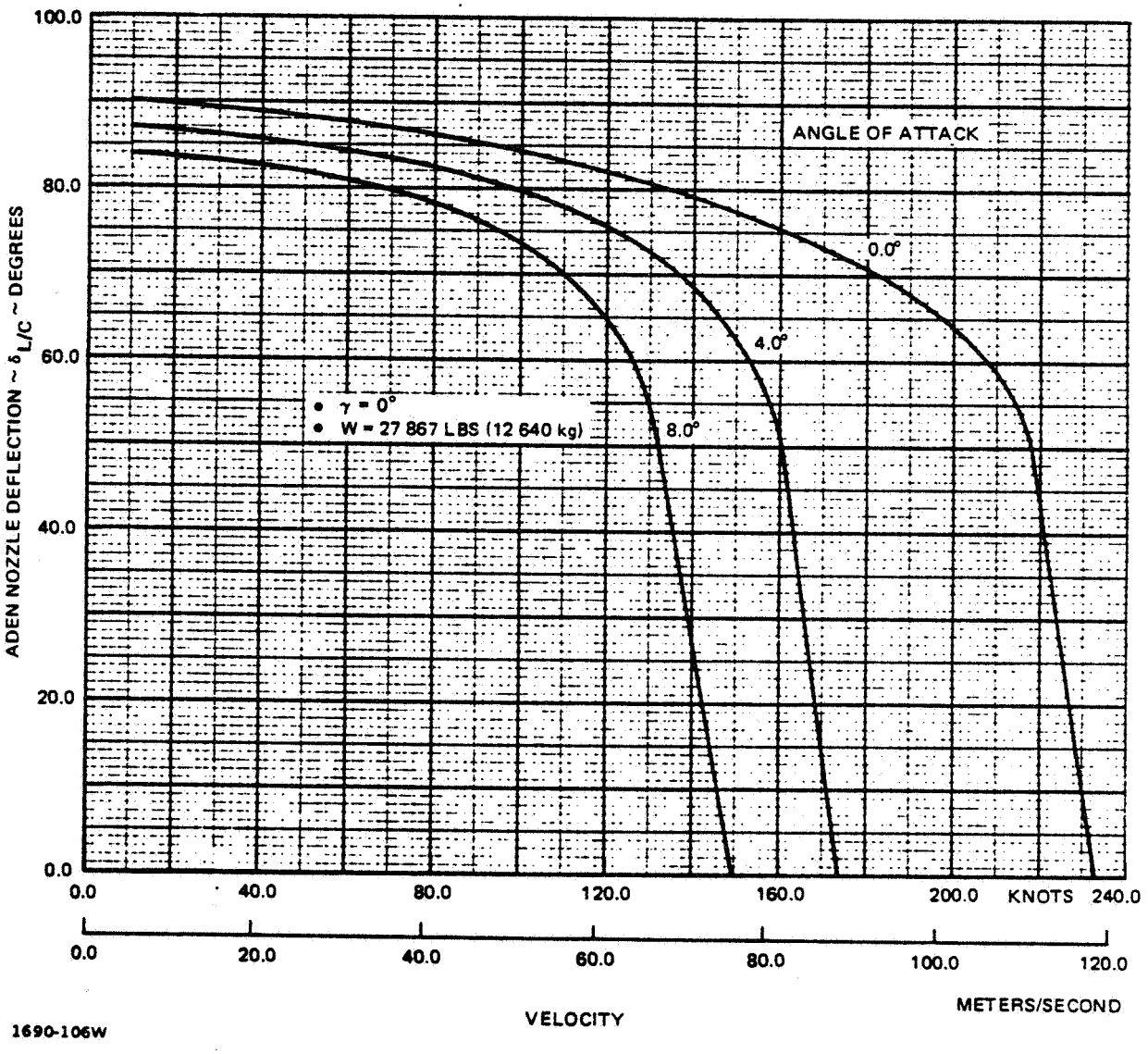

Figure 7.5-6 Design 623 - 2024 Landing Trasition, Effect of Angle of Attack

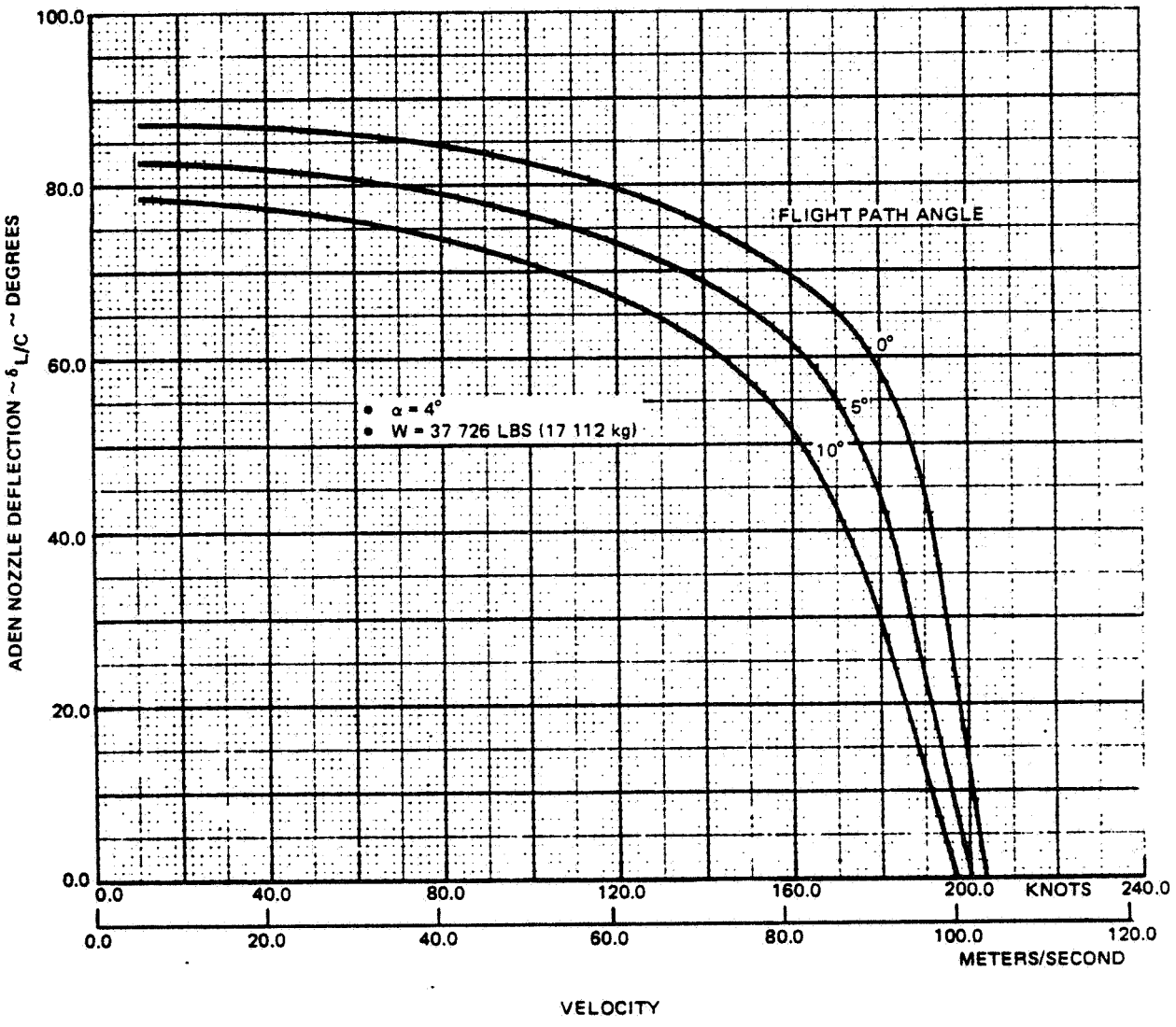

Figure 7.5-7 Design 623 - 2024 Takeoff Transition, Effect of Flight Path Angle

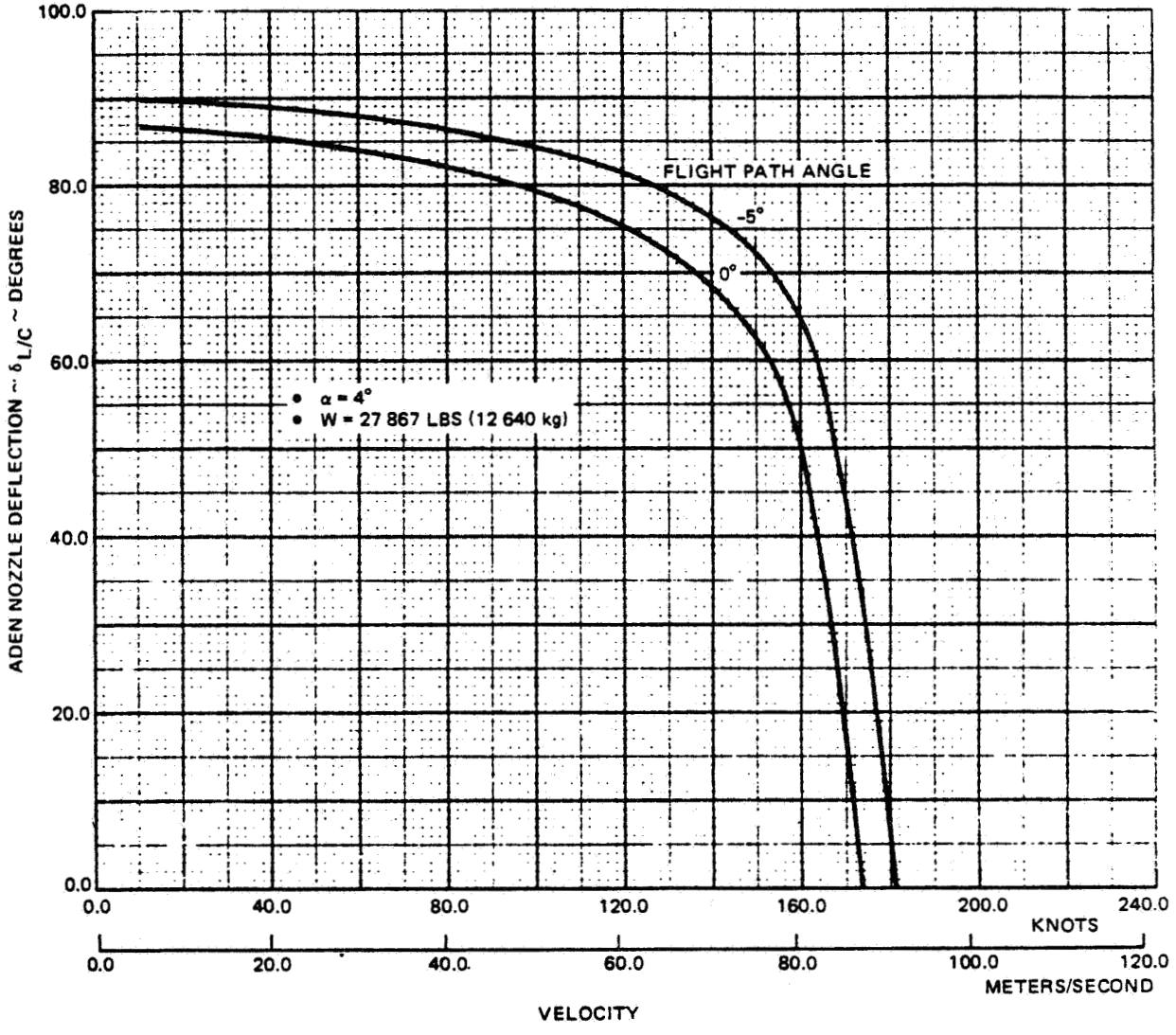

1690-108W

Figure 7.5-8 Design 623-2024 Landing Transition, Effect of Flight Path Angle

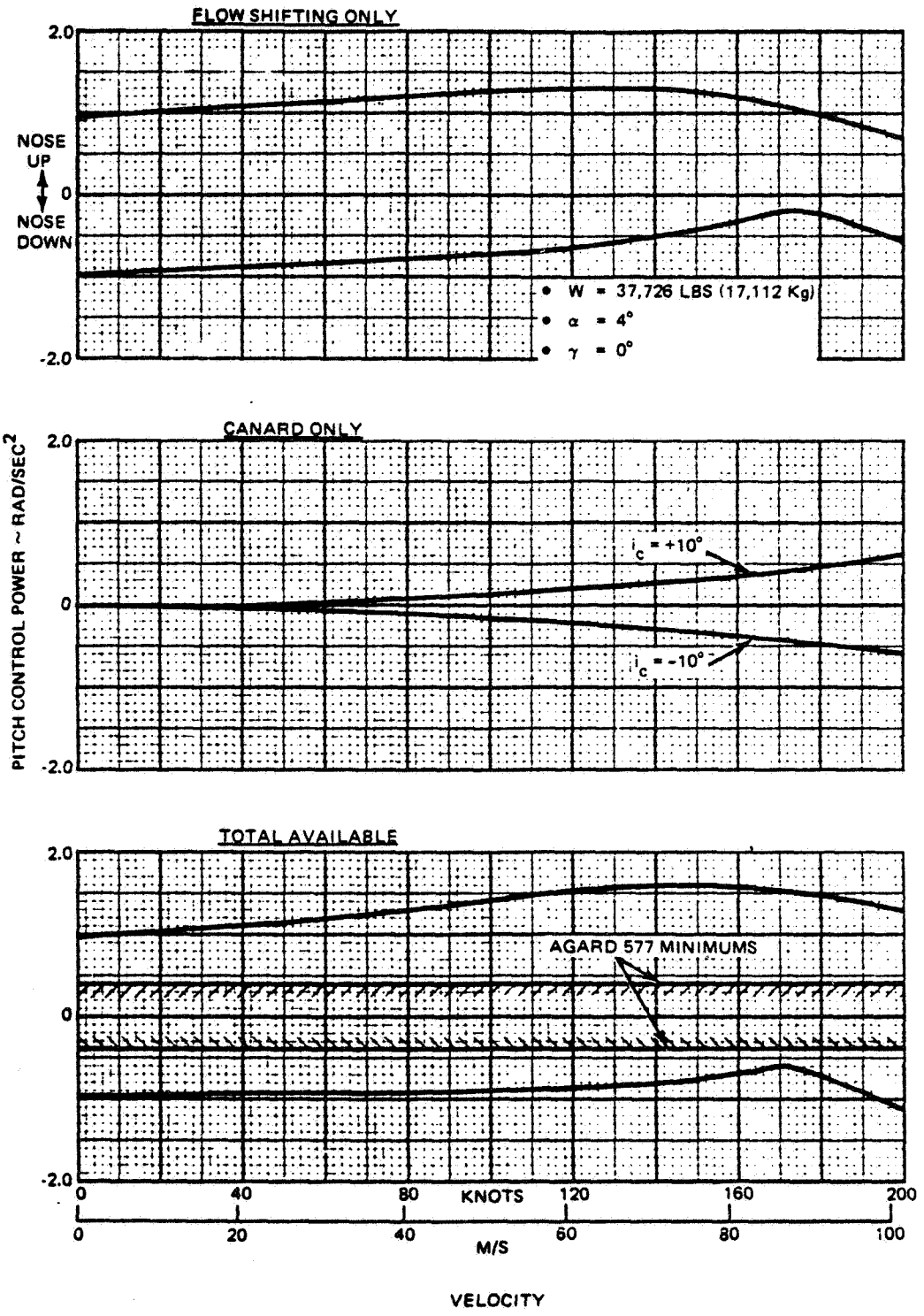

1690-122W

Figure 7.5-9 Design 623 - 2024 Maximum Available Pitch Control Power; Takeoff Transition

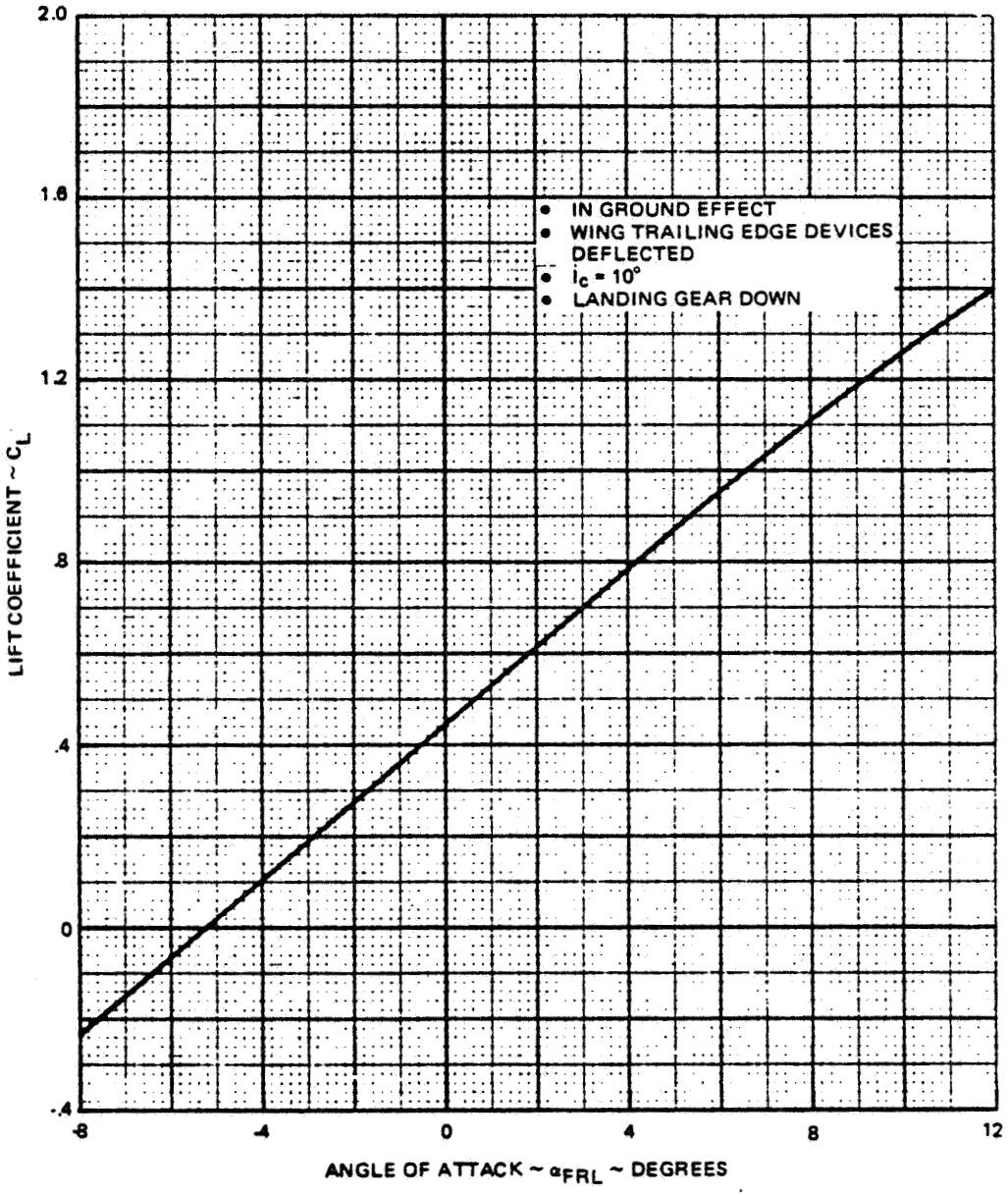

1690-046W

Figure 7.6-1 Design 623-2024 STO Lift Characteristics Power Off

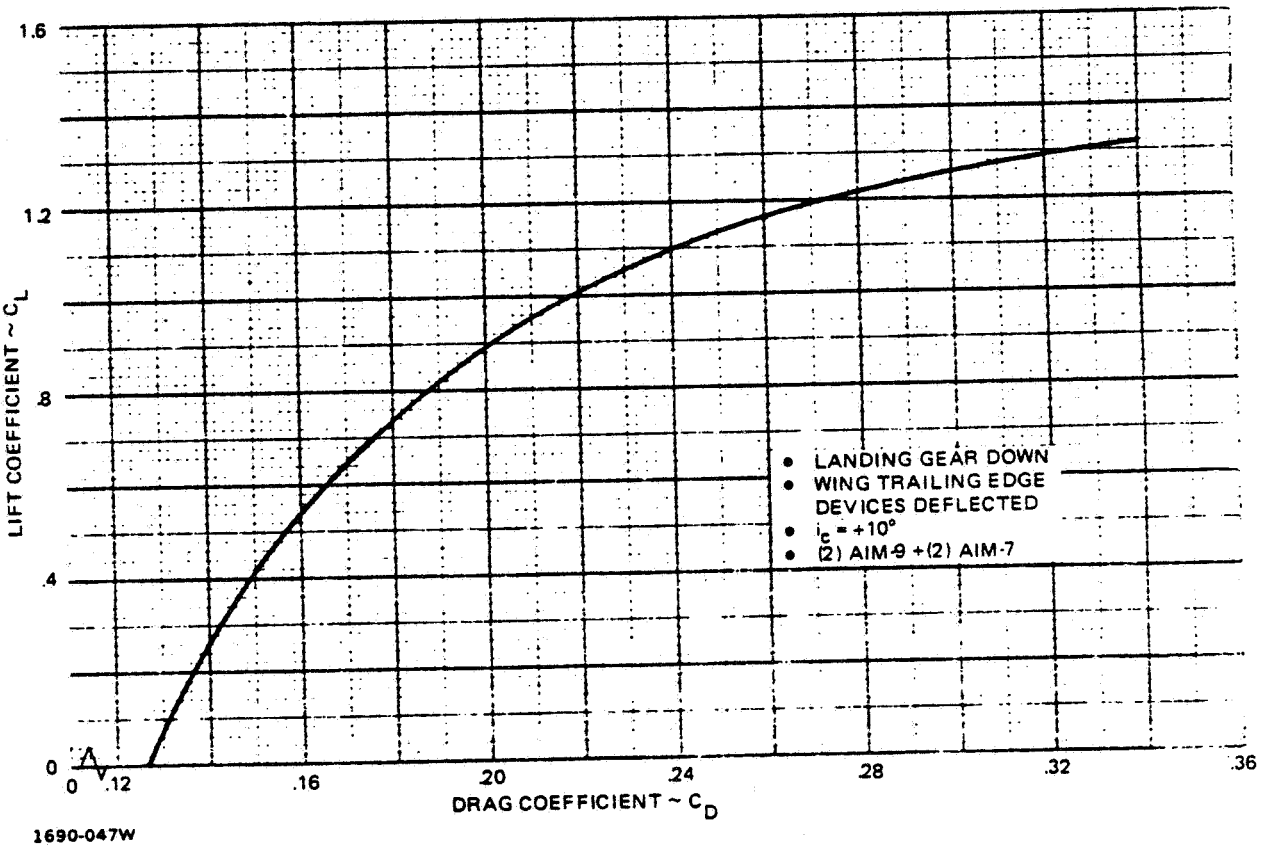

Figure 7.6-2 Design 623-2024 STO Drag Characteristics

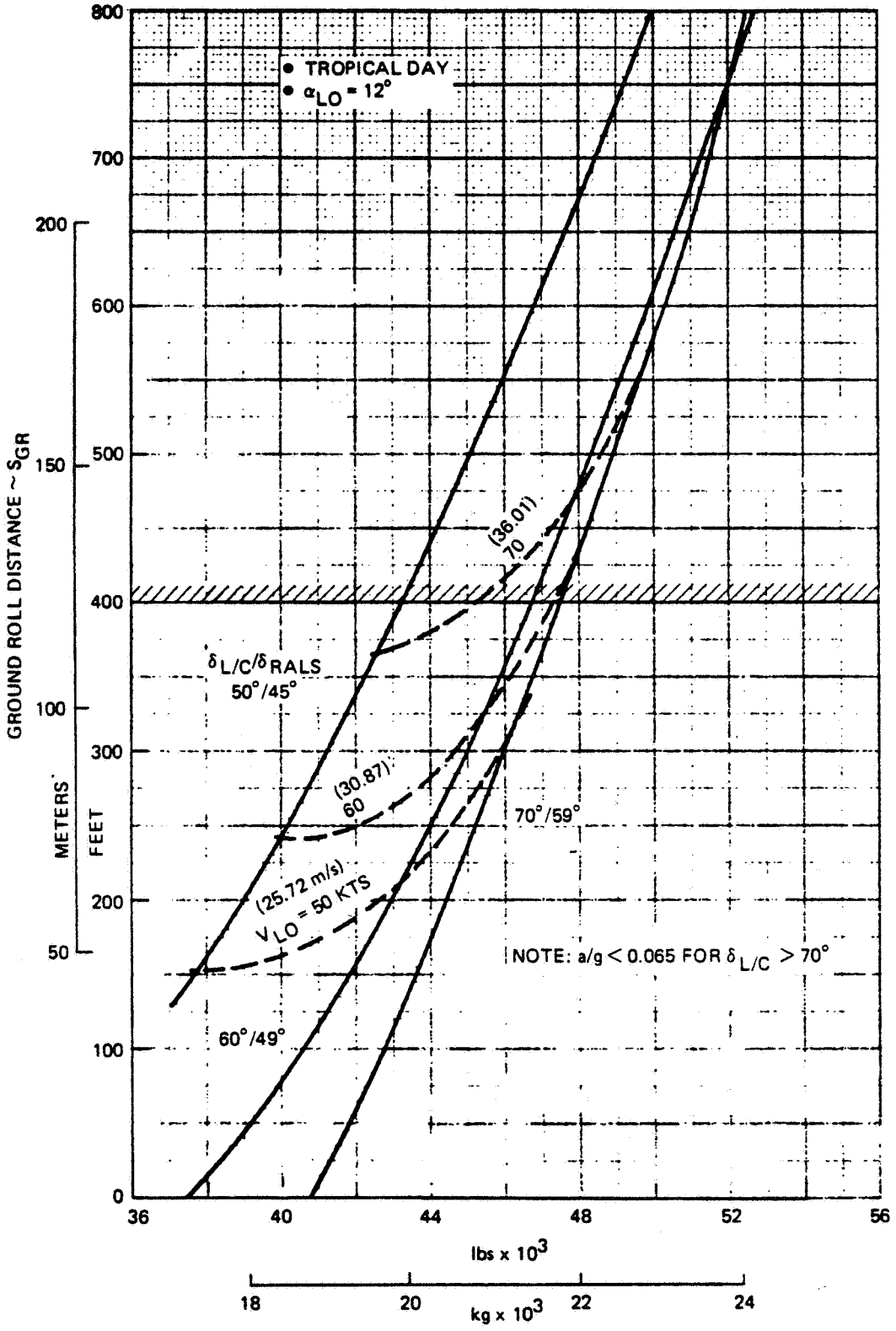

1690-048W

Figure 7.6-3 Design 623 – 2024 STO Performance
WOD = 0

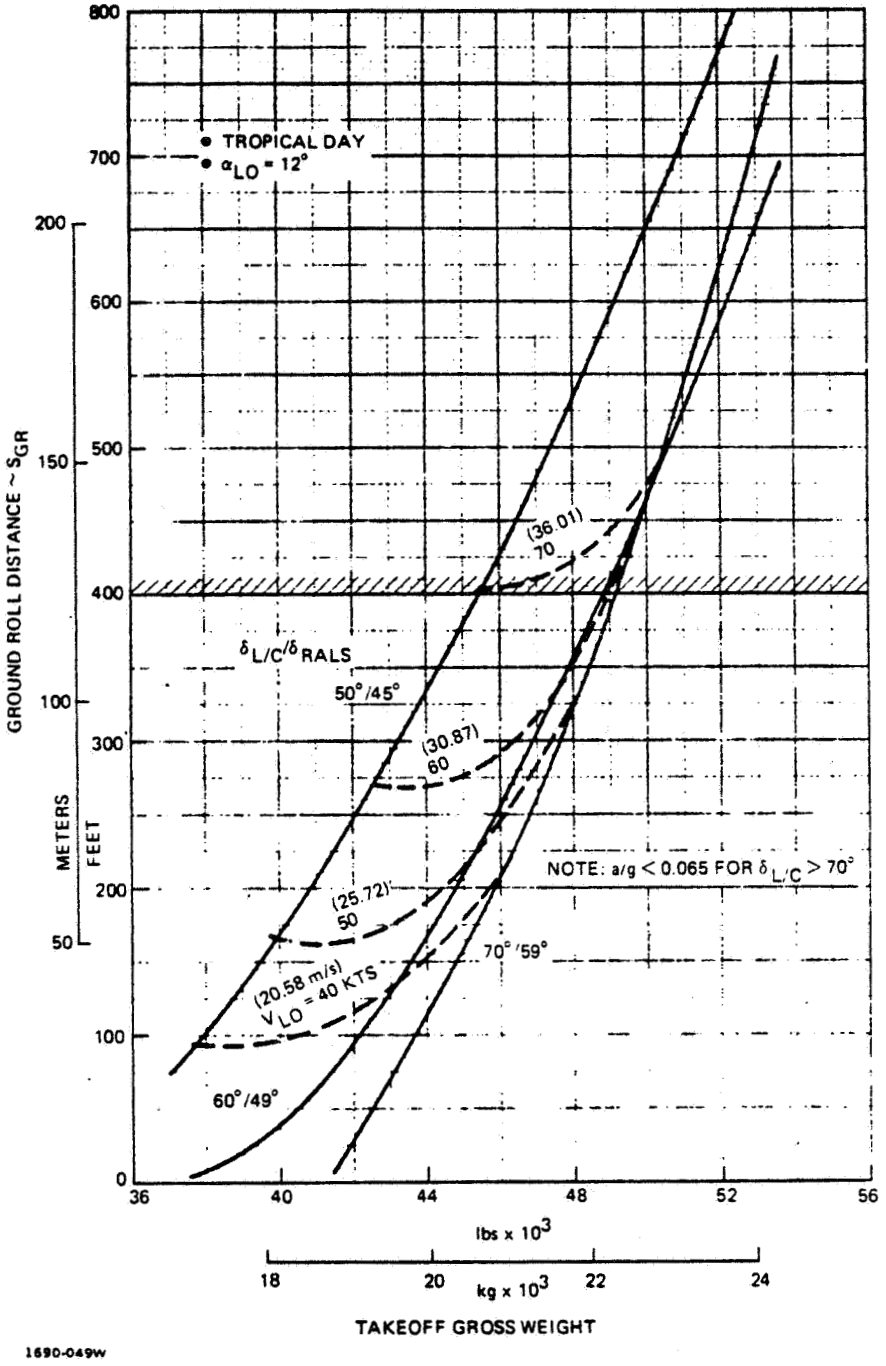

Figure 7.6-4 Design 623 – 2024 STO Performance
WOD = 10 KTS (5.14 m/s)

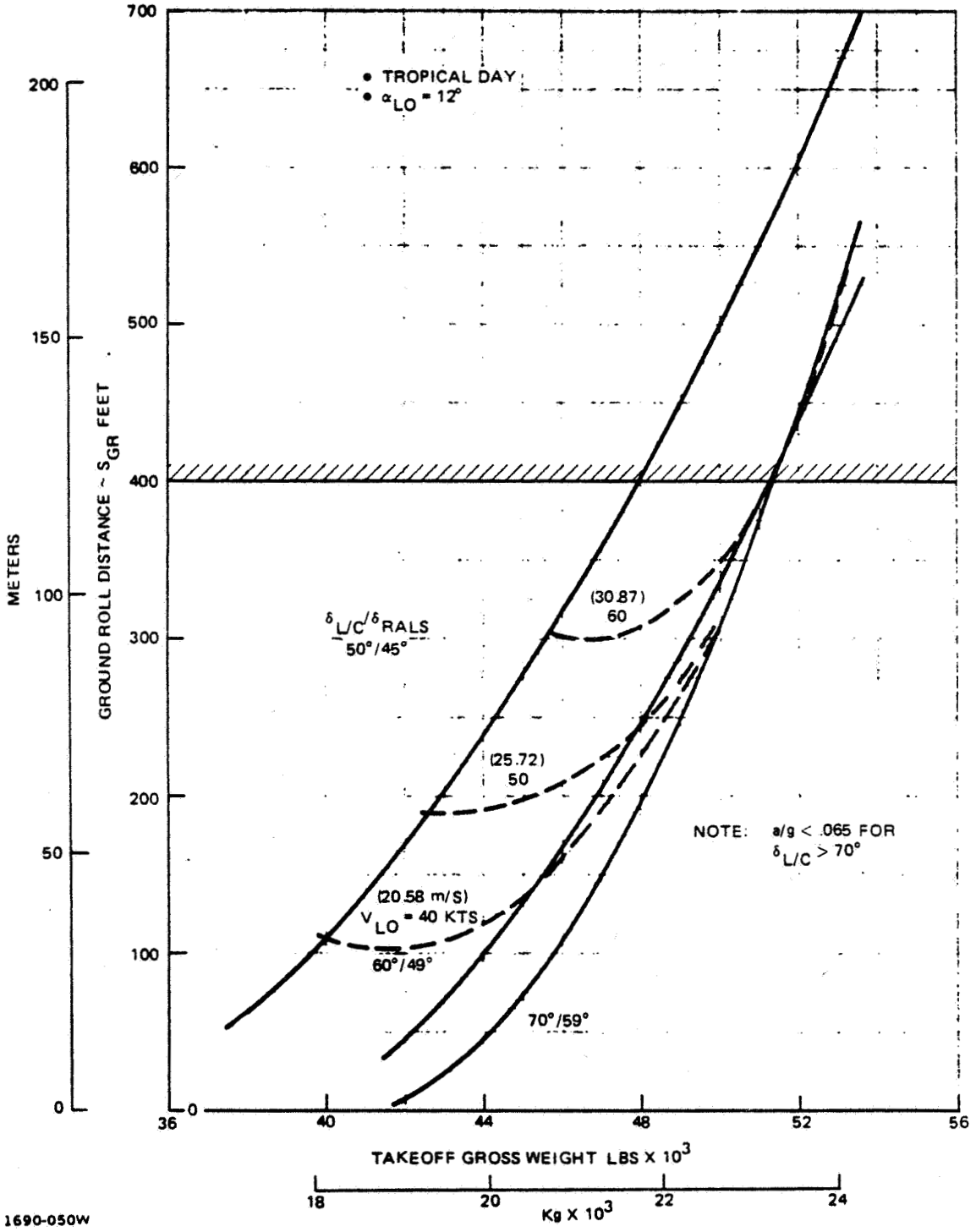

Figure 7.6-5 Design 623-2024 STO Performance WOD = 20 KTS (10.28 m/S)

8 - AERODYNAMIC UNCERTAINITIES

The following have been identified as areas of aerodynamic uncertainty that require additional research.

8.1 PROGRAMS AT AMES RESEARCH CENTER

8.1.1 Buffet Onset

Flight buffet is a dynamic aircraft behavior resulting from unsteady aerodynamic forces induced by flow separation. The primary mechanisms which initiate this unsteady flow condition are the existence of a shock wave on the wing and the boundary layer characteristics in the region of the separation. The location and strength of the shock greatly influence the buffet intensity. Many complex factors are involved in predicting buffet onset and present analytical techniques have been empirically derived from wind tunnel and flight test results.

An empirical data base does not exist for a configuration of the Design 623-2024 type, i.e. one employing a low aspect ratio supercritical wing. In addition, with a highly loaded wide-body and small exposed span, separation can occur initially on the fuselage, introducing another unknown in terms of predictability.

8.1.2 Aerodynamic Characteristics of Wide-Body, Low Aspect Ratio Wing Configurations

The methods available for determining the longitudinal and lateral/directional characteristics of an aircraft are largely based on slender body theory. These procedures are highly configuration dependent; proper definition of the wing and load carrying glove/pod are required. Design 623-2024 with the wide body/nacelle and a small exposed wing span, does not lend itself readily to math modelling with the majority of the presently available methods. An empirical data base must be established and correlation factors determined before an acceptable analytical method can be satisfactorily developed which can be applied with confidence to configurations of this type.

8.1.3 Close-Coupled Canard/Wing Interaction

Earlier Grumman studies, References 4.1.2-4 and 4.1.2-5, have indicated that the proper use of canard surfaces on a maneuvering aircraft can offer several positive features such as positive trim lift during maneuver and reduced trim drag. These same studies have also shown that canard control effectiveness is greatly influenced by canard/wing

geometry, with potentially large adverse mutual interference effects. Wind tunnel test results have shown that canard/wing interaction produces a complex flow field. State-of-the-art methodology is inadequate in predicting the aerodynamic characteristics of such configurations with a high degree of confidence. For optimum canard/wing design, adequate knowledge of the flow field is essential and can only be obtained at present from wind tunnel tests.

8.1.4 Thrust Vectoring/Supercirculation

Thrust vectoring/supercirculation (TV/SC) has indicated promise as a technology capable of potentially significant gains in performance and maneuverability for advanced fighters. The basic theoretical concept of supercirculation is the effective cambering of the buried wing-body, which, for a conventional configuration arrangement, would generate no camber lift of its own and only support carryover loads from the exposed wing panels. The non-axisymmetric nozzles essentially act as a jet flap in the buried wing area and ideally imparts to it the benefit of cambered wing loading. The effective cambering of the exposed wing panel is also increased thereby improving the load distribution. For an advanced supercritical variable camber wing design the benefits of (TV/SC) have not been established.

A major design aspect of incorporating (TV/SC) technology into a vehicle is the placement of the nozzle exhaust in the immediate vicinity of the wing trailing edge to induce supercirculation. Design 623-2024 has this feature, by virtue of other design considerations, and the accrued benefits should be assessed. These benefits are configuration dependent and generalizing such a technology can lead to questionable results. In order to gain insight into the basic flow phenomena occurring from the interaction of the deflected jet and wing flow field and the mutual interference effects with a close-coupled canard, parametric wind tunnel testing is required.

8.1.5 High Angle of Attack Characteristics

No exact analytical method is available for estimating high subsonic/transonic aerodynamics at high angles of attack. The unavailability of rigorous methods have been discussed in the literature, References 8.1.5-1 and 8.1.5-2. The difficulty is in the inability to account adequately for the location of the shock wave and the boundary layer characteristics around the region of separation.

There are empirical methods available that satisfactorily determine the lift characteristics of conventional wings but are inadequate for supercritical wing designs. More importantly, there are no procedures available for predicting drag, pitching moment and

lateral/directional characteristics at high angles of attack. Wind tunnel and flight testing are the only source for such data at present.

8.2 ADDITIONAL RESEARCH PROGRAMS

The following are additional aerodynamic areas of uncertainty not explored during the Phase II wind tunnel test program at the Ames Research Center but which, nevertheless should be part of a high speed V/STOL Research Program.

8.2.1 Jet Induced Interference Effects in Hover and Transition

Successful design and development of V/STOL aircraft requires an understanding and accurate prediction of aircraft forces and moments caused by jet-induced phenomena. This phenomenon is attributable to a number of complex flow/airframe/ground interactions. The flow interactions almost invariably result in an effective lift loss (suckdown) during the vertical mode of operation.

Grumman has been pursuing, both analytically (Reference 8.2.1-1) and experimentally (Reference 4.3-1), the parameters which contribute to jet-induced interference. Extensive wind tunnel test programs have been conducted and the results give some insight as to the complexity of the problem. Levels of jet-induced interference are sensitive to both airframe and nozzle configuration.

The efficient utilization of a model as a vehicle design guide is dependent on the simulation of several scaling parameters. A wind tunnel/flight test correlation and comparison study, Reference 8.2.1-1, has shown that real engine flow characteristics, i.e., effective velocity ratio, nozzle flow turbulance and mass flow control, are the critical parameters that must be properly simulated.

8.2.2 Reingestion

Recirculation of exhaust gases into the inlet(s) reduces the thrust available and can possibly result in compressor stall. The effects are configuration dependent and changes which alleviate this problem (i.e. reduction of fountain effects) can amplify another problem area (i.e., suckdown effects). The severity of the problem is a function of nozzle deflection angle, height above ground, aircraft attitude, wind velocity and direction.

Recirculation is usually classified into two categories: farfield effects, which are caused by heating of the ambient air and dependent on wind strength and direction, and near-field or fountain effects which are caused by the upward deflection of the jet plume. Both

phenomena require careful study, since small inlet temperature increments can result in significant thrust loss. The only means to accurately assess the impact on performance for preliminary design purposes is by model testing.

8.2.3 In Ground Effect at Forward Speed (STO) Characteristics

Short take-off (STO) performance may be limited by operational problems (i.e., recirculation/reingestion), which are not relevant to a conventional aircraft. Unlike the classical techniques representatively shown in Reference 4.1.2-8, theoretical and/or semi-empirical methods to define the ground effects of a V/STOL aircraft during a ground roll take-off do not exist.

The flow field surrounding a short take off is complicated by the free jet, wall jet and vortex recirculation (i.e., rolling up the wall jet field in a stable vortex sheet under front or crosswind conditions), which are a function of wind strength and direction. The effects of farfield hot gas reingestion, vortex recirculation and suckdown effects can only be established by model or full scale testing.

8.3 RANKING OF AERODYNAMIC UNCERTAINTIES

The areas of aerodynamic uncertainties, Sections 8.1 and 8.2, are ranked in order of their importance. Ranking is performed on the basis of two factors: 1) impact on vehicle design performance and 2) degree of predictability. The overall ranking of each aerodynamic parameter is obtained by a combination of the two numerical ranking factors. From this overall ranking the parameters requiring experimental evaluation are identified (see Table 8.3-1).

Based on overall ranking, jet-induced interference effects and reingestion are the areas of uncertainty which are most critical to the successful evolution of a high speed V/STOL design. Although these areas will not be investigated during the Phase II test program at NASA/AMES, considerable effort should be expended in reducing the degree of uncertainty of these high impact items. The next important areas of uncertainty (aerodynamics of wide-body configurations, buffet onset, high angle of attack characteristics) will be investigated during the Phase II program. The experimental program described in Section 9.0 explores these as well as the other conventional flight areas of uncertainty in depth.

TABLE 8.3-1

AERODYNAMIC UNCERTAINTY	RANKING *IMPACT	**PREDICT-ABILITY	OVERALL RANKING
• Buffet Onset	2	3	6
• Aerodynamic Characteristics of Wide Body Configurations	3	2	6
• Close-Coupled Canard/Wing Interaction	2	2	4
• Thrust Vectoring/Supercirculation	1	3	3
• High Angle of Attack Characteristics	2	3	6
• Jet-Induced Interference Effects in Hover and Transition	3	3	9
• Reingestion	3	3	9
• STO Characteristics	1	3	3

* 1 Minimal

2 Significant

3 Major

**1 Increasing degree of difficulty

2 ↓

3

9 - PROPOSED RESEARCH PROGRAM

9.1 OBJECTIVES

The wind tunnel model to be designed and fabricated during Phase II of this contract will be initially tested in a flow-through configuration. Therefore, the test program at the Ames Research Center will investigate the areas of uncertainty associated with the conventional flight regime which are not power dependent. Power-on testing may be done at a later date, when the XM2R propulsion simulators are available. The important areas of aerodynamic uncertainty which will be investigated have been delineated in Section 8.

9.2 MODEL DESCRIPTION

The model will feature modular construction to permit parametric investigation of the aerodynamic uncertainties identified during Phase I. The existing 1/8th scale Design 623 model will be extensively modified to be representative of the conceptual aircraft design developed in Phase I. Should differences exist between the model and Design 623-2024 due to model design considerations, appropriate adjustments to the estimated aerodynamic characteristics presented in this report will be made to establish a valid baseline for comparison with tunnel results.

Identifiable features which the model will incorporate are:

- Wing panels with multi element leading and trailing edge devices to establish relative benefits of supercritical variable camber concept
- Variable wing/exhaust nozzle longitudinal position and nozzle flap position to assess thrust vectoring supercirculation effects (during future power-on testing)
- Assymetric deflection of the wing trailing edge devices (aileron control panels) to assess roll control effectiveness
- Symmetric deflection of both wing leading and trailing edge segments (nose droop/flaps) to assess power-off short take-off, landing, and transition characteristics
- Canard with provisions for
  - o various vertical positions relative to the outer wing panel
  - o trailing edge flap
  - o leading edge droop device

- o variable incidence capability

- Removable vertical fins with provision for simulating rudder deflection

A straight sting model support will be utilized to enable aerodynamic investigation with variable sideslip. This support will only be used for the unpowered aerodynamic investigations. A means will be provided to evaluate any violations in aft fuselage contours and any interference associated with this installation. Power-off investigations will be conducted with flow-through nacelles. The wind tunnel model size will be compatible with the XM2R compact simulators for future powered testing as required in the Statement of Work. Replacement or modification of the existing bifurcated twin boom model support/air supply system to accommodate the operational requirements of the simulators may be necessary. The twin boom attaches to the vertical tail assemblies.

The wind tunnel model will be instrumented to acquire aerodynamic force, pressure and wing buffet data. Complete model force and moment data will be recorded on a primary 6-component strain gage balance. Spanwise rows of surface pressure instrumentation will be distributed on the canard and the wing. In addition, the wing will incorporate a root bending gage, tip accelerometer and trailing edge pressures for buffet analysis. For future powered model testing, nozzle internal and external forces will be measured in a secondary 6-component strain gage balance. Both the main and secondary balances are designed and fabricated as flow-through systems to permit effective passage of supply air for powering the model.

9.3 TEST PLANS

The test plans for the subsonic (12 ft Pressure), transonic (11 ft Unitary) and supersonic (9x7 ft Unitary) program are presented in Tables 9.3-1, 9.3-2 and 9.3-3, respectively. Table 9.3-4 lists the model nomenclature along with definitions of the pertinent test parameters. A schematic illustrating the variable camber orientation is shown on Figure 9.3-1.

Table 9.3-1 Grumman Design 623-2024 Subsonic Run Schedule; ARC 12-Ft. Pressure (1 of 2)

RUN NO.	CONFIG.	M	*α	β	ReN X10⁶	CAN. LOC.	ι_c/δ_{F_C}	δ_R	$*\delta_{W_1}$	$*\delta_{W_2}$	$*\delta_{W_3}$	$*\delta_{W_{4_I}}$	$*\delta_{W_{4_O}}$	$*\delta_{W_{5_I}}$	$*\delta_{W_{5_O}}$	WING PRESS.	REMARKS
1	BNWCV	.3	A	0	4.0	HIGH	0/0	0	0	0	0	0	0	0	0	NO	RAKE ON • RAKE OFF FOR REST OF TEST • BUFFET DATA
2	↓	↓	↓	↓	↓	↓	↓	↓	↓	↓	↓	↓	↓	↓	↓	YES	
3			0	C													
4			5														
5			10														
6			15				↓										
7			A	0			+5/0										
8			0	C													
9			5														
10			10														
11			15													↓	
12	↓		A	0		↓	↓									NO	INVERTED
13	BNWV		↓	↓		OFF	–									YES	
14	↓		0	A		↓	↓									↓	
15			5														
16			10														
17			15					↓									
18	BNW		A	0				OFF								NO	
19	↓		0	A				↓								↓	
20		↓	5	↓	↓	↓	↓		↓	↓	↓	↓	↓	↓	↓		
21	BNW	.3	10	A	4.0	OFF	–	OFF	0	0	0	0	0	0	0	NO	
22	↓		15	↓					↓	↓	↓	↓	↓	↓	↓		
23	BN		A	0					OFF	OFF	OFF	OFF	OFF	OFF	OFF		
24	↓		0	A					↓	↓	↓	↓	↓	↓	↓		
25			5														
26			10														
27			15														
28	BNWCV		A	0	5.0	HIGH	0/0	0	0	0	0	0	0	0	0		BUFFET DATA
29	↓		↓	↓	6.0							↓	↓	↓	↓		
30					4.0							+15	+15	+15	+15	YES	
31			0	A												NO	
32			5														
33			10														
34			15														
35			A	0					+5	+5	+5					YES	
36			0	A												NO	
37			5														
38			10														
39			15														
40	↓	↓	A	0	↓	↓	↓	↓	0	0	0	+10	+10	+10	+10	YES	

NOTES: *SEE FIGURE 9.3-1 αSCHEDULE A: -4° TO +40° Δ2° B: -4° TO +16° Δ4° βSCHEDULE A: -15° TO +15° ΔZ° B: -10° TO +10° Δ4° C: -30° TO -30° ΔZ°

1690-139W-1

Table 9.3-1 Grumman Design 623-2024 Subsonic Run Schedule; ARC 12-Ft. Pressure (2 of 2)

RUN NO.	CONFIG.	M	α	β	ReN X10^6	CAN. LOC.	$^{c}/_{b}F_{C}$	δ_R	$*\delta W_1$	$*\delta W_2$	$*\delta W_3$	$*\delta W_{4_I}$	$*\delta W_{4_O}$	$*\delta W_{5_I}$	$*\delta W_{5_O}$	WING PRESS.	REMARKS
41	BNWCV	.3	0	A	4.0	HIGH	0/0	0	0	0	0	0	+10	+10	+10	NO	
42			5														
43			10														
44			15														
45			A	0			5/0		3	3	3	6	6	6	6	YES	
46			0	C													
47			5														
48			10														
49			15														
50			A	0					0	0	0	0	0	0	0		BUFFET DATA
51							+5/5										
52							+5/10										
53							-5/5										
54						MID	0/0									NO	
55			0	A													
56			5														
57			10														
58			15														
59			A	0		LOW											
60			0														
61			5														
62			10														
63			15														
64			B	0		HIGH		+10									
65			0	B													
66			10														
67			B	0				+20									
68			0	B													
69			10														
70			B	0				+30									
71			0	B													
72			10														
73			B	0				0				±5	±5	±5	±5		RT. WING-T.E. UP LT. WING-T.E. DWN
74	BNWCV	.3	0	B	4.0	HIGH	0/0	0		0	0	±5	±5	±5	±5	NO	
75			5														
76			10														
77			15														

NOTES *SEE FIGURE 9.3-1

α SCHEDULE A: -4° TO +40° Δ2°
B: -4° TO +16° Δ4°

β SCHEDULE A: -15° TO +15° Δ2°
B: -10° TO +10° Δ4°
C: -30° TO -30° Δ 2°

1690-139W-2

Table 9.3-2 Grumman Design 623-2024 Transonic Run Schedule; ARC 11-Ft. Unitary (1 of 8)

RUN NO.	CONFIG.	M	α	β	ReN X10^6	CAN. LOC.	i_c/δ_{F_C}	δ_R	$*\delta_{W_1}$	$*\delta_{W_2}$	$*\delta_{W_3}$	$*\delta_{W_{4_I}}$	$*\delta_{W_{4_O}}$	$*\delta_{W_{5_I}}$	$*\delta_{W_{5_O}}$	WING PRESS.	REMARKS
1	BNWCV	.6	A	0	4.0	HIGH	0/0	0	0	0	0	0	0	0	0	NO	RAKE ON
2		.8															
3		.85															
4		.9															
5		.95															
6		1.2															
7		1.4															
8		1.4														YES	RAKE OFF FOR REST OF TEST
9	BNWCV	1.2	A	0	4.0	HIGH	0/0	0	0	0	0	0	0	0	0	YES	
10		.95															
11		.9															
12		.85															
13		.8															
14		.6															
15		.6														NO	INVERTED
16		.9															
17		1.2															
18		1.2	0	A												YES	
19			5														
20			10														
21		.9	0														
22			5														
23			10														
24			15														
25		.6	0														
26			5														
27			10														
28			15														
29		.6	A	0	5.0											NO	
30		.8															
31		.9															
32		.9			6.0												
33		.8															
34		.6															
35	BNWV	.6			4.0	OFF	–									YES	
36			0	A													
37			5														
38			10														
39			15														
40		.8	A	0													

NOTES: *SEE FIGURE 9.3-1

α SCHEDULE A: -4° TO +26° Δ2°
B: -4° TO +16° Δ4°

β SCHEDULE A: -15° TO +15° Δ2°
B: -10° TO +10° Δ4°

1690-121W-1

Table 9.3-2 Grumman Design 623-2024 Transonic Run Schedule; ARC 11-Ft. Unitary (2 of 8)

RUN NO.	CONFIG.	M	α	β	ReN X10^6	CAN. LOC.	i_c/δ_{F_C}	δ_R	$^*\delta_{W_1}$	$^*\delta_{W_2}$	$^*\delta_{W_3}$	$^*\delta_{W_{4_I}}$	$^*\delta_{W_{4_O}}$	$^*\delta_{W_{5_I}}$	$^*\delta_{W_{5_O}}$	WING PRESS.	REMARKS
41	BNWV	.85	A	0	4.0	OFF	–	0	0	0	0	0	0	0	0	YES	
42		.9															
43			0	A													
44			5														
45			10														
46			15														
47		.95	A	0													
48		1.2															
49			0	A													
50			5														
51			10														
52		1.4	A	0													
53	BNW	1.4						OFF								NO	
54		1.2															
55			0	A													
56			5														
57			10														
58		.95	A	0													
59		.9															
60			0	A													
61			5				–										
62			10														
63			15														
64		.85	A	0													
65		.8															
66		.6															
67			0	A													
68			5														
69			10														
70			15														
71	BN		A	0					OFF	OFF	OFF	OFF	OFF	OFF	OFF		
72			0	A													
73			5														
74			10														
75			15														
76		.8	A	0													
77		.85															
78		.9															
79			0	A													
80			5														

NOTES: *SEE FIGURE 9.3-1 α SCHEDULE A: -4° TO +26° Δ2° B: -4° TO +16° Δ4° β SCHEDULE A: -15° TO +15° Δ2° B: -10° TO +10° Δ4°

1690-121W-2

Table 9.3-2 Grumman Design 623-2024 Transonic Run Schedule; ARC 11-Ft. Unitary (3 of 8)

RUN NO.	CONFIG.	M	α	β	ReN X10^6	CAN. LOC.	i_c/δ_{FC}	δ_R	$*\delta_{W_1}$	$*\delta_{W_2}$	$*\delta_{W_3}$	$*\delta_{W_{4_I}}$	$*\delta_{W_{4_O}}$	$*\delta_{W_{5_I}}$	$*\delta_{W_{5_O}}$	WING PRESS.	REMARKS
81	BN	.9	10	A	4.0	OFF	–	OFF	OFF	OFF	OFF	OFF	OFF	OFF	OFF	NO	
82			15														
83		.95	A	0													
84		1.2															
85			0	A													
86			5														
87			10														
88		1.4	A	0													
89	BNWCV	.6	A	0		HIGH	0/0	0	3	3	3	6	6	6	6	YES	BUFFET DATA
90			0	B													
91			5														
92			10														
93			15														BUFFET DATA
94		.8	A	0													
95			0	B													
96			5														
97			10														
98			15														BUFFET DATA
99		.9	A	0													
100			0	B										6			
101			5	B													
102			10														
103			15										0		0		BUFFET DATA
104		.6	A	0													
105			0	B													
106			5														
107			10														
108			15														BUFFET DATA
109		.8	A	0													
110			0	B													
111			5														
112			10														
113			15														BUFFET DATA
114		.9	A	0													
115			0	B													
116			5														
117			10														
118			15									12	6	12	6		
119		.6	A	0													
120				B													BUFFET DATA

NOTES: *SEE FIGURE 9.3-1 α SCHEDULE A: -4° TO +26° Δ2° B: -4° TO +16° Δ4° β SCHEDULE A: -15° TO +15° Δ2° B: -10° TO +10° Δ4°

1690-121W-3

Table 9.3-2 Grumman Design 623-2024 Transonic Run Schedule; ARC 11-Ft. Unitary (4 of 8)

RUN NO.	CONFIG.	M	α	β	ReN X10^6	CAN. LOC.	i_c/δ_{F_C}	δ_R	$*\delta_{W_1}$	$*\delta_{W_2}$	$*\delta_{W_3}$	$*\delta_{W_{4_I}}$	$*\delta_{W_{4_O}}$	$*\delta_{W_{5_I}}$	$*\delta_{W_{5_O}}$	WING PRESS.	REMARKS
121	BNWCV	.6	5	B	4.0	HIGH	0/0	0	3	3	3	12	6	12	6	YES	
122			10														
123		↓	15	↓													
124		.8	A	0													BUFFET DATA
125			0	B													
126			5														
127			10														
128		↓	15	↓													
129		.9	A	0													BUFFET DATA
130			0	B													
131			5														
132			10														
133		↓	15	↓					↓	↓	↓	↓		↓			
134		.6	A	0					6	6	6	6		6			BUFFET DATA
135			0	B													
136			5														
137			10														
138		↓	15	↓													
139		.8	A	0													BUFFET DATA
140			0	B													
141			5														
142			10														
143		↓	15	↓													
144		.9	A	0													BUFFET DATA
145			0	B													
146			5														
147			10														
148		↓	15	↓			↓		↓	↓	↓						
149		.6	A	0			+5/0		3	3	3						BUFFET DATA
150			0	B													
151			5														
152			10														
153		↓	15	↓													
154		.8	A	0													BUFFET DATA
155			0	B													
156			5														
157			10														
158		↓	15	↓													
159		.9	A	0													BUFFET DATA
160	↓		0	B	↓	↓	↓	↓	↓	↓	↓	↓	↓	↓	↓	↓	

NOTES: *SEE FIGURE 9.3-1 α SCHEDULE A: -4° TO +26° Δ2° B: -4° TO +16° Δ4° β SCHEDULE A: -15° TO +15° Δ2° B: -10° TO +10° Δ4°

1690-121W-4

Table 9.3-2 Grumman Design 623-2024 Transonic Run Schedule; ARC 11-Ft. Unitary (5 of 8)

RUN NO.	CONFIG.	M	α	β	ReN X10^6	CAN. LOC.	i_c/δ_{F_C}	δ_R	$*\delta_{W_1}$	$*\delta_{W_2}$	$*\delta_{W_3}$	$*\delta_{W_{4_I}}$	$*\delta_{W_{4_O}}$	$*\delta_{W_{5_I}}$	$*\delta_{W_{5_O}}$	WING PRESS.	REMARKS
161	BNWCV	.9	5	B	4.0	HIGH	+5/0	0	3	3	3	6	6	6	6	YES	
162			10														
163			15														
164		.6	A	0									0		0		BUFFET DATA
165			0	B													
166			5														
167			10														
168			15														
169		.8	A	0													BUFFET DATA
170			0	B													
171			5														
172			10														
173			15														
174		.9	A	0													BUFFET DATA
175			0	B													
176			5														
177			10														
178			15														
179		.6	A	0								12	6	12	6		BUFFET DATA
180			0	B													
181			5														
182			10														
183			15														BUFFET DATA
184		.8	A	0													
185			0	B													
186			5														
187			10														
188			15														BUFFET DATA
189		.9	A	0													
190			0	B													
191			5														
192			10														
193			15														BUFFET DATA
194		.6	A	0					6	6	6	6		6			
195			0	B													
196			5														
197			10														
198			15														BUFFET DATA
199		.8	A	0													
200			0	B													

NOTES: *SEE FIGURE 9.3-1 α SCHEDULE A: -4° TO +26° Δ2° B: -4° TO +16° Δ4° β SCHEDULE A: -15° TO +15° Δ2° B: -10° TO +10° Δ4°

1690-121W-5

Table 9.3-2 Grumman Design 623-2024 Transonic Run Schedule; ARC 11-Ft. Unitary (6 of 8)

RUN NO.	CONFIG.	M	α	β	ReN X10^6	CAN. LOC.	i_c/δ_{F_C}	δ_R	$*\delta_{W_1}$	$*\delta_{W_2}$	$*\delta_{W_3}$	$*\delta_{W_{4_I}}$	$*\delta_{W_{4_O}}$	$*\delta_{W_{5_I}}$	$*\delta_{W_{5_O}}$	WING PRESS.	REMARKS
201	BNWCV	.8	5	B	4.0	HIGH	+5/0	0	6	6	6	6	6	6	6	YES	
202			10														
203			15														BUFFET DATA
204		.9	A	0													
205			0	B													
206			5														
207			10														
208			15					0	0	0	0	0	0	0	0	NO	
209		.6	A	0													
210		.8															
211		.9															
212		1.2															
213		1.4															
214		1.4					+10/0										
215		1.2															
216		.9															
217		.8															
218		.6															
219		.6					-5/0										
220		.8															
221		.9															
222		1.2															
223		1.4				MID	0/0										
224		1.2		A													
225			5														
226			10	A													
227		.9	A	0													
228			0	A													
229			5														
230			10														
231			15														
232		.6	A	0													
233			0	A													
234			5														
235			10														
236			15														
237		.6	A	0		LOW											
238			0	A													
239			5														
240																	

NOTES: *SEE FIGURE 9.3-1 α SCHEDULE A: -4° TO +26° Δ2° B: -4° TO +16° Δ4° β SCHEDULE A: -15° TO +15° Δ2° B: -10° TO +10° Δ4°

1690-121W-6

Table 9.3-2 Grumman Design 623-2024 Transonic Run Schedule; ARC 11-Ft. Unitary (7 of 8)

RUN NO.	CONFIG.	M	α	β	ReN X10^6	CAN. LOC.	$i_c/\delta F_C$	δR	$*\delta W_1$	$*\delta W_2$	$*\delta W_3$	$*\delta W_{4_I}$	$*\delta W_{4_O}$	$*\delta W_{5_I}$	$*\delta W_{5_O}$	WING PRESS.	REMARKS
241	BNWCV	.6	10	A	4.0	LOW	0/0	0	0	0	0	0	0	0	0	NO	
242			15														
243		.9	A	0													
244			5														
245			10														
246			15														
247		1.2	A	0													
248			0	A													
249			5														
250			10														
251			15														
252		.6	B	0		HIGH	+5										
253			0	B													
254			5														
255			10														
256			15														
257		.8	B	0													
258			0	B													
259			5														
260			10														
261			15				0/0	+5									
262		.9	B	0													
263			0	B													
264			5														
265			10														
266			15														
267		1.2	B	0													
268			0	B													
269			5														
270			10														
271		1.4	B	0													
272			0	B													
273			5														
274			10														
275		1.4	B	0				0				±5	±5	±5	±5		RT WING-TE UP LT WING-TE DWN
276			0	B	4.0	HIGH	0/0	0	0	0	0	±5	±5	±5	±5	NO	
277			5														
278			10														
279		1.2	B	0													
280			0	B													

NOTES: *SEE FIGURE 9.3-1 α SCHEDULE A: -4° TO +26° Δ2° B: -4° TO +16° Δ4° β SCHEDULE A: -15° TO +15° Δ2° B: -10° TO +10° Δ4°

1690-121W-7

Table 9.3-2 Grumman Design 623-2024 Transonic Run Schedule; ARC 11-Ft. Unitary (8 of 8)

RUN NO.	CONFIG.	M	α	β	ReN $X10^6$	CAN. LOC.	$c/\delta F_C$	δR	$*\delta W_1$	$*\delta W_2$	$*\delta W_3$	$*\delta W_{4_I}$	$*\delta W_{4_O}$	$*\delta W_{5_I}$	$*\delta W_{5_O}$	WING PRESS.	REMARKS
281	BNWCV	1.2	5	B	4.0	HIGH	0/0	0	0	0	0	±5	±5	+5	±5	NO	RT WING-TE UP LT WING-TE DWN
282	BNWCV	1.2	10	B	4.0	HIGH	0/0	0	0	0	0	±5	±5	±5	±5	NO	
283		.9	B	0													
284			0	B													
285			5														
286			10														
287			15														
288		.8	B	0													
289			0	B													
290			5														
291			10														
292			15														
293		.6	B	0													
294			0	B													
295			5														
296			10														
297			15														

NOTES: *SEE FIGURE 9.3-1 α SCHEDULE A: -4° TO +26° Δ2° B: -4° TO +16° Δ4° β SCHEDULE A: -15° TO +15° Δ2° B: -10° TO +10° Δ4°

1690-121W-8

Table 9.3-3 Grumman Design 623-2024 Supersonic Run Schedule; ARC 9 x 7 - Ft. Unitary (1 of 2)

RUN NO.	CONFIG.	M	α	β	ReN X10^6	CAN. LOC.	$\iota_c/\delta F_C$	δ_R	$^*\delta W_1$	$^*\delta W_2$	$^*\delta W_3$	$^*\delta W_{4_I}$	$^*\delta W_{4_O}$	$^*\delta W_{5_I}$	$^*\delta W_{5_O}$	WING PRESS.	REMARKS
1	BNWCV	1.6	VAR	0	4.0	HIGH	%	0	0	0	0	0	0	0	0	NO	RAKE ON
2		1.8															
3																YES	RAKE OFF FOR REST OF TEST
4		1.6															
5																NO	INVERTED
6		1.8															
7			0	VAR												YES	
8			5														
9			10														
10		1.6	0														
11			5														
12			10														
13	BNWV		VAR	0													
14			0	VAR												NO	
15			5														
16			10														
17		1.8	VAR	0												YES	
18			0	VAR												NO	
19			5														
20			10														
21	BNW	1.8	VAR	0	4.0	HIGH	%	0	0	0	0	0	0	0	0	NO	
22			0	VAR													
23			5														
24			10														
25		1.6	VAR	0													
26			0	VAR													
27			5														
28			10														
29	BN	1.6	VAR	0													
30			0	VAR													
31			5														
32			10														
33		1.8	VAR	0													
34			0	VAR													
35			5														
36			10														
37	BNWCV	1.8	VAR	0			+5/0									YES	
38		1.6															
39							+10/0										
40		1.8															

NOTES: *SEE FIGURE 9.3-1

1690-126-1W

Table 9.3-3 Grumman Design 623-2024 Supersonic Run Schedule; ARC 9 x 7-Ft. Unitary (2 of 2)

RUN NO.	CONFIG.	M	α	β	ReN X10^6	CAN. LOC.	i_c/h_{F_C}	h_R	$*h_{W_1}$	$*h_{W_2}$	$*h_{W_3}$	$*h_{W_{4_I}}$	$*h_{W_{4_O}}$	$*h_{W_{5_I}}$	$*h_{W_{5_O}}$	WING PRESS.	REMARKS
41	BNWV	1.8	VAR	0	4.0	HIGH	-5/0	0	0	0	0	0	0	0	0	YES	
42		1.6															
43		1.6				MID	0/0										
44			0	VAR												NO	
45			5														
46			10														
47		1.8	VAR	0												YES	
48			0	VAR												NO	
49			5														
50			10														
51		1.8	VAR	0		LOW										YES	
52			0	VAR												NO	
53			5														
54			10														
55		1.6	VAR	0												YES	
56			0	VAR												NO	
57			5														
58			10														
59		1.6	VAR	0		HIGH	+5										
60			0	VAR													
61		1.6	5	VAR		HIGH											
62			10														
63		1.8	VAR	0													
64			0	VAR													
65			5														
66			10														RT. WING T.E. UP
67		1.8	VAR	0			0					±5	±5	±5	±5		LT. WING-T.E. DWN
68			0	VAR													
69			5														
70			10														
71		1.6	VAR	0													
72			0	VAR													
73			5														
74			10														

NOTES *SEE FIGURE 9.3-1 α SCHEDULE -4° TO +15° Δ 2° β SCHEDULE -10° TO +10° Δ 2°

1690-121W-2

TABLE 9.3-4

I WIND TUNNEL TEST MODEL NOMENCLATURE

SYMBOL

B	Body
C	Canard
N	Nacelle (includes glove)
V	Vertical Tails
W	Wing (exposed panels)

II WIND TUNNEL TEST PARAMETERS

SYMBOL

δ_{F_C}	, deg	Canard Flap Deflection Angle
δ_{LE}	, deg	Canard Leading Edge Droop Angle
δ_R	, deg	Rudder Deflection Angle
$\delta_{W_{1,2,3}}$	, deg	Wing L.E. Deflection Angle (see Fig. 9.3-1)
$\delta_{W_{4,5}}$	, deg	Wing T.E. Deflection Angle (see Fig. 9-3-1)
i_c	, deg	Canard Incidence Angle

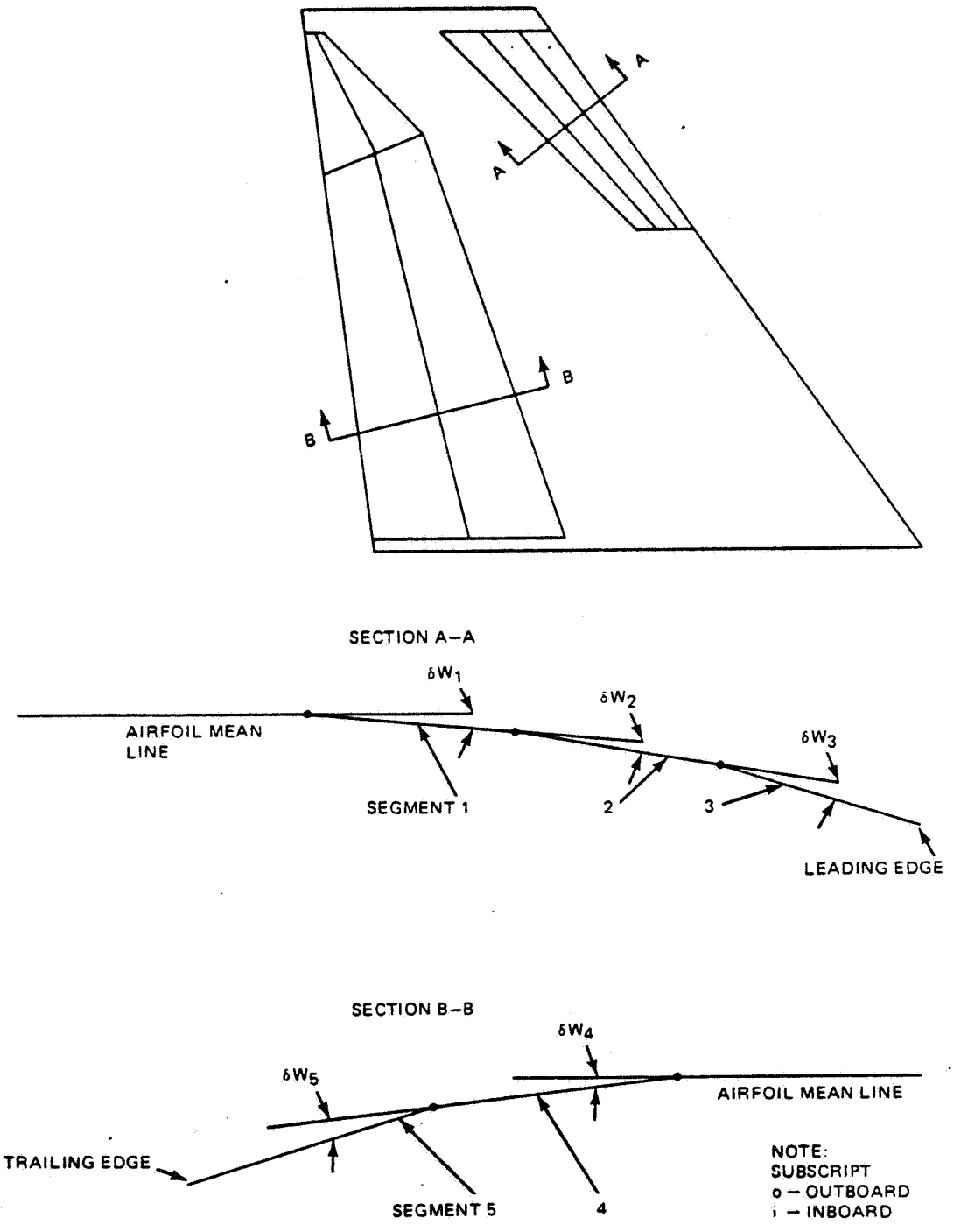

1690-109W

Figure 9.3-1 Schematic Drawing of the Variable Camber Segment Orientation

REFERENCES

4.1.1-1 Boppe, C.W.: The Effect of Planform Taper on Supercritical Wing Design. Grumman Memorandum PDM-653A-13, 1975.

4.1.1-2 Chow, R.; and Mead, H.R.: Theory of Viscous Transonic Flow Over Airfoils at High Reynolds Number. AIAA Paper 77-680, 1977.

4.1.1-3 Boppe, C.W.: A Computer Program for Calculating the Subsonic Aerodynamics of Complex Wing-Body Configurations. Grumman Report 393-73-1, 1973.

4.1.2-1 Margason, R.J.; and Lamar, J.E.: Vortex-Lattice Fortran Program For Estimating Subsonic Aerodynamic Characteristics of Complex Planforms. NASA TN-D-6192, 1971.

4.1.2-2 Glauert, H.: The Elements of Airfoil and Airscrew Theory. Cambridge University Press, 1948.

4.1.2-3 Campbell, G.S.: A Finite-Step Method For the Calculation of Span Loadings of Unusual Planforms. NACA RM L 50L13, 1951.

4.1.2-4 AFFDL/GAC Aerodynamic Configuration Transonic Wind Tunnel Tests, 1976. Results to be published.

4.1.2-5 Grumman Report PDR 651AA-5: Forward Swept Wing Feasibility Study, Second Monthly Status Report, 1977.

4.1.2-6 McGivern, D.: Results of The First Series of Wing Tunnel Tests of a 1/8 Scale Design 623 V/STOL-CTOL Aircraft. Grumman Report GWTT 328, 1974.

4.1.2-7 Jung, W.: Use of Lamar Vortex-Lattice Program For Preliminary Design Prediction of Longitudinal Aerodynamic Characteristics of Variable Wing Sweep Aircraft. Grumman Memorandum EG-ARDYN-78-31, 1978.

4.1.2-8 Hoak, D.E.; et al: USAF Stability and Control DATCOM. Revised 1972.

4.1.4-1 Hoerner, S.F.: Fluid Dynamic Drag. Published by the author, 1965.

4.1.4-2 Cerank, R.; et al: Semi-Empirical Methods for Systematic Drag Prediction of Arbitrary Aircraft Configurations. Grumman Report XAR-A-42, 1963.

4.1.4-3 Hayes, W.D.: Linearized Supersonic Flow. North American Aviation Report A.L. 222; 1947.

4.1.4-4 Graham, E.W.; Lagerstrum, P.A.; Lichen, R.M.; and Beane, B.J.: A Theoretical Investigation of the Drag of Generalized Aircraft Configurations in Supersonic Flow. NACA TM 1421, 1957.

4.1.4-5 Harris, R.V.: An Analysis and Correlation of Aircraft Wave Drag. NASA TMX 947.

4.1.4-6 Hendrickson, R.H.: The Wave Drag Program Users Manual; Grumman Report EG/RAVES-UM-226-75, 1975.

4.1.4-7 Hendrickson, R.H.: Correlation of Measured and Estimated Minimum Drag of the F-14A Wind Tunnel Model. Grumman Report 391-69-1, 1969 (C).

4.1.4-8 Hendrickson, R.H.: CISE Update for Drag Due to Lift. Grumman Memorandum EG-ARDYN-76-107, 1976.

4.1.4-9 Grumman Memorandum ASM-399-25: FX/VFAX UAL Wind Tunnel Test Results, 1966.

4.1.4-10 Naval Air Systems Command: External Store Drag Increments for HIPAAS Design Studies, 1969 (C).

4.1.4-11 Byars, L.T.; et al: A2F Substantiating Performance Data Report for the Standard Aircraft Characteristics Chart of September 1962. Grumman Report XA128-105-11, 1962.

4.1.5-1 Siske, T.R.: A Preliminary Assessment of the Transonic Maneuvering Capability of Two Advanced Technology Fighter Aircraft. NASA TMX 3439, 1975 (C).

4.1.5-2 Lindsay, Cdr. T.L.: A Procedure for Estimating Buffet Onset Normal Force as Effected by Wing Geometry. NSRDC Technical Note AL-70, 1968.

4.1.5-3 Grumman Report PDR-636A-2: Highly Maneuverable Aircraft Technology (HIMAT) - Phase II Final Report, 1974.

4.1.6-1 Schnell, W.C.; Grossman, R.L.; and Hoff, G.E.: Comparison of Non-Axisymmetric and Axisymmetric Nozzles Installed on a V/STOL Fighter Model; SAE Paper 770983, 1977.

4.2.1-1 Krepski, R.E.: A Method For Estimating Aircraft Static Directional Stability At Subsonic Speeds And Small Values of Angle of Attack. Grumman Memorandum PDM-AI-73-18, 1973.

4.2.2-1 Lowry, John G.; and Polhamus, Edward C.: A Method For Predicting Lift Increments Due To Flap Deflection At Low Angles Of Attack In Incompressible Flow; NACA TN3911, 1956.

4.3.1-1 Krepski, R.E.: Jet-Induced Interference Effects Test of a 1/8 Scale Multi-Jet V/STOL Strike Fighter Wind Tunnel Model. Grumman Report ADR 01-01-77.3, 1977.

4.3.1-2 Krepski, R.E.: Data Analysis Report of the First Series of Wind Tunnel Tests of the GAC Design 623-2004B V/STOL Strike Fighter Aircraft Conducted at the British Aircraft Corporation 5.5m V/STOL Wind Tunnel. Grumman Report PDR-623-20, 1975.

5.1-1 General Electric Preliminary Study Data: SYS-GE16/VVCE5 Study D3 Remote Augmented Lift System (RALS), 1978.

5.2-1 Tindell, R.H.: Advanced Inlet-Engine Matching Technology, Volume 1 - Aircraft-Mission Analysis. Grumman Report GAD-321-RT, 1976.

5.2-2 Brown, N.: Advanced Inlet - Engine Matching Technology, Volume 2 - High-Flow Inlet Wind Tunnel Test Results. Grumman Report GAD-321-RT, 1976.

5.3-1 Feddersen R.; and Migdal, D.: Airframe Studies of V/STOL Vectorable Nozzle for Twin-Engine Aircraft. Grumman Report PDR 623-6, 1973.

5.4-1 Grumman Progress Reports 1977 and 1978 for Contract F33615-77-C-3093, Propulsive Lift Enhancement Test. To be published.

5.4.4-1 Barron, W.A.: Hot Gas Tests of Grumman Design 623 VTOL 1/12 Scale Model at VFW-Fokker Gas Dynamics Facility - Phase I. Grumman Report ADR 01-01-76.2, 1976.

6.2-1 Air Force Flight Dynamics Laboratory: Air to Surface (ATS) Technology Evaluation And Integration Study, Task 7 - Manufacturing Technology, Structures And Materials Application, Final Report. Grumman Report, Contract F33615-76-C-3149, 1977.

7.5-1 AGARD Report No. 577: V/STOL Handling-Qualities Criteria, 1977.

7.6-1 Goranson, R. F.: A Method for Predicting the Elevator Angle Required to Land. NACA WR L95, 1944.

7.6-2 Krepski, R.E.: Wind Tunnel Test Data Report of the First Series of Wind Tunnel Tests of A 1/8 Scale Model Design 607A V/STOL Strike Fighter Aircraft Conducted At the British Aircraft Corporation 18 ft V/STOL Wind Tunnel. Grumman Report PDR-607A-11, 1973.

8.1.5-1 Smith, A.M.O.: High Lift Aerodynamics-1974 Wright Brothers Lecture. AIAA Journal of Aircraft, Vol. 12, 1975.

8.1.5-2 Chapman, D.R., Mark, H. and Pirtle, M.W.: Computers vs Wind Tunnels for Aerodynamic Flow Simulations. Astronautics and Aeronautics, Vol. 13, 1975.

8.2.1-1 Siclari, M.J., Migdal, D and Palcza, J.L.: The Development of Theoretical Models for Jet-Induced Effects on V/STOL Aircraft. AIAA/SAE Paper 75-1216, 1975.

8.2.1-2 Krenz, G.; et al: Propulsion-induced Forces and moments. NAVAIR Report 8R-76 USN/FMOD FRG VAK-191B Joint Flight Test Program Final Report, 1976.